The Effect of Pulsed Injection on Shear Layer Dynamics in a Scramjet Combustion Chamber

BY

Leslie Smith

Submitted to the graduate degree program in Aerospace Engineering

and the Graduate Faculty of the University of Kansas in partial fulfillment of

the requirements for the degree of Doctor of Philosophy.

_____

Chairperson: Dr. Saeed Farokhi

_____

Dr. Ray Taghavi

_____

Dr. Shawn Keshmiri

_____

Dr. Ronald Barrett-Gonzalez

_____

Dr. Bedru Yimer

Date Defended: May 6, 2015

The Dissertation Committee for Leslie Smith

certifies that this is the approved version of the following dissertation:

The Effect of Pulsed Injection on Shear Layer Dynamics in a Scramjet Combustion Chamber

_____

Chairperson Dr. Saeed Farokhi

Date approved: May 11, 2015

Abstract

One of the greatest problems that scramjet research faces is fuel air mixing. The residence time for a scramjet engine, or the time it takes for a volume of air to completely pass through the engine, is on the order of 0.1 ms. In that extremely short period of time fuel must be injected and fully mirco-mixed at stoichiometric ratios with the combustion chamber airflow. The fuel-air mixture must then be combusted and expanded through the nozzle to produce thrust. The goal of this research is to develop a new more efficient method of fuel air mixing within a scramjet combustion chamber.

A possible way to speed up the mixing process of parallel injection without incurring the total pressure losses that would occur in normal injection is to inject the fuel from the rear side of a backward facing step. Backward facing steps in supersonic flow produce a Prandtl-Meyer expansion fan followed by a shear layer. The instabilities in this shear layer have dominant resonant frequencies. It is believed that if fuel is injected in pulses that impinge on the shear layer at these dominant resonant frequencies that the shear layer will resonate. When the shear layer resonates the vortices that form in the shear layer will grow in magnitude, thus mixing the injected fuel with the air.

To test this hypothesis a new test section was designed and built that features a one inch step under which an injector can be housed. This new test section was installed in the supersonic facility at the University of Kansas. Two injectors were also designed that each feature a face plate, one with eight injection ports arranged in a ring and one with 5 injection ports. Between the face plate and a back plate there is a cavity that houses a rotating valve that is powered by a pneumatic motor. Five valves were built: one with 8 teeth, one with 16 teeth, one with 5 teeth that are the same size as the gaps between the teeth, one with 5 teeth where the teeth are 50% larger than the gaps, and one with 5 teeth where the teeth are 50% smaller than the gaps. The 8 tooth valve and 16 tooth valve where used with the 8 port injector face plate. The 5 tooth valves were used with the 5 port injector face plate. As the valve rotates the teeth block and unblock the injection ports injecting carbon dioxide gas into the test section. The 8 port injector was tested over a range of frequencies from 1.6 kHz to 10.0 kHz. The 5 port injector was tested for each valve over a range of frequencies from 1.0 kHz to 4.0 kHz. Static pressure data was taken along the upper and lower walls of the test section by means of an array of pressure sensors. The pressure data from the test section was compared to results generated using a three dimensional CFD simulation of the test section. Overall the pressure data on the lower wall agreed reasonably well with the CFD simulation.

The vorticity and turbulence contours generated by the STAR-CCM+ simulation suggest that as a pulse is injected into the test section from the step it causes the shear layer to curve outward near the

point of injection. After the pulse the shear layer returns to the state it was in before injection. The shear layer showed no resonance behavior as a result of pulsed injection. A spectral analysis was performed on the wall static pressure data. The results of this analysis showed no indication of resonance behavior of the shear layer in the wind tunnel tests.

Acknowledgements

I would like to first and foremost thank my advisor Dr. Saeed Farokhi for all that he has taught me during my years at KU and for all his help and advice while I was working on the research presented below. I would also like to thank Madison and Lila Self for creating the Self Graduate Fellowship which funded me for most of my graduate studies. I would also like to thank Dr. Barrett for his advice and for letting borrow tools from his lab. I would also like to thank the other members of my committee: Dr. Taghavi, Dr. Keshmiri, and Dr. Yimer for all of their advice help and support. I would like to thank the Wes Ellison for all of his help with the experimental set up. I would like to thank Robin Kerth and Lauren Kerth for their help in machining and assembling the wind tunnel test section. I would also like to thank Lauren Schumacher, Eilish McGuiness, John Zhu, and Stephen Hicks for their help testing the injector. Finally I would like to thank my parents, Larry and Anita Smith, for all of their help, support, and patience.

Table of Contents

Page #

Continued

Table of Contents Continued

List of Figures

List of Figures Continued

List of Figures Continued

List of Figures Continued

List of Figures Continued

List of Figures Continued

List of Figures Continued

List of Figures Continued

List of Tables

List of Symbols

Symbol	Description	Units
a	Speed of Sound	m/s, ft/s
c	Speed of Sound	m/s, ft/s
D	Diffusivity	m^2/s, ft^2/s
d	Length Scale	mm, in
e	Error	%
F	Force	N, Lbs
f	Frequency	Hz
g	Acceleration due to Gravity	m/s^2, ft/s^2
GCI	Grid Convergence Index	---
J	Richardson Number	---
K	Turbulent Kinetic Energy	m^2/s^2
L	Length Scale	mm, in
M	Mach Number	---
P	pressure	Pa, PSI
p	Apparent Order	---
R	Reynolds Number	---
r	Grid Ratio	---
s	Mean Shear Rate	1/s
S_c	Schmidt Number	---
St	Strouhal Number	---

List of Symbols Continued

Symbol	Description	Units
T	Time	s
U	Velocity in the x direction	m/s, ft/s
u	Velocity in the x direction	m/s, ft/s
V	Velocity in the y direction	m/s, ft/s
v	Velocity in the y direction	m/s, ft/s
X	Body Force	N, Lbs
x	Horizontal Direction	---
y	Vertical or Out of Plane Direction	---
z	Vertical Direction	---

Greek Symbol	Description	Units
β	Propagation Angle	rad, deg
δ	Thickness	mm, in
ε	Error	%
θ	Local Wave Front Normal Angle	rad, deg
κ	Wave Number	---
λ	Lateral Orientation Angle	rad, deg
μ	Mach Angle	rad, deg
ν	Kinematic Viscosity	m^2/s, ft^2/s
ρ	Density	kg/m^3, $slug/ft^3$
1/σ	Legrange Multipiler	---

List of Symbols Continued

Greek Symbol	Description	Units
ϕ	Grid Refinement Parameter	---
Ω	Vorticity	1/s

Subscript	Description	
a	Approximate	---
c	Convective	---
crit	Critical	---
eff	effective	---
ext	extrapolated	---
g	gradient	---
j	jet	---
r	relative	---
t	trubulent	---
visc	Viscous	---
x	Horizontal Direction	---
y	Out of Plane or Vertical Direction	---
z	Vertical Direction	---
0	Initial	---
1	Flow Region	---
1	Course Mesh	---
2	Flow Region	---

List of Symbols Continued

Subscript	Description	Units
2	Medium Mesh	---
21	Medium to Course Grid Refinement	---
3	Flow Region	---
3	Fine Mesh	---
32	Fine to Medium Grid Refinement	---
4	Flow Region	---
5	Flow Region	---

1 Introduction

Aircraft powered by scramjet engines, capable of travelling at up to 10 times the speed of sound, promise drastically shortened travel times allowing businessmen and travelers to be whisked to the other side of the globe in a matter of a few short hours. Scramjet powered spacecraft could also potentially serve as the gateway to space for the common man. Scramjets, unlike the space shuttle and other liquid fueled rockets, do not require large tanks of liquid oxygen, as they use the oxygen from the air for combustion. Liquid oxygen must be kept at a very low temperature, and requires a large volume for storage. Using air from the atmosphere eliminates the need for these large tanks and thus scramjets have the advantage of being smaller and thus produce less aerodynamic drag than rockets. Less drag means less fuel used, which leads to cheaper tickets for customers.

Scramjets could also offer a strategic advantage during times of war. The extraordinary speeds promised by scramjets could allow for missiles capable of destroying time sensitive targets, such as terrorists on the move. Missiles powered by scramjet engines would also be capable of destroying any incoming cruise missiles before they could reach the airspace of the United States or that of our allies.

Scramjets could also be used to power transport aircraft delivering much needed supplies to our troops abroad. Such aircraft could also potentially be used to evacuate severely injured soldiers and have them back in the United States for treatment in a matter of hours saving many lives. Scramjets could also perform these same functions in the event of a natural disaster. Medical supplies, rescue teams, and other forms of aid could be flown to the most remote regions in a matter of hours, and those first few hours after a disaster strikes are crucial.

So what is a scramjet? The word “scramjet” is an abbreviation for “supersonic combustion ramjet.” A scramjet is a type of jet engine currently capable of accelerating vehicles to speeds approaching Mach 10. A ramjet is a type of jet engine that utilizes a series of shockwaves, rather than an axial or centrifugal compressor, to compress the air. While travelling at supersonic velocities, the inlet of a ramjet produces a series of oblique shocks followed by a terminating normal shock (Figure 1). These shocks compress the air as well as decelerate it to subsonic velocities. The subsonic air then enters the combustion chamber where fuel is added and mixed with the air. The fuel air mixture is then ignited and expanded through a convergent divergent nozzle to produce thrust. Ramjets have an operational range of about Mach 3 to Mach 5. Above Mach 5, the deceleration of the air produced by the normal shock creates total pressure losses which limit the upper operational Mach number of the ramjet

engine. The performance losses from the shockwaves become so great that the engine can no longer produce net thrust.[1]

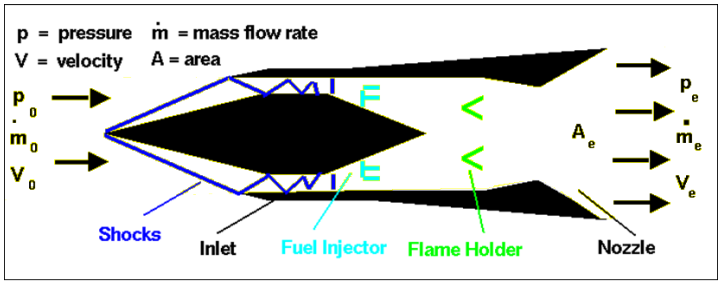

Figure 1: Ramjet Schematic[2]

Like ramjets, scramjets also utilize a series of shockwaves to compress the air. Unlike ramjets, however, scramjet inlets produce only a series of oblique shocks, without the terminating normal shock (Figure 2). These shocks compress and decelerate the air, but without the terminating normal shock the flow is still supersonic when it enters the combustion chamber. This minimizes the losses associated with decelerating the flow and allows the engine to produce thrust even at hypersonic (greater than approximately Mach 5) velocities.

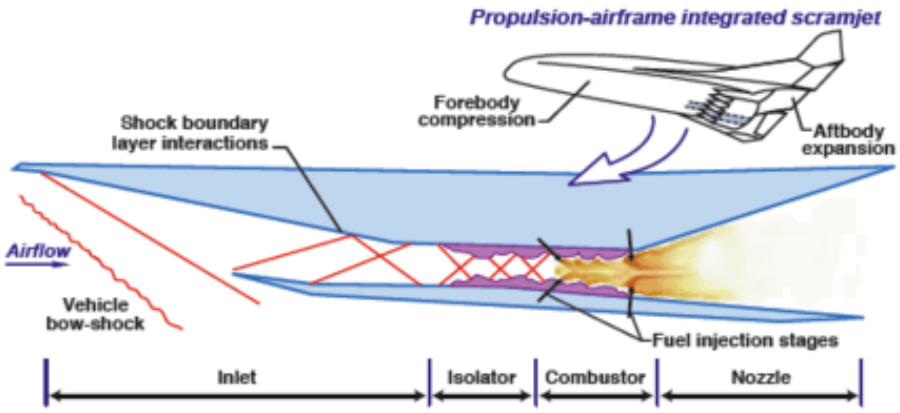

Figure 2: Scramjet Schematic[3]

There are so many possibilities for working, reliable scramjet engines, but this field is still in its infancy. There are plenty of improvements that will need to be made to the engine design before any applications are possible beyond pure research. But just like an infant this field is growing and beginning to take its first steps. NASA and the US Air Force, among others, have flown several unmanned prototypes, and various universities and research institutes around the world are working feverishly to bring this bright future one step closer.

One of the greatest problems that scramjet research faces is fuel air mixing. The residence time for a scramjet engine, or the time it takes for a volume of air to completely pass through the engine, is on the order of 0.1 ms. In that extremely short period of time fuel must be injected and fully mirco-mixed at stoichiometric ratios with the combustion chamber airflow. The fuel-air mixture must then be combusted and expanded through the nozzle to produce thrust. If the fuel and air are not micro-mixed, or mixed at the molecular level, quickly enough then the fuel air mixture will not have time to fully combust before being expelled. Thus the scramjet exhaust will contain unburned fuel, wasting the potential for greater thrust.

The goal of this research is to develop a new more efficient method of fuel air mixing within a scramjet combustion chamber. Injecting fuel normal the main flow of the combustion chamber has been shown to have good near field mixing, but poor far field mixing. Normal injection also causes bow shocks which create total pressure losses within the engine. Parallel mixing has been experimentally shown to cause lower total pressure losses than normal injection, but the mixing rate is extremely slow. A possible way to speed up the mixing process of parallel injection without incurring the total pressure losses that would occur in normal injection is to inject the fuel from the rear side of a backward facing step.

Backward facing steps in supersonic flow produce a Prandtl-Meyer expansion fan followed by a shear layer (Figure 3). The instabilities in this shear layer have dominant resonant frequencies. It is believed that if fuel is injected in pulses that impinge on the shear layer at these dominant resonant frequencies that the shear layer will resonate. When the shear layer resonates the vortices that form in the shear layer will grow in magnitude, thus mixing the injected fuel with the air.

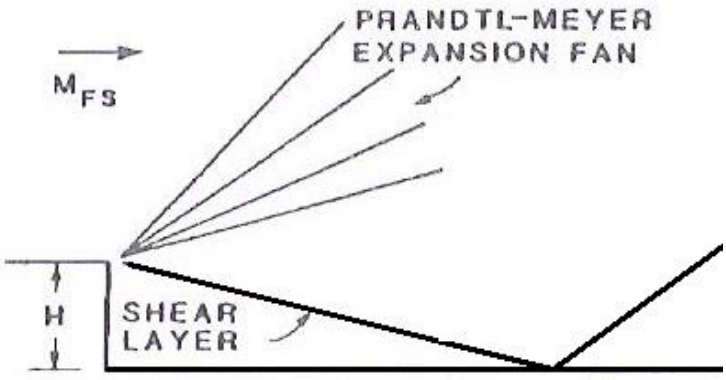

Figure 3: Flow Over a Backward Facing Step[1]

2 Review of Literature

In order to determine how to improve supersonic mixing in a scramjet combustion chamber it is necessary to first understand the processes that govern mixing at supersonic velocities as well as previous successful methods used to improve mixing. For mixing to occur the flow must be turbulent, so it is first necessary to study how instabilities arise in the flow, particularly the Kelvin-Helmholtz instability which plays such a crucial role in shear layer mixing. The behavior of the Kelvin-Helmholtz instability at subsonic and supersonic Mach numbers also needs to be understood. From there the behavior of the Kelvin-Helmholtz instability in supersonic shear layers can be exploited to enhance fuel and air mixing at supersonic Mach numbers.

2.1 Transition

All known laminar solutions of the hydrodynamics differential equations are valid for flows with high enough Reynolds numbers. The origin of turbulence, therefore, must be due to instabilities in the laminar flow. In laminar flow, small disturbances are superposed on the basic laminar flow. The small disturbances are composed of harmonic oscillations that propagate in the direction of the flow.[1]

For the two-dimensional boundary layer there exists a Reynolds number, R_{crit}, where the flow begins to transition from laminar to turbulent flow. For laminar flow with horizontal streamlines, two-dimensional oscillations are most likely to induce transition. In Couette flow, all oscillations are damped except for Tollmien-Schlichting waves.[1]

In boundary layer flows with pressure gradients, such as the gradients that boundary layers on airfoils might encounter, is was found that positive, or adverse, pressure gradients help to damp out oscillations and negative, or favorable, pressure gradients amplify oscillations. This is why boundary layer transition tends to occur on the back side of the airfoil. With increasing Reynolds number, as the Reynolds number approaches R_{crit}, it was found that the beginning of instability jumps from the rear of the airfoil to the front of the airfoil.[1] Friction or other elements on the surface of the airfoil can still cause instabilities in the boundary layer even with the adverse pressure gradient.[1] Transition in the airfoil boundary layer can also be caused by boundary layer separation. The transition of the boundary layer from laminar to turbulent can cause the boundary layer to reattach.[5]

The pressure gradient has less of an effect on transition at higher Mach numbers. However, compressible boundary layers are also much less sensitive to roughness than incompressible boundary layers.[1] The stability of supersonic boundary layers is problematic because of the significant increase in the number of parameters that much be considered. For compressible flows, vertical oscillations in stratified fluids will produce density fluctuations. Below about Mach 3 the instabilities that exist in the

two-dimensional supersonic boundary layers are of the resistivity variety. Above Mach 3 instability is related to a form of acoustic resonance in the shear flow and the effect of velocity is actually stabilizing.[6] In three-dimensional supersonic flows with instabilities at low frequencies, the rate of instability amplification increases with the obliquity of the disturbance. Instabilities at high frequencies are the most unstable when the waves are parallel to the main flow.[6] Heating and cooling walls has an effect on the speed of sound and the density of the fluid near the wall. It was found that boundary layers can be stabilized through cooling.[6] On concave walls cellular or recirculating flows arise. These cellular flows influence the transition from laminar to turbulent flow.[1]

The stability of the boundary layer can also be controlled by suction and blowing. When suction is applied, the boundary layer separation shifts further downstream. The stability of the boundary layer is also increased and the transition of the flow from laminar to turbulent occurs later. Blowing normal to the wall has the exact opposite effect. Blowing parallel to the flow is, in theory, stabilizing, but it is technically very difficult to do without introducing other disturbances. Moving walls parallel to the flow also have a stabilizing effect.[1]

Fully developed turbulent flow contains velocity fluctuation components in all three dimensions. The Tollmien-Schlichting method only shows the lower threshold for two-dimensional disturbances, but this does not excluded the presence of three-dimensional disturbances.[1]

When a weak shock wave strikes a laminar boundary layer a small disturbance is produced analogous to the effect of a small roughness element. Strong shock waves can cause transition directly or cause boundary layer separation.[5]

Once the flow passes the stability limit, there is a region where the flow is in transition but is not yet fully turbulent. Just beyond the stability limit Tollmein-Schlichting waves begin to amplify. The flow then becomes intermittent. There are regions of the flow where turbulent flashes are seen and there are other regions of the flow that are almost laminar. As the flow moves downstream, the regions of turbulence grow until the flow becomes fully turbulent.[1]

2.2 The Kelvin Helmholtz Instability

Given two stratified fluids, the Kelvin Helmholtz instability occurs when the static arrangement, that is to say the stratified fluids in the absence of streaming, is unable to inhibit the instability in the presence of streaming for disturbances of sufficiently small wavelengths. The Kelvin-Helmholtz instability arises by the crinkling of the interface between the two fluid layers. This crinkling is caused by the shear that occurs due to a difference in velocity between the two fluid layers. The crinkling of the

interface occurs for even the smallest velocity differential. However, surface tension has a stabilizing effect on the Kelvin-Helmholtz instability, damping the instability out if the velocity differential is small enough. The source of the instability lies in the energy stored in the kinetic energy of relative motion of the different layers. The tendency towards mixing and instability will be greater at larger shear values. The shear in the interface layer is the derivative of velocity with respect to distance normal to the shear layer.[7] In Figure 4 it can be seen how the Kelvin Helmholtz instability arises and leads to the formation of vortex structures.

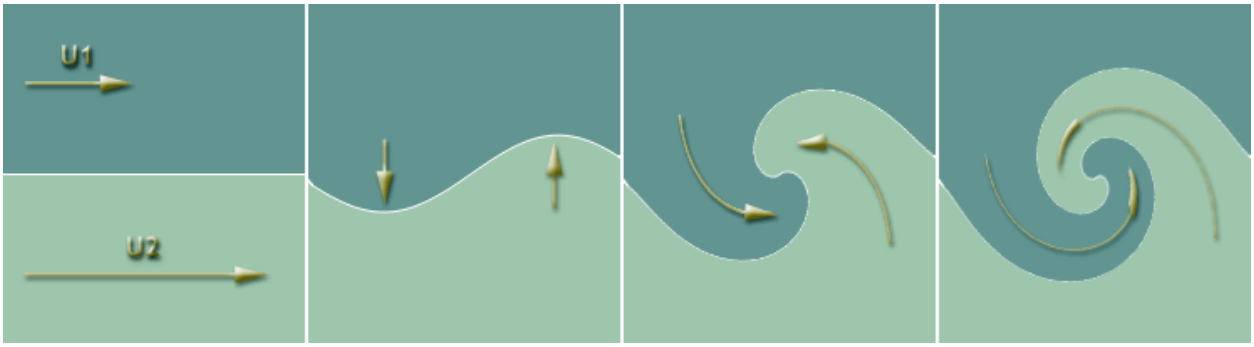

Figure 4: Kelvin Helmholtz Instability[8]

The presence of the instability has been verified both mathematically and experimentally. In a wind tunnel test, an air stream was directed over still oil. Ripples in the oil were seen to appear suddenly and grow rapidly after a sharply defined point.[7]

If the velocity is varied continuously throughout a fluid, rather than suddenly at the interface between two fluids, then there is no surface tension to damp out the instability. The results of the mathematical derivation for this case show that the instability is still present even in the continuously varying case. For the shear interface case, this implies that no matter how many times the interface is subdivided there will always be bands of unstable wave lengths. The Kelvin-Helmholtz instability cannot be avoided for any Richardson number.[7]

The Richardson number can be defined according to Equation 2.1:

$$J = -\frac{g\frac{d\rho}{dz}}{\rho\left(\frac{du}{dz}\right)^2} \qquad (2.1)$$

Where g is acceleration due to gravity, ρ is density, u is velocity in the streamwise direction, and z is distance normal to the streamwise direction. In essence the Richardson number measures the ratio of the buoyancy force to the inertia. Inertia dampens mixing. If inertia can maintain a sufficient pressure gradient, then the mixing will be prevented and instability will not occur. For Richardson numbers greater than 0.25 the flow will most likely be stable. It has been found that higher Richardson numbers

have a stabilizing effect on many flow instabilities, not just the on Kelvin-Helmholtz instability. For Richardson numbers less the 0.25 the flow could be unstable. The stability occurs because although there is enough stored energy for the instability to occur no mixing mechanism is present for transforming the energy into hydrodynamic modes.[7]

2.3 Mixing in the Subsonic Shear Layer

Brown and Roshko studied subsonic plane turbulent mixing between two streams of different gases, especially nitrogen and helium.[9] A new test section, shown below in Figure 5, generated two parallel streams of gas that pass over a splitter plate to form a two-dimensional shear layer. Measurements were taken with Pitot static probes and hot wire probes. Shadowgraph images were also used to study the flow field.[9]

Figure 5: Shear Layer Test Facility[9]

Spark shadowgraph images, such as the one shown in Figure 6, showed that for all density ratios the mixing layer between the two parallel streams is dominated by large coherent structures. These structures consist of vortex like waves, or rollers, which are essentially two-dimensional and well organized. These structures convect at nearly constant velocities, near to the average velocities of the two jet streams. This speed is independent of size and location of the eddy.[9]

Figure 6: Brown and Roshko Shear Layer Shadowgraph Image[9]

The structures form from Kelvin Helmholtz instabilities occurring at the interface between the two layers of moving fluid. As the waves grow they distort and tend to roll up into a vortex on the decreasing amplitude face of each wave. In the laminar instability layer, the spacing of the vortex structures is equal to the wave length of the initial small disturbance from which they have developed. In the turbulent layer the spacing between the structures increases with increasing distance downstream of the splitter plate. The eddy diameter also increases with increasing distance downstream. Brown and Roskho's results show that there does not appear to be a fixed repeatable pattern in the vortex arrangements, only a general resemblance in that the scale increases.[9]

It is to be noted that a true mixing layer is a type of free shear layer. However, a true mixing layer requires turbulent flow. A laminar layer exhibits shear between the fluid streams but no real mixing because the fluids each retain their organized streamlines.[10]

As the structures move downstream, they increase their size and spacing discontinuously by amalgamation with neighboring structures. Turbulent mixing and entrainment within the mixing layer is basically a process of entanglement on the scale of the large structures. The vortex growth process is believed to be vortex paring, where two vortices become entangled and rotate around each other until they become one new structure. The vortices also grow through entrainment, where fluid from both sides of the shear layer is pulled into and entangled within the coherent eddies. Fine scale mixing along the shear layer occurs by means of instabilities within the vortex structures themselves.[9]

Large changes in the density ratio across the mixing layer were found to have only a relatively small effect on the shear layer spreading angle.[9] The growth rate of the incompressible, variable-density, shear layer changed only by about 50% when the density ratio was varied by a factor of 50.[11] The slower spreading rate and other effects observed when one stream is supersonic are believed to be compressibility effects rather than density effects. Brown and Roshko tested this by using different gases to achieve different density ratios. Helium and Nitrogen gas have roughly the same density ratio,

approximately 7, as a jet of air at Mach 5.5. Even with the comparable density ratios the supersonic shear layer had a much lower spreading rate than the subsonic shear layer. Thus the slower spreading rate was determined to be due to compressibility.[9]

Plesniak et al. performed an experimental study on the influence of small changes in initial conditions on the near and far field evolution of the three-dimensional structure in a subsonic plane mixing layer. A two stream mixing layer with a velocity ratio of 0.6 was generated with the initial boundary layers laminar and nominally two-dimensional. The initial conditions were changed slightly by interchanging the high and low speed sides of the wind tunnel while maintaining the same velocity ratio. This meant the nature of the perturbations present in the boundary layers on each side of the splitter plate were interchanged between the high and low speed sides. The results show that the near field regions of the two cases differ significantly with the peak Reynolds stress levels varying by up to 100%.[12]

For the two cases, the distribution of the individual streamwise vortical structures differs in intensity and position. The reorganization and streamwise decay of the vortical structures is also very similar for the two cases. In the far field both mixing layers achieve comparable growth rates and asymptotic values of the peak Reynolds stresses. The development of plane mixing layers was largely influenced by the formation and interaction of large scale spanwise vortices within the layer.[12]

The formation of the spanwise vortical structures was primarily caused by the inviscid Kelvin-Helmholtz instability operating on the velocity distribution across the mixing layer. Once these structures form, the layer grows linearly. Several time averaged, plan view photos also showed distinct streamwise streaks which were believed to be distinct streamwise oriented, vortical structures. Cross sectional views show that there are pairs of counter rotating streamwise vortices riding within the spanwise structures. Streamwise vortices are believed to be a result of an unstable response of the layer to three-dimensional perturbations in the upstream conditions.[12]

Small, naturally present, disturbances in the flow were initially amplified just downstream of the first spanwise roll-up leading to the formation of streamwise vortices. Streamwise vortices with average circulation equivalent to about 10% of the initial spanwise circulation first appear in clusters containing vortices of both signs. Further downstream, the vortices reorganized to form counter rotating pairs.[12]

The purpose of Plesniak et al.'s study was to establish the sensitivity of shear layer three-dimensionality to small changes in initial conditions. One side of the shear layer had a velocity of 15 m/s the other had a velocity of 9 m/s. No strong three-dimensional disturbances existed in the boundary layers. A cross wire probe was used for measuring velocity.[12]

The spanwise properties were averaged to obtain an accurate representation of the behavior of the mixing layer due to the large spanwise variations experienced in the near field. Spanwise vortex rollup is more coherent in the reversed case. In both cases the behavior of the streamwise vorticity is similar. Vorticity appears in clusters, then reorganizes into counter rotating pairs and decays and grows in scale with downstream distance such that by the last measurement station the mixing layer is nominally two-dimensional. The instability leading to the formation of the streamwise structures occurs in the braid regions, the regions between the rollers, where the combined effects of the large positive strain and the normal shedding make the mixing layer unstable to small three-dimensional perturbations. Relatively small changes in initial conditions, while affecting the details of the near field three-dimensional structure and Reynolds stress distributions, do not change the mixing layer global properties significantly. The behavior of the streamwise vortices, after their formation, is not dependent on initial conditions.[12]

Flow visualization investigations of plane mixing layers with laminar initial boundary layers have shown the presence of streamwise vortical structures riding among the primary spanwise vortices. Bell and Mehta made measurements in the mixing layer with both initial boundary layers tripped which showed that such organized streamwise structures did not exist in that case. While the asymptotic turbulent shear layer structures were comparable, the growth rate of the shear layer for the untripped case was higher. The difference was attributed to the presence of organized streamwise vortices in the untripped case which would be expected to increase entrainment, and hence the growth of the mixing layer.[13]

Strong streamwise vorticity was injected into the mixing layer with tripped boundary layers. While the vorticity injection increased the growth rate in the near field, the asymptotic growth rate was reduced by a factor of about two. This result is attributed to the effect of the relatively strong, and short wavelength, streamwise vorticity. The vorticity makes the spanwise structures more three-dimensional and slows down their pairing process, thus reducing entrainment and shear layer growth. It was expected that the vorticity injection would increase the growth rate of the mixing layer. While this effect was observed in the very near field, the asymptotic growth rate was drastically reduced. This result is attributed to the effect of the relatively strong and short wavelength vorticity in making the spanwise structures more three-dimensional. It is believed that this effect decreases their pairing rate, thus reducing entrainment and the growth of the shear layer. The streamwise vortices were found to decay rapidly within the mixing layer, but their spacing remained unchanged.[13] There is some evidence that this mixing layer with vorticity injection will eventually achieve an asymptotic self-similar state

comparable to that of the undisturbed cases. It is clear, though, that the effects of the injected vorticity persist until well after all direct signs of the injected streamwise vorticity have decayed.[13]

Some researchers have reported that the large-scale vortical motions found within the shear layer are rolled up, or spooled, laminae resembling a helical spring with small vortices on their periphery. A thermal tagging technique was used by Disimile to show that the vortex core was well mixed and relatively quiescent, whereas large fluctuations were found on the vortex peripheries. The internal structure of the vortices is lost by viscous diffusion.[14] Brown and Roshko, while observing species concentration in a mixing layer, noted convoluted distributions. Their observations indicate that the surrounding ambient fluid is entrained and entangled within the structure causing the vortical structure to exhibit large fluctuations in concentration.[14]

Ambient fluid can be found throughout the jet. Indications were found of a two level instantaneous concentration field where concentration levels differ by a factor of 2 or 3. Vorticity measurements were taken in a weakly excited incompressible shear layer generated from a backward facing step, using hot wire testing. A relatively large, two-dimensional, turbulent boundary layer and low frequency periodic excitation allowed for the creation of vortical structures approximately 20cm in width. The phase averaged vorticity contours display the coherent structure generated by phase averaging 1000 cycles. High levels of vortical activity in the core of the vortex structure were observed. Rapid mixing is accomplished by inertial interactions. The rate of the core vorticity changes very rapidly. This indicates the high level of activity and non-equilibrium present in the mixing layer. The vorticity distribution is highly active and entangled, which leads to a high degree of uniformity of density and temperature in this region. Reduced vortical activity at the periphery of these large vortical structures confirms the higher degree of non-equilibrium found. The role of viscosity is negligible because inertia dominates mixing down to the micro scale.[14]

Three-dimensionality appears in subsonic transitioning mixing layers in the form of streamwise vortical structures. The effects of velocity ratio, the velocity difference across the layer, on near field generation and development of three-dimensionality in mixing layers have been investigated by Wiecke and Mehta.[15] Time-averaged velocity measurements were obtained using a single rotatable cross wire probe on fine cross plane grids at four streamwise locations in the near field region. The effects of five velocity ratios ranging from 0.5 to 0.9 were investigated by keeping the velocity of one stream constant while varying that of the other. One stream was set for 12 m/s, while the other stream was varied between 6 m/s and 10.8 m/s. The results indicate that the mixing layer three-dimensionality is indeed affected by velocity ratio.[15]

The peak, mean streamwise vorticity levels decrease monotonically with increasing velocity ratio at all the streamwise locations investigated. The rate of decrease is highest at the most upstream station and it decreases with increasing downstream distance. The mean streamwise vorticity contours at the first station show that their distribution is quite similar at the different velocity ratios, implying that the generating mechanism and initial disturbance fields remain unchanged with velocity ratio. It is conceivable that the amount of stretching in the braid regions, the regions connecting adjacent spanwise rollers, is affected by velocity ratio.[15]

As the velocity ratio decreases, and the velocity difference across the layer increases, stronger spanwise rollers are generated which increase the amount of stretching in the braid regions and hence the streamwise vorticity is amplified. The splitter plate wake has a lasting effect on the three-dimensional structure of the mixing layers at the higher velocity ratios. Secondary structures, in the form of spatially stationary streamwise vortices also appear. The streamwise structures first formed in the braid region, a region connecting adjacent spanwise vortices which lacks significant spanwise vorticity and is dominated by large scale strain. Three-dimensional mixing models showed an inclined vortex tube structure, referred to as ribs, in the braid region which wound back and forth between adjacent spanwise rollers. Small spanwise disturbances originating upstream in the boundary layer flow were amplified leading to the formation of spatially stationary streamwise vortices. The vortex structure grew in size and weakened with downstream distance.[15] Pairs of counter rotating streamwise vortices can develop as a result of stretching of the primary roller.

2.4 Mixing in the Supersonic Shear Layer

The growth rate and turbulent structure of the compressible, plane shear layer were investigated in 1986 by Papamoschou and Roshko. Ten combinations of similar and dissimilar gases at different densities and Mach numbers were studied. The Mach numbers in the study ranged from 0.2 to 4.[16] The mixing layer growth rate can be defined as the measure of bulk entrainment into the layer.[17]

It had been previously found that shear layers with one stream supersonic and one stream at rest, such as supersonic jets injected into stagnant air, spread more slowly than incompressible shear layers. It had also been noted that the growth rate of the shear layer decreased with increasing freestream Mach number. Increasing Mach number, accompanied by decreasing temperature, increases the density of the jet, thus the thinning of the shear layer was originally thought to be due to the density ratio between jet and gas. Brown and Roshko tested incompressible shear layers with large density

differences using different gases and saw that density difference had some effect on the spreading rate but could not account for the slow spreading rate in the supersonic case.[16]

The main difference between supersonic and subsonic flow is that in subsonic flow disturbances, propagating at the speed of sound, are felt throughout the flowfield. In supersonic flow these disturbances do not propagate upstream, as the air stream has a higher velocity than the disturbances, and remain confined within a Mach cone.[16]

The growth of the shear layer is primarily governed by large scale instability. Subsonic turbulent shear layers contain large coherent structures similar to those formed in the early stages of instability. Schlieren photography of the shear layer reveals very slow spreading rates and large scale structures.[16]

To better understand the behavior of these large scale structures Papamoschou and Roshko defined the Convective Mach number, M_c, or the Mach number observed in a coordinate system that is convecting with the velocity of the dominant waves and structures of the shear layer.[16] This convective frame of reference is also referred to as the Galilean frame of reference.[18] For these shear layer studies M_c ranged from 0 to 1.9.[16]

In two-stream compressible shear layers the effects of compressibility were found to be coupled with the density and velocity ratios. The density ratio has the effect of causing the growth rate to be smaller when the heavier gas is the high speed gas and causing the growth rate to be greater when the heavier gas is on the low speed side. The growth rate of the shear layer also increases with decreasing velocity ratio.[16]

To study only the effects of compressibility on the shear layer, the shear layer growth rates were normalized to the incompressible shear layer growth rates that would occur at the same velocity and density ratios. It was found that the normalized shear layer growth rate was only 20% of the incompressible shear layer growth rate at supersonic convective Mach numbers.[16] Thus it can be concluded that the growth rate of the shear layer is a strong function of the convective Mach number.[19] It can also be concluded that compressibility suppresses mixing.[19]

For a freestream Mach number of 0.5, large structures engulf pure fluid from both sides of the shear layer, and the shear layer grows, doubling its size. For a freestream Mach number of 1.5, similar behaviors were observed, except at a reduced rate. These shear layers show characteristics of the Kelvin Helmholtz instability. For a freestream Mach number of 2.9, the growth rate is smaller than for the incompressible case but is still of the same magnitude. For the unbounded shear layer at Mach 2.9 the growth rate was much smaller. Shear layer mixing appears to be very slow with no pure fluid

engulfment by the large structures as in the low Mach number case. At higher Mach numbers the extent of contact surfaces is also significantly reduced.[20]

Compressibility plays a crucial role in the stability and mixing of shear layers. As the convective Mach number increases, the disturbances act less in perturbing the flow in the vicinity of the shear layer, and thus the shear layer itself, and more in perturbing the flow away from the shear layer. At supersonic convective Mach numbers energy is radiated away from the shear layer. This could cause energy removal from the potential pairing of spanwise vortices, thus impeding the process of amalgamation. It is uncertain if this is actually the case, but regardless, the loss of energy would slow down all interactions responsible for shear layer growth.[16]

Another important factor in the stability of compressible shear layers is that there is a portion of the flow near the center of the shear layer where the local velocity, relative to the convective velocity, is subsonic. This is the case even if both freestreams are supersonic. The extent of this subsonic layer decreases as the convective Mach number increases, but the region never completely vanishes. This subsonic region is potentially dominated by subsonic instabilities and, as the flow velocity in these regions is less than the disturbance velocity, these disturbances can propagate upstream. The upstream propagation of disturbances in this subsonic region could be essential for shear layer instability at supersonic speeds. The fact that this subsonic layer never completely vanishes could be the reason why the shear layer remains unstable no matter how high the freestream Mach number.[16]

The shear layer becomes turbulent immediately after passing the trailing edge of the splitter plate. As the shear layer is fully turbulent, it is expected (and has been proven by experimental results) to grow linearly. The static pressure also rises rapidly near the trailing edge of the splitter plate, then levels off in the far field. The compressible mixing layer in a constant area duct exhibits a strong pressure recovery similar to that seen in a supersonic diffuser.[16] The cause of the pressure rise is the increased entropy due to mixing. [21] As the entropy is due to the mixing it is also strongly coupled to compressibility.[21] The microscopic mechanisms responsible for causing entropy rise are shocklets, or small shocks that are attached to the turbulent eddies.[21]

This increase in entropy also causes a decrease in the total pressure and Mach number.[16] The static pressure rise is a result of the shear layer displacement thickness, which acts like a solid wedge inserted between the two streams.[16] The mixing of two parallel streams up to the point where the mixing layer takes up the whole channel has total pressure losses equivalent to a normal shock in a single stream equivalent flow.[21]

Schlieren photography revealed large scale vortical structures in the shear layer. It is believed that the structures seen in this experiment were quasi-two-dimensional because the Schlieren images were very distinct.[16]

Clemens et al. performed an experimental investigation of the evolution of these large scale structures in a flow consisting of two planar turbulent shear layers formed by a Mach 3 planar jet bounded by a Mach 5 freestream at a convective Mach number of 0.28. The two shear layers were initially independent, but interacted further downstream. Measurements were taken with a fast response hot wire probe and planar laser scattering from a condensed alcohol fog. The hot wire data was used to calculate power spectra and cross correlations from which large scale structure length scales and orientation were inferred. The images reveal roller like structures but these structures are not as dominant or as coherent as those seen in low Mach number shear layers at similar Reynolds numbers. The hot wire data confirmed the relatively unorganized and three-dimensional natures of the independent shear layers. In the far field the visualizations reveal that the shear layers interact to form a more organized structure. This is similar to vortex shedding in incompressible turbulent wakes.[22]

The organized structures result in a distinct peak in the power spectrum and larger spanwise coherence lengths than for the independent shear layer. Upstream the shear layer is quite unorganized. This could be because the independent shear layer has not recovered from the unorganized turbulence of the initial high speed boundary layer. The increase in organization with increasing downstream distance was shown to be attributable to the interaction of the two shear layers to form a new instability that appears wake-like. This new instability exhibits a sharp peak in the power spectra, and has approximately twice the spanwise correlation length as the upstream shear layer. There is a significant increase in the characteristic structure angle from the upstream to the downstream location. The increase in angle is related to the development of the new instability. The large scale structure in the near field independent shear layer is more organized than that found in previous studies of incompressible and low convective Mach number supersonic shear layers at the same or higher Reynolds numbers. Power spectra sharpen with increasing streamwise distance which indicates an increase in shear layer structure organization.[22]

2.4.1 Shear Layer Transition

Demetriades and Brower performed an experimental study of the free shear layer between two dissimilar parallel high speed streams. A Mach 3 supersonic nozzle, in combination with either a Mach 1.6 or a Mach 2.0 supersonic nozzle, was used to produce a two-dimensional flow field where laminar

flow, transitional flow, and turbulent flow were observed. Data was taken on the laminar flow profiles in the shear layer, the frequency and intensity of the fluctuation in the laminar flow, and the appearance of transition to turbulence and its role in mixing. The shear layer appears as a quiescent layer for a streamwise distance of about 200 times the fast side momentum thickness aft of the trailing edge. For the next 200 momentum thicknesses the hot wire film spectra show the appearance of a strong instability with a frequency on order 120 kHz. Further downstream the instability decreases in intensity, its spectrum disperses, and the flow width increases.[23]

Hot film anemometer, continuous Schlieren and spark Schlieren were used to quantify and qualify the results (Figure 7). The boundary layer being shed from the splitter plate must be laminar to achieve a laminar mixing layer.[23]

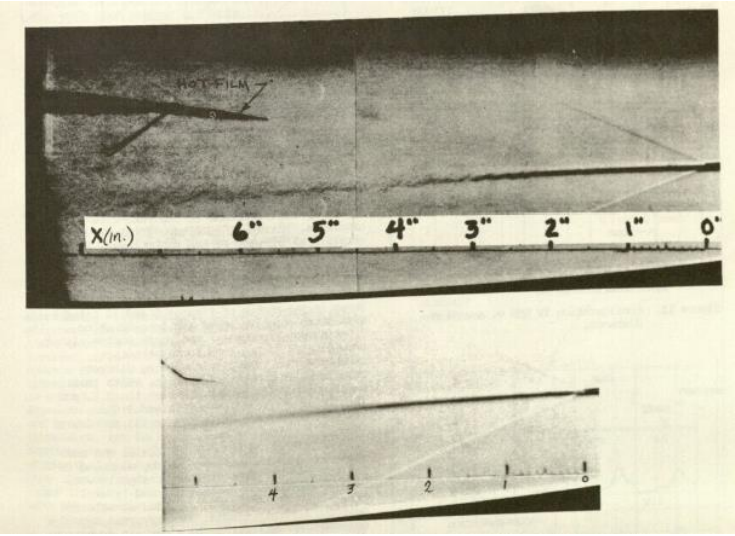

Figure 7: Spark and Continuous Schlieren Images of the Laminar Mixing Layer[23]

The shear layer showed an orderly progression from a quiescent laminar flow at the trailing edge to the disordered motion typical of turbulence at far downstream positions.[23] The onset of turbulence is marked by accelerated spreading of the layer and a decrease of the mean flow gradients.[23] The decrease in the density gradients is also detectable by the loss of Schlieren contrast.[23] No distinguishing discrete structures were observed in the turbulent zone.[23]

Following a quiescent period just downstream of the trailing edge, instability waves appeared and grew in the downstream direction.[23] The waves seem to vanish long after transition had occurred.[23] This shows the existence of density waves of a phase independent of the spanwise coordinate.[23] In the initial quiet period, the appearance of the oscillation caused by the wave and gradual dispersion of the waves into turbulence can be clearly seen.[23]

2.4.2 Turbulence

Papamoschou et al. performed exploratory tests of a new optical method which directly measured two components of the three-dimensional power spectrum of the refractive index fluctuation. The method was applied to a Mach 2 turbulent shear layer. Length scales of 0.1mm to 1mm were resolved within a shear layer with shear layer thicknesses ranging from 5mm to 10mm. The spectra slopes were in agreement with prevailing theoretical predictions for anisotropic, or low wave number, and isotropic, or high wave number, turbulence.[24]

One of the fundamental concepts in the theory of turbulence is the so called energy cascade. This is where the large turbulent eddies transfer their energy to small eddies which in turn transfer energy to smaller ones until the energy is dissipated at the very small scale eddies. The energy in question may be kinetic energy associated with fluctuation of scalars, such as temperature and density.[24]

The spectral description of turbulence deals with the distribution of energy among eddies of size, L, and wave numbers κ:

$$\kappa = \frac{2*\pi}{L} \qquad (2.2)$$

If the turbulence is isotropic, eddies do not have a preferred direction, which means they can be thought of as spherical and a single wave number, κ, is sufficient to characterize them. However, turbulence in most cases is anisotropic and the turbulent eddies need to be described by the three-dimensional wavenumber, i.e. κ_1, κ_2, and κ_3.[24]

Wantanabe and Mungal investigated two-dimensional velocity fields of mixing enhanced compressible planar shear layers measured via PIV to study the mechanism of mixing enhancement by sub-boundary layer triangular disturbances. The convective Mach numbers studied were 0.63 and 0.25. Titanium dioxide particles were used as seeds for PIV measurement. Schlieren photography was also used to show global effects of the enhancement technique on the shear layer growth rate.[25]

The results show that at a convective Mach number of 0.63 the streamwise velocity profile across the shear layer has double inflection points while it has periodical inflection points in the spanwise directions. A pair of counter-rotating streamwise vortices, due to the disturbances, was also observed. It was found that the enhanced case shows higher turbulent intensity at a convective Mach number of 0.63, suggesting mixing enhancement effects through large momentum transportation.[25]

The Schlieren results reveal the present mixing enhancement technique increases the shear layer growth rate by 45% at a convective Mach number of 0.63, although it does not show a distinguishable growth rate increase in a far-field at a convective Mach number of 0.25. With the disturbances at a

convective Mach number of 0.63, the streamwise velocity profile across the shear layer has double inflection points, which is rarely observed in compressible shear layers. It also has periodical inflection points in the spanwise direction corresponding to the spacing of disturbances. The various inflection points appear to enhance shear layer instability, leading to mixing enhancement.[25]

A pair of counter-rotating streamwise vortices, generated by an individual disturbance, was observed at both higher and lower compressibility conditions. At a convective Mach number of 0.63, the enhanced case shows higher turbulent intensity in terms of streamwise and transverse components and Reynolds stress in the transverse plane, suggesting mixing enhancement effects through a larger momentum transportation condition than the no-disturbance case. In addition the disturbances have effects abbreviating anisotropy at high compressibility conditions. At a convective Mach number of 0.25, peak values of the quantities have little differences between the cases.[25]

Side views of instantaneous velocity fields in the disturbed case show two thin sheets of vortices near the upper and lower edge of the shear layer at a convective Mach number of 0.63 while the layers are not so apparent at a convective Mach number of 0.25.[25]

The present mixing enhancement technique using sub boundary layer triangular disturbances increases shear layer growth rate by 45% at a convective Mach number of 0.63. It does not show a distinguishable growth rate increase in the far-field at a convective Mach number of 0.25, although shear layer thickness becomes thicker due to an initial mixing enhancement effect near the splitter tip. It is inferred that two-dimensional structures, dominant in low compressibility shear layers, could suppress the mixing enhancement effect by introducing streamwise vortices while highly three-dimensional structures in highly compressible conditions are susceptible to the vortices.[25]

2.4.3 Compressibility Effects

The gradient Mach number, M_g, is a parameter based on the mean shear rate, the integral length scale of the turbulence and the speed of sound in the fluid. It has been shown to be an important indicator of compressibility. In the simulations performed by Sarkar, when the gradient Mach number was increased there was a large reduction in the growth rate of turbulent kinetic energy. The stabilizing influence of compressibility in the high speed regime is due to the reduced efficiency of turbulence production and not due to mean density variation or explicit dilatational effects.[26]

An estimate of the gradient Mach number showed that it is substantially larger in the compressible mixing layer than in the compressible boundary layer for the same mean flow Mach number. Thus the

stabilizing effect of compressibility is expected to be larger in the mixing layer with respect to the boundary layer. This is in agreement with experimental observations.[26]

One explanation for lower shear layer growth is that the growth rate of small disturbances decreases when the convective Mach number increases. The second explanation is that the dissipative effects of dilatational velocity fluctuations become progressively more important with compressibility, which reduces the turbulent energy and thereby decreases turbulent mixing. This explanation still needs direct validation.[26]

The turbulent Mach number and the gradient Mach number are respectively defined in Equations 2.3 and 2.4:

$$M_{t0} = \frac{u_0}{c_0} \tag{2.3}$$

$$M_{g0} = \frac{S*L_0}{c_0} \tag{2.4}$$

Where s is the constant mean shear rate, L_0 is the initial integral length scale of u in the transverse shearing direction and c_0 is the initial mean speed of sound. The variable u_0 is defined according to Equation 2.5:

$$u_0 = \sqrt{2K_0} \tag{2.5}$$

Where K_0 is the initial turbulent kinetic energy.[26]

Compressibility effects on the flow evolution increase when either M_{g0} or M_{t0} increases. The asymptotic growth rate of the turbulent kinetic energy depends on the eventual balance between the turbulent production by shear, the turbulent dissipations, and dilatational effects. The reduction in the Reynolds shear stress anisotropy, and consequent reduction in the turbulence production level, is predominantly responsible for the reduced growth rate of the turbulent kinetic energy.[26]

The parameter M_g increases significantly more rapidly in the mixing layer relative to the boundary layer when the mean Mach number of the flow increases. This is because the reduction in turbulence production by the mean shear and the consequent stabilizing effect of compressibility in turbulent shear flows appears to be a strong function of the gradient Mach number.[26] A possible reason for the difference between the extent of compressibility effects in the high speed mixing layer and boundary layer is the large difference in values of the gradient Mach number.[26]

Urban et al used Particle Image Velocimetry (PIV) to measure the instantaneous two-dimensional velocity field in turbulent, planar mixing layers at varying levels of compressibility. The structure of the

instantaneous velocity and vorticity fields are seen to display similar variation with compressibility as the scalar field with the spatial intermittency of the velocity field tied to the interfaces of the large-scale structures. The compressible case displays multiple thin sheets of vorticity within the layer rather than diffuse regions spanning its transverse extent. The PIV data may also be used in large ensemble fashion to provide turbulence statistics previously obtained using a point wise measurement technique. The effect of sub-boundary layer mixing enhancement techniques on the velocity field is observed by means of plan-view measurements. The convective Mach numbers tested were 0.79, 0.63, and 0.24.[27]

PIV was used to obtain side view and plan view planar velocity fields of turbulent shear layers over a range of compressibility. The resulting well resolved high-yield data sets lend themselves to both structural and statistical interpretation. The instantaneous velocity fields are seen to display structure similar to that observed in instantaneous scalar visualizations.[27]

Details of the vortical structure, particularly in the compressible case, are revealed through direct velocity measurement. At high convective Mach numbers thin sheets of vorticity appear within the layer thickness and appear to be isolated from one another. This situation was predicted by linearized stability analysis and is possibly related to the shear layer growth rate suppression. Steep velocity gradients exist at the local sonic speed in the lab frame suggesting a sensitivity to wall disturbances. This sensitivity is confirmed by the success of small scale perturbations as mixing enhancements. Transverse turbulence intensity and Reynolds stress also decrease due to compressibility.[27]

Elliot and Samimy studied high Reynolds number compressible free shear layers experimentally to explore the effects of compressibility on the turbulence field. In the developing region of shear layers, the developments of mean flow and turbulence fluctuation profiles have similar trends as those seen in incompressible shear layers. Not only is the growth rate decreasing as the convective Mach number increases but the turbulence quantities are also decreasing. There is also a nearly universal dependence of the normalized maximum amplification rate of disturbances on the convective Mach number.[28]

In this study three cases were tested. In case 1, the convective Mach number is 0.51 and the static pressures of the two streams are matched. In case 2, the convective Mach number is 0.64 and the supersonic stream was under-expanded. In case 3, the convective Mach number is 0.86, once again the static pressures are matched, but the velocity of the second stream is high, M_2=0.45.[28]

A two component Laser Doppler Velocimetery system was used in these experiments. Both sides of the shear layer were seeded with atomized silicone oil. Two Schlieren systems were used for flow visualization, one was a normal light based system and one was a laser based system.[28]

The mixing layer thickness grows linearly with streamwise distance. The shape of the mean velocity profile is independent of downstream distance when scaled by layer thickness. The profiles of all turbulence quantities are independent of streamwise location when scaled by mixing layer thickness. The peak values of the turbulence stresses should be independent of streamwise location. The lateral extent of the streamwise turbulence decreases with increasing convective Mach number. This means that less of the thickness of the shear layer is turbulent as the convective Mach number increases. The level and lateral extent of both small and large scale fluctuations decreased with increasing convective Mach number on the high speed side of the flow. The maximum levels of the turbulence fluctuations decreased almost linearly with increasing convective Mach number. The level and lateral extent of the skewness and flatness were also reduced with increased convective Mach numbers. This is believed to be a reason for the lower entrainment and growth rates for compressible shear layers.[28]

Development of the mean flow and turbulence fluctuation profiles were found to have similar trends as seen in incompressible shear layers. It was found that the shape of the velocity profile is not sensitive to Mach number and is nearly the same for supersonic layers with moderate convective Mach numbers and in low speed flows with variable density. In such conditions the only compressibility effect is on the rate of spread. It was also found that the turbulent friction is a function of Mach number and a function of the ratios between velocity and density. The level of turbulence and turbulent friction depends on compressibility. The shapes of the velocity profiles in subsonic and supersonic mixing layers look very much the same.[29]

In self-similar supersonic mixing layers with density gradients the conditions for self-preservation are that all quantities depend on a single local scale of space for both velocity and temperature. Several length scales for temperature and velocity prevent self-preservation. Flows that assumed isobaric-density and temperature in-homogeneities are directly related to each other. For flows to have the same length scales they need to have a unity Prandtl number.

Two sorts of flows were considered: flows where density distribution is known and will be specified as an input to compute velocity profiles and supersonic flows for which velocity and temperature distribution follow Crocco's law. The level of friction in the shear layer can be significantly altered by density gradients. The efficiency of mixing can also be enhanced by increasing the turbulent intensities.[29]

The relationship between velocity and the inverse of density will produce very asymmetric distributions of density and this asymmetry will be enhanced at high Mach numbers. For moderate convective subsonic Mach numbers, the velocity profile depends only weakly on the convective Mach

number. Compressibility is felt by self-similar mixing layers through the spreading rate but not by the shape of the velocity profiles.[29]

It was found that the level and lateral extent of the turbulence fluctuations were reduced as the compressibility, by means of the convective Mach number, is increased. The reductions in both level and the lateral extent of turbulence fluctuations with increasing convective Mach number, which was reported earlier for the convective Mach number range of 0.51 to 0.64, was much higher at a convective Mach number of 0.86. The higher order moments of turbulence fluctuations, such as skewness and flatness, were reported which show that the intermittency, due to the excursion of large scale structures into the free streams at the edge of the shear layers, was significantly reduced due to increasing Mach number.[28]

Samimy and Elliot also performed tests where a high Reynolds number, two-dimensional, constant pressure, compressible shear layer was formed. Convective Mach numbers of 0.51 and 0.64 were investigated using two component coincident Laser Doppler Velocimetry for the measurements.[30]

For the shear layer with the lower convective Mach number the non-dimensional shear layer and vorticity thickness growth rates were over 20% higher and the momentum thickness growth rate was over 30% higher than the shear layer with the higher convective Mach number. The results indicate that both small scale and large scale mixing are reduced with increasing convective Mach number. Beyond 120 mm downstream of the splitter plate all the shear layer mixing rate measurements show linear growth of the shear layer. The momentum thickness growth rate is closely related to shear layer entrainment rate. The mean velocity profiles for shear layer growth rates were found to collapse to a single curve. As the convective Mach number is increased, levels of streamwise and lateral turbulence fluctuations, shear stress, and transport of kinetic energy in the lateral direction are decreased but the correlation coefficient level does not change. The level of both large and small scale turbulence fluctuations is also reduced as the convective Mach number is increased. The reduction of shear layer growth rate with increased convective Mach number is due to a reduction in both small and large scale mixing.[30]

Zhuang et al. studied the linear spatial instability of inviscid, compressible laminar mixing of two parallel streams, comprised of the same gas, with respect to two-dimensional wave disturbances. The effects of velocity ratio, temperature ratio, and the temperature profile across the shear layer have been examined. The normalized maximum amplification rate, which depends on the convective Mach number, decreases significantly with increasing convective Mach number in the subsonic region. The flow is unstable with respect to supersonic disturbances, although the amplification rate is smaller than

that for subsonic disturbances. Increasing the angle between the disturbance wave number vector and the principle flow direction tended to increase the instability.[31]

A turbulent compressible mixing layer with a relative Mach number of 1.59 has been investigated experimentally by Gruber et al. using a two component laser Doppler Velocimetry system. Two sets of profiles were obtained at each streamwise measurement location to compile the streamwise, transverse, and spanwise turbulence statistics. Results from the fully developed region of the mixing layer showed similar peak values of streamwise and spanwise turbulence intensities along with reduced peak values of transverse turbulence intensity, normalized primary Reynolds shear stress, and normalized turbulent kinetic energy in comparison to the respective quantities from incompressible shear layers. The Reynolds normal stress ratio was found to decrease with increasing relative Mach number. It was concluded that the spanwise component of the mixing layer turbulence becomes more important as compressibility is increased.[32]

Various turbulence profiles demonstrated a reduction of lateral extent on the high speed side of the mixing layer as compared to profiles in incompressible mixing layers. Significant reduction of the transverse turbulence intensity and normalized primary Reynolds shear stress with increasing compressibility were observed. Increases in compressibility produce a large scale turbulence structure that is reoriented in a direction more oblique to the streamwise flow directions. A less organized more oblique structure develops with increasing compressibility. Three-dimensional instabilities are more dominant at higher levels of compressibility.[32]

The relative Mach number of 1.59 falls within the region of moderate compressibility as defined by Papamoschou and Roshko. The peak value of streamwise turbulence intensity within the mixing layer was observed to be about 0.17. Streamwise turbulence intensity remains relatively constant with increasing relative Mach number. The streamwise turbulence intensity profile also seems to suggest a reduction of lateral extent on the high speed side of the mixing layer. This reduction is demonstrated by the tendency of the streamwise turbulence intensity within the mixing layer to decay very quickly to the freestream value on the high speed side, whereas the same decay occurs more gradually on the low speed side. Transverse turbulence intensity also suggests a reduction of lateral extent on the high speed side in the same manner as the streamwise component. The transverse turbulence intensity had a peak value of 0.072. Substantial reduction is observed for transverse turbulence intensity as compressibility increases.[32]

A major effect of compressibility on the mixing layer turbulence is the suppression of the transverse velocity fluctuation resulting in an increasingly anisotropic structure in terms of the streamwise and

transverse components. The spanwise turbulence intensity profile is more symmetrical than the other two components. This is due to a smaller reduction in lateral extent on the high speed side of the mixing layer. The spanwise turbulence intensity has a peak value of about 0.13, which is comparable to the value achieved in incompressible mixing layers. There was no significant reduction in spanwise turbulence intensity with increased compressibility.[32]

The turbulence structure of the mixing layer becomes more dependent on the spanwise turbulence level as compressibility increases due to the suppression of the transverse component. The effect of compressibility on the mixing layer turbulence structure is a tendency toward more three-dimensional behavior, such as obliquely oriented large scale structures with enhanced spanwise, compared to transverse, velocity fluctuations. The peak normalized turbulent kinetic energy decreases with increasing compressibility which is a direct result of the transverse velocity fluctuation suppression.[32]

Goebel and Dutton conducted an experimental investigation of compressible turbulent mixing layers using pressure measurements, Schlieren photographs, and velocity measurements with a two component Laser Doppler Velocimetry system. TiO_2 was used as the seed particle because it can withstand the high temperatures of the heated conditions. Seven cases were examined with relative Mach numbers ranging from 0.4 to 1.97. The spatial development and similarity of the mixing layers were examined as well as the entrainment process and the effects of particle dynamics.[33]

In the fully developed regions of the mixing layers it was found that transverse turbulence intensities and normalized kinematic Reynolds stresses decreased with increasing relative Mach number. Conversely, the streamwise turbulence intensities and kinematic Reynolds stress correlation coefficients remained constant.[33]

The normalized growth rate of a compressible shear layer decreases proportional to the normalized kinematic Reynolds stress and the transverse turbulence intensity similarly decreases while the streamwise turbulence intensity remains nearly constant with increasing relative Mach number. The reduction of transverse turbulence intensity is due to the suppression of the pressure-transverse velocity correlation, which redistributes turbulent kinetic energy from the streamwise to the transverse direction. This may be caused by the decrease in the domain within which pressure waves can propagate due to the increasing relative Mach number of the flow.[33]

From the Schlieren photographs, organized, large scale structures were not observed under the conditions studied here. For the mixing layers to be fully developed the local Reynolds number needed to be approximately 10^5. Higher levels of free stream turbulence and shock waves inhibited and disrupted the mixing layer development process.[33]

Normalized mixing layer growth rates decreased with increasing relative Mach number. The relative Mach number seems to be an adequate parameter for correlating the effects of compressibility. Transverse turbulence intensity and normalized kinematic Reynolds stresses both decreased like normalized growth rates with increasing relative Mach number. The mixing lengths also decreased with increasing relative Mach number. The kinematic Reynolds stress correlation coefficients were also found to remain approximately constant with relative Mach number, and the profiles were fairly flat across the mixing layers. Fully developed streamwise mean velocity profiles were well approximated by an error function profile even for the more compressible cases.[33]

By using the observed velocity profile shape and the Crocco-Busemann temperature profile an analysis of mixing layer mass entrainment fractions was performed. From the single stream seeding experiments it was found that fluid within the mixing layer had the same mean streamwise velocity regardless from which freestream the fluid originated. It was also shown that particle concentration biasing did not affect the velocity measurements. It was found that the seed particles which were used could adequately follow the turbulent velocity fluctuations, therefore, particle dynamics effects were not a problem [33]

Papamoschou studied the physical interpretation of the stabilizing effect of compressibility on shear layers. Compressibility hinders communication between regions in a shear flow by distorting the rays originating from an acoustic source in a shear layer. This distortion results in sound-intensity distributions quite different from the incompressible case. The intensity diminishes rapidly as the Mach number at the source increases. As the Mach number increases, regions of very little or no sound-intensity are evident not far from the source. Poor communication among regions of the flow field causes the inherent stability of compressible shear flows.[11]

Physically, compressibility suppresses the shear layer growth and instability. The vortex sheet, which is formed due to Kelvin Helmholtz instability, becomes stable when the relative Mach number exceeds a critical value.[11] The shear layer growth rate decreases with increasing Mach number partially due to the decrease in the maximum growth rates of the large-scale Kelvin-Helmholtz instabilities.[34] Amplification rates of the linearized, compressible, finite-thickness, shear layer decrease sharply with increasing Mach number. As previously stated, the shear layer growth rate decreases as Mach number increases until the growth rate is only 20% of incompressible shear layer growth rate.[11]

Upstream and crossflow communication is essential for instabilities at supersonic and hypersonic speeds. If a fluid particle, A, in the shear flow moves at a Mach number greater than 1 with respect to another fluid particle, B, particle B does not “know” of particle A until it is enveloped in the Mach cone

of Particle A. This is similar to how an observer on the ground cannot hear the approach of a supersonic airplane.[11]

At high Mach numbers the acoustic wave length, λ, of the dominant instability is of a similar size or smaller than the characteristic thickness of the shear layer, δ. The following geometric acoustic analysis using ray theory is accurate for λ< 0.16 and order of magnitude accurate for when the wave length, λ, is the same order of magnitude as the thickness of the shear layer, δ. For the two-dimensional theoretical considerations it is assumed that the shear layer is parallel, with velocity dependent only on the transverse coordinate, y. If the shear layer is observed from the frame of reference of the fluid particle, a velocity distribution U(y) on the y=0 plane is observed with a source on the y=y1 plane where the velocity is U_1. The least travel time principle was used to find the path of the ray emanating from the source. The signal velocity along the ray, V, consists of the geometric sum of the local velocity vector and the local speed of sound vector.[11] Equations 2.6 and 2.7 give the velocities in the x and y directions respectively.

$$V_x = U(y) - a(y)\sin\theta = \frac{dx}{dt} \tag{2.6}$$

$$V_y = -a(y)\cos\theta = \frac{dy}{dt} \tag{2.7}$$

Where a(y) is the speed of sound, and θ is the local wave front normal angle with respect to the vertical. The above equations were solved to find the travel time and the location at which the ray crosses the x-axis. From that, the angle that minimized the time for the ray to pass through any given point can be found from Equation 2.8:

$$\sin\theta = \frac{a}{U+\sigma} \tag{2.8}$$

Where $\frac{1}{\sigma}$ is a constant Lagrange multiplier.[11]

As the Mach number increases, the rays become more and more distorted. Thus, an acoustic source disturbs fewer and fewer fluid particles as the Mach number at the source location increases. Thus the Mach number inhibits acoustic interactions in the shear layer.[11]

2.4.4 Structure Angle

Petullo and Dolling performed an experimental investigation to study the orientation of large-scale structures in a compressible, turbulent shear layer bounded by Mach 5 and Mach 3 air streams with a convective Mach number of 0.28. The shear layer structure was investigated using dual normal wire

hotwire probes at five vertical positions at 17.8 cm (848 initial momentum thicknesses) downstream and 48.3 cm (2300 thicknesses) downstream of the origin. The shear layer structure was found to be more organized than that of the boundary layer. The shear layer becomes increasingly organized with distance downstream and the highest degree of organization is evident at the shear layer center. Although large scale structures are clearly discernible and appear to have a preferred angle, they do not appear to be as organized as in the incompressible case.[35]

Compressibility plays a role in the degree of organization of the turbulent structure. Increasing convective Mach number (increasing compressibility) generates more three-dimensional, less organized structures. The structures tend to be more organized further downstream from the splitter plate at a convective Mach number of 0.28. According to Hussain, a coherent structure is a connected turbulent fluid mass with instantaneously phase-correlated vorticity over its spatial extent.[35]

Petullo and Dolling's study attempted to detect structures through mass flux fluctuation measurements and to examine their degree of organization through quantitative assessment of histograms of structure inclination angle. At 48.3 cm downstream of the splitter plate, the average structure angle is oriented at a 46˚, at 17.8 cm the average structure angle is 39˚. An increasing fraction of the structures fall within a narrow range of angles with increasing distance downstream. The range of angles is still quite broad, however.[35]

Bowersocks and Schetz used overheated cross-wire probes, parallel hot wire probes, shadowgraph image processing, and high frequency response Pitot probes to survey a two-dimensional, adiabatic, supersonic, free mixing layer consisting of Mach 1.8 air injected tangentially into a Mach 4 freestream. (See Figure 8) Turbulence intensity profiles in three dimensions were acquired and the axial component was found to be about 25% larger than the transverse and spanwise components. Velocity fluctuation data indicated that the axial component was negative, while both the transverse and spanwise components were positive.[36]

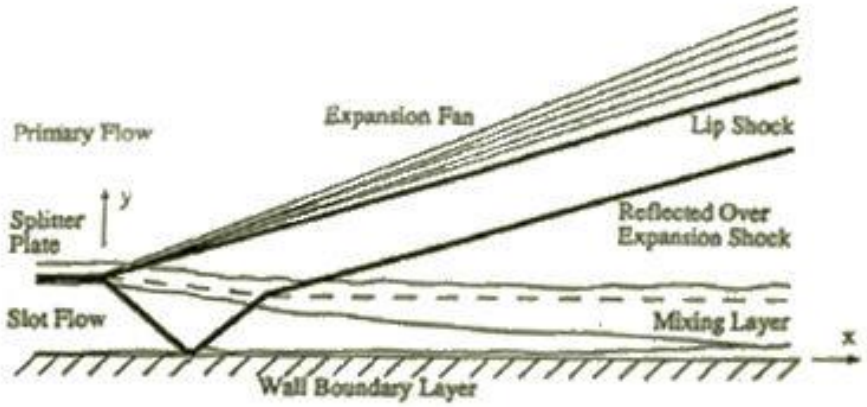

Figure 8: Experimental flowfield[36]

Turbulent flow structure angles and length scales were measured in the fully developed region of the flow. The structure angles were found to be consistent with previous compressible boundary layer results. However, the magnitude of the structures here was found to decrease across the mixing layer. The Mach number fluctuation levels were also measured and the peak Mach number fluctuation level in this flow was about 10%.[36]

In a study of the structure of a high speed, high Reynolds number mixing layer, the effects of compressibility have been found to dominate the levels of turbulence. Tangential injection of air at a Mach number of 1.8, and a Reynolds number of $7*10^6$ into air at a freestream Mach number of 4 with a Reynolds number of $67*10^6$, where the convective Mach number was 0.39 was studied.[36]

The results of this study described the temporal and spatial structure of this highly compressible turbulent mixing layer. The axial mass flux turbulence intensity levels were found to be about 25% higher than those for the transverse and spanwise components, which were found to be nearly equal. The large scale turbulence, which occurs at a lower frequency, contributed most of the energy. The large sale structure angles and integral length scales were found to be dependent on the spatial location within the shear layer indicating that the large scale turbulence was influenced by the mean flow field. The micro-length scales however were found to be independent of the mean flow field, reinforcing the notion that the smaller scales of turbulence are nominally independent of the mean flow. The measured Mach number turbulence intensity peaked at a level of about 10%.[36]

An experimental study was performed by Shau and Dolling to determine if two-point fluctuating Pitot pressure measurements can be used to detect and quantify the large scale structure in a two-dimensional, high Reynolds number, compressible, turbulent shear layer bounded by Mach 5 and Mach

3 air streams. Three cases were tested: the undisturbed shear layer and two cases where the initial conditions at the shear layer origin were changed by planar shockwaves impinging on the boundary layer about 6 and 11 boundary layer thicknesses upstream of the shear layer origin (Figure 9). The fluctuating Pitot pressures were recorded using probes with high frequency response Kulite transducers projecting from their tips.[37]

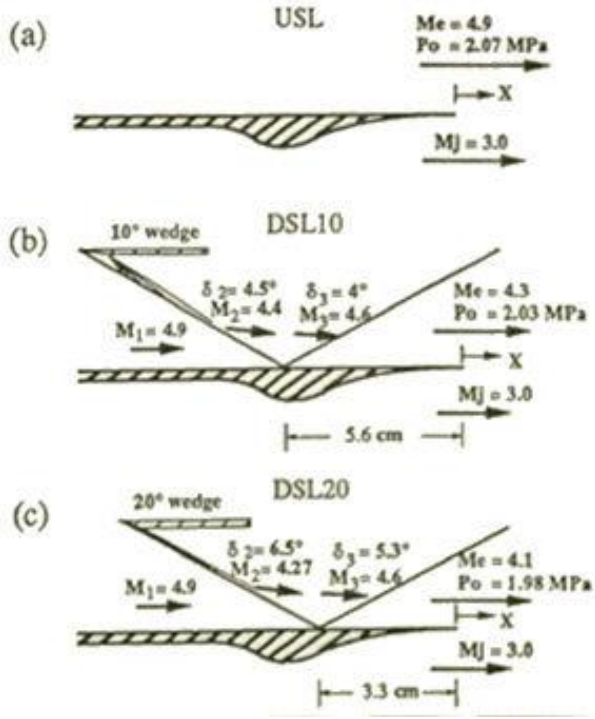

Figure 9: The Undisturbed Shear Layer (a), the disturbed shear layer with a 10° wedge shock (b), and The disturbed shear layer with a 20° wedge shock [37]

In the disturbed cases the rms of the Pitot pressure fluctuations rapidly returned to undisturbed values downstream of the shear layer origin. The same can be said for the details of the large scale structure development, although there are certainly measureable differences between the disturbed and undisturbed flows these differences are not large. There is evidence that large scale structures exist and they span the width of the shear layer. Because of the way the layer is generated the flow has a wake like character which affects the large-scale structure orientation. The width of the large scale structure measured streamwise from front to back is estimated from the cross correlations to be about 0.6 to 0.8 shear layer thicknesses. Independent estimates from the VITA technique support this value and also suggest that the width is essentially constant across the shear layer. The spacing of the large scale structures, defined as the streamwise distance from the trailing edge of one to the leading edge of

the other, is estimated to be about 1.8 thicknesses for undisturbed flow and slightly less, about 1.5 thicknesses, for the disturbed flow.[37]

Cross correlations in the upper part of the boundary layer at the shear layer origin have shown that the large structures are inclined at about 30°. Cross correlations in the upper part of the shear layer for USL show angles of 30° to 35°. Thus there is little evidence of any change in the structure orientation as the shear layer evolves. For the disturbed shear layer the structure angles in the upper part of the shear layer vary from 30° to 40° and appear to be 10% to 20% higher than in the disturbed boundary layer at the origin.[37] Because of the wake like character of the flow and the corresponding change in sign of the shear stress, the structure angle increases rapidly in the lower part of the shear layer. The exact structure orientation is not clear, but it appears to be normal to the flow or even inclined in the upstream direction as seen from below.[37]

Although there is clear evidence of large scale structures which span the shear layer, they are not highly organized. It is possible that the measuring station which is about 20 initial shear layer thicknesses from the origin is in the transition region in which a highly organized structure is only just beginning to evolve.[37]

2.4.5 Shear Layer Asymmetry

For shear layers with a convective Mach number between 0.64 and 0.9, flow images confirm the phenomenon of structure asymmetry at high compressibility. Structure asymmetry is defined as occurring in a two freestream shear layer when a vortical structure is dragged by one of the freestreams rather than travelling with a velocity closer to the average freestream velocity.[19] This occurs when the densities of the two gases are not very different.[21] The velocity at which the vortical structure travels is called the convective velocity, U_c. If both the freestreams are supersonic then the convective velocity will approach the low speed stream velocity. If, however, one of the freestreams is subsonic, then the convective velocity will approach the high speed stream velocity. This asymmetrical behavior may have an impact on the entrainment, growth rate, and mixing rate of the shear layer.[19] The entropy causing shocklets are also stronger if the eddies propagate asymmetrically.[21]

The evolution of large turbulent eddies in supersonic shear layers were studied by Papamoschou and Bunyajitradulya via a two-laser single detector planar laser-induced fluorescence technique, with gaseous acetone as the tracer molecule. The method enables measurement of the convective velocities and provides detailed visualization of the evolution of the flow structure.[38] The Method was applied to

supersonic shear layers with average convective Mach numbers ranging from 0.23 to 0.97. The flow images confirm the phenomenon of structure asymmetry at high compressibility where one convective Mach number is large (sonic or supersonic), while the other is subsonic. This phenomenon may have a profound effect on supersonic mixing and combustion.[38]

Schlieren photography of the evolution of large shear layer eddies showed nearly frozen patterns convecting with a velocity very different from the mean flow velocity. In shear layers where both streams were supersonic the eddies traveled with a velocity close to the slower freestream velocity, while in shear layers where one stream was supersonic while the other was subsonic they traveled with a velocity close to the velocity of the faster freestream. Investigations using Mie scattering and pressure traces also observed this behavior.[38]

The phenomenon of asymmetric eddy propagation may affect fluid entrainment into the layer and has a profound impact on supersonic jet noise. In shear layers surrounding supersonic jets the eddies travel at velocities very close to the jet velocity. This generates Mach waves earlier than conventional theories had predicted. These Mach waves are a dominant source of supersonic jet noise.[38]

At an average convective Mach number of 0.57 there is no spanwise coherence and the structure looks fairly chaotic. The convective velocity vector, however, is well aligned with the flow direction. Therefore, the propagation of those eddies is two-dimensional. There was no evidence of eddy paring or merging in any of the tests.[38]

In another study, Papamoschou used a two stream supersonic wind tunnel to investigate large scale structures in the turbulent compressible shear layer. Double exposure Schlieren photography was used to study the flow field. The system used was a two spark variant where two slightly off axis beams are produced by two different spark gaps. The focal points of the two beams coincide at a single knife edge and two distinct images appear on the film. The exposure time is 20 ns and the time between the two sparks is controllable. When a large structure moves a certain distance the convective velocity and convective Mach number can be calculated within ±5% error.[39]

The two convective Mach numbers corresponding to each side of the shear layer are very different. One is sonic or supersonic while the other is low subsonic. This contradicted the, at the time, current isentropic model of the structure of the shear layer which predicted the convective Mach numbers to be equal or very nearly equal. The addition of shock wave effects to the isentropic model allows for the asymmetric trends seen in the experiments.[39] The convective Mach numbers for the high and low speed streams are given below in Equations 2.9 and 2.10:

$$M_{c1} = \frac{U_1 - U_c}{a_1} \quad (2.9)$$

$$M_{c2} = \frac{U_c - U_2}{a_2} \quad (2.10)$$

The relation between the higher convective Mach number, M_{c1}, and the lower convective Mach number, M_{c2}, was obtained by requiring that the total pressures of the two streams in the convective frame be equal. This idea stems from an argument, used mostly in subsonic flows, that there exists a stagnation point between two structures that must be stable. Thus the pressures at that point must be in balance. It was assumed by Papamoschou and Roshko that the flow comes to rest at the stagnation point isentropically. This means that there were no losses due to shockwaves even for supersonic convective Mach numbers.[39]

For streams with equal ratios of specific heat (i.e. $\gamma_1 = \gamma_2$) the two convective Mach numbers can be related according to Equations 2.11 and 2.12:

$$M_{c1} = M_{c2} = \frac{\Delta U}{a_1 + a_2} \quad (2.11)$$

Where:

$$\Delta U = U_1 - U_2 \quad (2.12)$$

For shear layers where the specific heat ratios of the two streams are not equal, $\gamma_1 \neq \gamma_2$, then M_{c1} is assumed to be approximately equal to M_{c2}.[39]

Papamoschou and Roshko chose the convective Mach number in the high speed stream as the compressibility effect parameter against which the shear layer growth rate was correlated. All the data for a wide range of tests collapsed onto one curve, so using the convective Mach number as a measure of shear flow compressibility is highly applicable. But the question still remains whether or not the convective Mach numbers on either side of the shear layer are still equal when shock waves form on the structures. At high compressibility, the convective velocity closely approaches one stream velocity or the other depending on the test case. The side of the shear layer with the higher convective Mach number is not the same for each case. No consistency in which side had the higher convective Mach number was found based solely on density ratio or specific heat ratio. Consistency was found based only on the free stream Mach number. In cases where both streams are supersonic, the convective Mach number on the side of the faster stream is always the highest. In cases where one stream is supersonic and the other stream is subsonic the convective Mach number on the slower stream side is always the highest.[39]

This could be due to the flow field change that occurs when the low speed stream goes from subsonic to supersonic. In the convective frame, fluid engulfed into the mixing zone has to come to rest at some point between the two structures and the pressures there must balance for that point to be stable. The flow is turbulent so this point is not necessarily stationary, although from the photos the effect of turbulence seems small. The existing model assumes the fluid comes to rest isentropically, but for the compressible case the dissipative effects of shocks must be added. A shock wave on a structure could lead to a considerable total pressure drop along the streamline leading to the stagnation point. If shock waves appear symmetrically on the structure the losses would be similar and assuming the convective Mach numbers on either side of the stream to be equal would still be a good approximation.[39]

In asymmetric situations, if in the convective frame of reference, the two free streams are assumed to have equal static pressures. If the convective Mach number on the side of the faster stream is supersonic, like with flow around a cylinder or a thick airfoil, the Mach number near the structure is higher than the free stream Mach number. The flow along the top edge of the structure turns and accelerates through a Prandtl Meyer expansion fan. As a result, the Mach number ahead of the stagnation point is substantially higher than the fast side convective Mach number. The flow comes to rest by means of a normal shock located just upstream of the stagnation point. A shock at that Mach number is strong enough that the total pressure downstream of the shock is reduced to the level of the static pressure in the freestreams.[39]

The freestream Mach number of the lower speed side convective Mach number, M_{c2}, must be such that the stagnation point is pressure balanced. This creates two potential scenarios. The first being a symmetric case where similar shocks form on either side of the structure and the convective Mach numbers on both sides are equal. The second case is the asymmetric case where the convective Mach number on the slower stream side of the structure is subsonic with the resulting free stream total pressure close to the free stream static pressure. No shocks form on the slow speed side and total pressure remains fairly constant until it comes to rest.[39]

Why does flow always prefer the asymmetric case? For M_c^* to be critical it should fall within the range of $0.5<M_c^*<1.0$. For asymmetry to occur, M_c^* must be less than the convective Mach number on one side of the shear layer or the other (i.e. $M_{c1}>Mc^*$ or $M_{c2}>Mc^*$).[39] This means that Equation 2.13 must be satisfied:

$$M_c^* < \frac{\Delta U}{a_1 + a_2} \quad (2.13)$$

No matter what the convective velocity is, at least one of the convective Mach numbers will exceed M_c^*.[39] If Equation 2.14 is satisfied:

$$M_c^* > \frac{\Delta U}{a_1 + a_2} \quad (2.14)$$

Asymmetric solutions are still possible, but flow has the choice of a subsonic structure where both convective Mach numbers are less than M_c^* and the isentropic model applies. If the convective Mach number is greater than about 0.6 the shear layer will be asymmetrical. If the convective Mach number is less than about 0.6 the shear layer will be symmetrical. The physics of mixing depend on the individual convective Mach numbers, especially the higher convective Mach number. The lower convective Mach number is always low subsonic, so its influence is weaker.[39]

Hall et al. studied two-dimensional compressible turbulent shear layers. Helium, nitrogen, and argon were used in various combinations to produce shear layers with isentropically computed convective Mach numbers that range from 0 to 1. Schlieren photos are generally devoid of the two-dimensional large scale structures seen in incompressible flows. Traveling shock and expansion waves are observed in the high compressibility flows. Evidently these features are created by turbulent structures convecting at supersonic velocities with respect to one of the freestreams. The shocks and expansion fans were seen only in the low speed fluid suggesting that the apparent convective velocities of the structures are much higher than the velocities predicted by the usual isentropic pressure matching arguments.[40]

The shear layer growth rate is relatively insensitive to the effects of incident shock and expansion waves on the shear layer. The convective velocity measurements of Papamoschou suggest that grossly unequal total pressure losses must occur on the two sides of the shear layer, if the requirement of a pressure balance at the convective frame stagnation points is to be observed, otherwise the convective velocities of the two streams would be equal. This could be caused by shock wave generated by turbulent structures on only one side of the shear layer in these flows. These shocks could provide a mechanism for the unequal total pressure losses (Figure 10).[40]

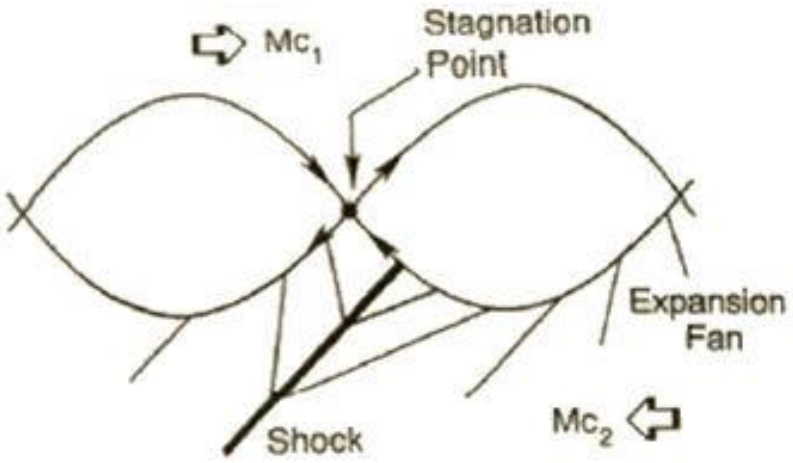

Figure 10: Model for shear layer recompression shock[40]

The wave angles were used to estimate the convective Mach number of the structures. Large scale structures were not clearly visible in the Schlieren images. It could be that the large scale structure is obscured by the signal from many small scale high gradient turbulent interfaces superimposed on it, or else the large scale structure is highly distorted by spanwise three-dimensionality.[40] The convective Mach number of the slower stream can be computed by Equation 2.15 where μ is the Mach wave angle.

$$M_{c2} = \frac{1}{\sin \mu} \qquad (2.15)$$

The convective Mach numbers vary more widely from the theoretical values for highly compressible flows. The recompression shocks could be several weaker oblique shocks rather than one strong normal shock. During testing, traveling shocks and expansion waves were seen in the low speed fluid. The waves were created by unseen shear layer structures convecting at supersonic Mach numbers. The measured convective velocities of these structures are considerably higher than those predicted by isentropic pressure recovery models at the stagnation point in the convective frame. To the extent that large scale structure appears, it is not as conspicuous as in incompressible shear layers. Generally no large scale structure is discernible in the early part of the flow in the present data but there is some evidence of large scale structure further downstream.[40] For convective Mach numbers on the fast stream side, M_{c1}, greater than 0.3, the measured shear layer growth rates agree with previous results by other experimenters. It was also observed that the shear layer growth rate was not affected significantly by the impact of strong planar waves created by a pressure mismatch at the splitter tip.

Tang et al. imposed small amplitude velocity disturbances at selected frequencies over an otherwise steady flow at the juncture of two streams to promote mixing. It was found that disturbances are

selectively amplified at certain frequencies while disturbances at other frequencies are rapidly damped out. In studies where the relative Mach number of the disturbances relative to one of the streams is high, shocklets were found to form on one or both sides of the shear layers. In such a situation the relative Mach numbers of the eddies were different in coordinate systems attached to the upper and lower streams.[41] The relative Mach number is defined by Equation 2.16: [33]

$$M_r = \frac{2(U_1 - U_2)}{a_1 + a_2} \qquad \textbf{(2.16)}$$

This study was performed at very low convective Mach numbers (convective Mach numbers of less than 0.2) and at very high convective Mach numbers (convective Mach numbers of greater than 1). The response of supersonic shear layers at low convective Mach numbers to arbitrary user specified acoustic disturbances over a broad range of frequencies was studied. Sinusoidally varying velocity disturbances at a number of frequencies are introduced at the initial laminar mixing region of the shear layer. These disturbances grow with time as they are convected downstream and eventually lead to well organized vortical structures.[41] At high convective Mach numbers vorticity and pressure contour plots at a number of time levels were used to track the velocity of the dominant eddies and compute the relative Mach number of these eddies in a coordinate system attached to either the faster stream or the slower stream. If supercritical Mach numbers arise relative to either stream, then the resultant pressure field is examined for the occurrence of shock waves, expansion waves, and their effects on the shear layer growth.[41]

In the case of shear layers at subsonic and supersonic convective Mach numbers, the imposition of acoustic disturbances over a large range of frequencies lead to the transfer of this energy from the high frequencies to the low frequencies. As the flow progressed from the upstream boundary to the downstream boundary, the energy content at the lowermost frequencies rapidly reached asymptotic values. Following this, eddies in the shear layer were convected downstream with no further alteration in their structure.[41]

In the case of shear layers at a supersonic convective Mach number, situations were found where the convective Mach number relative to the faster stream is low. This leads to a situation where shocklets arose only on the lower side of the shear layer. Conditions were also found where the convective Mach number relative to both the streams is high leading to shocklets on either side.[41]

Ragab and Sheen investigated the nonlinear development of two-dimensional supersonic instability waves in a mixing layer by solving the full unsteady Navier-Stokes equations. Both confined and unconfined shear layers were simulated. The development of rollup structures is enhanced by confining

the layer between parallel walls. Rollup structures form on the subsonic side of the shear layer, oblique shock waves form on the supersonic side.[42]

In the unconfined case the shockwaves form in the farfield as a result of the coalescence of compression waves initiated at the shear layer. In the confined shear layer case, the shockwaves appear as reflections of compression waves off the side wall. In the case of supersonic relative Mach numbers on both side of the layer no vortical roll up is observed, only a staggered pattern of oblique shock waves was found. The unconfined temporal simulations predict vortical formations on the side of the layer where the convective Mach number is subsonic. Oblique shock waves formed on the side where the convective Mach number is supersonic as a result of the coalescence of compression waves generated on the growing wave.[42]

Over the eight wave lengths simulated, the unconfined spatial case shows weak deviation from linearity. Convergence of the compression fans is evident in this case but shock waves have not formed yet in the simulated domain. Two modes of the confined case were simulated. The first mode is the most amplified. The convective Mach number is supersonic on the slow stream side and subsonic on the fast stream side of the shear layer. Vortical structures form on the fast stream side while strong oblique shock waves form on the slow stream side. A study of the velocity vector field, in a frame of reference moving with the wave, shows that the shock waves are formed by reflection of compression waves generated on the concave bottom side of the shear layer which turns the relative flow towards the confining wall.[42]

A comparison between the unconfined case and the confined case shows that confining the layer enhances the development of the vortical structures which have not formed yet in the unconfined case over comparable length. The vorticity contours of the regular mode in which the convective Mach numbers are supersonic on both sides of the layer show no vortical formations on either side of the layer only a staggered pattern of oblique shock waves is possible. The layer growth is dominated by laminar diffusion.[42]

If the upper stream of the shear layer transitions from a convective Mach number of 1 to a supersonic convective Mach number and the lower half transitions from a convective Mach number of 1 to a subsonic convective Mach number, the speed change will cause the layer to develop asymmetrically. Eddy shocklets will form only on the top half of the layer and a Kelvin Helmholtz like instability will develop in the bottom half of the layer. The flow is then locally accelerated and a local supersonic region occurs.[20] Pure fluid engulfment occurs mostly in the bottom half of the layer whereas the top layer, to some extent, appears to form a wall mode with a characteristic saw tooth pattern. The

saw tooth pattern elongates the contact surface somewhat but it is not a very efficient mixing mechanism. This type of mixed instability only occurs near Mach 2.0.[20]

2.4.6 Shear layer Three-Dimensionality effects

For convective Mach numbers between 0 and 0.6, two-dimensional instabilities are amplified most rapidly resulting in a shear layer dominated by spanwise two-dimensional structures. For convective Mach numbers between 0.6 and 1.0, oblique three-dimensional instability modes become dominant while two-dimensional instabilities are still significantly amplified resulting in a shear layer which is composed of both two-dimensional and three-dimensional structures. For convective Mach numbers greater than 1.0, two-dimensional instabilities are amplified by a factor five times less than the amplification factor for the three-dimensional modes resulting in a flow dominated by large scale three-dimensional structures with little or no organized two-dimensional structures. At high convective Mach numbers no coherent spanwise structures are readily apparent, but lots of fine scale structures are visible.[43]

Risha performed an extensive computational study of three-dimensional air to air supersonic shear layers. Convective Mach numbers of 0.20, 0.50, 0.75, 1.00, 1.15, 1.25, 1.5, and 1.56 were resolved using a full, time dependent, three-dimensional Navier Stokes code called SPARK3D. The shear layer growth rates were determined using the mean streamwise velocity criteria to define the shear layer boundaries. The boundaries for the mixing layer growth rate were determined using the O_2 mass fraction.[44]

The three-dimensional shear layer and the mixing layer growth rates dramatically increase in the convective Mach number range from 0.75 to 1.25. In this range three-dimensional effects on growth rates, as determined by the large scale oblique structures, are much greater than the compressibility effects that result from increasing the convective Mach number. The orientation of the growth rate calculations as defined by the oblique angle to the streamwise direction has very little impact on the magnitude of the growth rates.[44]

There are three stages of molecular mixing. In the first stage fluid elements must be engulfed into the shear layer to a relative transverse extent. The fluid elements then mix molecularly to occupy some fraction of the shear layer thickness at a streamwise position. Finally the fluid elements, reacting to form the chemical product, represent some fraction of the mixed fluid.[44]

There are also three physical characteristics that affect the three Lagrangian steps of molecular mixing. The shear layer growth rate represents the upper limit of the mixed fluid and is dependent upon

the convective Mach number of the flow. The mixture fraction depends on the fluid Schmidt number which is equal to Equation 2.17:

$$S_c = \frac{v}{D} \quad \textbf{(2.17)}$$

Where D is the diffusing/mixing species diffusivity and v is the kinematic viscosity. The fraction of molecularly mixed fluid that is converted to chemical product depends upon the probability density function of the molecular mixture composition within the shear layer. If the chemical kinetics are not fast enough, chemical product formation will lag behind the rate at which reactants are mixed on a molecular scale. The mass fraction for the upper and lower flows deviated slightly from that of actual air to allow O_2 to act as a trace substance while still maintaining the properties of air.[44]

For three-dimensional disturbances, if β is the angle between the direction that oblique disturbances propagate and the mean flow direction, then the shear layer becomes more unstable if β is increased.[16] The effective convective Mach umber can be defined according to Equation 2.18:

$$M_{c_{eff}} = M_c \cos \beta \quad \textbf{(2.18)}$$

The effective convective Mach number can be completely subsonic even if the convective Mach numbers of the flow are supersonic, and thus can allow oblique disturbances to propagate upstream. This in turn makes the shear layer more unstable, which allows for a higher growth rate. [16]

The three-dimensional growth rate greatly increases in the convective Mach number range from 0.75 to 1.25. The growth rate bump represents the effects of three-dimensionality on air to air supersonic shear flow fields. When the oblique angle, β, is 0 the normalized shear layer growth rate varies between 1.0 and 7.25 times the two-dimensional value depending on the convective Mach number. This implies that the lateral effects caused by the three-dimensional simulation increase the growth rate by a factor of 7.25 for a convective Mach number of 1.15. For the normalized three-dimensional shear layer growth rate on the convective Mach number range of 0.75 to 1.25, there is a small increase in shear layer growth for when the oblique angle, β, is approximately equal to 15˚ then declines with increasing β. All other convective Mach number values, high and low, show an immediate decrease in growth rate with increasing β. The lateral effects of the three-dimensional simulation significantly increase the mixing layer growth rate.[44]

For convective Mach numbers ranging from 0.75 to 1.25 the flow is dominated by two-dimensional large scale oblique structures. Linear stability theory states that in the medium convective Mach number range, oblique waves are more rapidly amplified then the two-dimensional waves. The

normalized three-dimensional shear layer growth rate as a function of oblique angle, β, ranges from 1 to 7.5 times the two-dimensional value depending on the convective Mach number. A shear layer growth rate "bump" exists as a function of convective Mach number and normalized three-dimensional shear layer growth rate for the range of convective Mach numbers from 0.75 to 1.25. The magnitude of the "bump" is only slightly dependent on the oblique angle, β, and strongly dependent on the lateral orientation angle, λ, of the large scale structures. The normalized three-dimensional mixing layer growth rate as a function of β ranges from 1 to 4.7 times the two-dimensional value, depending on the convective Mach number.[44]

The lateral orientation angle, λ, of the two-dimensional large scale structures adheres to the relation from linear stability theory for the angle of the most unstable inviscid linear instability wave, as defined in Equation2.19.

$$M_c \cos \lambda \cong 0.6 \qquad (2.19)$$

Risha also performed a computational study of three-dimensional air to air supersonic shear layers at convective Mach numbers of 0.2, 0.5, 0.75, 1, 1.15, 1.25, 1.5, and 1.56. Peak turbulence statistical quantities are weakly dependent on the convective Mach number when the convective Mach number is greater than 0.75 and less than 1.25. The characteristics of the Reynolds stress tensor account for the transfer of momentum by velocity fluctuations. Kinematic Reynolds shear stress and transverse turbulence intensity also decrease with increasing convective Mach number. Streamwise turbulence intensity remains nearly constant regardless of convective Mach number and the spanwise turbulence intensity increases as convective Mach number increases. This is due to the increasingly three-dimensional nature of the large scale motion of the mixing layer with increasing compressibility. The Reynolds normal shear ratio decreases with increasing convective Mach number.[45]

The spanwise component of mixing turbulence becomes more important as compressibility is increased. The reduction in the shear layer growth rate with increasing convective Mach number reduces the size of both the small scale and large scale structures. The normalized streamwise turbulence intensity increases up until the flow reaches a convective Mach number of 0.75. For convective Mach numbers between 0.75 and 1.25 the normalized streamwise turbulence intensity dramatically decreases. At higher convective Mach numbers the intensity continues to decrease but at a slower rate. The normalized transverse turbulence intensity peaks at a convective Mach number of 0.5 then quickly decreases until it reaches a convective Mach number of 1.15. These are two-dimensional simulations, so the turbulences statistics are only affected by compressibility.[45]

One three-dimensional effect is that the normalized transverse turbulence intensity and the normalized lateral turbulence intensity decrease only slightly with increasing convective Mach number. For convective Mach numbers between 0.75 and 1.25, the three-dimensional effects enhance the turbulence character of the shear layer more than the compressibility effects suppress the turbulence of the flow. This range of convective Mach numbers corresponds with the high value three-dimensional shear layer growth, and the existence of oblique structures.[45]

Unconfined supersonic shear layers are relatively stable to two-dimensional disturbances but are unstable to three-dimensional disturbances at angles sufficiently oblique to the flow direction. The preferred direction of instabilities for confined three-dimensional shear layers was found to be three-dimensional. As the Mach number was increased, the most unstable disturbances clearly became more and more oblique to the mean flow. For convective Mach numbers greater than 1 the two-dimensional unconfined shear layer appeared to be stable to any two-dimensional perturbations. Initially the two-dimensional modes caused the three-dimensional modes to become much more unstable, but the persistent pairing of the two-dimensional modes to some extent suppresses the growth of lower amplitude three-dimensional modes. This serves to maintain the predominant two-dimensional structures in the flow.[20]

The two-dimensional modes act as a catalyst and appear to be unaffected by the growth of three-dimensional modes. Relative phases affect the structure of a mixing layer but they were found not to affect the layer energetically. Two-dimensional energy grows much faster and saturates at much higher levels compared to the three-dimensional modes in incompressible flow.[20]

For a free stream Mach number of 0.5 and a convective Mach number of 0.25, the primary instability is two-dimensional. For a freestream Mach number of 1.5 and a convective Mach number of 0.75 the most unstable disturbance in a supersonic shear layer is three-dimensional. This type of three-dimensional instability has the same characteristics as Kelvin Helmholtz instability. For freestream Mach numbers of 2.9 and convective Mach numbers of 1.45 the fastest growing instability is very oblique to the mean flow. This instability also has characteristics that correspond to the Kelvin Helmholtz modes.[20]

The initial magnitude of the two-dimensional Kelvin Helmholtz perturbation energy is about three times the three-dimensional (oblique 45°) perturbation energy. The two-dimensional perturbation energy also grows much faster than the three-dimensional perturbation energy. Two-dimensional modes roll up into a coherent structure and the structure grows until it reaches its maximum size. At Mach 0.5, the single three-dimensional Kelvin Helmholtz mode shows a coherent two-dimensional rollup in a frame rotated 45˚ from the streamwise direction. At Mach 1.5, a single three-dimensional

Kelvin Helmholtz mode is the mode with the highest growth rate for this Mach number that is the Kelvin Helmholtz mode oriented at 36.25˚ to the mean flow. Initially, the two-dimensional perturbation energy is about twice the three-dimensional perturbation energy. In this case the three-dimensional mode grows faster than the two-dimensional mode in the linear regime. At Mach 2.0, the vortex rollup is consistent with the initial conditions, however, the rollup is quite small even at this late time, and no shocks are observed in this simulation. Due to the obliqueness of the rollup, a disturbance is not felt as strongly by the adjacent supersonic flow.[20]

The superposition of more than one unstable mode forces the two-dimensional structure not to remain coherent and to quickly become nonlinear and three-dimensional. The nonlinear development of the two-dimensional wall mode is significantly different than the two-dimensional Kelvin Helmholtz mode so it strongly affects the nonlinear development of the three-dimensional mode. The active nonlinear interaction of the competing modes can force the compressible mixing layer to be more unstable, to elongate the saturation time, and to have a much higher energy level than could be reached by a single isolated mode. When the two-dimensional mode travels at the same speed as the three-dimensional Kelvin Helmholtz mode, then the two-dimensional mode is relatively unaffected and the phase relationship is important. When the two-dimensional wall mode and the three-dimensional Kelvin Helmholtz mode move at different speeds the two-dimensional mode is strongly affected, but the phase relationship is unimportant.[20]

Clemens and Mungal performed an experimental study whose results compare the structure of the turbulent, planar mixing layer for three different values of convective Mach number: 0.28, 0.62, and 0.79. Mie scattering visualizations were used such that either the mixed fluid or the high speed fluid was marked. The supersonic mixing layer, when driven to low convective Mach number, behaves as an incompressible layer with characteristic two-dimensional, organized, Brown-Roshko structures. As the convective Mach number increases the mixing layer becomes highly three-dimensional with little apparent two-dimensional, large-scale organization. This is due to a compressibility effect, not a Reynolds number effect. The structure or topology of the mixing layer is important because of its effect on entrainment and the subsequent mixing process. [46]

Schlieren photography is not good for studying three-dimensional effects because it uses spatial integration. The droplet fog method is a visualization method where ethanol vapor is seeded into the low-speed stream and condenses as a result of mixing with the very cold supersonic stream within the mixing layer. Ethanol liquid is sprayed into the stream using an atomizing spray nozzle which produces droplets less than 100 μm in diameter. The ethanol vapor condenses in about 50 μs. The fog, therefore,

is a marker only of the mixing fluid since neither pure high nor low speed fluid contains droplets. This method could potentially be biased by non-uniform seeding or the finite rate of droplet formation. Thus, a second visualization technique was employed that used the vapor screen method to uniformly mark the high speed fluid. Seeding the high speed side of the shear layer rather than the low-speed side of the shear layer caused the ethanol vapor to condense within the supersonic nozzle and produced a fine fog which uniformly marked the high-speed fluid. The first method, the product formation method, is analogous to combustion systems were a new species is formed. The second method is similar to the dilution of a passive scalar, called the passive scalar method, which has been extensively used in incompressible mixing layers. [46]

Pitot tubes with 1/16" needles were used to take pressure measurements in the flow. Such small needles only create a small disturbance to the flow. Earlier measurements using larger probes caused blockage effects to occur in the subsonic stream so they were not employed in this experiment. A pulsed light source with a 20 ns pulse length was used to capture Schlieren images. [46]

Planar Mie scattering images were obtained using a frequency doubled Nd: YAG laser with a 6 ns pulse width, 150 mJ pulse energy, and a repetition rate of 10 Hz. The laser beam is formed into a sheet which is typically 15 cm wide and 150 μm thick. The detector is a standard CCD video camera which outputs to a frame grabber. The Stokes number is the ratio of the particle to flow time constants. The Stokes number must be sufficiently small for the particles to satisfactorily track the flow.[46]

The boundary layers on the splitter plate were turbulent in all cases. The experimental results match well with existing data of decreasing growth rate with increasing convective Mach number. Differences in the data could be from how the thickness of the shear layer was measured by different researchers. For the case when the convective Mach number is 2.8, the shear layer thickness is less than what was observed in similar experiments at this convective Mach number. This could be because the growth rate is dependent on the splitter plate boundary layers. If the boundary layers are tripped it can decrease the growth rate by up to 30%.[46]

In the case when the convective Mach number is 0.28, relatively weak shocks emanate from the splitter tip and from the supersonic nozzle/test section wall junction. Large scale Brown-Roshko structures appear at about 7 cm downstream and persist to the very end of the test section. The structures do not show signs of breaking up into three-dimensional turbulence with increasing streamwise distance. The structures appear the most robust near the exit station of the test section. Certain positions of the knife edge, used in the Schlieren set up, were optimal for visualizing the large-scale structures while other positions highlighted only the small scale turbulence. Both the product

formation method and the passive scalar method reveal the same structures seen in the Schlieren images, but with much greater detail. Large coherent vortex cores separated by thinner braid regions can be seen in both images. The product formation method is superior in visualizing the details of the mixing layer due to its natural contrast on both the high and low speed side interfaces. In the passive scalar method, the limited dynamic range makes it difficult to distinguish the high speed interface. The structures in both images are similar. The product formation method highlights turbulent motions which bring mixed fluid next to unmixed fluid. The passive scalar method highlights motions which bring pure high speed fluid next to pure low speed fluid. Small scale structures that reside on the large scale structures can be seen using this method. Variations of concentration in the vortex cores can also be seen. Planar imaging shows that the structures span the width of the layer in agreement with previous studies in incompressible flows.[46]

In the case when the convective Mach number is 0.62, two weak shock waves are seen in the Schlieren images near the nozzle exits. The large scale organized structures clearly seen in the low compressibility case are apparently no longer present. The Mie scattering images show structures that appear different from those seen at a convective Mach number of 0.28. The structures seen here are not as distinctly roller like and not as regularly spaced. Sometimes the rollers are seen but they are not preceded or followed by rollers. The planar images do not show structures that are highly two-dimensional and the structures lack all spatial regularity. Near the end of the test section small "jets" of mixed fluid are ejected from the layer. These jets seem to be mushroom structures caused by small scale counter rotating vortices. The Reynolds numbers when the convective Mach number is 0.28 at 45 cm, and when the convective Mach number is 0.62 at 15 cm, are nearly the same but the structure is quite different, so differences in structure must be due to compressibility effects.[46]

In the case when the convective Mach number is 0.79, large scale structures are not readily apparent in the Schlieren images, but planar cuts show large three-dimensional structures. The spatial integration of the Schlieren technique averages out the effects of the large scale structures. In the Mie scattering images, structures appear similar to the case where the convective Mach number is 0.62, but the structures occur further downstream. No roller structures were seen in this case. All of the structures that were observed were highly three-dimensional, fine scale structures.[46]

Images of all three cases show that the mixing layer structure transitions from two-dimensional behavior at low compressibility to three-dimensional behavior at high compressibility. At a convective Mach number of 0.5, both rollers and three-dimensional structures can be seen, which is the behavior that was expected in the transitional convective Mach number range.[46]

Hataue performed a computational study of the mixing layer between two parallel high speed streams. The second order TVD scheme and LUADI implicit scheme were applied to solve the two and three-dimensional compressible Navier-Stokes equations without using any turbulence model. The results show a large-scale coherent structure clearly in the two-dimensional incompressible case at a Mach number of 0.588. The three-dimensional results show the spanwise unsteady fluctuation of the vorticity fields, clearly. The models agreed well with experimental data. The compressible mixing layer also has a large scale vortical structure and the growth rate decreases with increasing Mach number at the same density and velocity ratios.[47]

The objectives of this study were to answer the question of whether two-dimensional turbulent compressible mixing layers between two streams have large scale vortical structures, also known as coherent structures. Also, to clarify the compressibility effects, such as decrease of the growth rate of mixing layer with increasing Mach number. Three cases were run for a two-dimensional mixing layer: the Mach 0.588 case, the Mach 1.125 case, and the Mach 2.352 case.[47]

Mixing occurs by momentum or vorticity transfer. Reynolds stress decreases with increasing Mach number. The lowered Reynolds stress is responsible for the reduced growth rate of the shear layer. Almost all of the Reynolds stress transferred by momentum is not included in the small eddy, but in the large one, and the large scale vortices induce the instability of the shear surface. Therefore, the growth of large scale vortices is impeded by compressibility effects and the mixing layer never grows.[47]

Three-dimensional computations were performed for Mach 0.588 and Mach 2.352. At the lower Mach number, flow fields appear not to be disturbed very strongly and spanwise bands can be seen. The cores of two-dimensional rollers are also visible. Three-dimensionality is not notable at the lower Mach number. In the supersonic case, no spanwise bands can be seen but fine vortical structures that look like spanwise structures from the planar view can be seen. Three-dimensionality becomes more effective in the compressible case. The findings agree with Clemens research, that flow fields become more three-dimensional in the middle of the compressible layer than those in the incompressible layer.[47]

Morkovin proposes that oblique structures begin dominating the flow field once the convective Mach number becomes supersonic. To enhance three-dimensional effects in order to enhance mixing, trailing edge devices for the splitter plate were tested. These devices included vortex generators, trip wires oriented at an angle of 60° to the trailing edge, and saw tooth extensions with teeth inclined at 40°. None of these devices enhanced the growth rate by more than 5%.[39]

Schlieren images taken with the knife edge perpendicular to the flow enhanced the gradients in the streamwise direction, which are generally much weaker than the density gradients in the transverse direction. The shear layer becomes turbulent immediately downstream of the trailing edge. Waves roughly normal to the flow direction and of smooth texture appeared consistently on every photo. The waves extend into both free streams and are relatively stationary. The waves cannot be fully explained. They are not normal shock waves, and are not radiating directly from the structure, and they do not appear to be caused by gradients external to the test section. The waves are thought to be caused by an intricate interaction between a supersonic structure, the test section walls, and the test section wall boundary layers. The waves do not convect with the structures but remain almost stationary.[39]

What is the appropriate compressibility effect parameter for the shear layer? If the maximum convective Mach number is used, it directly defines the compressibility associated with the large scale structure. A more indirect method is to use Equation 2.20:

$$\frac{\Delta U}{(a_1+a_2)} \qquad \textbf{(2.20)}$$

This equation determines when a structure has to be supersonic regardless of the value of the convective velocity. This is a more consistent measure of compressibility. Generally, large scale structures appear frozen from one exposure to the next even though the velocity difference across the structure is on the order of the convecting velocity and the structure has typically traveled two of its body lengths. No evidence of pairing or coalescence was seen in this study.[39]

Where are the structures "born"? If they are only formed at the trailing edge and then expanded downstream, the flow field in the vicinity of the trailing edge may influence their behavior. The shocks on the structures are not clearly seen in the photos, which could be due to rapid weakening. The effects of the surrounding walls cannot be neglected, as the strange waves could be due to wall interactions.[39]

One possible method of increasing the mixing in a shear layer is through the generation of three-dimensionality in the flowfield. Linear theory predicts that, for a certain Mach number range, a shear layer becomes more unstable with increasing three-dimensionality of the disturbance wave. The simplest type of three-dimensional structure is one propagating at an angle, β, with respect to the direction of the free stream. This is the so called oblique structure. The disturbances propagate at the velocity calculated in Equation 2.21 where ΔU is the average speed across the shear layer.

$$\mathbf{V} = \Delta U \cos \beta \qquad (2.21)$$

The incompressible three-dimensional growth rate is equal to the incompressible two-dimensional growth rate multiplied by cosβ. The three-dimensional incompressible disturbances are more stable than the two-dimensional disturbances. [48]

A study by Wantanabe et al. found that forcing the mixing layer with unstable oblique modes caused a growth rate 1.4 times larger than if the mixing layer is forced by random disturbance. Oblique unstable modes with 2% amplitude yield Lambda-shaped vortices. These vortices appear intermittently downstream, and cause the turbulent mixing layer to grow quickly and show a high spreading rate far downstream.[49]

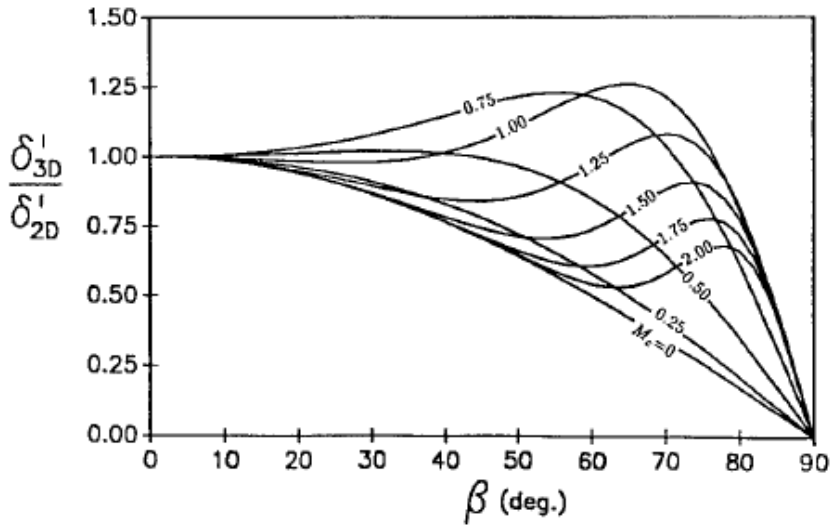

Figure 11: Ratio of three-dimensional to two-dimensional growth rate vs. angle β and for various convective Mach numbers[39]

The results of a study by Papmoschou show the ratio of two-dimensional to three-dimensional shear layer thicknesses for various convective Mach numbers and oblique perturbation angles (See Figure 11). The overall trend in Figure 11 is a reduction of growth rate with increasing β with the exception at Mach 1 when β=60˚ where growth rate rises by a maximum of about 25%. There are two counteracting mechanisms at play as β increases: the reduction of the effective convective Mach number generally destabilizes the flow and the decrease of the effective velocity difference that drives the instability of the structure stabilizes the flow. The latter is the dominant cause for stability. For shear layers with convective Mach numbers above 1, increasing three-dimensionality can only decrease the growth rate. High three-dimensionality is unlikely to trigger order of magnitude improvement in the growth rate. [48]

Island et al tested mixing enhancement methods for compressible planar shear layers perturbed by two-dimensional and three-dimensional disturbances located within the supersonic side splitter tip boundary layer. The disturbances were varied in shape, spacing, and thickness. Discrete three-dimensional disturbances induce appreciable spanwise convolution, streamwise structure, and thickening of the mixing layer with disturbances as thin as 5% of the boundary layer displacement thickness. For equivalent blockage, three-dimensional disturbances are significantly better mixing enhancers than two-dimensional perturbations. The optimal disturbance appears to have an angle of 30° to the streamwise direction and be located at the splitter tip rather than further upstream. The farfield growth rate is unchanged implying that enhancement effects are due to changes in initial conditions.[50]

At a convective Mach number of 0.63, the perturbed layer shows a slight improvement, 7%, in mixing efficiency and a large increase, 48%, in layer thickness. This indicates that gains in the total amount of mixing fluid occur primarily by layer thickening. Disturbances range in height from 0.05 to 0.5 the thickness of the boundary layer.[50]

Mie scattering was used for direct visualization of the mixed fluid. Finely atomized ethanol droplets are evaporated into the low speed stream well upstream of the splitter tip. When the vapor laden stream mixes with the cold supersonic stream the ethanol condenses into small diameter droplets. Laser light scattered from the droplets thereby qualitatively marks the mixed fluid. Laser light is formed into a sheet about 300 μm thick and directed through the test section. The laser light scattering from the ethanol droplet is collected at a right angle to the sheet with a CCD video camera. A filter is attached to the camera to block out the room light.[50]

PLIF also was used for quantitative mixing measurements. The seeding fluid was nitric oxide (NO). The technique employs collisional quenching of excited state NO molecules to provide a resolution-independent measurement of pure fluid from which the probability of mixed fluid is derived.[50]

Two-dimensional disturbances do not seem to encourage two-dimensionality as easily as the discrete three-dimensional disturbances induce three-dimensionality. As the mixing layer becomes thicker with the stronger perturbation, the scale of the vortices equals or exceeds the spanwise spacing of the disturbances thus diminishing the apparent convolution. A limit to the enhancement is expected to occur when the local layer thickness is roughly equal to the spanwise scale imposed by the perturbation.[50]

The optimal disturbance shape is an equilateral triangle. The thickness is 20% greater for an equilateral triangle compared to the more and the less acute triangles tested. Square shapes were

found to be the least effective at enhancing thickness even though the images do show a moderate increase in streamwise structure. The flow area blockage is the same for all the shapes tested. Staggering the tape elements to introduce array obliquity results in a decrease in the enhancement effect.[50]

The optimal disturbance angle of 30° may be related to the susceptibility of the high speed boundary layer to oblique perturbations, as stability calculations have shown that the maximum temporal amplification rate occurs for a 30° wave when the free stream Mach number is near 2. Shock waves are generated at the leading edge of the boundary layer disturbances, and for discrete disturbances result in spanwise variations in pressure. At the end of the splitter tip the pressure differential would likely generate axial vorticity. This would explain the poor performance of the two-dimensional disturbances, which produce no spanwise pressure variations. The results also suggest that discrete three-dimensional disturbances increase only the near field growth rate and do not impact the far field growth rate. Discrete three-dimensional disturbances induce spanwise convolution, streamwise structure, and a thickening of the mixing layer for disturbances as thin as 5% of the boundary layer displacement thickness. The shape of the disturbance appears to be significant with an optimal angle approximately 30° to the streamwise direction for the present flow conditions. Close proximity to the end of the splitter tip results in greater layer convolution and thickening. For equivalent flow area blockage and pressure field disruption discrete three-dimensional geometries generated much thicker mixing layers than two-dimensional perturbations. These enhancement effects are due to changes in initial conditions and near-field growth rate and do not appear to change the far field growth rate. Quantitative measurements of molecularly mixing fluids indicate a slight increase in mixing efficiency and a large increase in layer thickness for enhancement geometry.[50]

Martens et al. performed experiments in which two streams of air are produced in adjacent supersonic sliding block nozzles. The high speed Mach number ranges from 3 to 4, whereas the low speed stream was held at Mach 1.2, with a low to moderate Reynolds number. The shear layer was studied in the laminar to turbulent transition region as well as under fully turbulent conditions. Standard hot wire anemometry was used to analyze the flow. Glow discharge techniques were used to excite the shear layer. Schlieren photography was also used to qualitatively document the flow.[51]

The glow discharge excitation has a significant effect on the shear layer in terms of growth rate and spectral content of the fluctuations. The increased instability of oblique waves was observed for the higher Mach number conditions. At reduced Reynolds numbers the viscous stresses suppress the small-scale turbulence which allows the large scale instabilities, which are concentrated in a limited frequency

range, and typically coherent over large distances in the flow, to be characterized with much greater accuracy. In the supersonic shear layer the large-scale motions grow from instability waves which form early in the shear layer and then over a relatively long distance develop into large scale vortices.[51]

Glow discharge can artificially excite the shear layer increasing the mean growth and allowing for some control over the instability waves and turbulent structures. The glow discharge technique uses a strip of copper wire attached to the centerbody, just upstream of the trailing edge on the low speed side of the splitter plate, with an AC voltage of 350 V peak to peak with a DC offset voltage of -400 V applied to the copper strip. At low pressures the high voltage ionizes the air and a local glow is produced from the copper to the aluminum centerbody. The ionization produces a very high temperature next to the surface of the centerbody. The variations in voltage produce variations in the air density which perturbs the airflow. Tests were performed with the strip normal to the flow and at 45˚ to the flow to excite oblique instabilities. Large scale structures can be seen in the excited case but not in the undisturbed case. When the strip was at a 45˚ angle, 69˚ oblique instabilities were formed. The velocity differential along the center body means the actual excitation angle is 64˚.[51]

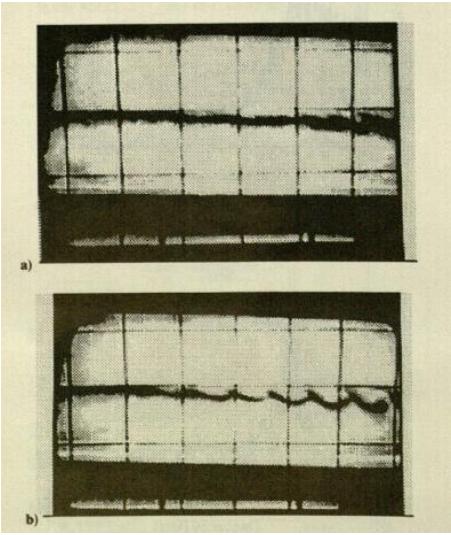

Figure 12: Natural and excited shear layers[51]

Martens et al. also performed detailed measurements of the instabilities present in supersonic shear layers. A high speed stream of Mach 3 or Mach 4 and a low speed stream of Mach 1.2 are produced and begin mixing at the trailing edge of the dividing centerbody. Glow discharge excitation is used to excite either two-dimensional or oblique instability waves. Mach number profiles for the Mach 3 case show little effect of excitation on the growth rate. The higher Mach number case shows enhanced mixing with both excitation geometries.[52]

Four hot wires are used simultaneously to measure the axial and spanwise wavelengths for each case. With these wavelengths, the propagation angles of the instabilities were calculated. The instability waves in a two-dimensionally excited shear layer remain two-dimensional. The three-dimensionally excited shear layer results in waves that travel at a nominal angle of approximately 60° to the mean flow direction even with three widely different excitation angles.[52]

Increasing the convective Mach number of the shear layer creates a slightly oblique instability wave angle. The conclusions support the predictions of previous analytical and numerical studies. Increasing the Reynolds number does not affect the Kelvin Helmholtz instabilities but increases the smaller scale turbulence.[52]

The electrodes were used to stimulate instabilities at angle of, 0°, 10°, 25°, and 45°. The 25° electrode warps to an instability angle of 35° for the Mach 3 case and 44° for the Mach 4 case. The 45° electrode warps to an instability angle of 57° for the Mach 3 case and 64° for the Mach 4 case. For the higher Mach number case, a significantly thicker Mach number profile was observed compared to the natural case. In both Mach number cases, 2D excitation resulted in instability waves that remained virtually two-dimensional throughout the test section. The three-dimensional excitation angles resulted in oblique instability waves. For different excitation angles a similar resulting oblique wave angle developed in each experimental condition. Also, the higher Mach number case resulted in a higher propagation angle.[52]

2.4.7 Shear Layer Merging Processes

The planar shear layer, planar jet, radial jet, and planar wake-coherent structures were first observed by Brown and Roshko. Since then there have been many attempts to relate coherent and large eddy structures in free shear flows to different mixing rates. Some believe that the mixing process is dominated by large eddies and suggest that shear layers grow through a doubling process where pairs of vortices combine to form a new vortex structure (Winant and Browand). It is also believed by some that the mixing rate is sensitive to the detailed structure of the vortices and that the turbulent mixing will continue to depend on the initial turbulent structure. This belief leads to the hope that turbulent mixing can be controlled by controlling the initial conditions.[53]

However, while initial conditions may persist for a while downstream (especially for planar wake flows), spreading rates always approach asymptotic states that are unique for each flow, regardless of the initial conditions. Some consider mixing rates to be describable without considering the turbulent

structures. This party believes that just because spreading follows the vortex doubling that does not necessarily mean that the vortex doubling causes the shear layer spreading. Experimental results have shown that the absence of the doubling process does not affect mixing layer spreading rates. In some cases the eddies can die out completely before a later group of eddies starts to develop. This would seem to show that the initial eddies are not the cause of downstream mixing.[53]

It is argued that the sensitivity of the turbulent mixing to the detailed structure of the turbulent eddies can vary considerably. Some flows are very insensitive to the structure of the large eddies, and in some cases changes in mixing appear to be directly related to the changes in structure of the eddies. Mixing in planar flows is a function of the non-dimensional axial gradient of the turbulent viscosity. Large eddy structures have length scales in the two cross stream directions that are approximately equal. Some experiments have shown that the degree to which the large eddies are two-dimensional does not appear to affect the growth rate of the mixing layer. Other experiments show that the spreading rate of a mixing layer can be insensitive to even fairly large changes in the structure of the large eddies.[53]

Choong and Loth conducted shear layer experiments at convective Mach numbers of 0.35, 0.45, and 0.7. Reduction in eddy coherency as compressibility increases was found to be related to modifications in the eddy merging process. Sensitivity to initial conditions was also found to be greater at higher convective Mach numbers due to the reduction of large scale structure development. Distributions of vorticity, perturbation frequencies, and perturbation amplitudes were all shown to significantly influence the development of the compressible shear layer.[54]

Two types of eddy merging phenomenon were noted in the study. In the one case, the eddies slapped into each other. In the other case, the eddies spin around one another to form a new eddy. The phenomenon where the eddies spin around each other to form a new eddy was observe in the case where the convective Mach number was 0.35. The slapping phenomenon first appears in the case where the convective Mach number is 0.45 and becomes the predominant merging process for the case where the convective Mach number is 0.7. The slapping mechanism resembles a wave hitting a beach, with structure dissipations, and can be seen in Figure 13 (b). It is presumably found as the convective Mach number increases due to the suppression of perturbations by the supersonic ambient flows as the ratio of gas dynamic forces to vorticity forces increase and the reduction in pressure signal propagation from the downstream vortex to the upstream vortex which tells the upstream vortex to move up. A result of this process is that a large portion of the vortex coherency and growth rate are directly lost.[54]

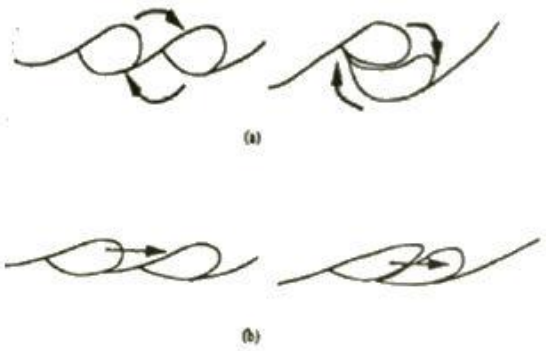

Figure 13: Vortex merging processes: (a) rotational pairing, and (b) slapping[54]

Large scale structures exhibit an elliptical shape, with the major axis inclined to the streamwise flow direction. For increasing convective Mach number, the shape of the eddy is more elongated, the inclination is decreased towards the freestream, and the size is reduced. The structure is also more flattened to the streamwise direction as convective Mach number increases. The tilting of the eddy due to gas dynamic forces and the slapping processes due to merging appear to be the main mechanisms for the shear layer growth rate reduction and decreases in shear layer structure coherency as the convective Mach number increases. The decreased transverse height of the eddy as convective Mach number increases results in decreased high speed side convolutions of the organized lump of fluid.[54]

2.4.8 CFD Simulations

Billig and Schetz numerically modeled injection at angles other than 90˚ and included turbulent mixing into the plume after the Mach disk with a new simulation model. Data is usually reported as the decay of the maximum concentration in the plume at any axial station and the analysis predicts the one dimensional average concentration in the plume. Their analysis was able to predict the effects of angle reasonably well. The mass flow of external stream fluid in the plume at three axial stations was measured and those results can be used to approximately infer an entrainment rate.[55]

2.4.8.1 Reynolds Averaged Navier Stokes Models

There are two largely contradictory approaches to turbulence research. One is the Reynolds Averaged Navier Stokes based method, or RANS Method, which is used for many practical engineering calculating procedures. The other method places emphasis on organized or coherent structure in turbulent flows and is the basis flow of many experiments. The averaging process by its very nature destroys phase information. The RANS method implies that the behavior of the turbulent flow is, to a degree, independent of the detailed structure of turbulent eddies. Some researchers believe that it is the coherent structures that are responsible for turbulent mixing.[53]

There are several problems with the RANS models. Flows where changes in the turbulent mixing have causes that cannot be readily accommodated within the context of a conventional Reynolds average single point model are not represented accurately. The RANS models also have difficulty with problems associated more with the detailed implementation of the models than with general flow situations. It is important to decide how practical a model is to use for real engineering calculations. RANS models tend to over predict the spreading rate of the wall jet. RANS models also do not work well for planar or axisymmetric jets because the constants in the equations would need to change at each cross section. For three-dimensional jets there is a need to model turbulence driven secondary flows.[53]

In the supersonic mixing layer, the growth of the large eddy structures is constrained in ways that are difficult to model with RANS models. For subsonic flows the turbulent mixing in a planar mixing layer is essentially independent of Mach number. However, in supersonic flow the turbulent mixing in the planar mixing layer becomes very dependent on the convective Mach number. It is very difficult for the RANS models to mimic the reduced mixing rate in supersonic mixing layers in a way that correctly models the physical processes present in such flows.[53] However, two-dimensional unsteady RANS simulations have been successfully used to capture the trends of pulsed jet penetration.[56]

Ota and Goldbeg used the USA (United Solution Algorithm) series multizone Reynolds-average Navier-Stokes solver, which is a Total Variation Diminishing or TVD scheme, to model turbulent supersonic shear layer mixing. Three models were used: an algebraic model, a one equation K-L model, and a two equation K-ε model. The one and two equation models matched the experimental velocity profiles better than those using the algebraic model. The shear layer spreading and shear layer thickness results for the K-ε model match well with the experimental values.[57]

Three cases were tested. In the first case the two streams had Mach numbers of M_1=1 and M_2=2. All three models match the velocity profiles better for the high speed side than for the low speed side at x=0.1 in. The algebraic model deviated the most from the experimental values. The K-L model and the K-ε model have similar results which both match well with the experimental data. The algebraic model over predicts shear layer thickness further downstream. The K-ε model had the least error showing only 3% deviation from the experimental results. In the second case, the two streams had Mach numbers of M_1=1.2 and M_2=2. Once again the algebraic model deviated the most from the experimental results. Once again the K-L model and the K-ε model both match well with the experimental data. In the third case the two streams had Mach numbers of M_1=1.25 and M_2=3.06. The K-L model and the K-ε model both match well with the experimental data. In Cases 2 and 3 the experiments showed flow structures

not predicted by the models. From the results, it was concluded that the K-ε model is best for predicting shear flows.[57]

2.4.8.2 Large Eddy Simulation Models

Two different computational approaches were used to perform calculations for forced shear layers. One method was a direct numerical simulation and the other was a large eddy simulation. The Direct Numerical Simulation used full three-dimensional Navier Stokes equations for a temporally evolving mixing layer. The Large Eddy Simulation model used the two-dimensional Navier Stokes equations with a subgrid scale turbulence model. The calculations were shown to agree qualitatively with several aspects of the experiment.[58]

The hope is that through the application of very low amplitude forcing one can significantly alter the flow development of a shear layer such that a large amplitude effect is produced. A well organized, periodic, large-scale motion can be produced in a shear layer by forcing at a single frequency. The forced flow structure evolves in a turbulent flow, extracting energy from and later returning energy to the mean flow. The manner in which these large scale structures interact with small scale random motions (turbulence) yields a great deal of information on flow dynamics and presents an important challenge to those interested in predicting forced flows.[58]

Shear layers are known as a convectively unstable type of flow. This means that small perturbations upstream grow exponentially as they are convected with the flow. Initially the shear layer is subject to very rapid growth due to the rollup of vortices scaling with the forcing wavelength. Further downstream, the rollup process saturates and the shear layer stops growing. This is followed by a collapse of the layer width and then by a slow, secondary growth (Figure 14).[58]

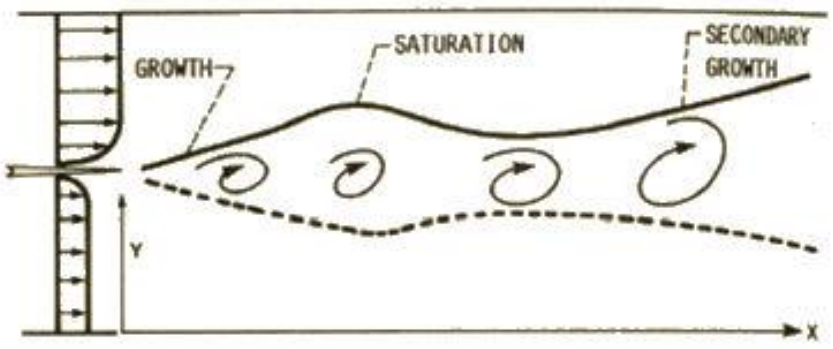

Figure 14: Shear layer growth and saturation[58]

The laminar and the Large Eddy Simulation calculations display very different small scale behavior but the initial rollup is largely dominated by the forced structure, a feature that all of the calculations

present. The Direct Numerical Simulation calculations indicate that the small scale streamwise vortices grow very rapidly. The transition from two-dimensional forced motion to three-dimensional and eventually rather random motion seems likely to be the cause of the slow secondary growth found experimentally. The LES calculations do display increased levels of turbulence kinetic energy in the braid regions where the streamwise structures originate, but this has no significant effect on the mean flow. The oscillatory motion dominates the stresses in the LES calculations up until very near the outflow. Near the outflow, the turbulence model significantly alters the stresses to the extent that the negative stresses contributed by the oscillatory motions are entirely offset making the total stresses positive. Although this trend is in agreement with the experimental data it is quantitatively too small to significantly affect the mean velocity profile and display some secondary growth. The Direct Numerical Simulation calculations may overestimate the important of the streamwise vortices due to their inability to cascade energy to scales both larger than the computational domain and smaller than the computational mesh.[58]

2.5 Thrust Loss Due to Mixing

Supersonic mixing results in total pressure losses that result in thrust losses in scramjet engines. Fuel can be injected into a scramjet combustion chamber either transverse to the main flow, parallel to the main flow, or at some angle in between. Transverse injection produces good near-field mixing, but is inevitably accompanied by shocks which reduce the total pressure recovery of the combustion chamber. Parallel injection could conceivably be achieved without shocks and thus appears to be a more efficient way to mix the fuel and air streams provided that the combustor is long enough to enable the desired amount of mixing. However, at high Mach numbers, viscous dissipation may become powerful enough to create losses comparable to the losses suffered through a shock. These losses would manifest themselves not just in parallel mixing but in any kind of mixing where the characteristic velocity difference is on the order of the speed of sound or higher.[59]

Papamoschou performed a study to examine the effect of Mach number on the total pressure distribution inside a plane shear layer composed of similar and dissimilar gases. He estimated the maximum thrust developed by a device in which two streams mix in a parallel configuration at supersonic velocities.[59]

The total pressure distribution in a compressible shear layer is function only of velocity, provided that the Prandtl and Lewis numbers are both equal to 1. As the convective Mach number increases, the total pressure distribution acquires a defect that becomes increasingly larger for supersonic convective

Mach numbers. For shear layers with equal freestream total pressures, an explicit relation for the defect versus convective Mach number can be obtained. These trends are insensitive to details of the shear layer velocity profile, as well as to the freestream values of velocity, density, and specific heat ratio. The magnitude of the defect does not depend on the shape of the velocity profile, as long as that profile is monotonic.[59]

Papamoschou connected the loss of total pressure to the loss of thrust in a simplified model of a scramjet. The thrust loss due to supersonic mixing is approximately 10% at a convective Mach number of 1, 30% at a convective Mach number of 2, and 50% at a convective Mach number of 3. The effect of specific heat on the thrust versus convective Mach number relation is secondary.[59]

2.6 Flow over a Downstream Facing step

Flows over a downstream facing step in both subsonic and supersonic flow result in the flow area expansion as it moves over the step. In subsonic flows the expansion diffuses the flow and causes it to decelerate. In supersonic flows this expansion is takes place through a Prandtl-Meyer expansion fan which causes the flow to accelerate. In both cases the main flow is separated and a slower recirculation region forms in the step. A shear layer forms between the slower moving recirculating flow and the faster main flow. The shear layer begins where the turbulent boundary layer detaches from the lip of the step and ends where the shear layer reattaches to the lower wall. In supersonic flow where the shear layer reattaches a reflected oblique shock wave forms which abruptly decreases the velocity of the flow and raises the static pressure. Figure 15 shows a definition sketch for supersonic flow over a backward facing step.

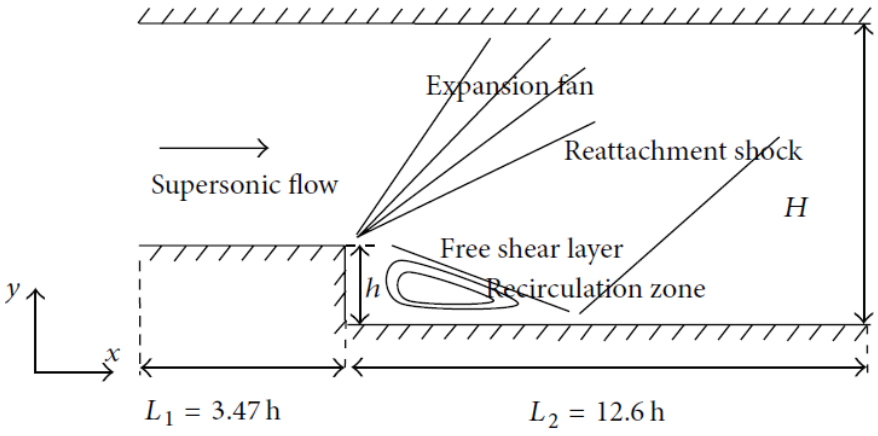

Figure 15: Supersonic Flow over a Downstream Facing Step[60]

Liu et al. used both RANS and LES simulations to study supersonic flow over a backward-facing step at different inflow Mach numbers and expansion ratios. The simulated results were then compared with experimental data and showed a good comparison. Higher inflow Mach number was found to cause a stronger reattachment shock, resulting in a more adverse pressure gradient, which accounts for the boundary layer separation and the formation of the recirculation region. The high pressure after the shock pushes the region of recirculating flow back toward the step. At first the reattachment length was found to decrease with increasing Mach number. However, as the Mach number increase more and more work has been transferred to the kinetic energy in the recirculation region, resulting in the increasing absolute velocity and slight changes in reattachment length.[60] Figure 16 shows a comparison between the simulated shear layer reattachment point and the shear layer reattachment points measured in previous experimental studies at various Mach numbers.

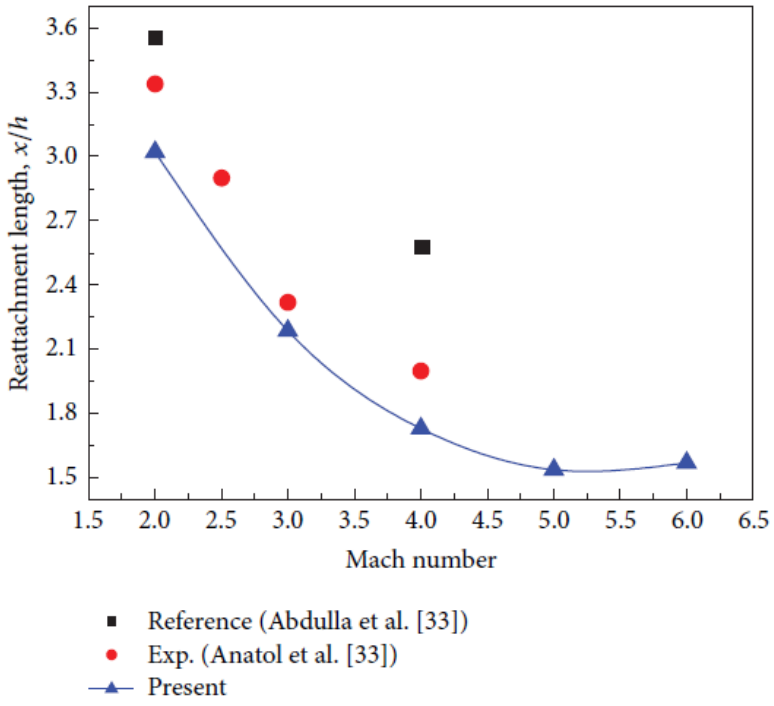

Figure 16: The Effect of Inflow Mach number on Shear Layer Reattachment Length[60,61,62]

2.7 Mixing Enhancement Methods

2.7.1 Confined Shear Layers

Sigalla et al. studied the spatially developing shear layer using both linear stability theory and numerical simulations. Temporal and spatial linear stability solutions were compared and it was found that the temporal and spatial wave numbers are equal. The temporal frequency is a function of the

spatial frequency and the temporal and spatial growth rates have a one to one correspondence. Numerical simulations of the Euler equations were performed for the spatially developing shear layer using a linear stability forcing function. Spatially developing simulations of the acoustic instabilities and the Kelvin Helmholtz instability of shear layers where both streams are supersonic and shear layers where one stream is supersonic and the other is subsonic were compared to temporally developing simulations and found to be in agreement. The purpose of the study was to show the effects of confinement on two-dimensional compressible spatially developing shear layers and to show the relationship between the spatially and temporally developing shear layers.[60] Figure 17 and Figure 18 show the temporal and spatial frames of the shear layer, respectively.

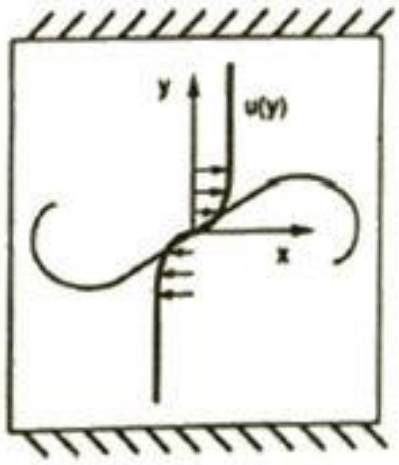

Figure 17: Shear Layer Temporal frame of reference [60]

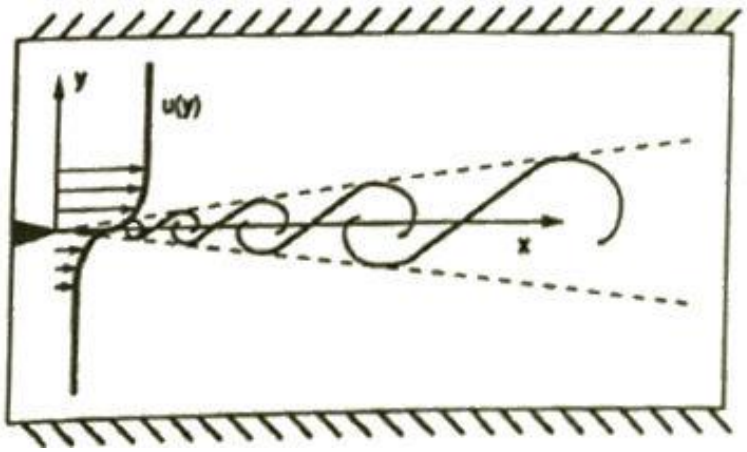

Figure 18: Spatial frame of reference[60]

Viewed from a temporal frame of reference, a wave system grows in amplitude with respect to time. Viewed from a spatial frame of reference, a perturbation generates a train of waves which grow spatially as they travel away from the source. The temporal frame of reference travels at the average velocity of the upper and lower streams of the equivalent spatial frame. There are no direct transformations between the two frames except for certain limiting cases. Temporal and spatially growing waves with the same wave number have equal frequencies and growth rates that can be linked using the group velocity.[60]

The acoustic type instability is characterized as supersonic /supersonic or supersonic/subsonic depending on the relationship between the flow velocities and the instability phase velocity, better known as the coherent structure velocity. The acoustic modes are important since they take energy from unstable three-dimensional Kelvin Helmholtz modes and radiate it away acoustically. These acoustic modes do not engulf fluid and so are inefficient mixers compared to the Kelvin Helmholtz modes, but they are also more energetic.[60]

Unstable modes exist at all convective Mach numbers, but the modes may have relatively small growth rates. When the convective Mach numbers of both the fast and slow streams are supersonic, the instabilities are supersonic/ supersonic acoustic type instabilities. When the convective Mach number of the fast stream is supersonic but the convective Mach number of the slow stream is subsonic, the instabilities are supersonic / subsonic acoustic type instabilities. When the convective Mach numbers of both the fast and slow streams are subsonic, the instabilities are Kelvin Helmholtz instabilities. As the convective Mach numbers increase there is a smooth transition between the instability types.[60]

For every temporal wavenumber there is an equal spatial wavenumber and a corresponding frequency. The temporal and spatial growth rates also correspond well with each other. According to linear stability theory the temporal and spatial wavenumber, phase speed, growth rate, and instability type are in excellent agreement. For every spatial wavenumber there is an equal temporal wave number corresponding to the same type of instability. The temporal frequency is related to the spatial frequency and the temporal growth rate is related to the spatial growth rate.[60]

Soetrisno et al. studied the effects of walls on three-dimensional compressible mixing layers. They studied the effects of two-dimensional wall modes and two-dimensional Kelvin-Helmholtz modes on the dynamics of three-dimensional Kelvin-Helmholtz modes.[20]

Theoretically in a confined compressible shear layer, reflected Mach waves can interact such that perturbation growth is from the reinforced-wall modes. The wall modes were found to grow to large

amplitude but they do not rollup for supersonic convective Mach numbers in the two-dimensional case. Numerical simulations of individual Kelvin Helmholtz modes, super-positions of different Kelvin Helmholtz modes, super-positions of Kelvin Helmholtz modes and symmetric wall modes, and super-positions of Kelvin Helmholtz modes and Asymmetric wall modes were performed using three-dimensional non-steady Euler equations governing the motion of inviscid, non-heat conducting gases.

The wall modes were found to have growth rates that are smaller in magnitude yet still of the same order as the Kelvin Helmholtz disturbances. It was expected that if the channel is narrower than the one in this experiment that the growth rate of the most unstable wall modes would exceed that of the Kelvin-Helmholtz modes.[20]

The nonlinear-behavior of two and three-dimensional Kelvin Helmholtz instabilities and their interactions in confined mixing layers were also studied by Soetrisno et al. These types of instabilities exist together for convective Mach numbers less than 1. For supersonic convective Mach numbers the two-dimensional Kelvin Helmholtz mode does not exist but is replaced by a large family of acoustic modes. At convective Mach numbers less than 1, Kelvin Helmholtz modes exist as unstable modes in two dimensions. As the convective Mach number exceeds about 0.6 the most unstable disturbance becomes a three-dimensional Kelvin Helmholtz mode. Since the two and three-dimensional Kelvin Helmholtz instabilities exist at similar magnitudes it is important to understand their interactions to obtain a better picture of mixing at high subsonic convective Mach numbers.[64]

Persistent paring of the two-dimensional modes suppresses to some extent the growth of low amplitude three-dimensional modes, thus maintaining a predominantly two-dimensional flow. The two-dimensional modes act as a catalyst and appear to be unaffected by the growth of the three-dimensional modes. These effects are suspected to be different in compressible flows, but this study only looked at subsonic convective Mach numbers where two-dimensional modes exist. When the convective Mach number is 0.25, the primary instability is two-dimensional in nature. When the convective Mach number is 0.75, most unstable mode is now a three-dimensional mode. The two-dimensional mode simulations showed that for different channel widths and momentum thickness the behavior of the results were essentially identical. For different channel widths, only the growth rate magnitudes are different. The Kelvin Helmholtz instability still exists at higher subsonic convective Mach numbers, but the growth rates are relatively small and meaningful calculations are difficult.[64]

Initially mixing is diffusion dominated for all cases, but after the Kelvin Helmholtz instability becomes nonlinear the mixing mechanism is taken over by the rollup and entrainment of the Kelvin Helmholtz instability. The saturation of the Kelvin Helmholtz instability is indicated by the slowed

formation of the total integrated product concentration. Finally the product is formed mostly by diffusion again as the primary instability is saturated.[64]

The coherent structures become more elongated and flattened as the effects of compressibility become more dominant. The rollup process is almost undetectable at a convective Mach number of 0.85 which indicates that the Kelvin Helmholtz instability is very weak for this case.[64]

Three-dimensional single mode simulations were performed at convective Mach numbers of 0.25 and 0.75. At a convective Mach number of 0.25 the most unstable mode is two-dimensional. If an oblique perturbation, 45˚ to the mean flow, is used instead of the most unstable two-dimensional mode, then the three-dimensional Kelvin Helmholtz mode saturates at a lower kinetic energy than the two-dimensional mode. For perturbations at 45˚ and -45˚ to the main flow, the nonlinear development of the structure is significantly different. The additional three-dimensionality of two crossed oblique Kelvin Helmholtz modes does not show any significant effect on the mixing extent in the shear layer, thus mixing at a convective Mach number of 0.25 is dominated by two-dimensional Kelvin Helmholtz instability. When the convective Mach number is 0.75, two-dimensional and three-dimensional modes saturate at about the same level. The three-dimensional modes are perturbed at 36.25˚ and -36.25˚ to the mean flow. For this Mach number the two-dimensional mode is not the fastest growing disturbance. The additional three-dimensionality of two crossed oblique Kelvin Helmholtz modes show an effect on the mixing extent in the shear layer. Faster mixing can be achieved when the three-dimensional Kelvin Helmholtz instability is used.[64]

When a two-dimensional mode and a three-dimensional mode are superposed, it appears that the two modes are competing to extract energy from the mean flow so that they can grow. In the early part of the interaction it is found that the two-dimensional mode always wins this energy competition and hence inhibits the growth of the three-dimensional instability. In the later part of the nonlinear interaction the three-dimensional mode suppresses the two-dimensional rollup resulting in faster saturation and lower saturation energy of the two-dimensional mode. After the two-dimensional mode saturates the three-dimensional mode does not have any other mode with which to compete allowing it to saturate at a higher saturation energy level. Shocklets only develop for convective Mach numbers greater than 0.75 where local supersonic regions occur because of the acceleration imposed by the rollup of the Kelvin Helmholtz instability.[64]

At a convective Mach number of 0.25 interactions between the three-dimensional Kelvin Helmholtz modes and the two-dimensional Kelvin Helmholtz modes were found to be affected by the choice of the three-dimensional modes used to create the secondary instability. When the three-dimensional growth

rate was at least half an order of magnitude of the two-dimensional mode growth rate the two-dimensionality was not affected by the growth of the three-dimensional mode. (The two-dimensional mode acted as a catalyst in the interactions.) When the three-dimensional mode growth rate is of the same order of magnitude as the two-dimensional mode growth rate the two-dimensional mode saturation energy was somewhat suppressed. (The two-dimensional mode was not a catalyst in this case.) In this case, the three-dimensional disturbances were found to be inhibited by the two-dimensional instability growth.[64]

Interactions between three-dimensional Kelvin Helmholtz modes and two-dimensional Kelvin Helmholtz modes at higher convective Mach numbers, between 0.25 and 1, were found to be different than interactions at low Mach numbers. At higher convective Mach numbers the growth of the three-dimensional instability was found to suppress the rollup process of the two-dimensional mode resulting in a faster two-dimensional saturation time and lower two-dimensional saturation energy. The two-dimensional mode growth was also found to significantly inhibit the growth of the three-dimensional instability. As soon as the two-dimensional mode saturated the three-dimensional mode grew at the actual rate and was allowed to saturate at a higher three-dimensional saturation energy (compared to the case with only the saturation of three-dimensional oblique Kelvin Helmholtz). For convective Mach numbers less than 0.6, when the most unstable disturbance for the given Mach number is two-dimensional the presence of two-dimensional instability as a secondary instability to the three-dimensional flowfield would increase the extent of mixing. For convective Mach numbers less than 0.6, when the most unstable disturbance of the given Mach number is three-dimensional the presence of a two-dimensional mode as a secondary instability would decrease the extent of mixing.[64]

Morris et al. modeled two-dimensional shear layers to study shear layer axisymmetry. The model assumes that large scale coherent structures dominate the mixing process in free shear layers. These large structures were modeled locally as instability waves. The effects of confining walls on the development of two-dimensional shear layers were also considered, mainly the effect of changing the wall locations in both the spanwise and normal directions. It is shown that the growth rates of instabilities may be maximized by the correct choice of duct width to height ratio.[65]

The present model assumes that the mixing process at high speeds continues to be dominated by large scale coherent motions, though the nature of these motions changes with the operating conditions. A co-flowing jet was used to simulate axisymmetric shear layers. For convective Mach numbers close to 1 the two-dimensional shear layer growth predictions continue to decrease, whereas the axisymmetric shear layer predictions level off. This is because the two-dimensional shear layer

calculations only include two-dimensional instability waves. At higher convective Mach numbers three-dimensional instability waves are expected to dominate. The axisymmetric shear layer predictions include three-dimensional waves so the predictions should be valid at supersonic convective Mach numbers. The predicted spreading rate of the axisymmetric shear layer is slightly less than for the two-dimensional case, especially at low convective Mach numbers. Both experiments and predictions indicate a decrease in the vorticity thickness growth rate for the axisymmetric shear layer for all velocity ratios. The agreement between the experimental results and the predictions was very good. The development of the free shear layer is related closely to the stability characteristics of the mean flow.[65]

Confining the shear layer creates duct acoustic modes. Duct acoustics decompose the higher order normal modes or acoustic waves into a superposition of oblique waves travelling at the speed of sound and reflecting back and forth between the confining walls. Confined shear layers can impose a constraint on possible three-dimensional modes. In spanwise confined shear layers this is determined by the width of the ducts. In axisymmetric shear layers it is set by the azimuthal periodicity condition. Altering the width of the duct for the two-dimensional case has the equivalent effect of changing the ratio of the jet radius to the local width of the shear layer in the axisymmetric case. Both modifications lead to changes in the growth rate of a given instability wave. For unconfined shear layers, instability waves may be convectively supersonic with respect to either one of the freestreams, with the Kelvin Helmholtz instability as the dominant instability.[65]

In these simulations Mode 1 waves have a higher growth rate at lower frequencies, whereas Mode 2 waves are unstable for a wider range of frequencies. Mode 1 waves are dominant when three-dimensional instability waves are considered.[65] Decreasing the wall height increases the instability wave growth rate. The growth rates for Mode 2 waves are always less than the growth rates for Mode1 waves. The choice of width to height ratio of the tunnel cross section could be used to maximize the growth rates of instability waves. This would also be likely to increase the spreading rate of the shear layer.[65]

2.7.2 Flow Trips

Cenkner performed a cold flow laser Doppler Velocimetery study in the mixing region of supersonic mixing nozzles that employed gas-trips for enhanced mixing. The nozzles were operated with room temperature nitrogen under simulated laser flow conditions. The primary, secondary, and trip streams were simultaneously seeded with 0.357 µm diameter latex spheres. The objectives of this activity were to acquire basic cold flow information on trip nozzles in order to help develop some insight into the

tripped mixing phenomenon and to acquire information that could be correlated with sophisticated computer models of the mixing process.[66]

Gas trips have been installed in various mixing nozzles in an attempt to enhance mixing and thereby improve device efficiency. In this approach gas is injected through small orifices that are located in the nozzles near the exit plane in an attempt to trip the flow. Tripping the flow triggers premature transition from laminar to turbulent flow. Laser induced Fluorescence of selectively seeded iodine vapor was used to study the flow. The mixing region was probed with a laser Doppler velocimeter. Measurements were made of three mean and turbulent velocity components as well as two turbulent shear stress elements.[66]

Supersonic turbulent velocities where the mean velocity could exceed 3000 m/s were measured. The measurement volume had to be small enough so that reasonable spatial resolution could be achieved. The LDV system needed to be a single burst system that would respond to Doppler frequencies as high as 300 MHz. A special high frequency signal processor was also needed.[66]

Mean and turbulent velocities were measured in the mixing region of a slit nozzle array under both tripped and untripped conditions. The flow field is three-dimensional even under the untripped condition. The three-dimensionality of the flow is related to a mismatch in nozzle exit and cavity back pressures and to side feeding of the secondary nozzles. The gas trips do not enhance the turbulence in the untripped wake region rather the trips locally spread the turbulence into the adjacent lower turbulence regions. The LVD results appear to be consistent with the flow visualization work that shows that the trip jets act like solid deformable bodies near the nozzle. The tripped and untripped axial turbulent intensity is low level, being no more than 10% at peak locations. The peak vertical and horizontal turbulent velocities exceed their respective mean velocities. The untripped secondary nozzles are filled with higher levels of turbulence sooner than the primary nozzles this is probably related to the differences in the widths of these nozzles. The untripped centerline velocity of the secondary stream also drops off faster than that of the primary stream. The LDV measurement volume is small enough so that localized flow phenomenon can be resolved.[66]

Cenkner and Driscoll refined a laser- induced iodine fluorescence visualization technique and used it to study supersonic cold-flow mixing. The visualization studies were performed in the mixing region between supersonic slit nozzles that employed gas trips for enhanced mixing. The nozzles were operated with room temperature helium under simulated chemical laser flow conditions. Three-dimensional information was acquired on the size, shape, location, structure, and interaction of the primary, secondary, and tripped jets under both the tripped and untripped conditions.[67]

Three trip induced convective mechanisms appear to contribute to enhancements in mixing. The mechanisms appear to depend on the type of trip configuration used, the nozzle width, and the flow-field location. One mechanism appears to dominate in the primary nozzle and another in the secondary nozzles. The gas trips inject non-reacting gas through small orifices that are installed in the side walls of the mixing nozzle near the exit plane. The gas trips enhance mixing by tripping the flow from laminar to turbulent prematurely. Gas jet injection from a circular hole into a cross flow creates a shock wave which causes the upstream Boundary Layer to separate.[67]

For testing, a small stainless steel slit nozzle array was fabricated consisting of three contoured secondary nozzles and two contoured primary nozzles.[67] See Figure 19

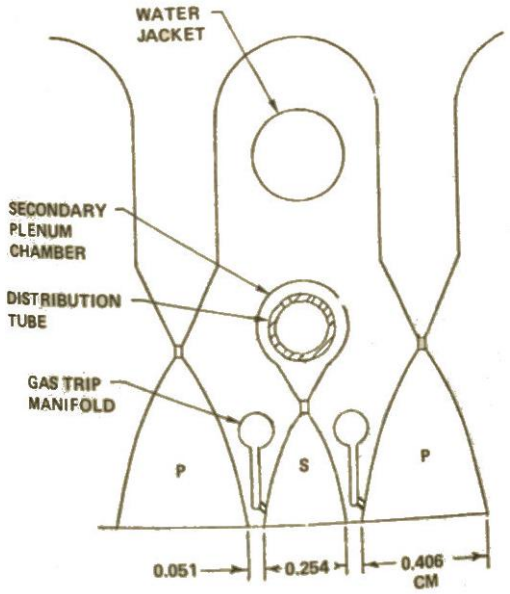

Figure 19: Primary and secondary nozzles[67]

The fluid stream of interest was seeded with molecular iodine vapor. The flowfield was then illuminated by a green (514.5 nm wavelength) argon ion laser beam to pump the I_2 to an excited electronic energy level. When the excited iodine spontaneously decays to an intermediate energy level, yellow fluorescence is emitted. When it then decays to and even lower energy level, red fluorescence appears. If a narrow band optical filter is used to block the green pumping beam, a planar cross section of the fluorescencing stream can be observed or recorded using standard electro-optical or photographic techniques.[67]

Three convective mechanisms have been proposed as contributing to enhancements in the mixing of adjacent gas streams. The low pressure wake of the solid body trip jets draws gas from the adjacent secondary flow. A high pressure region is established in the nozzle main flow by the trip jets in the same

nozzle which pushes this main flow into the adjacent stream. Trip jet breakup, which may trigger a nibbling/spreading effects on the adjacent main flow, or which may work in conjunction with the second mechanism. Which mechanisms are active and which dominate appears to depend upon the type of trip configuration used, position in the flowfield, and nozzle size. Interaction of the injected jets is the most likely cause of the premature breakup of the jets.[67]

2.7.3 Wavy Wall

A potential technique for improving the growth rate of compressible shear layers is to use a wavy-wall geometry in a confined supersonic shear-layer facility to generates Mach waves in the flowfield that impinge upon the shear layer. The Mach waves create a three way resonant interaction between the spatial Mach waves, duct acoustic waves, and the Kelvin Helmholtz waves, causing excitation of certain modes within the shear layer. A tuned pure tone excitation of Kelvin Helmholtz waves can be coupled with the wavy wall induced disturbances and duct acoustic waves to produce local shear layer growth rates that are approximately 50% higher than the natural, smooth walled baseline case.10

The experimental setup for testing this technique is shown in Figure 20. A glow discharge excitation system used to excite specific spectral components of the Kelvin Helmholtz instability. The 20 kHz excitation case appears to have the largest growth rate of the cases tested. The 30 KHz case shows the quickest initial growth but then the growth rate decreases considerably. The 10 and 15 kHz cases exhibit increased shear layer thicknesses at further upstream locations compared to the unexcited case. All of the wavy wall cases show improved growth over the baseline smooth wall unexcited case. The smooth wall, 20 KHZ excitation case shows comparable growth in the upstream region but begins to level off farther downstream10

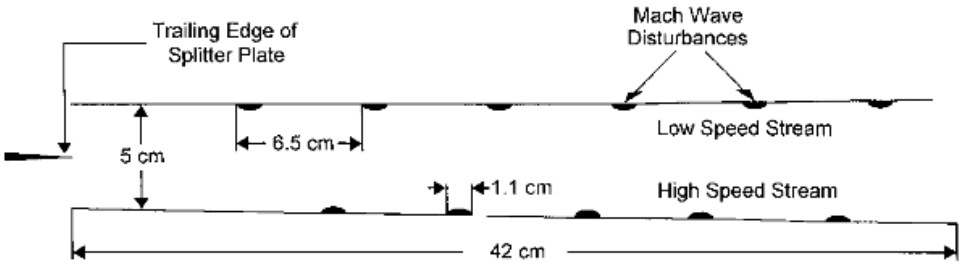

Figure 20: Wavy Wall schematic10

As shear layers thickens, their dominant lengths scale increase and their dominant frequencies decrease. A decrease in dominant shear layer frequency with downstream distance results in the eventual ineffectiveness of higher excitation frequencies. Such excitations can at that point result in

destructive interference and excited shear layers can actually show less growth than their unexcited counterparts. With the standing Mach wave pattern present, a three wave interaction is theoretically taking place in which the Mach waves and neutral acoustic waves interact to drive the Kelvin Helmholtz instability to resonance.10

Figure 21 and Figure 22 show Schlieren images of the flow field beginning 12 cm downstream from the splitter plate. Figure 21 shows the natural shear layer with no excitation. Figure 22 shows the shear layer excited by a 30 kHz glow discharge. Figure 23, Figure 24, and Figure 25 show Schlieren images of the shear layer approximately 18 to 24 cm downstream of the splitter plate with wavy-wall geometry in place. Figure 23 shows the shear layer with only the impinging Mach waves. Figure 24 shows the shear layer excited by a 20 kHz glow discharge with impinging Mach waves. Figure 25 shows the shear layer excited by a 30 kHz glow discharge with impinging Mach waves. 10

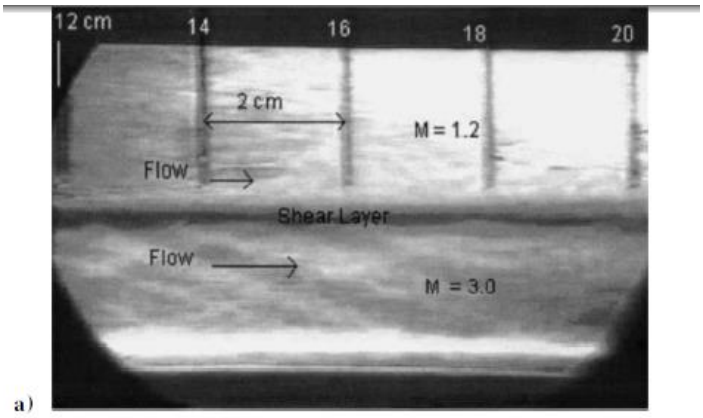

Figure 21: Natural Shear Layer10

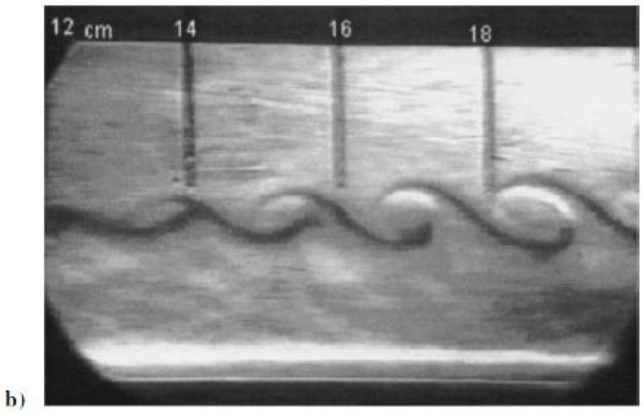

Figure 22: Shear layer excited with 30 kHz glow discharge10

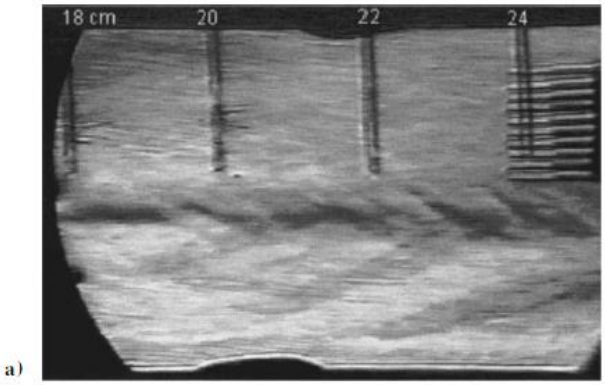

Figure 23: Shear Layer with wavy wall geometry and no excitation10

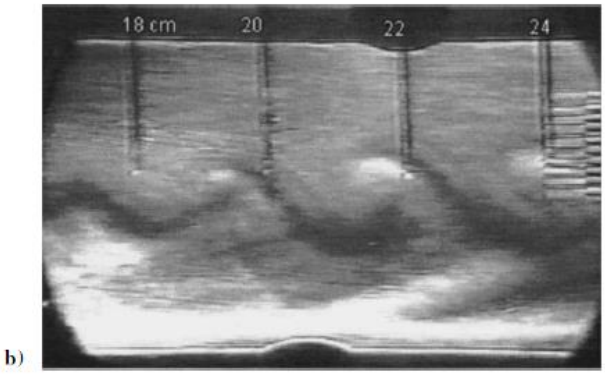

Figure 24: Shear layer with wavy wall geometry and 20 kHz excitation10

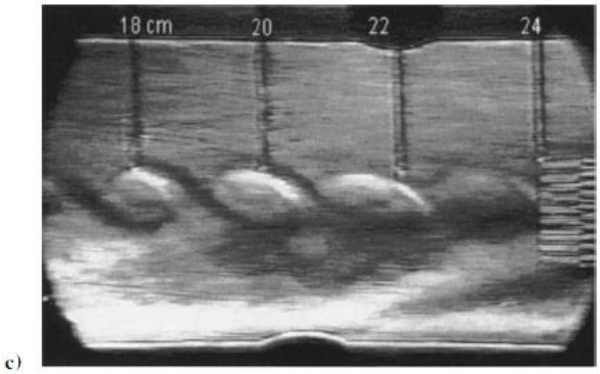

Figure 25: Shear layer with wavy wall geometry and 30 kHz excitation 10

2.7.4 Cross Stream Pressure Gradients

Another possible method of enhancing the fuel air mixing in supersonic flows by cross stream pressure gradients. Baroclinic torque is the generation of axial vorticity by cross stream pressure gradients normal to density gradients. If the two streams on either side of a shear layer have different densities then a density gradient exists across the shear layer. Shock waves and expansion fans create

pressure gradients so vorticity is generated when a shock wave or an expansion fan intersects with a mixing layer.[68]

If two streams with different densities have the same pressure, temperature, and velocity, then the speed of sound in the low density fluid is greater than that of the high density fluid so a compression shock or expansion fan propagates much faster in the low density fluid. This causes the low density fluid to deflect while the high density fluid continues to go straight which induces the cross stream shear flow or vortex sheet along the contact surface. The pressure change in the high density fluid is greater than in the low density fluid inducing a cross flow or large scale displacement of the contact surface. This large scale displacement can also be analyzed as the induced velocity of the vortex sheet.[68]

In most scramjets the flow is turned in the inlet and nozzle where the Mach numbers, and therefore the total pressure losses, are high (See Figure 26). An alternative is to turn the flow down on the forebody then turn the flow upward in the combustor where the Mach number is lower and where the turning can enhance fuel mixing. With the flow upward out of the combustor the nozzle may be more effective due to less nozzle pluming. These installation advantages may be offset by the additional cowl frontal area [68]

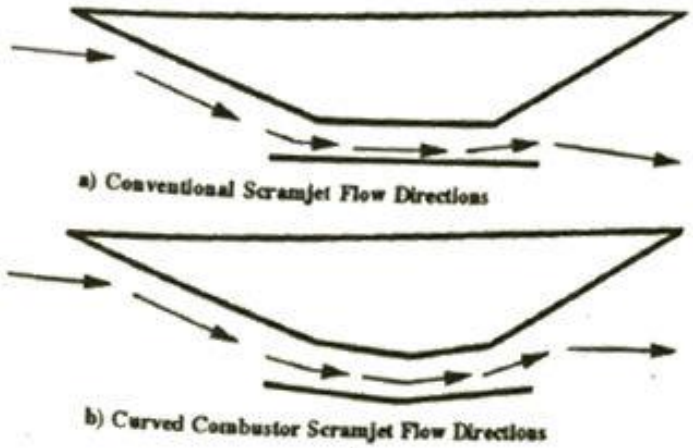

Figure 26: Scramjet configurations[68]

Modeling the curved combustion chamber has shown that the pressure waves do generate vorticity and large scale displacements that increase mixing rates. Fuel penetration is not significantly improved by the vorticity. However, the fuel spreading on the expanding surface could possibly increase film cooling effectiveness. The vorticity generated by an expansion fan is the same magnitude or greater than the vorticity generated by an equivalent strength shock wave. It was found than an expansion fan was slightly more effective at generating vorticity than a shock wave and that the installation

advantages of the curved combustor increased net thrust. It was also found that the efficiency of vorticity generation is better for smaller turning angles.[68]

The flow turning interactions do improve the mixing which gives higher predicted system performance even with the higher combustor total pressure losses. The expected improvement in combustion efficiency for a full combustor could be on the order of 5 to 10% by using small turning angles. The installation advantages of curving the combustor improves propulsion system performance even without the effects of the enhanced mixing simply by decreasing the total pressure losses. Curving or turning the combustor should improve the high speed performance of a scramjet engine, possibly with net thrust increases of at least 10%.[68]

2.7.5 Transverse Injection into a shear layer

Maddalena and Dimotakis investigated a shear layer formed between a supersonic upper stream with a Mach number of 1.5 and a subsonic lower stream with a velocity of 8.5 m/s injected at an angle of 30° with respect to the horizontal. The coupling of streamwise vortices generated by five jets inclined at 30° with respect to the freestream and the shear layer was investigated and the influence of the jet injection on shear layer entrainment was studied.[18]

In the experiments a high speed upper stream is expanded over a ramp inclined 30° to the flow while a low speed stream is injected through perforations in the ramp generating a mixing layer. To increase mixing at higher convective Mach numbers five transverse jets, injected at an angle of 30° with respect to the freestream, were incorporated to exploit the excitation of instabilities to streamwise vortices in the shear layer in order to enhance mixing.[18] Figure 27 and Figure 28 show the test section with the modular inclined jet injection insert.

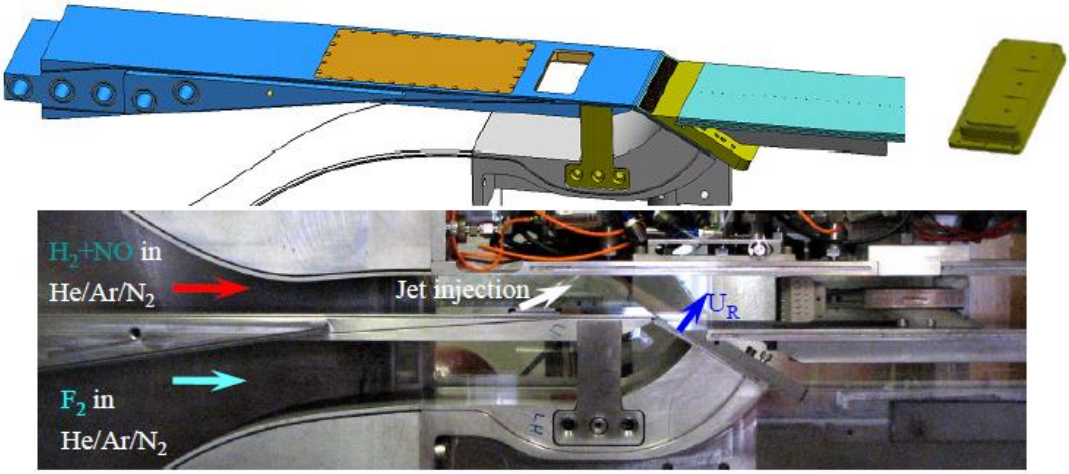

Figure 27: Experimental Setup[18]

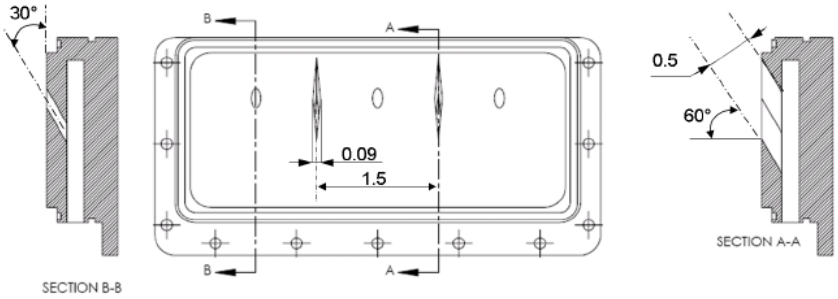

Figure 28: Injector insert, Dimensions in Inches[18]

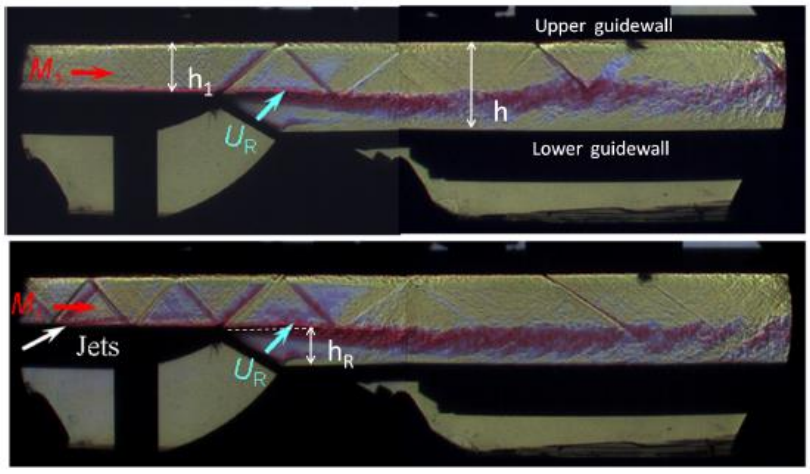

Figure 29: Schlieren Images with and without injection[18]

Because the low speed stream and the jets are injected at an angle to the free stream flow oblique shocks form at the sites of injection. For the case with no jet injection the shocks are weak because

their angle is close to the Mach angle. The mixing layer grows approximately linearly from a virtual origin upstream of the splitter plate/perforated grid connection point. The shear layer is substantially thicker with jet injection. This appears to be an enhancement in the growth rate rather than just a local phenomenon due to the injected mass from the jets. A weak oblique shock is present downstream near the normal shock where the two plates constituting the upper guide wall attach. A corrugation layer is visible for both cases where the oblique shock impinges the shear layer [18]

A predominant increase in growth occurs along the low speed interface, 22% to 39% increase in growth rate in the range of downstream distances. Experiments at lower momentum flux ratios did not show the same effectiveness on enhancing the shear layer thickness. Due to the fact that Schlieren photography integrates across the shear layer it is not possible to distinguish between the entire layer thickening and the presence of other streamwise structures. However, a substantial increase of the shear layer thickness compared to the unperturbed case is reported for a jet to freestream momentum flux ratio of 2.[18]

2.7.6 Coaxial Jets

Compressible jets are unstable over a wide range of Mach numbers. Countercurrent shear layers caused by reverse flow around a supersonic jet result in enhanced mixing. Tiny disturbances in the boundary layer caused by roughness in the nozzle or on the splitter plate propagate into the shear layer.[17] This self-induction of flow instability is considered the main reason for mixing enhancement of coaxial jets.[69] Counter flowing shear layers are also better at mixing because of three-dimensional structures not seen in co-flowing shear layers.[17] When the single coaxial jet mixes with the main flow it decays into two smaller jets. The spacing of these jet is important as the merging of neighboring jets can prevent mixing enhancement.[69]

Rectangular supersonic free and coaxial jets were used to enhance mixing relative to a circular jet over a convective Mach number range of 0.5 to 2.2. Non-circular nozzles such as nozzles with elliptic, rectangular, and other non-conventional cross sections geometries have unique shear flow development and have been used to improve performance of various types of subsonic ramjets. Elliptic and rectangular free jets having an aspect ratio 3:1 were studied and compared to a circular jet in a Mach number range of 0.15 to 2.4. The major and minor axes switched at a distance of less than 3 diameters from the nozzle in the underexpanded elliptic and rectangular jets, for a Mach number of 1.3, which was significantly closer to the nozzle than in the corresponding subsonic jets.[70]

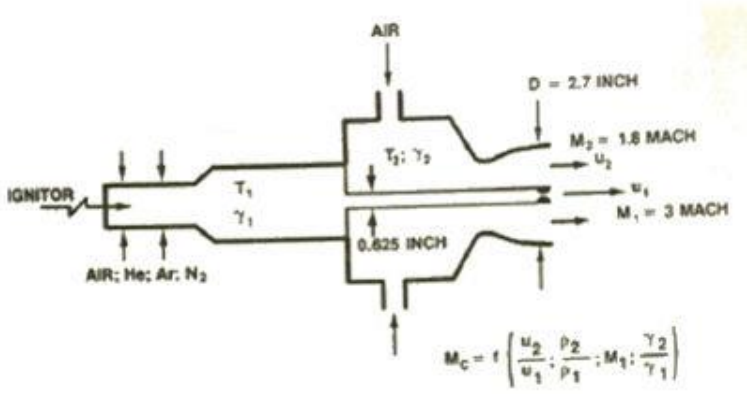

Figure 30: Coaxial Supersonic Jet[70]

In the coaxial jet configuration (Figure 30) the mixing between the two jets is strongly dependent on the convective Mach number. Increased shear and high density ratios increase the instability of the jet and subsequently the jet spreading rate. Irrespective of the convective Mach number the spreading rate increases with increasing shear and reduction of the center jet density.[70]

Direct measurements of mixing rates were performed using supersonic circular and rectangular jets. The rectangular jets tested included the REC 1 jet which diverges only at the narrow sides and the REC 2 jet which diverges only on the wider sides. The convective Mach numbers of the tests were varied over a range of M_c=0.5 to M_c=2.2 by varying the density of the inner and outer jets either by changing the gas composition or by varying the temperature.[70]

In all test conditions both rectangular jets showed enhanced mixing relative to the circular jet. Free jets tend to spread faster radially relative to the coaxial jets. For the rectangular jets the centerline total pressure decreased faster with larger spreading of the jet at the major axis plane relative to the minor axis. The minor axis spreading rate was nearly equal to the circular jet spreading rate. No axis switching was observed for the present test conditions. Improved mixing was obtained by the rectangular jets relative to the circular jet.[70]

The gas sampling data shows in more detail the actual location of the mixing and its volumetric fraction, which is the parameter relevant to evaluate the mixing necessary for complete reaction between the two streams. In free jets most of the mixing occurs in the jet circumference and the ambient fluid does not penetrate the circular jet, even at great distances downstream. With coaxial flow more of the ambient fluid is entrained deeper into the central jet.[70]

With rectangular jets, the mixing in the entire jet is enhanced. A better mixing performance was measured for REC 1 than for REC 2. For all test conditions the rectangular jets showed substantial

improved mixing relative to circular jet. The free jets showed high mixing in the circumferential region of the jet while the coaxial jet had a high mixing rate inside the central jet.[70]

Murakani and Papamoschou performed experiments on the morphology and evolution of large turbulent eddies in co-annular supersonic jets. They tested 430 m/s round, perfectly expanded jets composed of air, 745 m/s helium and air mixed jets, and helium and air co-annular jets that have a core flow of Mach 1.5 and a secondary flow of Mach 0.82. A double exposure planar laser induced fluorescence (PLIF) system using gaseous acetone as the tracer molecule enabled visualization of the turbulent structure of the jet and its evolution. The convective velocity of the eddies was extracted from the PLIF images by means of 2D cross correlations.[71]

Eddies in the air jet propagate with a speed approximately 80% of the local centerline velocity and are subsonic with respect to the ambient air. The helium-air jet which is faster than the air jet emits Mach waves and exhibits substantial turbulent motions in the azimuthal direction.[71]

In the helium-air jet addition of the Mach 0.82 secondary flow reduces the convective velocity of the primary eddies from 72% to 63% of the primary exit velocity. The speed of the secondary eddies is 44% of the secondary exit velocity. All turbulent motions in this co-annular helium-air jet are intrinsically subsonic leading to elimination of Mach waves and substantial reduction in noise[71]

Strong parallels between the development of the vortex-sheet (Kelvin Helmholtz) instability and the behavior of fully turbulent shear layers suggest that large eddies constitute the dominant instability of the flow. A key aspect of the instability is its phase speed or convective velocity, U_c. In subsonic shear layers the convective velocity controls the entrainment ratio and influences the growth rate. In high speed shear layers and jets the convective velocity determines the production of strong noise emission.[71]

At high compressibility, eddies behave asymmetrically with fast modes (high M_{c2} and low M_{c1}) in shear layers between a supersonic and a subsonic stream and with slow modes (low M_{c2} high M_{c1}) in shear layers between two supersonic streams. At high Mach numbers the shear layer of the jet (which is supersonic/subsonic) exhibits fast modes as evidenced by the onset of Mach wave radiation. These modes continue past the potential core and eventually decay as the jet slows down. Mach wave radiation occurs when the convective velocity exceeds the speed of sound of the ambient gas.[71]

In the 430 m/s jet eddies in the primary shear layer traveled with 80% of the local centerline mean velocity. In the 745 m/s jet which consisted of a helium air mixture the convective velocity of the primary eddies was 72% of the jet exit velocity and resulted in Mach wave emission. Addition of a Mach 0.82 secondary flow to the helium-air jet reduced the primary convective velocity by 12%. In addition

this secondary flow rendered all relative turbulent motions subsonic leading to elimination of the Mach waves and substantial noise reduction. As a result of its lower density the helium air jet spreads faster than the air jet. The turbulent structure of the helium air jet is more disorganized than that of the air jet and exhibits strong azimuthal notions.[71]

Yu et al. tested the passive control of coherent vortex formation on three axisymmetric compressible mixing layers, Mach 2 and Mach 1.3 co-flowing supersonic jets, Mach 3 and Mach 1.3 jets, and a free flowing Mach 2 supersonic jet. All the jets are fully expanded in these experiments. The convective Mach numbers tested are 0.23, 0.47, and 0.85.[72]

In the two cases which used coaxial jets, coherent vortex formation is controlled by having a finite thickness nozzle lip and varying its thickness. The interaction between the lip created wake and shear flow results in highly coherent large scale structures. The lip thickness is systematically varied and the resulting compressible shear layers are visualized using a planar Mie scattering technique. The results show that the streamwise wavelength varies monotonically with the lip thickness.[72]

Passively organized spanwise, or tangential, rollers were also used to modify compressible mixing. This is done by introducing other sources of instability into the compressible shear layer thereby promoting interaction with the shear flow instabilities.[72]

With a finite thickness lip much more coherent structures are seen then with other experiments at similar convective Mach numbers. The finite thickness lip creates a wake aft of the tip. With certain lip thicknesses the structures were very well organized and the wavelengths were very uniform. The wavelength was varied with the lip thickness and this is a clear indication that the dynamics of the wake flow is important for the stability characteristics of the shear flow downstream. For nozzles with fairly large lips, the supersonic flow continued to expand over the lip resulting in over expansion of the center jet. The wavelength increases with the size of the lip thickness. As a result, there was almost a linear relationship between the lip size and the coherent structure wavelength.[72]

2.7.7 Lobed nozzle

A radially lobbed nozzle is a potential candidate to enhance the mixing of supersonic jets. These nozzles are also referred to as clover nozzles. Reduction in the growth of shear layers due to compressibility renders the mixing of co-axial supersonic streams extremely slow. Multi-lobed force mixer nozzles have been shown to be efficient at promoting enhanced mixing of compressible jets.[73]

The mixing mechanism of lobed nozzles is characteristically different than from conical nozzles. For jets from circular nozzles, mixing is dominated by momentum transfer through viscous shear stresses

and small scale turbulence in the mixing layer. This results in a very slow growth rate. Rectangular nozzles are better than circular nozzles of same area because shear stresses in the flow are distributed over a larger area. Mixing for lobed nozzles is characterized by a parameter called momentum flux.[73]

Samitha studied two types of clover nozzle: a 4 leaf and a 6 leaf (shown in Figure 31 and Figure 32). The nozzles were then compared to the conical nozzle. All three nozzles had a throat diameter of 10mm, a converging angle of 25°, and a diverging angle of 3°. All of the nozzles had the same exit area and area ratio. All three nozzles also had an exit Mach number of 1.5.[73]

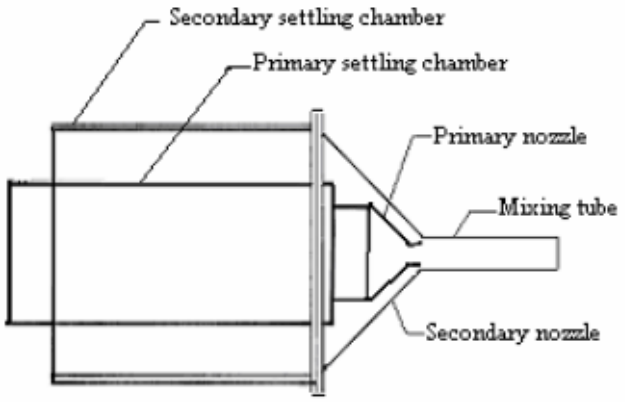

Figure 31: Side View Schematic of the Samitha Clover Nozzles[73]

The stagnation pressures in the primary and secondary settling chambers were 400 kPa and 200 kPa, respectively. The static pressure at the outlet of the mixing tube is 1 atm. The Reynolds number in the mixing tube was above 2300. The flow in the mixing tube was fully turbulent.[73]

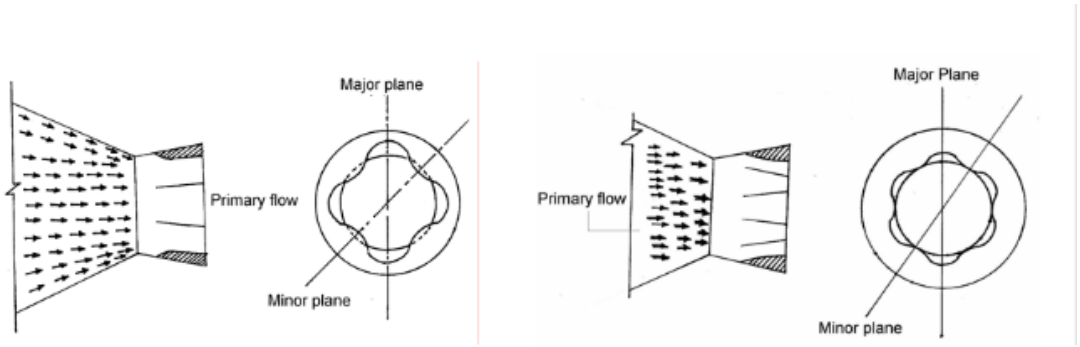

Figure 32: End View Schematic of the Samitha Clover Nozzles[73]

The clover nozzles were able to enhance mixing with only marginal total pressure loss. For the circular nozzle mixing is caused by small scale turbulence in the mixing layer. For the lobed nozzles mixing was caused by axial vortices at the lobe's tips. The pressure loss seen was due to shocks caused

by the nozzle's lobes. The four leaf nozzle was superior in degree of mixing to the six leaf and both were superior to conical nozzle. The four leaf nozzle was superior because it had deeper lobes than the six leaf nozzle and thus generated stronger vortices. The four leaf nozzle needed only 57% of the length that the conical nozzle required for the jet to fully mix with the flow.[74]

2.7.8 Lobed Mixers

Lobed mixers increase mixing in two ways: they increase the initial interface area associated with their convoluted trailing edge shape and they introduce streamwise vorticity. In addition to mixer generated vorticity, streamwise vorticity may be generated downstream of the mixer trailing edge via the interaction of trailing edge shocks and density gradients across the mixing layer. Depending on the density ratio between the high-speed and low-speed streams this baroclinic torque generated vorticity can either enhance or retard the mixing rate.[75]

Four different geometries were tested: one planar splitter plate and three lobed mixers. The lobed mixers with either a 15˚ or a 25˚ ramp angle were designed to shed streamwise circulation. The third mixer was a convoluted plate with the same trailing edge shape as the two lobed mixers but was not ramped and therefore shed little streamwise circulation. The mixers were of an approximately square lobe design with a height to wavelength ratio of 1.25. The estimated non-dimensional circulations for the 15˚ and 25˚ mixers were 0.5 and 0.9 respectively. The circulation shed by the convoluted plate mixer was estimated to be 0.1 based on the NS computations for similar geometries.[75]

The convective Mach number for the tests ranged from 0.3 to 0.8 and the primary stream Mach number ranged from 1.3 to 2.4. A decreasing mixing rate with increasing convective Mach number was observed. In mixing layers downstream of the lobed mixers, a mixing penalty did appear to be associated with increases in convective Mach number when the velocity ratio was held constant.[75]

The mixing augmentation, but not necessarily the overall mixedness of the flow, associated with streamwise vorticity at any location downstream of the mixer increases with increasing convective Mach number. Streamwise vorticity is increasingly important with increasing convective Mach number because of the decreasing shear layer growth rate.[75]

In supersonic/subsonic mixer flows shocks in the vicinity of the mixer trailing edge can interact with the density gradients across the mixing layer to generate levels of streamwise circulation comparable to that shed by the mixer. When pressures were matched at the trailing edge, the primary flow was turned back into approximately the axial direction. As the secondary/primary static pressure ratio was decreased, the turning of the primary trough flow at the trailing edge became less abrupt. If the ratio

was increased the trailing edge shock strengthened and in some cases the shock moved upstream into the trough causing the flow to separate within the lobed mixer. The interaction of shocks and density gradients can result in the generation of streamwise circulation. The secondary stream sees approximately the same pressure gradient due to the shock wave turning as the primary stream pressure gradient turns the secondary flow farther off axis increasing the streamwise circulations. The forced mixing rate will always be equal to (if all of the vorticity is canceled) or higher than the mixing rate downstream of the convoluted plate.[75]

Reduced shear growth rates associated with high convective Mach number give the streamwise vorticity more time to stretch the interface between the two streams and hence streamwise vorticity is more effective in compressible regimes than in incompressible ones. Vorticity may be generated downstream of the mixer by the interaction of trailing edge shocks and density gradients across the mixing layer, depending on the density ratio between the streams, this vorticity generation may either enhance or reduce the mixing rate.[75]

2.7.9 Normal Injection

VanLerberghe et al. studied the basic flowfield surrounding a single, underexpanded, sonic, transverse jet injected into a Mach 1.6 crossflow. Surface oil flow techniques were used to show the surface streakline patterns around the jet orifice. Shadowgraph methods, planar Mie scattering using ethanol droplets, and planar laser induced fluorescence (PLIF) using acetone droplets were used to reveal large scale turbulent structures in the streamwise and transverse side view planes of the jet.[76]

Figure 33 shows the flow features seen when a normal jet is injected into supersonic flow. Shadowgraph images of the jet show the bow shock, the barrel shock structure, the Mach disk, and turbulent structures in the jet crossflow interface (Figure 34). Acetone PLIF images show the rapid expansion of the jet fluid after it leaves the injector. These images also clearly reveal the barrel shock and Mach disk (Figure 37). The surface streakline patterns indicate primary and secondary flow separation regions are indicated upstream of the jet. The streaklines also suggest the presence of a horseshoe vortex system which originates upstream of the jet and extends downstream around the jet (Figure 35). Large scale structures were noted along the jet crossflow interface in the side view images obtained by planar Mie scattering and acetone PLIF images (Figure 36). The rotational direction of these eddies indicated that the jet fluid is moving faster than the crossflow fluid at the interface. The large scale structures vary in size and spacing along the jet crossflow interface and engulf large portions of crossflow fluid, which contributes greatly to the near field mixing.[76]

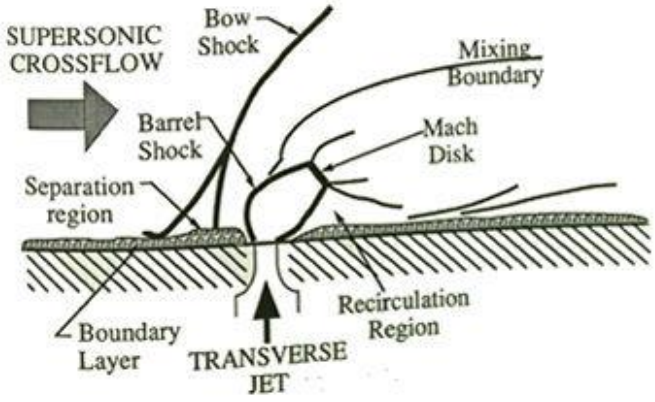

Figure 33: Features Transverse Jet Injection[76]

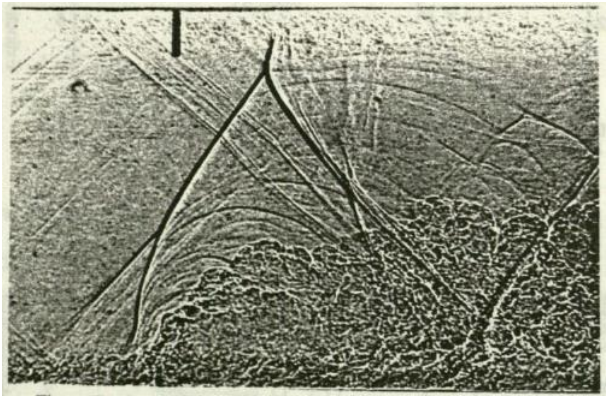

Figure 34: Shadowgraph image of the helium jet at J=2.2[76]

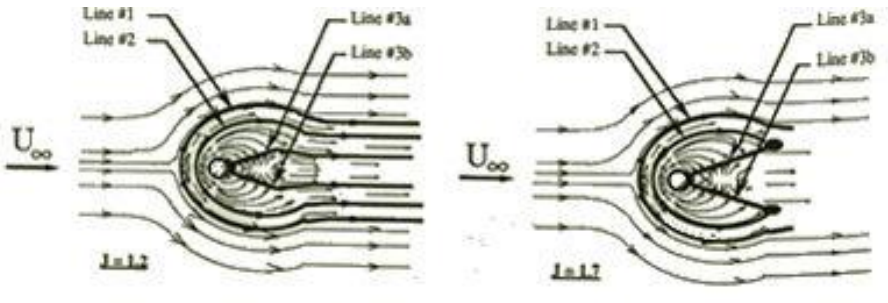

Figure 35: Sketches of the surface streakline patterns for J=1.2 and J=1.7[76]

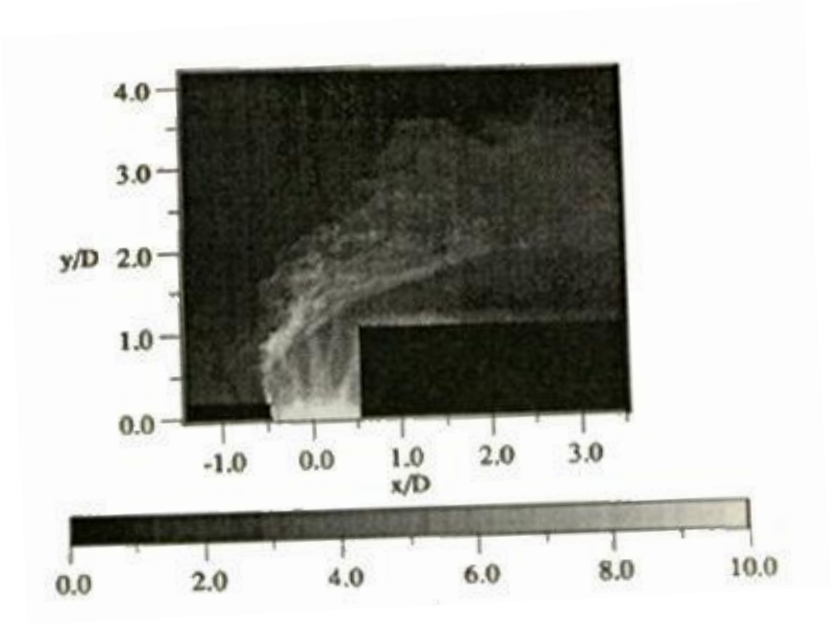

Figure 36: Average Mie scattering images, J=2.2[76]

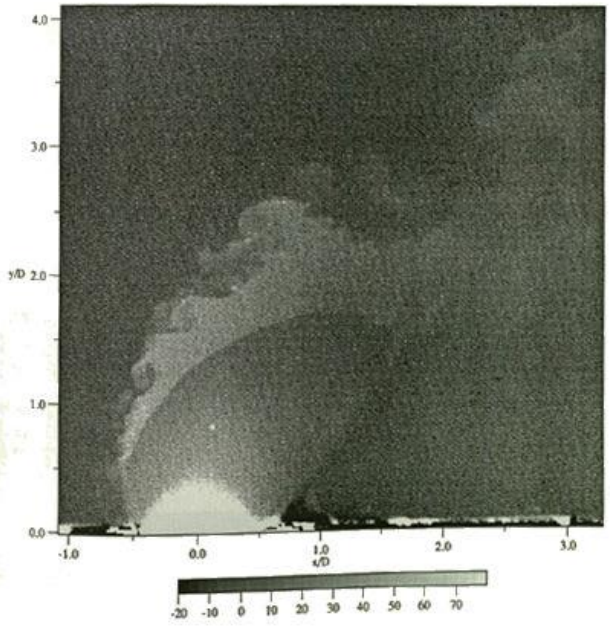

Figure 37: Acetone PLIF image for J=2.2[76]

Transverse jet injection of the secondary fuel stream into the supersonic primary air stream is one potential scheme which has been proposed to provide rapid and thorough mixing of the fuel and air so that efficient combustion can be achieved. The transverse jet acts as an obstruction to the supersonic freestream so a bifurcated bow shock forms in front of the jet and the wall boundary layer separates just upstream of the jet.[76]

After emerging from the jet orifice the high pressure underexpanded jet fluid passes through an expansion fan originating from the edges of the jet orifice. Where these expansion fans intersect the jet boundary they are reflected back into the jet as compression waves. The compression waves gradually coalesce to form a barrel shock structure which terminates in a Mach disk. The jet fluid loses most of its momentum as it passes through the Mach disk and thus is quickly deflected downstream. (Similar internal jet structure is present in underexpanded sonic and supersonic jets injected into ambient conditions.) Immediately downstream of the jet exit near the surface is another separated flow region similar to a bluff body wake region. Eventually the lower edge of the jet attached to the boundary layer on the wall farther downstream.[76]

The most important factor affecting penetration of transverse jet injection into the cross flow is the ratio of the jet to crossflow momentum flux ratio, J. The optimum jet penetration at a given value of J is achieved at the pressure matched condition, in which the jet exit pressure is equal to the effective back pressure of the flow field, P_{eb}. This is because at the pressure matched condition the shock structure within the jet seems to be the weakest. The effective back pressure of the flowfield is the average static pressure around the periphery of the injector hole. Determining the effective back pressure, P_{eb}, is difficult because the static pressure varies dramatically around the periphery of the jet due to the bow shock, the separation regions and other compressibility effects. Different approximations for the effective back pressure have been suggested based upon experimental observations. Jet penetration and jet spreading were found to increase with increasing jet to crossflow momentum ratio.[76]

The mixing process of transverse injection is strongly influenced by streamwise vortices which shed from both sides of the jet, similar to those found in incompressible jets. The transverse injection causes counter rotating vortex pairs to form in the streamwise direction. Large scale turbulent structures at the jet freestream interface, as far as 25 jet diameters downstream of the injector were observed. The structures developed at the jet freestream interface in a periodic manner and persisted far downstream of the orifice. Unmixed freestream fluid was found to penetrate well into the jet.[76]

The bow shock produced by normal injection caused the upstream wall boundary layer to separate providing a region where the boundary layer and jet fluids mix subsonically upstream of the jet exit. This region is important for its flame holding capabilities.[77] (Figure 38)

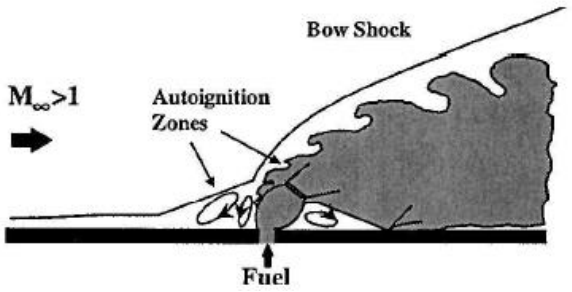

Figure 38: Underexpanded fuel injection normal to the crossflow

Backward facing steps followed by normal injection can be used for flame stabilization. The step creates a larger recirculation region with the hot gases serving as a continuous ignition source, which can provide sustained combustion. Backward facing steps have the disadvantage of large stagnation pressure losses and increases in drag due to the low pressure flow behind the step (Figure 39). Angled injection weakens the bow shock, thus decreasing the total pressure losses from normal injection. The jet axial momentum from injecting the fuel at an angle can contribute to the net engine thrust (Figure 40).[77]

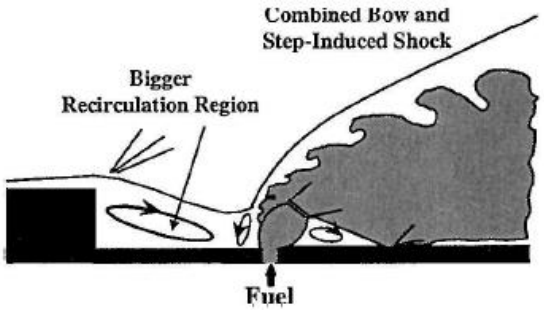

Figure 39: Injection behind a sudden expansion produced by a step

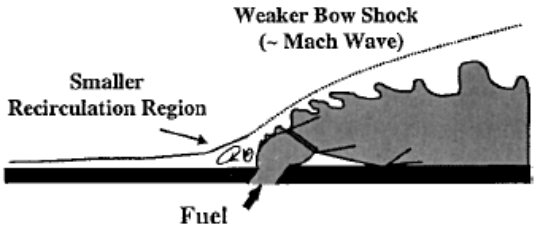

Figure 40: Fuel injection at an angle

When staged injection of two transverse jets injected into a supersonic crossflow was tested intense mixing of the injectant and freestream fluids in the region between the two jets was observed. This effect was perhaps due to subsonic flow interaction just upstream of the second injector. Streamwise vortices were observed just downstream of the injectors and it was determined that vortex-driven

mixing dominates in the near field while turbulent diffusion dominates in the far field with the transition between the two regions occurring between 10 and 20 jet diameters downstream of the injectors. Near field mixing was enhanced for the staged injectors compared to parallel injection, but the far field mixing did not seem to be improved to any noticeable degree.[76]

Takahashi et al. experimented with sonic transverse injection into Mach 2.0 airflow. Acetone PLIF was used to investigate single-time, two-point, spatial correlations of injectant concentrations in the mixing flowfield. Contour maps were obtained in several planes to characterize the turbulent structure and three-dimensionality of the mixing flowfield. Organized large scale structures were seen in the upper region of the jet. The shape of the dominating structures were elliptic and their major axes turned from backwards leaning to forward leaning as the reference point of correlation moved downstream. The instantaneous jet plume appeared by turns either in the top or in the lower sides of the time-averaged injectant plume in each cross section.[78]

The purpose of this research was to clarify details of the large-scale structures. Single time two point spatial correlations taken from multiple images give the shape and spatial extent of a large scale turbulent structure and resulting mixing mechanisms. These spatial correlations also show the influence of the surrounding flowfield on the structure.[78]

In shear layers structures are elongated and compressed toward the streamline flow direction with increasing compressibility. Large scale structures increase in size and decrease in eccentricity with increasing compressibility. For transverse injection, large scale eddies tend to break up rapidly in low compressibility whereas in high compressibility the structures remained coherent over a longer spatial distance.[78]

Generally, in investigations of high speed flows, it is very difficult to relate the scattered light intensity from fluid markers directly to a certain physical property. When using particles as a fluid marker, a disparity between the particle path and the streamline may result from a lag of the tracing particle. PLIF can provide high resolution quantitative data and can trace fluid behavior well. Gaseous acetone was seeded only in the injectant to represent the molar concentration (number of moles in the specific volume of the injectant) of the injectant, not the mole fraction.[78]

Large structures similar to the two-dimensional roller-type vortices produced by low-speed axisymmetric jets were observed. This is evidence of the highly intermittent nature of the scalar field on the outer boundary of the jet. The images were averaged out to smooth out the injectant plume. The most intensely fluctuating region appeared along the 50% averaged concentration track. A high correlation region was seen which proves the existence of the large scale structures around the upper

jet boundary region. The structure around the maximum concentration tack may be small-scale or not very well developed due to the remaining high concentration.[78]

The major axis of the elliptic structure switched at seven jet diameter distances downstream of injection. The structure first rotated in the clockwise direction as it went downstream until reaching six jet diameters downstream. At that point the structure changed its shape from an ellipse to a circle to another ellipse with switched major and minor axes. The axis switching is not as remarkable as the fact that the axis ratio remained less than 1.3.[78]

The reflected bow shock caused the structure to break up hence the correlation region had an almost circular shape. The pairing of the large scale structures was not observed. In the lower part of the plume there was an elongated correlation region that might be influenced by the turbulent structure in the boundary layer because this region was adjacent to the boundary layer. This could also have resulted from intermittent inflow of air from outside of the jet plume induced by the counter rotating vortex pair. No large scale structures appeared in the center of the plume.[78]

In general, fluid elements have four motions: transitional motion, rotation, stretch/compression, and shearing deformation. The velocity field strongly influenced the shape and motion of the correlation regions generated by the acetone markers. The increase of shear and velocity gradients between the main flow and the jet leads to the stretching of the large scale structures and the structure tends to tilt toward the fast flow direction. The velocity between the 10 and 50% tracks was slower than that in the region between the 50% and maximum tracks so the part of the large scale structure inside the 50% track traveled faster than the one outside so the structure became backward leaning. Downstream, the streamwise velocity outside of the 50% track gradually became close to that of the inside velocity and the streamwise velocity above the 10% track in this region is faster than that below the 50% track. The result was a turning of the major axis of the structure and deforming the elliptic structure to a circular one. There was no significant flapping motion of the jet in the transverse direction. The shape change of the correlation region is not due to jet dynamic motions but due to velocity distributions formed by the local flow structure.[78]

Sandham and Reynolds showed that at low convective Mach numbers, i.e. convective Mach numbers less than 0.4, the two-dimensional Kelvin-Helmholtz instability plays a dominant role in mixing. However, at higher convective Mach numbers, i.e. convective Mach numbers greater than 0.6, three-dimensional modes are dominant. The large scale structures similar to those in low speed jets could thus be formed and exist stably in this flowfield.[78]

The mean injectant mole fraction was distributed symmetrically, but there was some asymmetrical behavior observed. A counter rotating vortex pair was seen. The most fluctuating region is again near the 50% of max concentration track. There is slight asymmetry due to a flapping motion on either side due to the counter rotating motion. The two vortices act to draw main flow fluid up into the center of the jet. Large scale structure was circumferentially developed and did not exist in the center lower part of the jet.[78]

Averaged tracks of molar concentration and injectant mole fraction agreed very well in the region of less than four jet diameters downstream, though distributions differed due to density changes. The mean concentration profile in the upper half of the jet plume exhibited self-similarity in the region from the point of injection to twelve jet diameters downstream. A large scale structure was observed for correlation distributions and appeared along the upper 50% average concentration track where the fluctuation intensity was most intensive, the large scale structures appeared sequentially in an interval of three diameters to four diameters downstream, and possibly consisted of hairpin vortices. The size of the large scale structure grew linearly as it moved downstream until six jet diameters downstream where the fluctuation intensity began to have self-similarity then shrank gently or maintained a constant size. This tendency is different from that of the mixing layer.[78]

In the transverse direction the area became the maximum between the 10 and 50% averaged concentration tracks and sharply diminished below the maximum track. The structure first had a backward leaning elliptic shape and rotated itself in a clockwise direction then its shape changed to a circle and then to a forward leaning elliptic shape with switching major and minor axes. The streamwise velocity distribution might determine the shape and orientation of the large scale structure. This suggests that the structure may be controlled by giving such additional velocity distribution as incident shock waves. In the cross sections the upper center and both lower side regions were negatively correlated and both the right and left sides of the lower part were positively correlated. The features of the correlation region that appeared alternately in the upper or lower part of the jet plume were ascribed to the intermittent air inflow which was induced by the counter-rotating vortex pair at the lower part of the jet from outside of the jet plume.[78]

Gruber et al. performed a study of sonic transverse injection from circular and elliptic nozzles into a supersonic crossflow. The structural details show a highly three dimensional near-field interaction dominated by shear layer eddies and a pair of counter rotating vortices. The elliptic jet was found to spread faster in the lateral direction than the circular jet, but suffers a 20% reduction in penetration

compared to the circular jet. For both the circular jet and the elliptic jet mixing was found to be better at lower convective Mach numbers than at higher convective Mach numbers.[79]

2.7.10 Ramp injectors

As previously stated, at higher convective Mach numbers the mixing layer growth rate is suppressed and the "Brown-Roshko structures" that govern incompressible mixing layers tend to develop with less coherence because turbulent fluctuations decrease with increasing convective Mach number. In supersonic mixing it is necessary to rapidly increase the fuel/air interface area to enhance micro mixing.[80] Streamwise vortices can do this by stretching the fuel/air interface along the length of the vortex. Streamwise vortices have also been shown to increase penetration into the main flow.[81]

One common method used to enhance supersonic mixing is to use ramp injectors to generate streamwise vortices. In supersonic flow generating streamwise vortices is relatively easy and generates very little total pressure loss. The breakdown of streamwise vortices, which is necessary for mixing, can be controlled by the geometry of the injectors, by their spanwise row configurations, various combinations of their scales, and by the intensity of circulation and rotational directions the ramps generate. Ramp injectors also have the advantage of being able to directly inject hydrogen fuel into the core region of the streamwise vortices. Streamwise vortices are expected to be free from the compressibility effect unless the circumferential Mach number component exceeds about 0.6.[80]

Kawano et al tested parallel and oblique sonic helium injection from ramp injectors into Mach 4 flow. Helium was injected at 10° and 30° (see Figure 41 and Figure 42). Kawano found that injection from the upper face of the ramp improved mixing more than injection from the aft face of ramp. This is because injecting from the upper surface of the ramps allowed the injected gas interface to be better enlarged by the streamwise vortices generated by the ramp.[82] Oblique injection was also found to generate smaller disturbances on the plate than parallel injection.[82] The peak concentration of helium for oblique injection was smaller than for parallel injection implying better mixing.[82]

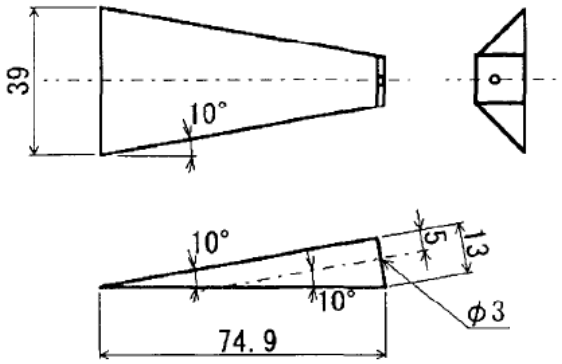

Figure 3: Parallel injector

Figure 41: 10 Degree, Parallel Injection Ramp Injector[82]

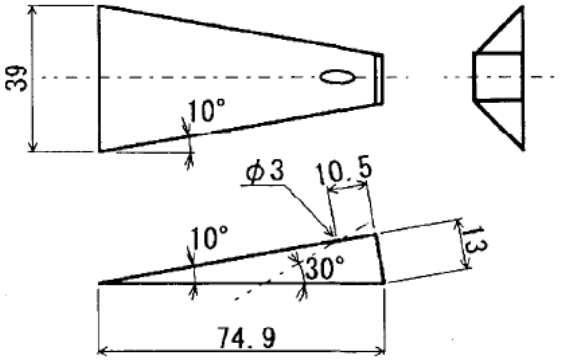

Figure 4: Oblique injector

Figure 42: 30 degree, Oblique Injection Ramp Injector[82]

Ramp injector sweep angle is known to change the strength of the streamwise vortices generated by the injector. Aso et al preformed a study on how the ramps' injector sweep angle affects the strength of longitudinal vorticity on the mixing flowfield. Ramp injectors with 0°, 10°, and 20° of sweep were tested. Nitrogen was injected parallel to the flow through a 5mm diameter nozzle in backward facing step of the injector.[83]

For the tests the free stream Mach number was varied between 3.85 and 3.88. As sweep is increased it was found that the separated region starting from the forward edge of the ramp injector becomes large. Downstream of the rear edge of the injector the interaction of separated flows with secondary flow is significant at sweep angles above 10°. For the injectors with 10° and 20° of sweep stronger vortices were produced than were produced by the injector with 0° of sweep. The pressure disturbances downstream of the nozzle are also stronger for the injectors with higher angles of sweep.

The optimum sweep angle seems to be between 10° and 20°. The highest vortical flow is for the 10 degree injector. Data for this experiment was recorded using Schlieren phtotgraphy, oil flow techniques, and surface pressure distributions.[83]

Sunami et al wanted to determine how fuel-air mixing is affected by the initial streamwise vortex arrangements. They wished to see how the vortex circulations and co- and counter-rotational configurations effected mixing. They also wished to study the interaction of the fuel-air equivalence ratio, mixing, and the combustion heat release. Four wedge fuel injector struts were tested in a Mach 2.48 direct connect supersonic combustor.[84]

The initial arrangement of vortices was found to significantly affect the mixing process. The co-rotating vortices show better mixing than the counter-rotating vortices. The structures of the fuel jet are strongly affected by combustion heat release resulting in a more uniform fuel distribution. Combustion causes the streamwise vortex structures to break down into more uniform turbulence. The spreading rates of hydrogen are also higher with combustion.[84]

Abdel-Salam et al also studied the effect of ramp injector sweep angle on mixing. Three ramps with different side sweep angles: 0°, 5°, and 10° were tested. All of the ramps had a 10° compression angle, a fuel jet diameter of 2.7 mm, and ramp height of 5mm. The jet is injected at 10° so that it is parallel to the ramp and thus parallel to the flow along the top of the ramp. The unswept ramp had an aspect ratio of 1.[85]

The swept ramps spread the fuel over a wider area than the unswept ramp. Just downstream of the point of injection the ramp with 5° sweep has better spread than 10° swept ramp, but further downstream the spread is wider for 10° ramp and counter-rotating plumes are seen, an effect of side sweep angle. The 10° ramp produces the strongest vortices. The locations of the vortex centers move out from the center lines. Downstream of the ramp injectors the vortices become weaker. The axial decay of maximum injectant mole fraction is more rapid for the swept ramps than for the unswept ramps. The mixing rates of the two swept ramps do not differ very much from each other.[85] The ramp with 10° sweep angle shows the highest entropy rise. The ramp with the 5° sweep angle has the highest mixing with less entropy produced. In theory, there should be a value of sweep after which sweep no longer effects mixing.[85]

Yamauchi et al studied the effect of Mach number on the supersonic mixing generated by hyper-mixers. Tests were performed at Mach 1.8, Mach 2.4, and Mach 3. The hyper-mixers, shown in Figure 43, were designed to generate a pair of counter rotating vortices. The HM1 hyper-mixer was also expected to introduce spanwise vortices into the flow. Turbulence from vortices was generated, and

the shock waves become weaker with increasing Mach number because the incoming boundary layer makes the transition from laminar to turbulent. The RMS density values also became large along the upper edge of the mixing region. The turbulent intensity increases behind the oscillating shock, and the expansion ratio decreases as the Mach number increases.[86]

The expansion ratio of HM1 is larger than that of HM2 due to HM1 having a wedge cut from the injector causing spanwise vortices and small turbulent eddies. Increasing the Mach number reduces difference between HM1 and HM2. The Power Spectrum of Brightness (The yellow region in Figure 44) for HM1 and HM2 are higher for HM1 than Hm2 at lower Mach numbers, but higher for HM2 at higher Mach numbers. This would indicate that HM1 is more effective at mixing at lower Mach numbers and HM2 is more effective at higher Mach numbers. PIV revealed that the vortex area decreases with increasing Mach number and that circulation decreases as Mach number increases. Mixing performance also decreases as Mach number increases.[86]

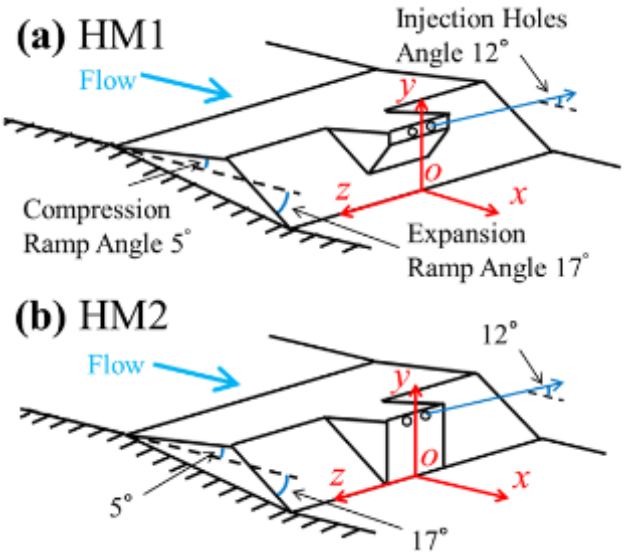

Figure 43: HM1 and HM2 Hyper-mixers[86]

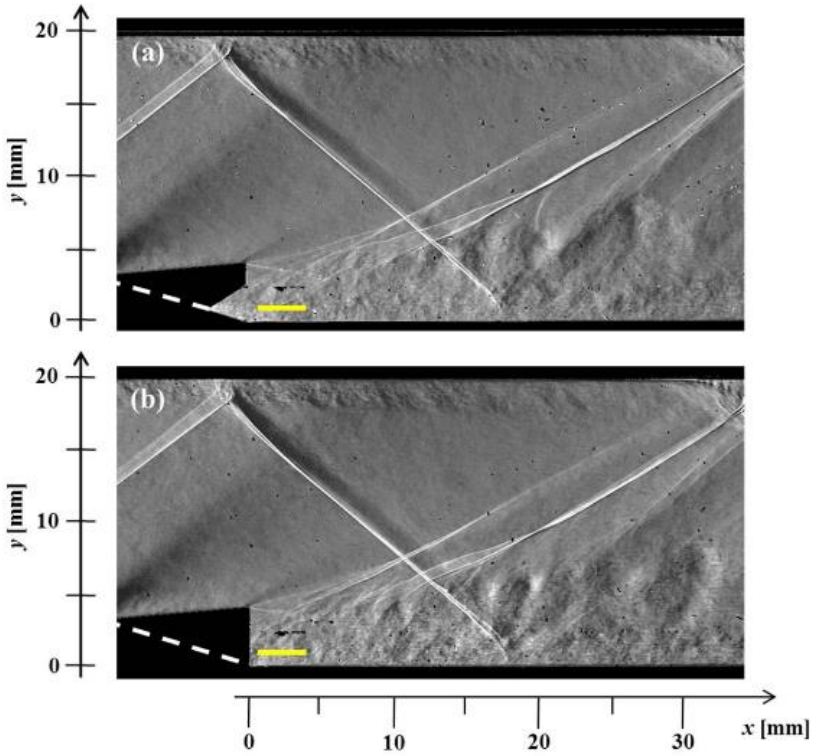

Figure 44: Pixels Analyzed for Power Spectrum Brightness[86]

Three ramp injectors (see Figure 45) were tested at Mach 1.8 and 2.4. All three ramps generate a pair of streamwise vortices 5mm in diameter with a vortex Reynolds number of 10^4. Helium was used as a fuel stand in and injected at Mach 1 from the aft end of the ramp injectors. The oil flow visualization for the HM1 type has more oil in middle due to spanwise flow near the wall, as expected (Figure 46). The BS type did not have as much oil in mid span, indicating that it was not generating spanwise flow near the wall.[81]

For Mach 1.8 the amounts of circulation for streamwise vortices of the BS type and HM1 (hyper-mixer) type are almost the same, at Mach 2.4 HM1 injector generates larger amounts of circulation. At low Mach numbers there is no difference in circulation because the incoming turbulent boundary layer is very thick, so the effect of the detailed shape of the injector may be spoiled. Circulation decreased further downstream. This is possibly because of the vorticity cancelation due to the mixing between a pair of counter-rotating vortices, which would cause the vortices to break down into small eddies.[81]

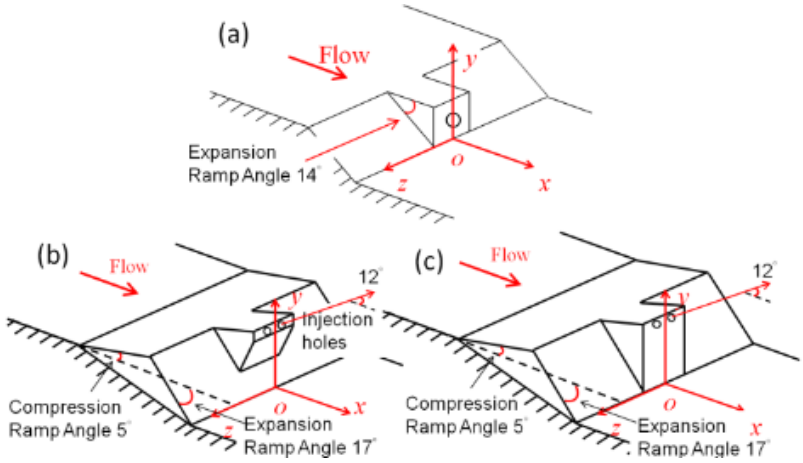

Figure 45: Ramp Injectors and Hyper-mixers[81]

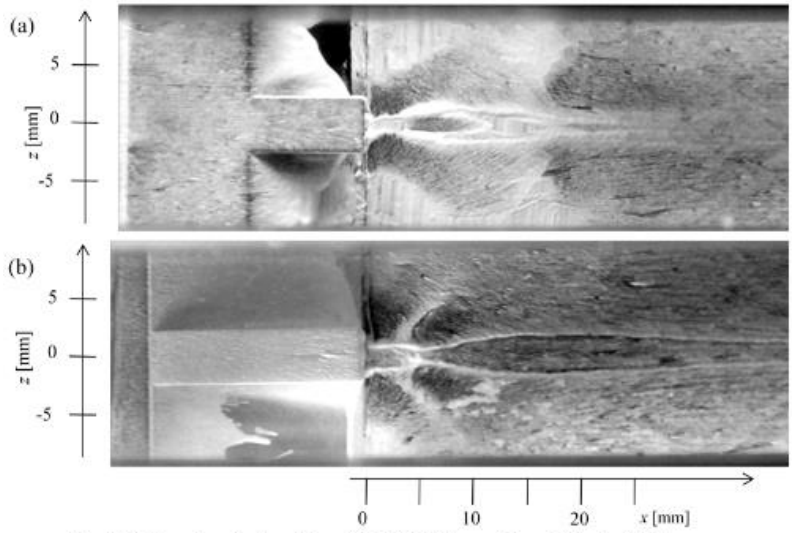

Fig.6 Oil flow visualization (M_c = 1.8): (a) HM1 type (Hyper-Mixer), (b) BS type

Figure 46: Oil Flow visualization[81]

Parent and Sislian tested cantilevered ramp injectors at s convective Mach number of 1.5 to determine the effect of ramp injectors on inert mixing in a shcramjet (shock induced combustion ramjet[87]) inlet. The mixing efficiency of a freejet was compared to the mixing efficiency of a cantilevered ramp injector. Both setups used the same fuel-air contact surface and the same fuel and air inflow conditions. For the free jet case, fuel was injected from a backward facing step.[88] (See Figure 47 through Figure 49)

Injection took place after the first shock in the inlet of an external compression shcramjet at a flight M of 11. Mixing efficiency is defined as the ratio between the reacting mass flux of oxygen and the predicted mass flow rate. In this case the increase in mixing efficiency is less from the streamwise

vortices and more from a planar jet becoming an axial free jet. The cantilevers ramp injector had the highest mixing efficiency, followed by the freejet. The planar jet had the lowest mixing efficiency. [88]

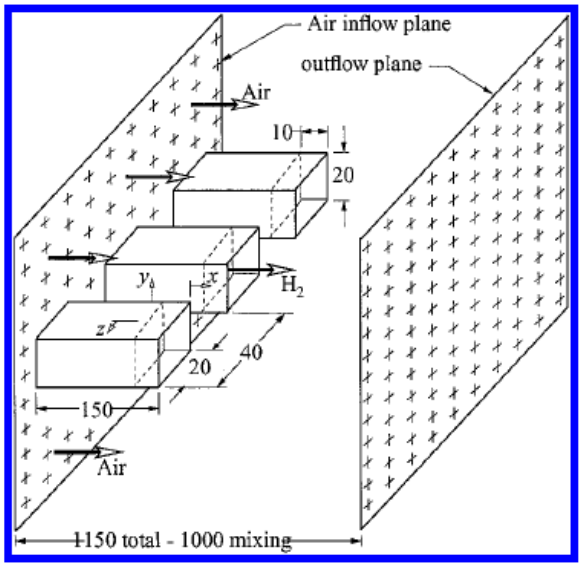

Figure 47: Design of the Freejet injector: All Dimensions are in Millimeters[88]

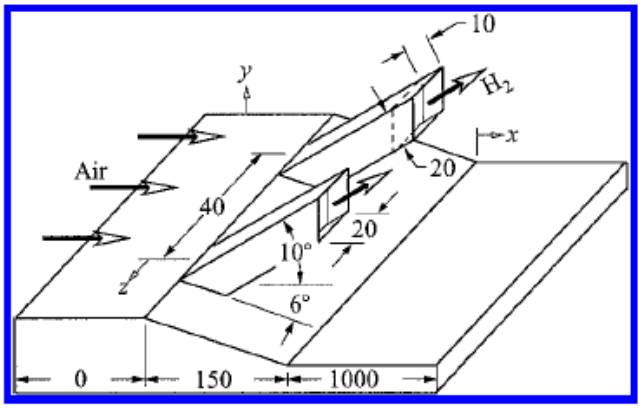

Figure 48: Design of the Cantilevered Ramp Injector: All Dimensions are in Millimeters Unless Otherwise Noted[88]

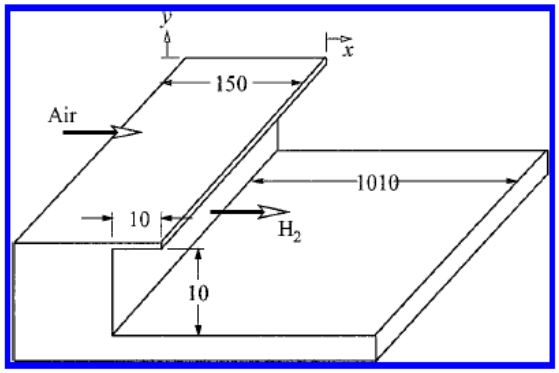

Figure 49: Design of the Planar Injector: All Dimensions are in Millimeters[88]

Tumin also sought to enhance mixing by using streamwise vortices, but on a smaller scale. Tumin found that putting small rough elements in the boundary layer can create small streamwise vortices. Sub-boundary layer elements seem to work well for convective Mach numbers less than 0.63. Optimal disturbances are defined as those disturbances that allow the flow to bypass transition and become turbulent. There is great potential for disturbance energy growth even if the flow is stable with respect to wave-like perturbations.[89]

Tumin's theory and experimental results both agreed that optimal disturbances are stationary streamwise vortices. These streamwise vortices need to be properly spaced in the spanwise direction to affect the shear flow. Tumin analyzed the optimal disturbances to predict the spanwise periodicity of the streamwise vortex generators to provide the strongest effect on the basic flow. The theory of optimal disturbances was then applied to the problem of mixing enhancement in compressible turbulent mixing layers. The results indicate that for a specific distance downstream of the vortex generators there is an optimum vortex generator spacing.[89]

The turbulent Reynolds number depends on the spreading rate of the mixing layer. The spreading rate of the mixing layer is a function of the velocity ratio and the convective Mach number. The energy growth in the mixing layer is scaled with the second power of the Reynolds number. An increase in Mach number is accompanied by an increase in transient growth effects. These effects can be used to estimate the optimal spacing of the vortex generators places on the splitter plate in parallel flow. There are two drawbacks for this model. An adequate description of the flowfield needs to include non-parallel flow effects, and the closer model used for disturbances in a turbulent mixing layer is justified by experimental comparison for travelling waves but the model may not be accurate for stationary disturbances.[89]

Inoue et al compared the performance of a ramp injector with a ramp injector cavity combination and a ramp injector shock generator combination. Helium was injected at sonic velocity into a Mach 4.0 freestream from a ramp with at 10° ramp angle (Figure 50). An oil flow technique was used on the surface to study the flow pattern generated by the ramp injector, Schlieren photography was also used. Swept ramp injectors with a sweep angle of 10° were used.[90]

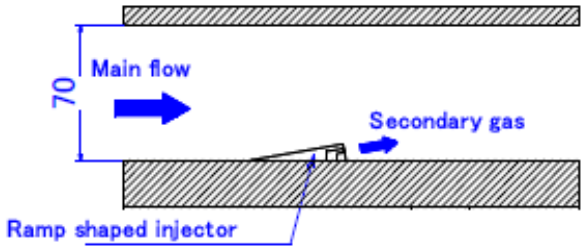

Figure 50: Ramp Injector Only Configuration[90]

The separation line due to the shock wave at the front of the ramp and the flow toward symmetry due to longitudinal vortices at the side of the ramp can be seen in Figure 51. To evaluate the mixing the volume fraction of helium in the mixing region was measured using a sampling probe with hole of 1 mm diameter. The measurements were then analyzed by using a gas chromatograph. The measurements were taken at a cross-section 100mm downstream of the injector. Eight points were analyzed in the vertical direction and four points were analyzed in the spanwise direction. The spanwise measurements were conducted at half cross section as it was assumed the flow was symmetrical. The peak concentration was found to be on the center line.[90]

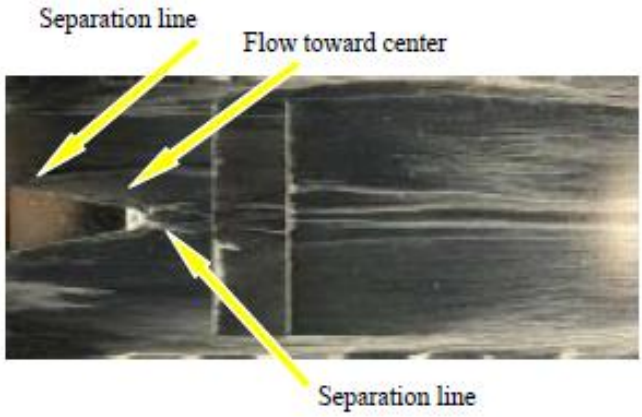

Figure 51: Ramp Only Oil Flow[90]

2.7.11 Shockwaves and Mixing

Inoue et al expected that shock waves would enhance mixing by interfering with the mixing layer. A ramp injector with a shock generator in the configuration shown in Figure 52 was tested. The shock generator generates a stable shockwave which causes downstream boundary layer separation which causes the separation shock wave. As with the case where only a ramp injector was tested, a shock is seen at the front of the ramp and flow toward center is seen. The recirculation region seen in Figure 54 is due to the interaction of the shock and the boundary layer.[90]

Downstream of the recirculation region, the flow towards center is stronger than it was for just the ramp injector. The vortices are believed to be strengthened by Baroclinic torque generated by the density gradient and the pressure gradient. More specifically, the torque is caused by the density gradient at the gas interface and the pressure gradient from shockwave. The vortex cores are not clear as was seen when only a ramp injector was tested. The maximum concentration of fuel is much smaller, about one third what it was for the ramp injector only set up. The stronger vortices generated with the help of the shock generator mean that the contact surface between the main flow and gas is large, and thus the mixing is better. Of the three test performed by Inoue et al, the shock generator test showed the smallest concentration of injected gas and the widest combustible area.[90]

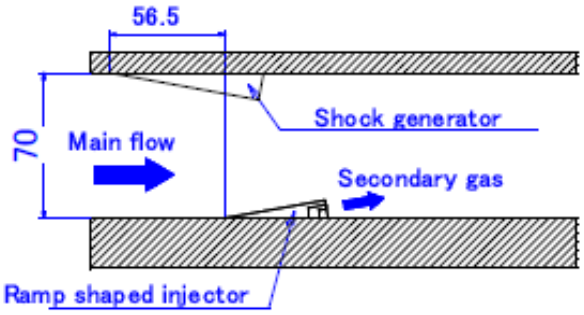

Figure 52: Ramp Injector with Shock Generator[90]

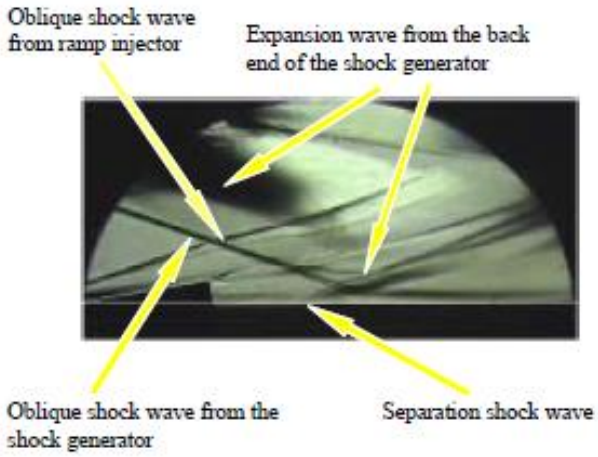

Figure 53: Shock from Ramp Injector and Shock Generator[90]

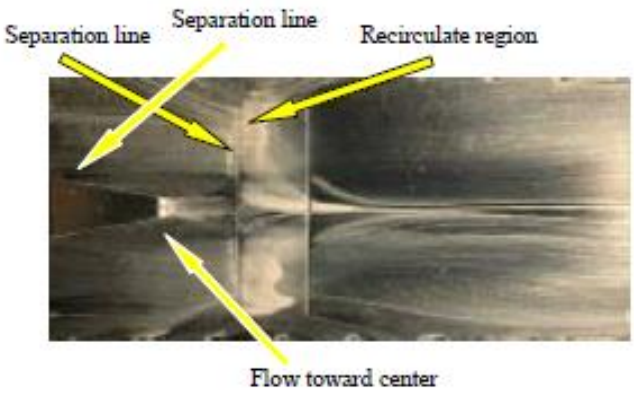

Figure 54: Shock Boundary Layer Interaction Oil flow[90]

Parent and Sislian studied the effect of oblique shocks and Prandtl-Meyer compression fans on the characteristics of turbulent mixing of a square cross section hydrogen jet in hypersonic flow. The conditions were designed to be similar to the external compression shcramjet inlet at a flight Mach number of 11 and at an altitude of 34.5 Km. The jet was perfectly expanded and the vortices generated had a convective Mach number of 1.2.[87]

The results obtained show an increase in the mixing efficiency growth by 5.7 and 6.3 times through the oblique shock and the compression fan, respectively. The compression fan produced the higher mixing efficiency because of it was able to produce a higher density increase. The interaction between the mixing layer and the oblique shock creates strong axial vortices that stretch the fuel-air interface. This is due to the Baroclinic torque term of the Helmholtz vorticity transport equation. The results show that the growth of mixing efficiency due to compression is a function of air density, convective Mach number, and the fuel-air interface length.[87]

2.7.12 Cavities

Inoue et al also investigated the effect on mixing of a ramp injector paired with a cavity (Figure 55). The cavity generated curved, unstable shockwaves. A shock wave was formed at the leading edge of the cavity. This shock was weaker than the shock wave that was created by the shock generator, thus the total pressure loss is smaller for the cavity case than for the shock generator case.[90]

Once again there was separation due to the shock wave at the front of the ramp. There was also flow toward the centerline downstream of ramp, and flow towards the centerline downstream of the cavity. The area of flow towards center is larger than the flow towards the center for just the ramp injector. The vortices were once again strengthened through baroclinic torque. The boundary layer developed quickly downstream of the cavity. As with the shock generator test, the vortex cores were

not clear. The fuel concentration was about half of what it was for the ramp injector only test. As with the shock generator test this was due to the Baroclinic torque. Some of the injected gas expanded near the lower wall and was captured by the boundary layer as it left the cavity. The cavity test showed the smallest maximum concentration and smallest total pressure loss of the three tests performed by Inoue et al.[90]

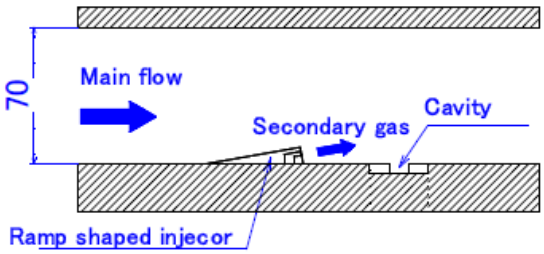

Figure 55: Ramp injector with cavity setup[90]

A novel use of a resonating cavity is used for passively controlling free shear layers. The cavity draws the acoustic energy from the supersonic jet noise and amplifies certain frequency oscillations by acoustic resonance. When forced in this manner the spreading rate of the compressible shear layer is drastically increased. At high convective Mach numbers, shear layer structures have a highly irregular wave length, and are increasingly three-dimensional.[72]

A cavity was placed just downstream of the jet exit plane and very close to one side of the shear layer. When the jet was forced on the lower side using the cavity, highly coherent large scale structures formed in the affected side of the shear layer. The cavity forcing significantly increased the spreading rate of the affected shear layer. On the forced side of the shear layer, the growth was more than three times faster than the unforced side. The cavity must force the shear layer at a specific frequency to see increased growth rate. Cavities of other sizes that resonated at other frequencies did not show the same increase in spreading and coherent structures as the initial cavity.[72]

Cavity forcing works when the transverse resonance of the cavity is matched by the longitudinal resonance along the direction of the flow. The transverse resonance of the cavity drives the flapping of the shear layer which results in pressure wave generation when the shear flow impinges on the trailing edge of the cavity. If the longitudinal resonance is such that the phase relation of the ensuing disturbances matches the flapping then a highly coherent driving may be expected.[72]

Cavity flame holders are used in scramjets for flame holding and for flame stabilization in supersonic combustors. At flight speeds above Mach 6 the air entering the combustor must be supersonic to avoid excessive dissociation of both nitrogen and oxygen gases. The time available for fuel injection and fuel

air mixing when the scramjet is travelling at such high velocities is on the order of 1 ms. Flame holding in scramjet combustion chambers can achieved by three techniques. The first is to create a recirculation area where the fuel and air can be mixed partially at low velocities. The second is the interaction of a shockwave with partially or fully mixed fuel and oxidizer. The third is the formation of coherent structures containing unmixed fuel and air wherein a diffusion flame occurs as the gases are convected downstream.[77]

For a length to depth ratio less than approximately 7 to 10, the cavity flow is termed open because the upper shear layer reattaches to the back face of the cavity. For a length to depth ratios less than approximately 2 to 3, cavities are controlled by transverse oscillation mechanism. In larger aspect ratio cavities longitudinal oscillation becomes the dominant mechanism. The high pressure at the rear face of the cavity caused by the shear layer impingement increases the drag of the cavity. For cavities with length to depth ratios of greater than approximately 10 to 13, the cavity flow is termed closed because the free shear layer reattaches to the lower wall of the cavity (Figure 56). The pressure increase in the vicinity of the back wall and the pressure decrease at the front wall results in large drag losses. The critical length to depth ratio at which a transition between different cavity flow regimes occurs depends on the boundary layer thickness at the leading edge of the cavity, the flow Mach number and the cavity width.[77]

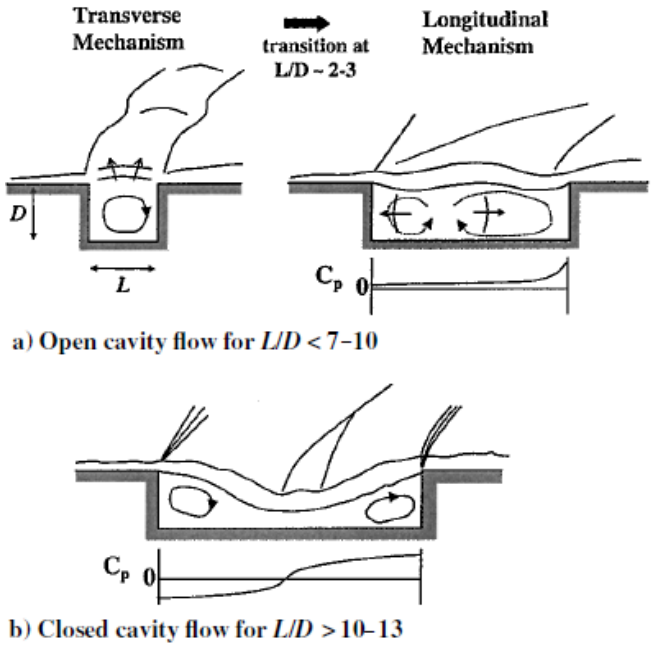

Figure 56: Flowfield schematics of cavities with different L/D in a subsonic flow[77]

Cavity pressure fluctuations depend on cavity resonance due to the cavity geometry and the small amplitude fluctuations from the shear layer. The unsteady motion of the shear layer above the cavity causes the cavity oscillations by causing mass addition and removal at the cavity trailing edge, the rear wall. The shear layer impinging on the rear wall causes freestream flow to enter the cavity. As a result of the impingement, the cavity pressure increases and creates an acoustic wave, a compression wave, which propagates upstream through the cavity at the local speed of sound and impacts the front wall of the cavity. This acoustic wave generates small vortices at the leading edge of the front wall which grow as they are convected downstream. The instabilities cause the shear layer to be deflected upward and downward resulting in a shock/impingement event on the rear wall of the cavity. (Another model assumes that the acoustic wave reflection from the front wall, rather than shedding vortices, is the cause of the shear layer deflection and therefore the impingement event on the rear wall.) The oscillation loop is closed when the instability caused either by vortex shedding or a reflected acoustic wave propagates downstream and the mass added in the beginning of the loop is ejected at the trailing edge again (See Figure 57).[77]

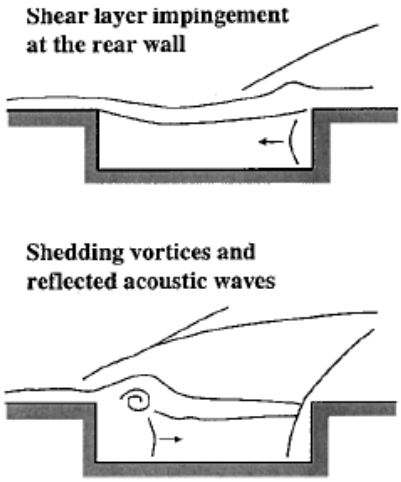

Fig. 3 Typical longitudinal cavity oscillations caused by the impingement of the free shear layer on the rear wall, which generates traveling shocks inside the cavity.

Figure 57: Longitudinal Cavity Oscillations[77]

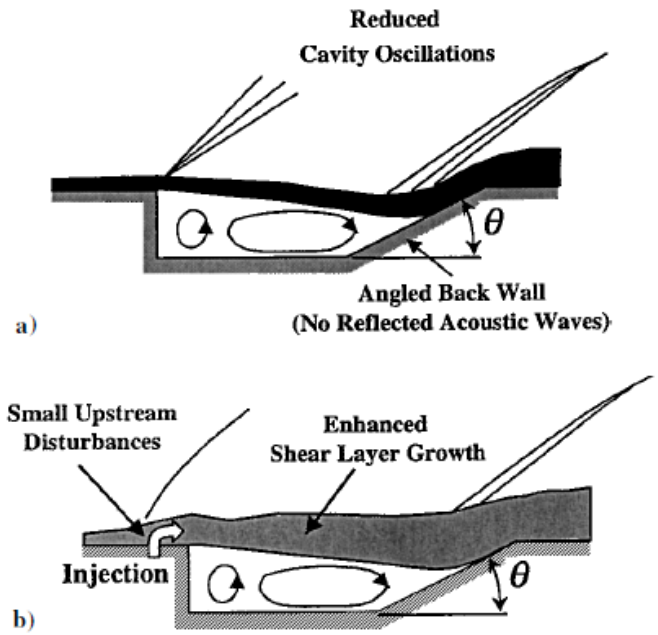

Figure 58: methods to suppress cavity oscillations: a) an angled back wall to suppress the unsteady nature of the free shear layer by eliminating the generation of the traveling shocks inside the cavity due to the free shear layer impingement and b) small disturbances produced by spoilers or by secondary jet injection upstream of the cavity to enhance free shear layer growth[77]

The oscillatory frequency of a particular mode in a shallow cavity decreases with increasing cavity length, or increasing length to depth ratio. The dominant oscillatory mode (the mode with the largest amplitude) jumps from a lower mode to a higher mode as the length to depth ratio increases. Controlling the shear layer can suppress cavity oscillations. One method in which cavities can be stabilized is by means of an oblique rear wall. In an open cavity with a 90° back wall the flow generates shock waves at the cavity trailing edge. As the shear layer reattachment point oscillates about a sharp corner periodic acoustic waves propagate inside the cavity. Some mass exchange is also seen at the cavity trailing edge. Utilizing angled back walls leads to a steadier shear layer reattachment process. Figure 59 shows the effect of the back wall angle on the flowfield structure of a cavity. A cavity with a length to depth ratio of 5 (a) shows the unsteady nature of the shear layer at the reattachment point. A cavity with a slanted back wall (b) stabilizes the shear layer reattachment process.[77]

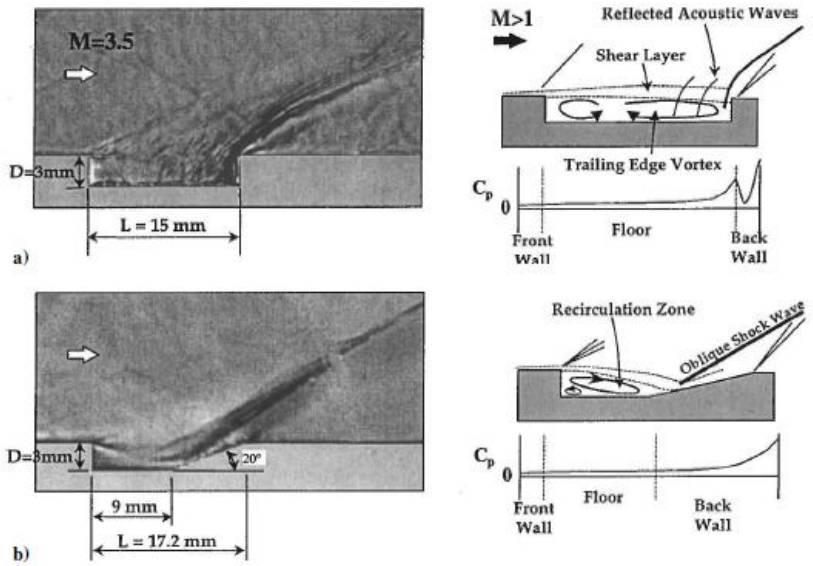

Figure 59: Cavity Shear Layer Stabilization[77]

Active control of the shear layer can be accomplished by mechanical or acoustical methods, or by fluid injection. Mass injection causes the shear layer to thicken and alters its instability characteristics such that the rollup frequency is shifted outside of the natural frequencies of the cavity.[77]

Cavities can also be used for mixing enhancement and for trapping vortices within the cavity for flame holding and stabilization of supersonic combustion. Studies by Yu and Schadow concluded that transverse acoustic waves emanating from cavities are powerful enough to affect mixing in a significant manner. Yu and Schadow suggest attaching the cavity to the exit of a jet circular nozzle to enhance mixing. When the cavity was tuned for certain frequencies, large scale highly coherent structures were produced in the shear layer substantially increasing the shear layer growth rate. The spreading rate of the shear layer was also increased by a factor of 3 for jets with convective Mach numbers or 0.85 and by 50% for jets with convective Mach numbers of 1.4. Sato et al. studied the effect of an acoustic wave emitted from a cavity and impinging on the initial mixing layer. The results showed that the mixing was enhanced by the acoustic disturbance and the rate of the enhancement was controlled by the cavity shape while the total pressure losses were small enough to be negligible (Figure 60). Stable cavities are better suited for flame holding. Unstable cavities are better suited for mixing enhancement.[77]

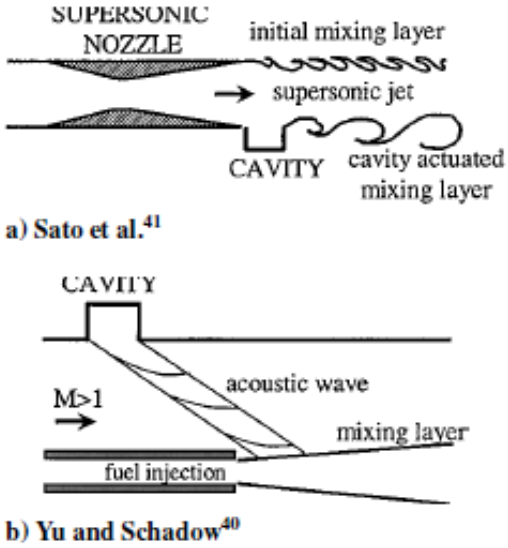

Figure 60: Cavity-Actuated Supersonic Mixing Enhancements

Rougeux and Malo-molina conducted numerical simulations to analyze the physical processes occurring within an analogous scramjet combustor three-dimensional cavity to determine the flow field and effects on varying freestream Mach numbers on typical operational values. They also wished to test the effect of three-dimensional cavity effects on performance and general flow field characteristics. Single cavities have been commonly used to provide flame holding and stabilization in a supersonic combustor environment.[91]

A common strategy to enhance fuel/air mixing utilizes a backward-facing step geometry within the combustor to produce streamwise vortices within the cavity formed by the step. The backward facing step generates a recirculation zone of hot gases within the cavity region located downstream of the step. The circulation of the hot gases provides a continuous ignition source within the combustor. Fuel injection locations can be optimized to take advantage of the vortex flow to supplement the fuel/air mixing and to stabilize the flame. The drawback to this strategy is that the step produces relatively large stagnation pressure losses.[91]

Cavities have better total pressure recovery than just a backward facing step. Most hydrocarbon scramjets now rely on flameholding cavities with flush mounted injectors. External ignition aids are commonly required at relatively low flight Mach numbers as the scramjet approaches Mach 4. The angled back wall of the cavity is to suppress the unsteady nature of the free shear layer and eliminate traveling shocks in the cavity. There is flow movement present in the transverse direction away from the wall towards the center of the channel, known as flow entrainment caused by the solid wall

interaction. The strength of the vortices within the cavity increase as the flow moves away from the solid wall towards the center of the channel.[91]

Zang et al and Yaga et al. investigated the effect of using a porous cavity with transverse injection of fuel into Mach 2.2 airflow. Helium was used as a substitute for the hydrogen fuel.[92] The number, positions, and alignment of the jets was the main parameter.[93] The experimental setup can be seen in Figure 61. A cavity with a porous wall surrounds the injected jet. The mixing is accomplished when the pressure difference causes the injected gas to circulate through the cavity. This type of cavity has the benefit of not producing drag in the engine during the off condition, as is the case with steps and wedges.[93]

The flow in the cavity was found to be driven by the pressure distributions on the bottom wall of the main duct. The jets cause bow shock waves to form in front of them, this raises the static pressure behind the shock waves forcing the fuel into the lower pressure cavity.[93] The improved mixing is due to flow induced cavity resonance.[92] The total mass flux through the porous holes increases with the number of jets. A three jet configuration was found to be the best, with one jet followed by two spanwise aligned jets.[93]

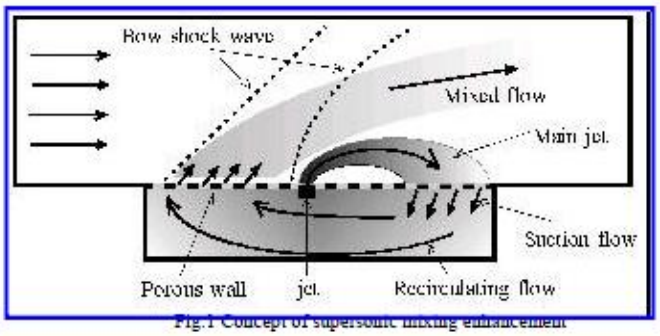

Figure 61: Porous Cavity with Injection[93]

Bueno et al investigated the effects of upstream mass injection, pulsed and continuous, on the mean and fluctuating pressures in a Mach 2 cavity flow in an attempt to control noise. Six pulsed jets with frequencies up to 1 kHz were located just upstream of the leading edge of the cavity. Continuous upstream injection can reduce the mean cavity floor pressure near the leading edge by as much as 8%. The RMS pressure at the same location on the cavity floor increased for longer cavities and decreased for shorter ones. Short cavities react differently than long cavities under both short and long duration single pulses. The longer cavities showed a larger degree of response to the pulses than shorter cavities. Thus it can be concluded that it may be easier to influence the pressure field of a longer cavity than a

shorter cavity. The fundamental and second cavity tones tended to decrease with continuous mass injection while overall sound pressure level was higher, potentially due to an increase in back ground turbulence. A peak reduction of about 5.5 dB in cavity tones and 2 dB in overall sound pressure level were achieved. It was found that continuous injection is better than pulsed injection in reducing the amplitude of the acoustic tones and overall noise.[94]

2.7.13 Pulsed Injection

For Scramjet combustion chambers, it is desirable to maximize the thrust and minimize structural weight and heat transfer. Flush injectors do not increase the drag and heat transfer but they have poor mixing and so increase the necessary length of the combustor. Ramps and struts can be designed large enough to have greater mixing than a flush wall injector, but struts and ramps also increase the drag and heat transfer. It is also required that the injectors have a capacity for flame-holding.[95]

It is also desired that the scramjet be able to operate over a large range of Mach numbers. A wide operating range means that the streamwise distribution of heat addition, and thus fuel addition, needs to be varied to avoid choking the engine and to optimize performance at each speed. Flush wall injectors distributed in the injector that can be turned on and off are more desirable than fixed structures if they can provide the required mixing.[95]

Studies have shown that continuous injection from flush injectors does not provide the necessary mixing. Jet skew and jet swirl effects while large in the vicinity of the jet tend to dissipate further downstream. Unsteady injection, or the use of small perturbations to excite the natural instabilities of the jet near the point of injection, is one way of potentially increasing the mixing of the jet. A variation on unsteady injection is pulsed jets, wherein the velocity of the jet is varied from zero to the operating velocity. So far there is very little previous work on pulsed injection.[95]

Miller et al used a three-dimensional unsteady CFD model to investigate the effect of pulsed injection on increasing the penetration and blockage of a stream into a confined, expanding, compressible, crossflow. The simulations were run with different injector conditions and geometries. The injection of a flow into the internal crossflow of a nozzle stream could be used to partially block the nozzle flow allowing for non-mechanical thrust vectoring.[96]

Pulsed injection was found to produce vortex ring structures that quickly entrain surrounding air. These ring structures had greater penetration into the crossflow and produced a larger diameter plume than steady injection.[96]

Bueno et al used a wide field PIV system in combination with fast-response pressure transducers to study the effects of upstream mass injection on a turbulent boundary layer shock interaction generated by a 0.5 inch diameter circular cylinder in Mach 2 airflow. PIV and pressure measurements were taken for a no injection case, a continuous injection case, and two pulsed injection cases with frequencies of 10 Hz and 100 Hz. The pulse duration for each case was 5 ms. Pulsed injection had big impact on the structure of the interaction depending on the type of forcing. Pulsed injection and continuous injection both cause the intermittent region to move downstream and to reduce the strength, i.e. the transverse deflection, of the separated flow. The injectors act like vortex generators in that they introduce high momentum fluid into the upstream boundary layer, making it more resistant to separation. The results show that the 100 Hz injection case approaches the results for continuous case.[97]

Kalidas and Kurian investigated pulsed injection into supersonic flow. A solenoid valve operated by means of voltage pulses was used to provide the pulsed injection. Eight combinations of frequencies and pulse widths were tested and compared to continuous injection. MIE scattering images were taken at various locations downstream of the point of injection. Mixing was quantified by calculating the mole fraction distribution and by estimating the five parameters: degree of unmixedness, mixed area, weighted area of mixing, penetration depth, and spread.[98]

The results show that the mixing was better with pulsed injection than with continuous injection. Also the mixing efficiency increases as pulse width decreases. The results also showed that perfectly expanded jets displayed better mixing than under expanded jets. If good mixing is desired it is best not to raise the total pressure of the jet in order to increase the mass flow rate.[98]

Malo-Molina and Ebrahimi used third order LES simulations to model a pulsed injector in a single cavity flame holding configuration supersonic combustor. The model had a rectangular cross section with a freestream Mach number of 2.2 that was intended to mimic the HIFiRE-II. Pulsed injection and steady injection, both with an equivalence ratio of 0.7, were compared. Fuel was injected in 0.8 ms pulses at 30° at a distance of three times the depth of the cavity upstream of the 30° cavity.[99]

The cavity had a length to depth ratio of 5 and a depth of 1 inch. The angled rear wall of the cavity serves to suppress the unsteady nature of the free shear layer and eliminates the traveling shock inside the cavity. The cavity produced strong coherent vortices. Long cavities, with length to depth ratios greater than 10 produce vortex shedding. This vortex shedding creates cavity oscillations and unstable flames, but short cavities are not as good for entrainment.[99]

The results show that pulsed injection leaves residual fuel in the cavity that increases between the pulsation cycles and slightly decreases towards the middle of the cycles. The pulsed injection case saw

larger fuel entrainment and overall mixing enhancement downstream into the core flow than the continuous case.[99]

Cutler et al developed a new injector designed to provide high frequency, on the order of 10 kHz, pulsed injection in a supersonic crossflow. The injector is formed from the fixed internal surface of the nozzle and a freely rotating 3 or 4 sided wheel embedded within the device. The flow induced rotation of the embedded wheel causes the nozzle throat to open and close. The injector was tested with helium being injection normal to a Mach 2 crossflow.[100] The injector and the experimental set up can be seen in Figure 62 and Figure 63.

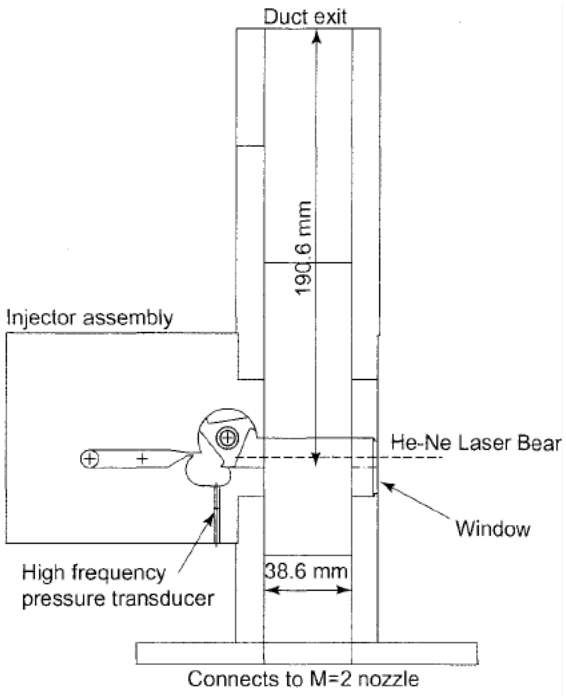

Figure 62: High Frequency Pulsed Injector Experimental Set Up[100]

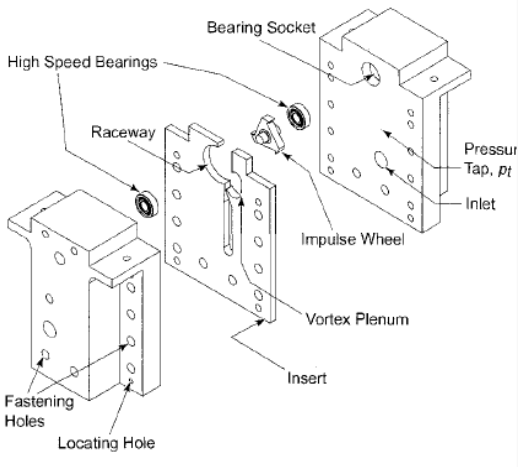

Figure 63: High Frequency Pulsed Injector Expanded View[100]

The mechanism of mixing for normal pulsed injection is vortex ring rollup. A vortex forms at the start of the injection pulse at the air fuel interface. The vortex then grows during the injection and then detaches at the end of the pulse.[100]

The target injection frequency calculated from the duct height and the velocity was 13.3 kHz. The pulsed jet was viewed with Schlieren photography. The helium jet was also seeded with ethanol and illuminated with a laser light sheet. Subsonic injection and supersonic injection into the crossflow were both compared.[95]

For a subsonic steady jet in crossflow after the jet enters the crossflow it turns downstream and forms a counter-rotational vortex pair embedded in the jet plume an in the supersonic flow.[95] Pulsing a subsonic jet in crossflow causes the jet plume to split into two streams. One stream consists of a series of compact vortex ring structures oriented roughly parallel to the wall and moving away from the wall due to self-induction. The other stream roughly follows the same path as the jet without pulsation.[95]

The Strouhal number is a non-dimensional number that describes oscillatory flows like vortex shedding. It is a function of injection frequency as seen below in Equation 2.22.[96]

$$St = \frac{fd}{u_j} \qquad \textbf{(2.22)}$$

In Equation 1, f is the pulsation frequency, or vortex shedding, frequency, d is the jet diameter, and u_j is the jet velocity. The duty cycle of the pulsed injection is the fraction of the cycle time that the jet is on. Shorter duty cycles tend to favor the formation of the vortex ring structures. The stroke ratio is the length of the column of fluid in a cycle divided by its diameter. It can also be defined as the duty cycle divided by the Strouhal number. The stroke ratio determines the structures seen in the injected plume.

For stroke ratios less than 4 the structures are compact vortex rings. For stroke ratios between 20 and 75 the structures are turbulent puffs. For stroke ratios between 4 and 20 the structures formed are something in between the coherent vortex rings and the turbulent puffs. For the subsonic pulsed jets, mixing is best improved around Strouhal numbers of 0.1.[95]

In a supersonic crossflow, injection creates a bow shock that is important in the formation and rollup of the dominant longitudinal vortex pair. Bow shocks or oblique shocks generated by ramps often causes boundary layer separation. This separation lifts the boundary layer vorticity away from the wall and reorients it downstream. The bow shock curvature may also create significant vorticity. This vorticity is often entrained into the jet plume. For a pulsed jet the bow shock is unsteady which leads to time dependent patterns of vorticity.[95]

The Strouhal number requirements for high speed mixing lead to very high frequencies being needed for pulsed injection, on the order of 10 kHz, that depend on the speed of sound of the injected gas and injector diameter. However the experimental results show the greatest unsteadiness at lower frequencies of injection. The results also indicate a modest reduction in mean plume cross sectional size, and thus a reduction in mixing, with pulsation as compared to the steady injection case. But the pulsed case did show an increase in mean helium penetration over the continuous injection case.[95]

Kouchi et al experimented to see how pulsed injection effected jet penetration and mixing performance in a Mach 2.5 crossflow. Helium and nitrogen were both used as injected gases. Helium was used because it is analogous to hydrogen and nitrogen was used because it is a good approximation of gaseous hydrocarbons. Both of the gases were injected at sonic velocities perpendicular to the flow. The results of the pulsed jets were compared to the continuous injection case.[101]

The jets were pulsed at frequencies up to 1 kHz, with Strouhal numbers of approximately 3.5*10^-3. The fuel supply rate was determined by the injectant pressure, the duty cycle, and the pulsation frequency. A smaller injector was found to be better for penetration and mixing. The pulsed injection requires increased injection pressure but has the same mass flow rate as constant injection so for pulsed injection the penetration into the main flow is better. Pulsed injection also had better penetration and better mixing through the fluctuation of large scale eddies associated with the flux of the bow shock in front of the jet. At the beginning of each pulse the starting vortex induced a vertical velocity component which resulted in better penetration, large scale vortices, and a mixing rate increase. When the pulse is short the injectant vortex rings interact with each other.[101]

Kouchi et al also experimentally and numerically looked at the penetration characteristics of pulsed helium gas, with a pulse rise time 0.25 ms, a pulse width 0.75 ms into Mach 2 crossflow. Fully

modulating pulsed injection was utilized where the flow is completely shut off for part of the cycle. This method of injection keeps the equivalence ratio constant while increasing the injection pressure.[56]

At injection frequencies above 10 kHz, vortex rings were generated for each pulse cycle. These vortex rings increased the jet penetration and mixing. At higher frequencies of injection the jet penetration rapidly decreased with increasing frequency. The jet penetration is dominated by the dynamic pressure ratio and the pressure ratio of the injection pressure to the back pressure of the crossflow. The eddy size was larger near the injector for pulsed injections than for continuous injection. Frequency is expected to have a great effect on mixing and penetration. At frequencies higher than 10 kHz the pulses tend to blend together and the advantage of pulsation is lost. It is expected that as the pulsation frequency is increased the flow will come to approximate the steady injection case. [56]

Randolph and Chew performed a study where gas is injected in pulses into a Mach 2.5 cross flow at various momentum flux ratios. For comparison, steady flow at matching exit pressures and momentum flux ratios was also injected. Schlieren video of the freestream/jet interaction was used to measure the jet penetration depths at six downstream stations.[102]

Increasing the jet pressure in an attempt increase the penetration of the jet into the main flow causes the jet to become underexpanded. Underexpanded jets create a Mach disk, which is a normal shock feature. The Mach disk reduces the dynamic pressure of the gaseous injectant to a fraction of its original value. This is detrimental because the dynamic pressure represents the energy available to cause turbulence and mixing in a supersonic flow. It is desirable to increase penetration without increasing the injectant to freestream flux ratio.[102]

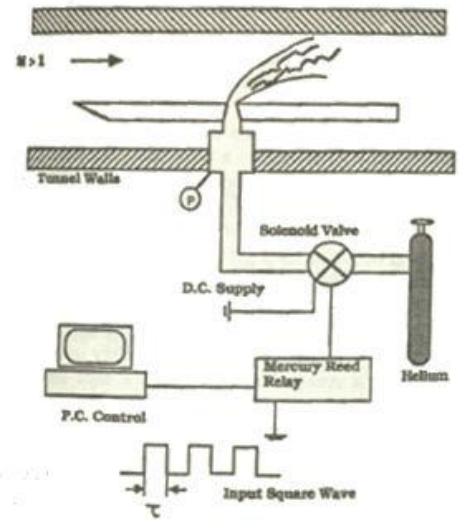

Figure 64: Schematic of Pulsed Injector set up[102]

Figure 64 shows a schematic of how the jets were injected into the main flow. Duty cycle, frequency, and injectant exit pressure could all be varied. Low pressure pulsed injection has been shown to have better fuel mixing and burning characteristics in the absence of a cross flow than steady injection at the same exit pressure. The injectant frequency in this experiment was 1 Hz with a pulse width of 250 ms. The free stream of Mach 2.5 and the injection pressures ranging from 206.8 kpa (30psia) to 696.4 kpa (101 psia) were used for steady and pulsed injection.[102]

The acceleration of the injectant through the time interval Δt for 0 velocity to Mach 1 at the injector exit produces an inertial force which pushes the Mach disk further into the cross flow in much the same way as increased injection pressure for the steady case does. The Mach disk is essentially the limit of penetration height for an underexpanded injectant in a supersonic flow. A finite time interval must pass before the Mach disk is established in the flow, during this interval the injectant may be able to penetrate the flow with little hindrance from shock effects. It was found that the pulsed jet penetrates the main flow 12% further on average than the steady jet at the same momentum flux ratio.[102]

2.8 Conclusion

Numerious methods to enhance the mixing between streams of fuel and supersonic airflow. As the supersonic mixing efficiency drops with increasing Mach number, many of these methods involve exciting the votical structures at the shear layer interface between the fuel and air structures. Other methods involve stretching the interface through the creation of streamwise votices. Compared to the other methods studied, pulsed injection is a relatively underdeveloped area with many new avenues of study yet to be researched.

3 Review of Facilities and Data Acquisition Methods

3.1 Supersonic Wind Tunnels

Typical supersonic wind tunnels have test section Mach numbers between about 1.3 and 5. If the test section Mach number is below Mach 1.3, then there are transonic effects. Transonic tunnels typically operate up to low supersonic Mach numbers to cover the range of transonic effects. If research needs to be performed at Mach numbers above Mach 5 a hypersonic facility is needed.[103]

Subsonic, transonic, supersonic, and hypersonic wind tunnels each have their own respective design problems. Supersonic wind tunnels can be designed to operate for short periods of time, at intermittent intervals, or designed to operate continuously at certain Mach numbers and Reynolds numbers. For one intermittent type of wind tunnel the air is evacuated from a large tank. Due to the high pressure

gradient atmospheric air is drawn through the tunnel and into the tank. The blow down type tunnel uses air from a high pressure air supply, usually on the order of 10-20 atmospheres. The air is then blown through the tunnel and exhausts into the atmosphere. The ability to change the total pressure and temperature at the entrance of the tunnel permits testing at various high test section Reynolds numbers. These two types of wind tunnels can be combined, wherein the tunnel has both high pressure tanks providing air to the wind tunnel which then flows into depressurized tanks providing for even higher wind tunnel pressure gradients.[103]

The third type of wind tunnel is the continuously operating, or closed circuit, wind tunnel. These types of wind tunnels must first be filled with dry air provided by an external dryer. Dry air is necessary because water condensation occurring during the expansion of the air in the supersonic nozzle would destroy the flow uniformity in the test section, leading to inaccurate test results. After the dryer, the subsonic air flows through several screens designed to reduce the airstream turbulence to a desired level. A convergent divergent nozzle is used to accelerate the previously subsonic flow to the desired supersonic test section Mach number. The test section Reynolds number can be varied by varying the supply pressure at a given temperature. After the test section, a convergent divergent diffuser decelerates the flow back to a low subsonic velocity. This deceleration process is non-isentropic and thus results in losses in total pressure. A compressor is needed to raise the air pressure back up to the supply pressure of the wind tunnel. Usually, axial flow or centrifugal compressors are used. The compression process raises the temperature of the air above the desired temperature so a cooler is needed to remove the heat from the air. The heat removed from the air must be equal to the power supplied to the compressor plant so that the internal energy of the air in the tunnel circuit remains constant and no work is done by the air.[103]

The contraction section of the supersonic nozzle must be shaped so that the flow is accelerated uniformly. This is done by designing the wall contours to have gentle curves that result in a flow with a monotonically decreasing pressure. The divergent nozzle section must be designed to produce uniform, parallel, shock free flow in the test section at the desired Mach number. Nozzles can be constructed from steel blocks that can be interchanged depending on the desired Mach number. These types of nozzle can only be used for one specific Mach number and often take time to change out. Far more common are nozzles made of flexible steel plates that can be bent by a set of pin-ended jacks. The advantages of these types of nozzles are that they can run at a wide variety of Mach numbers, the nozzle can be calibrated to give very uniform flow in the test section, and the test section Mach number can be changed while the tunnel is running.[103]

Tests section dimensions depend on the tests being performed but often include doors with glass windows so that optical measurements can be performed. Nozzles and diffusers are usually two-dimensional (which allows them to be easily variable) giving them square or rectangular cross sections, thus the test section should also be rectangular or square. Square and rectangular cross sections also make acquiring optical data easier as it allows for doors with flat plate windows that will not distort the light.[103]

For low Mach numbers the diffuser may simply be a diverging fixed duct in which transition to subsonic flow takes place by means of a pattern of shock waves and their interactions with the thick turbulent boundary layers. For higher Mach number tunnels (tunnels that operate above Mach 2.5) or if better total pressure recovery is desired, variable convergent divergent diffusers are used to decelerate the flow. During the starting process the throat of such a convergent divergent diffuser must be opened sufficiently to permit the establishment of supersonic flow in the test section. After the tunnel has started, the throat of the diffuser may be closed down to its running position, resulting in better pressure recovery.[103]

3.2 Data Acquisition Methods

3.2.1 Schlieren Photography

Schlieren Photography was used by Papamoschou and Roshko to study the growth rate of shear layers.[16] Schlieren and shadowgraph methods are the most common methods for visualizing compressible mixing flows.[107] Schlieren photography is a noninvasive flow visualization method. It consists of a light source, sometimes a condenser lens, two concave mirrors, two knife edge slits, a lens, and a camera (Figure 65). The light is projected from the source through the first knife edge slit and onto the first mirror. The first mirror reflected the light as a parallel beam through the region of interest of the flow field. Density gradients in the flow field (due to shock waves, expansion waves, etc.) distort the parallel beam of light by refacting the light that passes through the regions of higher density more so than the light that passes through regions with lower density. The beam of light is then collected by the second mirror and reflected through the second knife edge slit. This second knife edge cuts off the refracted light so that when the light is focused through the lens onto the recording device, the camera sees the denser regions as darker than the less dense regions.[104]

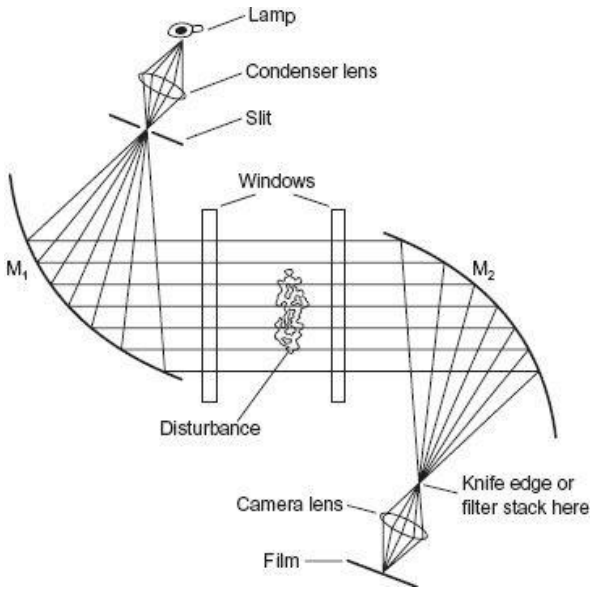

Figure 65: Schlieren Photography Set Up[105]

It is to be noted that the images generated by Schlieren methods are only a cross sectional average of the test section flow conditions because the image generated is integrate spatially through the flow. Schlieren Photography is very good for studying two-dimensional flows, but cannot always reveal all of the nuances of three-dimensional flows and thus can give a misleading picture if the flow is inherently three-dimensional.[106]

3.2.2 Surface Oil Flow Technique

An Oil tracer is applied directly to the wall of the wind tunnel where the flow along the surface is to be studied. This oil is composed of lamp black, STP motor oil, and kerosene.[76] During the wind tunnel test the oil tracer movements are recorded by video camera.[76] When the test is complete clear tape is applied to the wall and then carefully removed and stuck to piece of paper to preserve final pattern for later analysis.[76]

3.2.3 Pitot Probes

One of the most common instruments used to measure both the stagnation pressure and static pressure of a flow is the Pitot-static probe, also known as the Prandtl tube. This device is used to calculate the free stream velocity of the flow, either in a wind tunnel or mounted on an aircraft. Pitot tubes when used in wind tunnels are typically inserted through the wall of the tunnel and bent at a 90^{o} angle so that it points directly into the flow. The pobes may have several small holes drilled around the perimeter of the tube perpendicular to the direction of flow and a hole drilled down the center axis of the tube aligned parallel to the flow. The holes on the outside are used to calculate the static pressure of

the flow and are connected to one port of a pressure transducer. The center hole is used to determine stagnation pressure and is connected to a separate port of the pressure transducer. From there the pressure difference can be calculated. There are a few different options for the shape of the tip of the probe, and the designs vary for subsonic or supersonic flow. For use in supersonic flow, the ideal tip shape is a National Physical Laboratory modified ellipsoidal Pitot tube which provides the most accuracy results at higher velocities.[107]

Pitot probes were also used by Papamoschou and Roshko to define the thickness of the shear layer. Pitot probes allow for pressure and velocity measurements to be taken throughout the flow, but it is a highly invasive technique as the probe will generate shockwaves in supersonic flow. It is also difficult to obtain accurate data near a wall using a Pitot probe as the probe has a finite thickness and can only be brought so close to the wall.[16]

3.2.4 Double Hot Wire Probes

Another method of evaluating supersonic mixing is the double hot wire probe. The probe uses two kinds of wire with different characteristics of heat transfer to measure both the mass flux and the concentration, hence it is referred to as a double hot wire probe. Instantaneous fluctuations in mass flux and concentration can be simultaneously measured by using the double-hot-wire probe with a constant voltage anemometer circuit with 500 kHz bandwidth. While the probe is invasive it is advantageous in that most other processes cannot detect the instantaneous mixing process.[108]

The probe was first tested on an air-helium mixing layer and streamwise vortices with good results, though it tends to underestimate the helium concentration. Problems arise when the turbulence is very small scale because the two wires need to have some space between them and the wires themselves are not infinitesimally small so each wire is sampling a slightly different area. Electrical noise also made small differences difficult to measure.[108]

3.2.5 Laser Doppler Velocimetry (LDV)

Laser Doppler Velocimetry is an optical method for measuring the velocity and direction of particles seeded in the airflow. The airflow in the wind tunnel is first seeded with liquid or solid particles with diameters on the order of 1 μm. (Atomized silicone oil less than 1 micron in diameter has been successfully used.[30]) These particles are then entrained evenly throughout a fluid. The fluid with the entrained particles passes through the intersection of two laser beams. The particles cause the laser light to scatter. The scattered light received from these particles fluctuates in intensity. The frequency of the intensity fluctuation is equivalent to the Doppler shift between the incident light and the

scattered light, and is thus the fluctuation is proportional to the component of particle velocity which lies in the plane of the two laser beams and is perpendicular to their bisector. The velocity direction can be fixed if one of the laser beams has a frequency slightly different from that of the other. All three components of velocity can be measured by crossing 4 or 6 laser beams of different wavelengths or polarization in the same measuring volume, and then separating out the scattered light using filters. The frequency can be measured using digital counters (for high data rates of above 50 per second), photon correlators (for low data rates and signal levels), or spectral analyzers (for if the Doppler shift frequency is not over a few Megahertz). [109]

For Laser Doppler Velocimetry to be effective, the laser used must have excellent frequency stability, narrow line-width, small beam diameter, and a Gaussian beam intensity profile (meaning that it is brightest at the center). Typically, Helium/Neon or Argon ion lasers are used. These lasers typically have power levels that range from 10mwatts to 20 watts.[109]

Laser Doppler Velocimetry is capable of spatially precise point measurements, and can accurately measure speeds ranging from mm/s to supersonic velocities. Measurement point distances of up to 7m have been successfully used in large wind tunnels.[109]

Laser Doppler Velocimetry has a number of disadvantages. It is limited in that it can only measure at a single point. Also, data arrival times are dictated by the particle arriving in the measuring volume, not necessarily by when the user wants to sample data. Also, particle velocities and their derivatives can differ substantially from the flow velocity, especially in vortex cores and across shocks. Seeded particles small enough to follow the flow precisely may be too small to produce a signal above the noise threshold. Greater noise levels are often seen at higher speeds. It is also possible that radio frequencies interfere with the signal. The signal level depends on the angle of the detector, which can potentially pose optical access problems. Mie scattering intensity is much better in the forward direction, but it is difficult to set up forward receiving optics and have them remain aligned to the moving measurement volume. Optics alignment times range from 3 hours for a 1-component system to a day for a 3-component system. The Optical alignments may also be sensitive to vibrations. These problems can be alleviated with fiber optic probes, but this comes at the cost of signal level decrease due to fiber power loss. Ion lasers also tend to deteriorate in harsh, particle-laden labs. Breathing micron-sized metal oxide particles used for these studies can be hazardous to the health of the researchers, requiring them to wear particle masks. Class IV lasers pose severe eye hazards, yet aligning 2 to 6 beams in a 0.1mm cube of space 21 feet away is not easy when wearing laser goggles. [109]

3.2.5.1 Two Color Laser Doppler Velocimetry

The LVD system is characterized as a 320 MHz two color off axis single burst system. It can measure Doppler frequencies up to 320 MHz. Two different colored laser beams were used so that two velocity components could be measured simultaneously. The system collects forward scattered radiation off the axis of the focused laser beam. The velocities of single particles are measured as they individually pass through the measurement volume. Each optical cell is used to split, transmit, and focus one color beam while simultaneously receiving the forward scattered light of the opposite color beam. The measuring volume formed by each set of transmitted laser beams is essentially an elongated ellipsoid. When the two ellipsoids intersect, the spatial resolution is defined by the region that is common to both beams. The advantages of this type of arrangement are that two velocity components can be detected simultaneously from a single particle passing through the probe volume and the signal-to-noise ratio is greatly improved over the single beam method. The equipment needed includes two photomultiplier tubes (which convert scattered light to an electrical format), a dual channel signal processor (which measures the Doppler frequency of the single-particle burst, performs quality checks on the signal, and if the data is acceptable transfers it to the computer), a system minicomputer, CRT histogram display. Solid titanium dioxide, alumina, and spherical latex particles have been used.[66] See Figure 66 for set up.

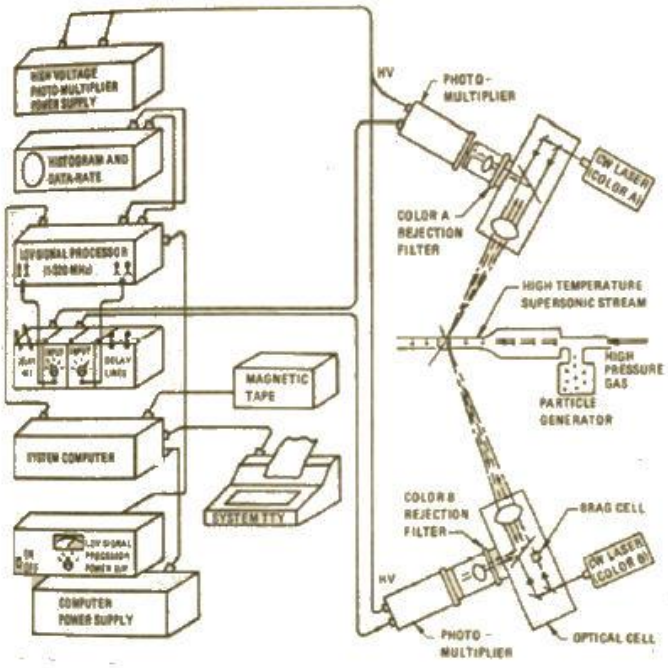

Figure 66: Two color, off axis, 320 MHz, sing burst laser Doppler velocimeter[66]

3.2.6 Particle Image Velocimetry (PIV)

In Particle Image Velocimetry, titanium dioxide particles are used as tracers. Illumination is provided by a pulsed Nd:YAG laser which can deliver collinear beams of 532nm light at up to 400mJ per laser per 8ns pulse. Particle velocity vectors are calculated by means of a Fast Fourier Transform based autocorrelation whose peaks are localized using a Gaussian curve fit. PIV is used to obtain side view and plan view planar velocity fields of turbulent shear layers over a range of compressibility. The resulting well resolved high-yield data sets lend themselves to both structural and statistical interpretation.[27]

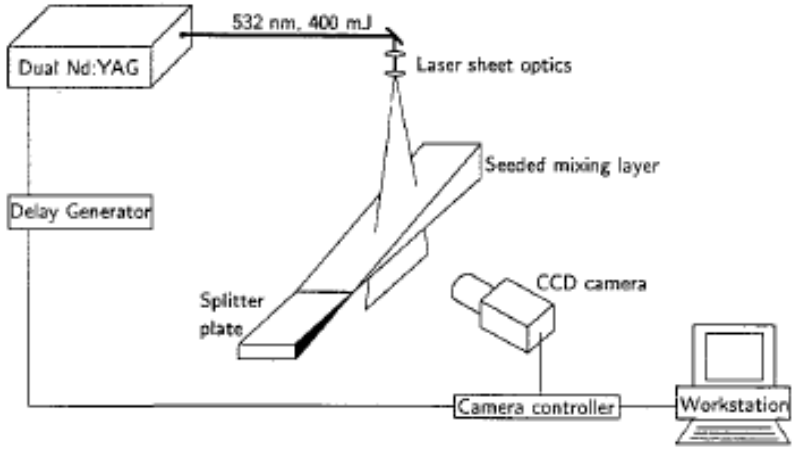

Figure 67: Particle Image Velocimetry Setup[27]

3.2.7 Planar Laser Induced Fluorescence (PLIF)

3.2.7.1 PLIF

Mixing is often characterized by local flow properties like concentration and density. These flow properties need to be measured accurately. Optical measurement methods are better than probes because they are non-intrusive. For planar laser induced fluorescence, a laser source, usually one that can be pulsed and is tunable in wavelength, is used to form a thin sheet of light which traverses the flowfield. Lasers commonly used in PLIF imaging are neodymium: yttrium aluminum garnet (more commonly referred to in literature as Nd:YAG) lasers, pumped, excimer-pumped, and flash-lamp pumped pulsed dye lasers, excimer and Raman-shifted excimer lasers, and less commonly, ion lasers and ion pumped dye lasers. Pulsed lasers are preferred because their short pulse lengths along with typically short fluorescence lifetimes, less than 100 ns, provide the ability to freeze motion in the flow field.[111]

If the laser wavelength is resonant with an optical transition of a species present in the flow a fraction of the incident photons will be absorbed at each point within the illuminated plane. A fraction of these absorbed photons may subsequently be re-emitted with a modified spectral distribution which changes for different molecules and varies with flow field conditions. The emitted photons, known as fluorescence, may be viewed as a form of molecular scattering and constitute the signal of interest in PLIF imaging. A fraction of the fluorescing light may be collected and imaged onto a sensitive, usually image intensified, solid state camera. This provides an image of the product of absorber number density. By various strategies the signal can be related to other flow field properties of interest. Other parameters can be computed such as gradients and dissipation factors from species data, heat flux vectors from temperature data, and vorticity from 2D velocity data. PLIF is good for detailed studies of flow field structure as well as for visualizing flames, shockwaves and recirculation zones.[111]

The resolution of the image is determined by the pulse length of the laser (typically 5-20 ns) and the resolution on the camera. PLIF imaging is more useful than Schlieren imaging because it provides imaging of a single plane rather than integrating through the flow field. Thus it is better for resolving three-dimensional flow structures. For PLIF imaging no seeding needed.[111]

The planar laser-induced fluorescence with acetone tracer method (PLIF) has good temporal and spatial resolution, a strong fluorescence signal, and is nonintrusive and safe to use.[110] Unlike several other flow imaging techniques, PLIF may be combined with particle image velocimetry (PIV). This allows for the simultaneous measurement of a fluid velocity field and species concentration. PLIF can also be used to indirectly determine species concentration, temperature, velocity, pressure, and density.[111]

The planar laser induced fluorescence method has some drawbacks as well. Maximizing the light gathering efficiency of an optical system typically degrades its spatial resolution. The flowfield must contain molecular species with an optical resonance wavelength that can be accessed by laser. Temperature measurements typically require two laser sources. Velocity measurements are practical only for high Mach number flows, i.e. Flows that are near sonic or supersonic. The signal-to-noise ratio is often limited by detector shot-noise. Fluorescence interference can be caused by other species in the flowfield, especially from hydrocarbons in high pressure reacting flows. The attenuation of the laser sheet across the flow field or the reabsorption of fluorescence before it reaches the detector can lead to systematic errors.[111]

The PLIF method cannot be directly related to physical quantities because the fluorescence signal depends on both the mole fraction of tracer molecules and the local thermodynamic properties. The fluorescence signal ratio approach is used to remove the thermodynamic dependencies of the laser

induced fluorescence signals so only mole fraction is measured. This is done by taking the ratio of two images recorded in two different seeding conditions. It is not clear whether this approach is applicable in all cases.[110]

Takahashi et al compared the injectant mole fraction distribution from the acetone PLIF method to the data from gas sampling in the flowfield of a sonic transverse injection into Mach 1.9 flow. Nitrogen gas was used as an injectant. The laser beam was expanded into a sheet 30 mm wide and 0.5 mm thick. The reason for the expansion was so that the flowfield could be measured with a parallel light sheet.[110]

Sonic injection was used because the flow is supposed to be choked at the jet orifice. The acetone concentration was kept below the saturation level. The air density change from the acetone was 1% at most. This small of a density change can be considered negligible for determining the injectant mole fraction. It was hard to get good data near the walls, but overall the generalized method agreed better with sampling data than Hartfield's method for determining the injectant mole fraction, thus validating the method.[110]

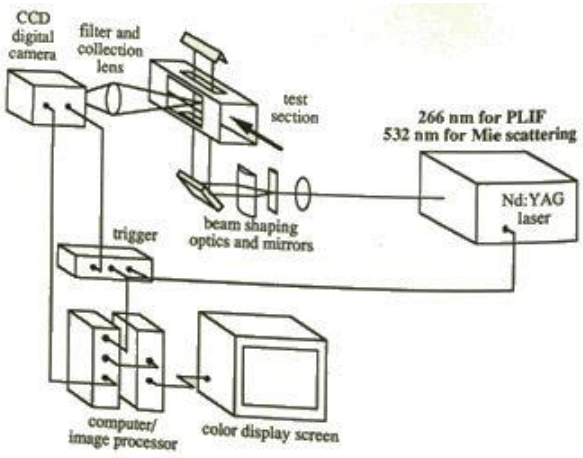

Figure 68: Planar Laser Induced Fluorescence setup[76]

3.2.7.2 DOEPLIF

Bunyajitradulya and Papamoschou developed an optical method for studying the evolution of large scale turbulent structures in high speed shear flows. The method is double offset exposure planar laser induced Fluorescence or DOEPLIF. As in the PLIF method the laser induces fluorescence with gaseous acetone as the tracer particle. In this method two laser sheets generated by a pulse laser (or the fourth-harmonic (266 nm) outputs of two independently pulsed Nd: Yag Lasers) enter the test section. The upstream sheet is triggered first and downstream sheet is triggered second with a time delay. Both sheets are then imaged onto a single detector. The DOEPLIF method enables measurement of

convective velocities and provides detailed visualization of the evolution of turbulent structures. If the time delay is right and the laser sheets are close enough together the turbulent features seen in the first sheet can be captured in the second.[19] By measuring the distance traveled by identifiable features one obtains their convective velocity.[38]

Gaseous acetone, at mole fractions around 1%, was used as the fluorescing agent. Acetone was injected in liquid form through atomizing nozzles approximately 1.2 m upstream of the settling chamber leading to the supersonic nozzle. The Acetone could be injected in the stream on either side of the splitter plate. Little variation in convective velocity is detected by injecting acetone in the fast or slow streams. Acetone appears to mark well the turbulent structure across the entire thickness of the shear layer.[38]

3.2.8 MIE Scattering

The planar Mie scattering technique is an optical technique that allows for the direct visualization of fluid mixing in supersonic flows. The mixed fluid is visualized by a laser light sheet scattering from small alcohol droplets which condense as a result of the mixing of a vapor laden subsonic stream with a cold supersonic stream. The condensation reveals details of the turbulent structure which are masked by the spatial integration of Schlieren and shadowgraph methods. Schlieren and shadowgraph methods are the most common methods for visualizing compressible mixing flows. Unfortunately these methods integrate spatially through the flow and can give a misleading picture if the flow is inherently three-dimensional. The details of the mixing process are often three-dimensional and thus are usually not revealed in such integrated methods. [107]

The need for instantaneous planar cuts has long been recognized and several methods have been demonstrated in supersonic flows. While these methods are effective they often require sophisticated equipment which may not be available in the typical laboratory.[107]

Mie scattering takes advantage of the large scattering cross sections of particles seeded into the flow. Detection of these images are now possible using less expensive pulsed lasers with 35 mm cameras and fast film or standard video cameras. Several different seed particles can be employed for Mie scattering, including smoke, liquid droplets and solid particles.[107]

Vapor screen methods have been used in continuous supersonic wind tunnels and require the global seeding of the entire test section. In these methods, the humidity in a continuous wind tunnel is allowed to rise to the point where the moisture condenses due to the cooling from the supersonic expansion. This method is usually used to obtain time averaged images of large scale stationary

structures such as wing tip vortices. The vapor screen method has generally not been used to investigate instantaneous turbulent structure.[107]

An alternative to global seeding of high flow rate wind tunnels is to locally seed near the region of interest. One example of this is creating smoke in the boundary layer. This is often done by painting titanium tetrachloride onto a surface which reacts with ambient water vapor thus forming a fine smoke. Another method is to bleed high vapor pressure liquid into the boundary layer of a supersonic flow. The large shear forces atomize the liquid forming a fine aerosol which can then be used for visualization.[107]

The Mie scattering visualization method is related to the vapor screen method but differs from it in that condensation occurs only as a result of the mixing of a relatively warm vapor laden subsonic stream with a cold supersonic stream. The droplets that are formed from the condensation mark the fluid that has been mixed in proportions such that condensation rapidly takes place, similar to a finite rate chemically reacting system where two non-premixing reactants meet within a mixing zone to form a reaction product. Mie scattering uses the condensation of alcohol vapor as a means of marking the mixed fluid between a supersonic stream and a subsonic stream within a planar mixing layer. Droplets are formed only where mixing occurs.[107]

In Mie Scattering, the scattering signal is related to the partial density of the high-speed fluid and not the local mass fraction as is expected of a conserved scalar. Mie scattering assumes single scattering for spherical particles of known index of refraction. Aside from alcohol, water vapor, and a fog generated carbon tetrachloride can be used to scatter the light.[107]

Using water vapor, however, can be problematic in blowdown wind tunnels because if the total temperature drops below the freezing point ice can form on the window. An additional problem with water occurs when it is seeded using an atomizing nozzle, as its relatively low vapor pressure can result in incomplete evaporation upon reaching the test section. High vapor pressure substances are best for this application. They also have the added benefit of low heats of vaporization thus perturbing the flow less upon condensation.[107]

In Laser Induced Fluorescence methods, or LIF methods, the laser is formed into a sheet which is typically 15 cm wide and 300 μm thick at the waist. The detector is a standard CCD video camera whose output is acquired using a computer with a frame grabber. The product formation and passive scalar visualizations of LIF and Mie are obtained in similar ways. The only difference being the stream into which the seed is injected. In Mie scattering, the high speed fluid which contains the condensed droplets appears as white, the low speed unseeded fluid appears black, and the mixed fluid appears gray.[107]

This method is seen to be superior to the Schlieren photographs in visualizing the details of the turbulent structure as it eliminates spatial averaging. It also reveals large-scale turbulent structures which appear to have been hidden by the Schlieren technique. The product formation planar cut shows considerably more detail of the turbulent structure as compared to the Schlieren images and even the passive scalar images, the cores of the large structures are seen to consist of mixed fluid and the cores are separated by thinner regions of mixed fluid. This technique also allows one to obtain other planar cuts such as plan view and end views which are particularly important in highly three-dimensional flows. The technique can be applied to other supersonic mixing flows of current interest and appears to be easily applicable to many existing supersonic facilities.[107]

The Mie technique affords a high resolution (200x200x200µm per resolution volume), but it still does not resolve finer structures known to exist in the turbulent regimes studied.[112] Spatial resolution using the Mie technique is limited by marker shot noise which is inversely proportional to the root of the number of seeded aerosols per unit volume.[112]

3.2.9 Rayleigh scattering

A technique based on Rayleigh scattering has been developed to measure the concentration filed in a cross section of a turbulent gas jet. This method enables one to quantitatively study turbulent mixing mechanisms and structures. The Rayleigh scattering technique provides better spatial resolution than Mie scatters, avoids the limitations due to aerosol seeding, and is capable of monitoring molecular diffusion. The Lorenz/Mie scattering techniques can not detect molecular diffusion, so the Rayleigh scattering technique is particularly useful in studying reacting flows.[112]

Rayleigh and Raman scattering have proved to be particularly valuable for making measurements at single points or along a line in the flow. In scattering techniques, the intensity of scattered light is proportional to the number of scatterers in the illuminated volume. In the Lorenz/Mie case the scattered light is proportional to the number of seeded particles per resolution element. In the Rayleigh case to the scattered light is proportional to the number of gas molecules per resolution element.[112]

The variation of scattered light intensity across a sheet of laser light in a plane of the jet is recorded with a computer controlled low-light-level V camera. The scattered light intensity is interpreted as being proportional to the injected fluid concentration. In regions where two gases mix the intensity of the Rayleigh scattered signal is proportional to a weighted sum of the injected and ambient gas concentrations, the weight being their different cross sections for Rayleigh scattering. If the ratio of injected gas to ambient gas cross section is sufficiently large, the contribution of the ambient gas term

can be ignored in solving for the injected gas concentration in these regions. In the case of low velocity jets (under constant pressure and temperature), it is not necessary to make this simplification as one can solve directly for the concentration of each component gas in the mixture. It is desirable to have two gases with a large difference in cross section, as small changes in number density are more detectable.[112]

The intensity of the scattered Rayleigh signal from gas molecules is several orders of magnitude lower than that of the Lorenz/Mie signal from the aerosols. The Rayleigh scattering technique requires higher incident laser power and a "clean" environment to eliminate scattering from particulates and stray light suppression. It is desirable to maximize the scattering cross section ratio between ambient and injected gases. A gas with a high refractive index such as Freon discharging into a gas of much lower index such as air or Helium is needed to maximize the contrast between scattered signal intensities from the injected and ambient gases.[112]

The argon ion lasers commonly used for Lorenz/Mie scattering and the Nd: YAG laser are also commonly used for the Rayleigh scattering technique. The laser is focused into a sheet approximately 50 μm thick over the injected jet. Two camera lenses (57 and 135 mm focal lengths) were used to collect and focus the scattered light from a portion of the illuminated sheet onto the face of the camera.[112]

To image the scattering, a two-dimensional concentration mapping is digitized at 10,000 points and stored in the computer, thus providing a measure of relative concentrations in two dimensions.[112]

The data must be corrected to account for the background signal, the camera response, and the non-uniformity of the laser sheet. This is done by taking a background picture without the jet on and subtracting it from the data frame. Then a rectangular glass cell holding a dilute fluorescent dye solution is placed in the path of the laser sheet so that a fluorescent sheet is imaged onto the camera face (optical filters are used to pass only the fluorescence). Since the fluorescence signal is constant across the sheet the actual recorded signal intensities reflect both the non uniform response of the camera and the intensity distribution in the sheet which drops off at either end in the direction of the jet axis and peaks in the center due to the Gaussian profile of the incident beam. The background corrected frame is finally divided by this response frame.[112]

The Rayleigh technique provides finer spatial resolution and avoids the limitations due to aerosol seeding density. Using the Rayleigh scattering technique it should be possible to take measurements in the jet far field and to attain even finer resolution given sufficient incident laser power. It should become possible to detect small scale turbulence using the Rayleigh technique.[112]

4 Methods

4.1 New Test Section Design and Construction

The University of Kansas Supersonic facility is a supersonic draw down type wind tunnel. The original wind tunnel consists of three large vacuum tanks and their respective depressurizing pumps, an initial variable throat to accelerate the airflow to supersonic Mach numbers, a short constant area test section, and a second variable throat to decrease the airspeed back to subsonic Mach numbers. See Figure 69. The original cross section is 3.515 inches high and 2 inches wide. The supersonic wind tunnel was designed to study quasi-two dimensional flow so the width of the wind tunnel is constant throughout. Each of the three vacuum tanks has a volume of 643 ft^3 which creates a total volume of 1930 ft^3.

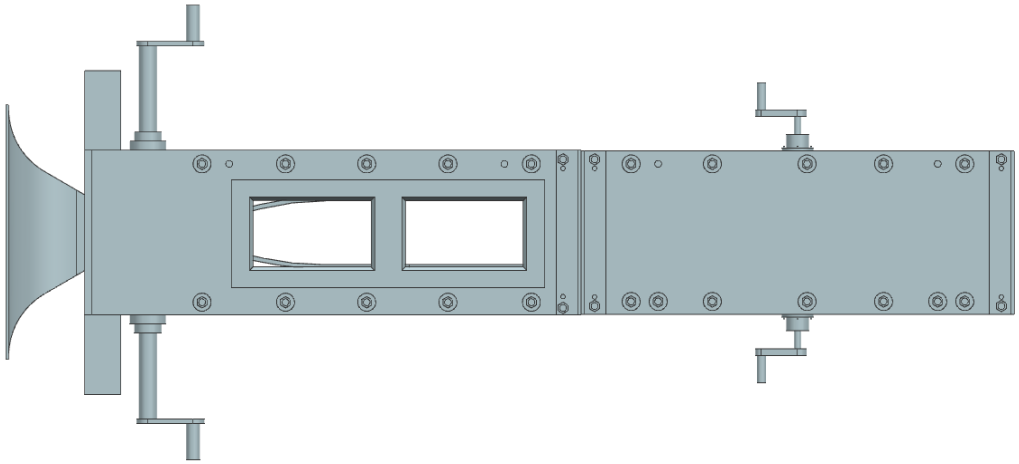

a) External View

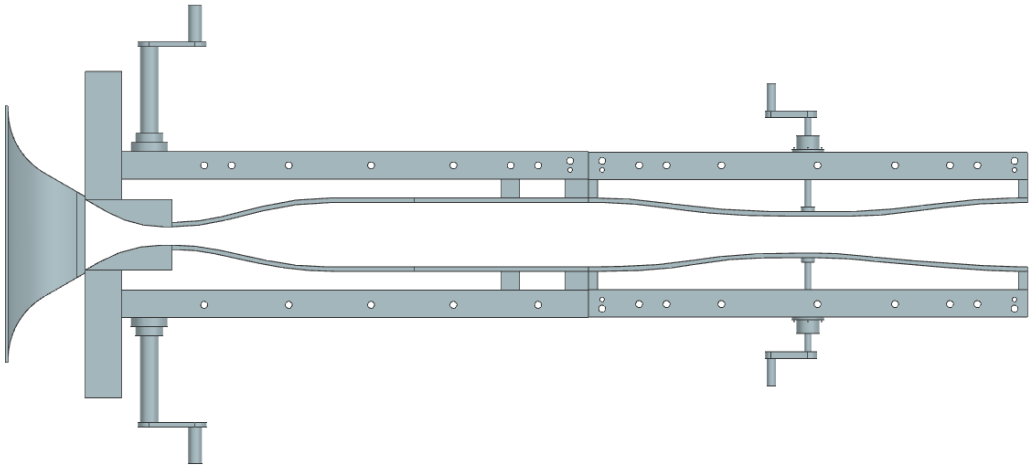

b) Internal View

Figure 69: Original Wind Tunnel: External and Internal Views

A new test section was designed to be incorporated into the supersonic wind tunnel which fits between the first and second throats. The purpose of the test section was to perform supersonic cold

flow mixing enhancement studies. The experimenters wished to study carbon dioxide gas injected in pulses from a step parallel to the main flow. A backward facing step was needed to produce the shear layer and to house the injector mechanisms. The injected gas then impinges on the shear layer that has been produced by the step. The test section also had to be sufficiently long enough to study the flow in the far field relative to the injector, or in this case 500 injector port diameters downstream.

The research of Soetrisno et al. has shown that forcing shear layers at certain frequencies can excite Kelvin-Helmholtz modes leading to shear layer growth.[64] Impinging of Mach waves and constant jet injection have also led to improved shear layer growth.[10, 18] The purpose of this research is to see if pulsating jets impinging on the shear layer at a specific frequency can excite the modes of the shear layer and lead to greater shear layer growth. As this experiment is a cold flow study, carbon dioxide gas was used as a fuel substitute because it is inert and produces clear Schlieren images.

Instead of reinventing the wheel, the new sections followed the same design as the existing sections. Calipers were used to take measurement of the existing wind tunnel sections which were used both to ensure that the new sections would match up perfectly with the old section to prevent leaks, and as inspiration for the CAD models of the new sections.

4.1.1 Initial Design

Originally four new sections were desired: a step test section where injection would take place, two parallel duct sections to study mixing further downstream, and a contraction section that would allow the new sections to mate with the second throat. The first section features a one inch step that mimics the step inside a Scramjet combustion chamber. The step will later house various fuel injectors. The internal height of the tunnel prior to the step is 3.515” which is the same as the height of the existing wind tunnel test section exit. All sections are 1.971” wide. The second and third proposed sections are both 19.75”. This length was chosen so that the side panels for the second and third sections could be made from the same design, in order to reduce tooling costs, without exceeding the length requirement for the tunnel. Also this length allows the wall static pressure ports to be spaced evenly. Section four contracts the wind tunnel cross section back to that of the original cross section. The originally proposed tunnel design can be seen incorporated with the existing tunnel structure below in Figure 70.

Downstream of the step there are wall static pressure ports drilled into the upper and lower walls of the tunnel. The pressure ports are attached to tubing which then attaches to pressure transducers to measure the distribution of static pressure along the wall during testing. Holes are drilled in the upper and lower structure of the wind tunnel to accommodate the tubing. The side panels are bolted to the

upper and lower structure of the section and overlap with the flanges to create an air tight smooth surface. The side panels are bolted to the upper and lower bars by double ended bolts with nuts that can be tightened or removed on either side so that the side panels can be easily removed without disassembling the entire section. Rods are used to help align the side panels and the flanges as seen in Figure 71.

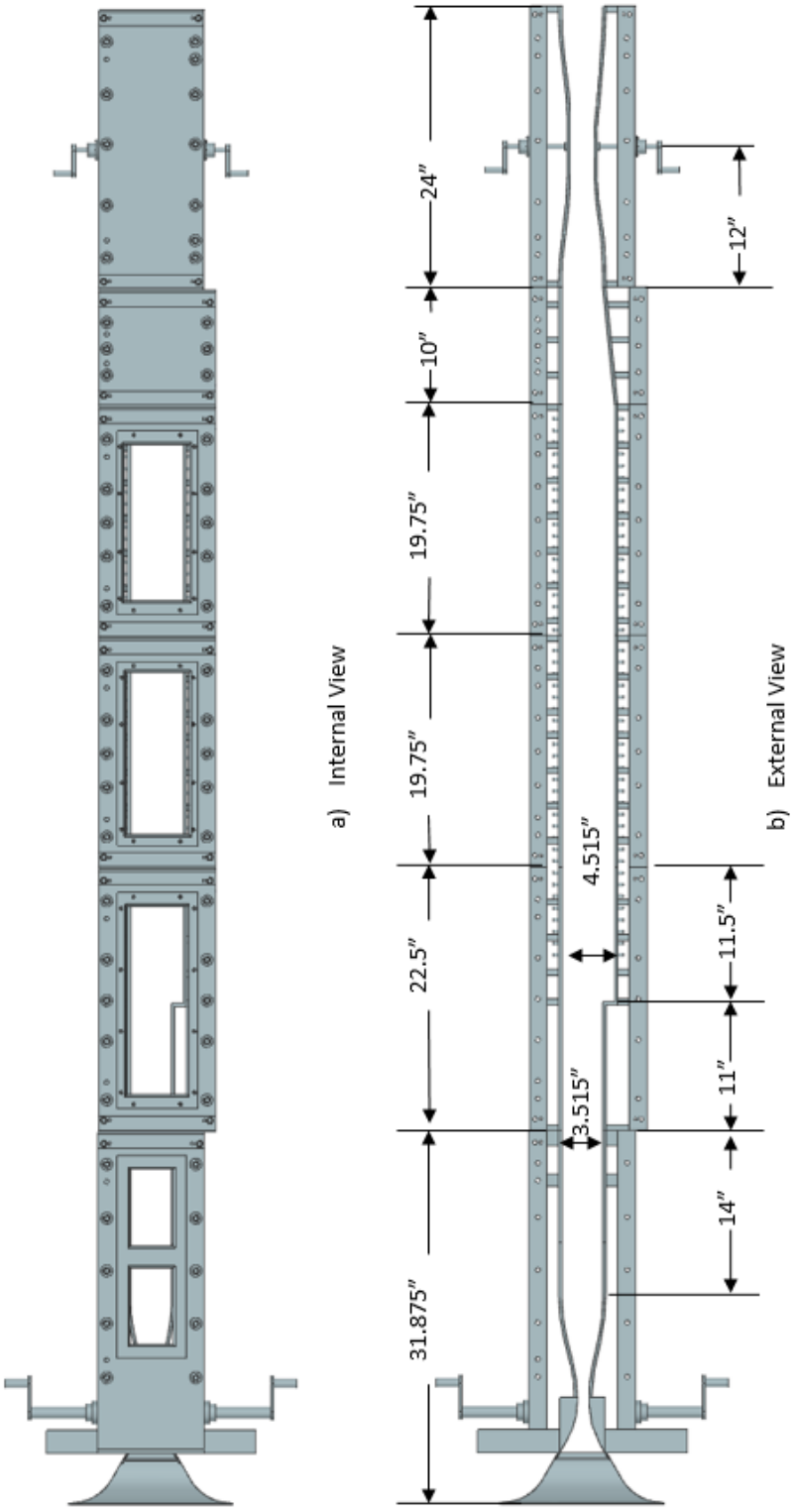

Figure 70: Original Proposed Supersonic Wind Tunnel Test Section

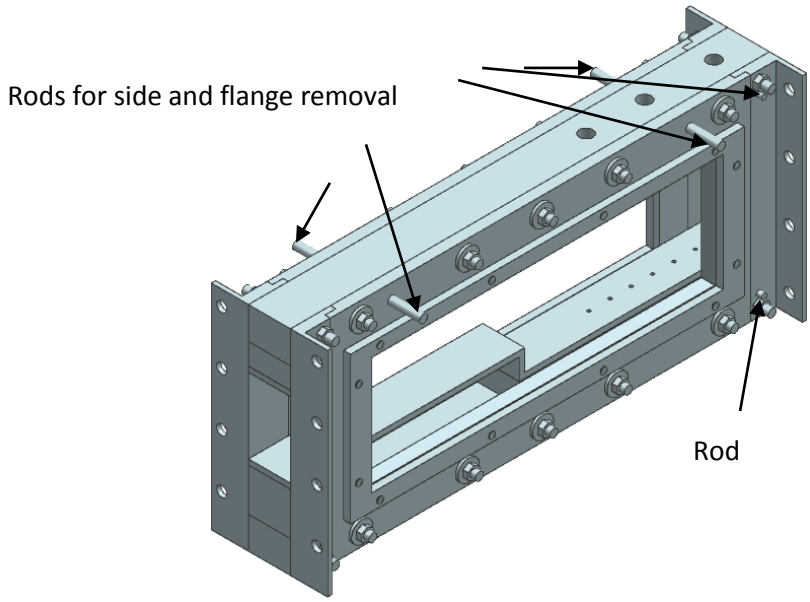

Figure 71: Alignment Rods

4.1.2 Re-Design

The design of the tunnel was discussed with Dr. Tam from the Air Force Research Lab. Dr. Tam expressed concern that the ramp of the contraction section would create an oblique shock, which would have ramifications on the back pressure of the tunnel. Dr. Tam also believed that the parallel walls should have a divergence angle to counteract any effects from a thickening boundary layer.

The tunnel was redesigned according to Dr. Tam's recommendations so that the test section features only three subsections. The first section mates with the exit of the initial throat of the existing wind tunnel and then features the 1 inch tall step under which the pulsed injector is housed. For the new test section the Mach number in the duct prior to the step can be varied from just over Mach 1 to Mach 2. The second half of the first test section and the second test section expand to accommodate the growing boundary layer at a divergence angle of 1.5˚. The upper and lower walls feature static pressure ports spaced one inch apart (Figure 72). Each port is fitted with plastic tubing which is attached to an array of pressure transducers.

The spacers shown along the upper and lower walls in Figure 72 are interchangeable so that different tunnel configurations can easily be tested (i.e. cavities or an expanding duct without the step).

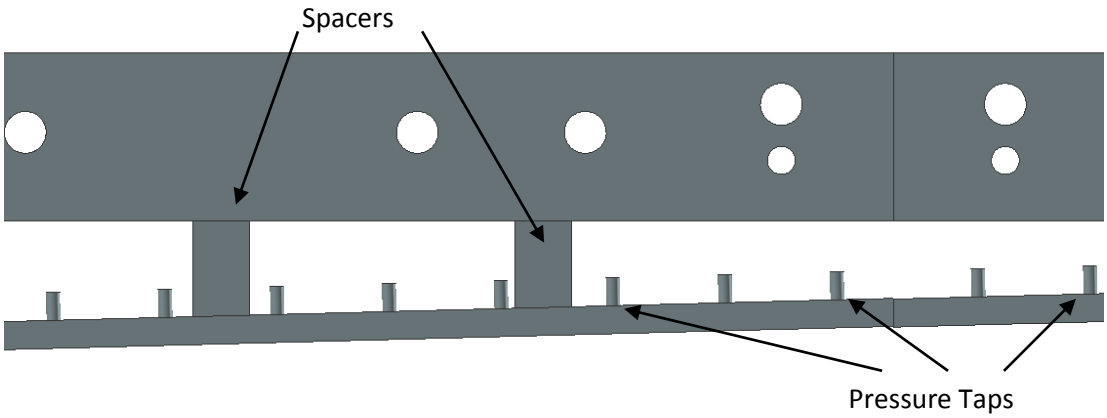

Figure 72: Close Up of Pressure Taps

The third section was redesigned to more smoothly contract the flow, and thus efficiently decelerate the flow, rather than the initial design with the sharp angled contraction ramp section. Pressure ports were removed from the end of the second section as they would interfere with the outer structure of the wind tunnel and there wouldn't be room for the tubing.

The spacers and internal plates are held in place by long bolts that pass through the upper and lower structural bar stock and through the spacers to screw into tapped holes in the inner wall plates. This means that there are no bolts or holes (other than the pressure taps) causing any disturbances to the air flow inside the test section. The edges of the glass window plates were beveled so that the glass could fit into the window slots. The bevel prevents the low pressure within the wind tunnel from pulling the glass panes inward slightly and disrupting the airflow. The windows are held in place with silicone and the gap between the glass and the aluminum was smoothed over with molding epoxy.

4.1.3 Wind Tunnel Assembly

The existing wind tunnel sections were split apart with the first throat section supported by an engine hoist. The inner plates and spacers were bolted to the upper and lower bars prior to assembly. The inner plates of the new sections were carefully aligned with the inner walls of the existing sections by means of shimming. Rubber gaskets were added to slots machined into the sides of each of the plates to prevent leakage. Cork sheeting was added to the sides of the upper and lower bars of each section to further prevent leakage. This method is also used on the original sections of the supersonic wind tunnel. Once the inner walls were aligned the brackets where bolted in place to hold the new upper and lower sections in place and the brackets were bolted to each other. The internal shimming was then removed. Caulk was used to seal any leaks that might occur between the sections. Tubing was attached to each of the pressure ports and threaded through the holes in the upper and lower walls.

The side panels were bolted in place. The tunnel was run to test for leaks and all leaks were sealed with clay putty. The assembly process can be seen in Figure 73 through Figure 77.

Figure 73: Splitting the Original Wind Tunnel

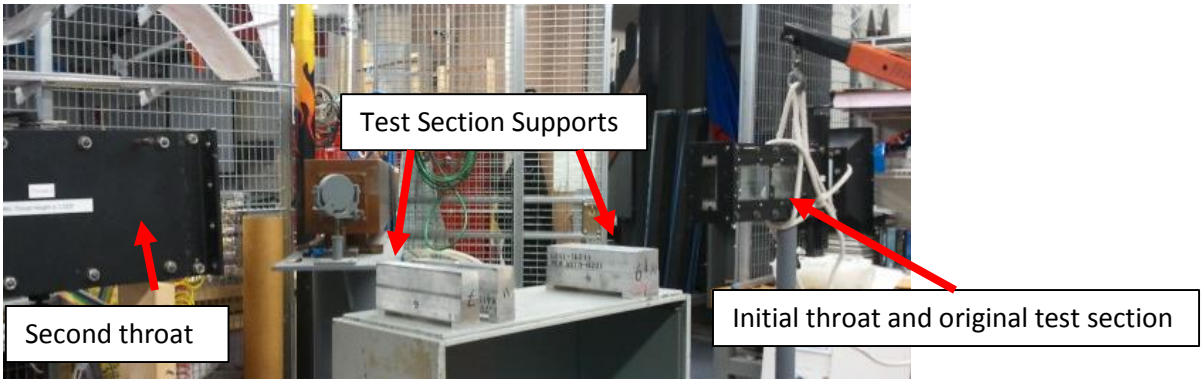

Figure 74: Wind Tunnel Supports

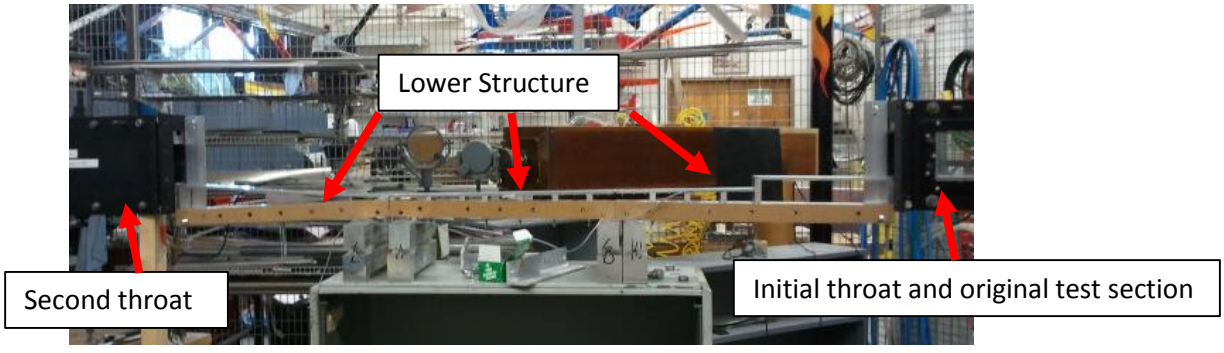

Figure 75: Lower Structure

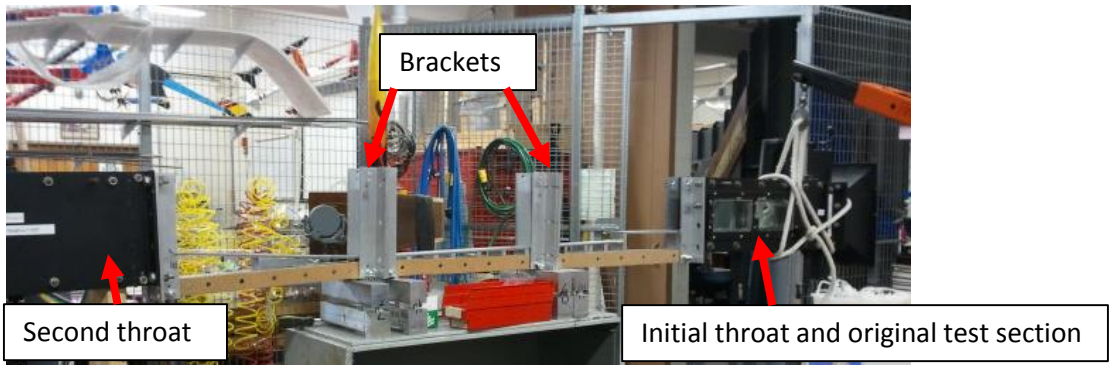

Figure 76: Brackets Installed

Figure 77: Completed Wind Tunnel with New Test Section

The three views for each of the parts are shown in Appendix A. All aluminum parts were machined from 6061 Aluminum plate and bar stock. All of the new sections were designed with a tolerance of ±0.002. The entire assembly of the original and new sections can be seen in Figure 78. The entire supersonic facility can be seen in Figure 79.

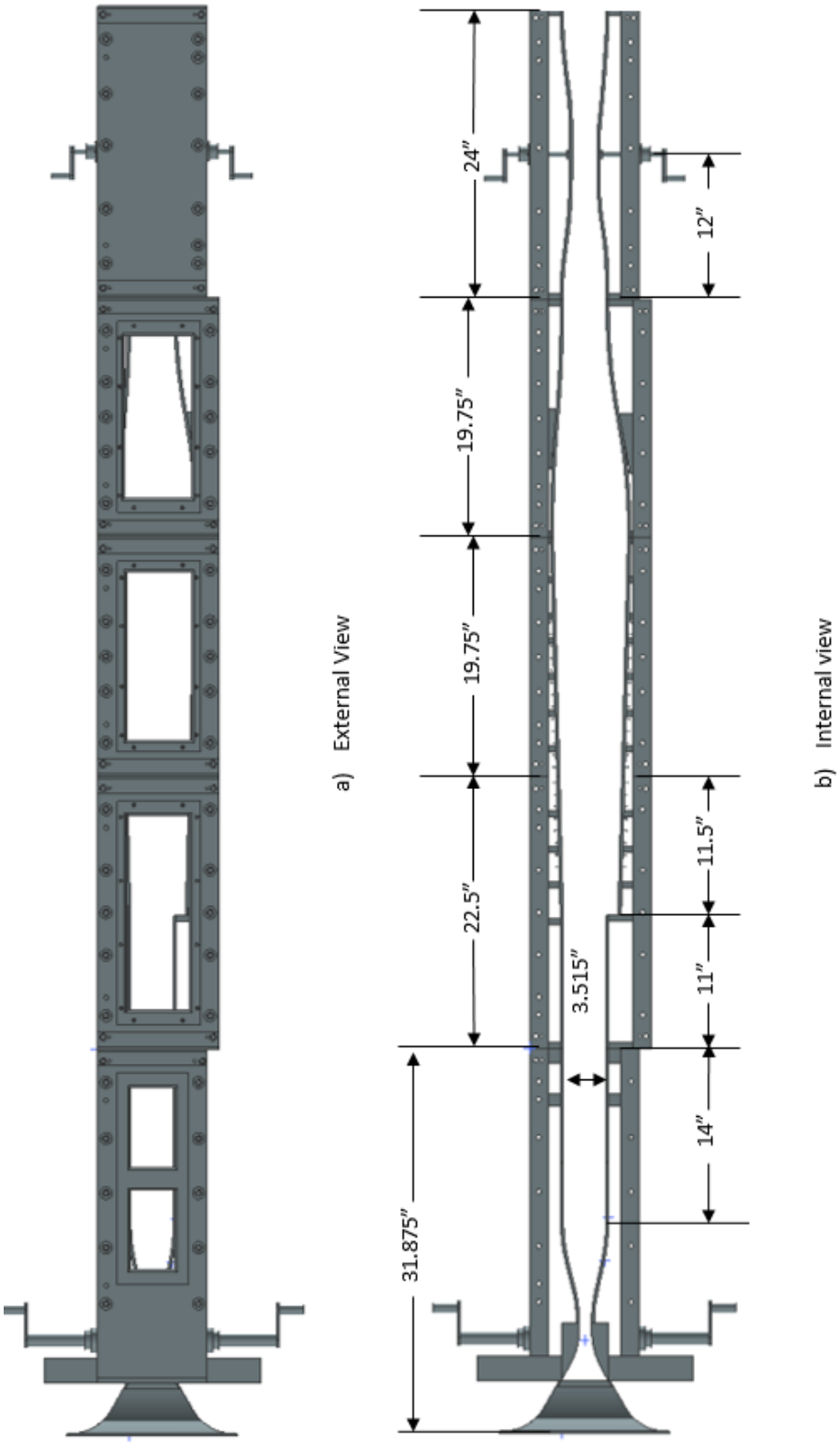

Figure 78: Supersonic Wind Tunnel with New Test Sections: External and Internal Views

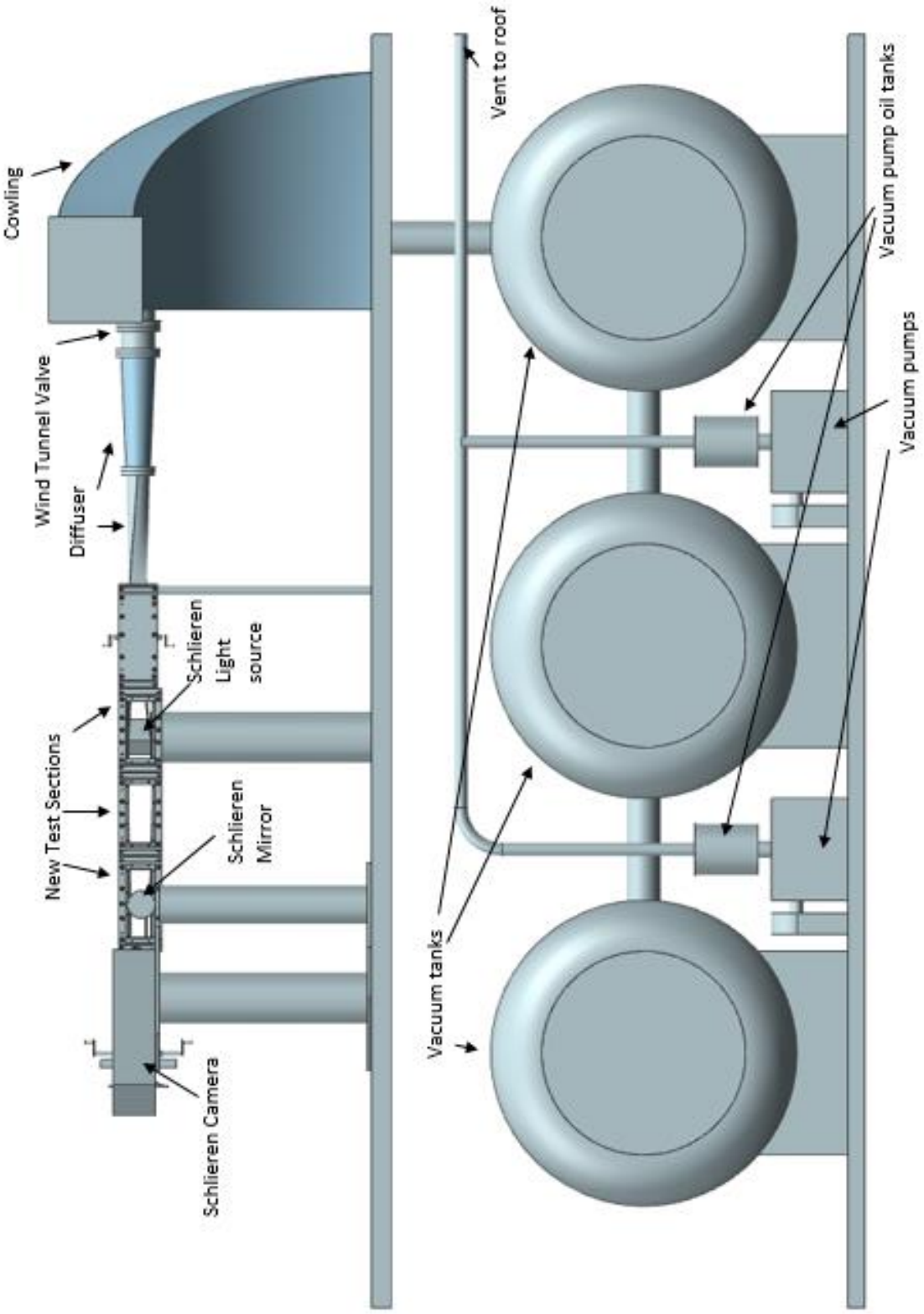

Figure 79: Supersonic Facility

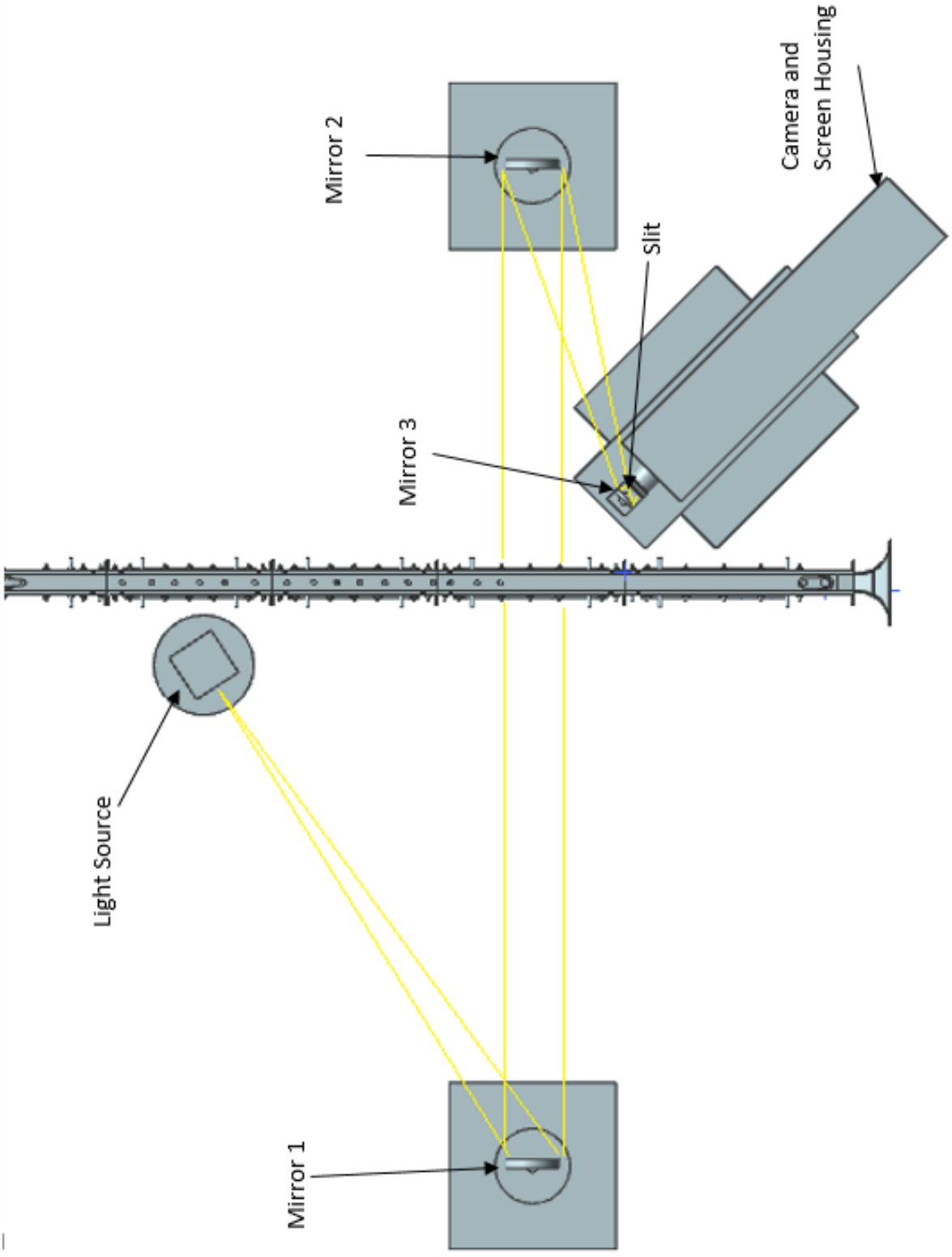

Figure 80: Schlieren Photography Setup

The overall 62 inch length of the new test section was chosen such that the effects of injection could be studied in the far-field relative to the injector length scales. The 11 inch section prior to the step was designed to allow adequate space for the injector, die grinder, and related components. The gap between the inner walls of the wind tunnel and the load bearing structure needed to be large enough to accommodate the tubing that would be attached to the pressure ports so initially the gap between the inner walls and the outer structure was 1 inch. The length of the divergent section was limited by when the diverging wall would come into contact with the outer structure. The convergent section needed to be long enough to smoothly transition the flow back to the original test section height.

The Schlieren photography set up consists of a light source which reflects off two mirrors to produce a parallel beam of light through the test section. The light is then reflected off of a third smaller mirror, through a slit, then through a lens, after which the image is projected onto a screen. The projected image is then recorded by the camera (Figure 80). No changes were made to the original Schlieren photography set up other than to move the mirrors, light source and camera so that images can be recorded in the region of the tunnel just downstream of the step.

4.2 Injector Design and Construction

The injector was designed to cause pulses of carbon dioxide to be injected into the wind tunnel. The injector features a modular design that allows for several different parameters to be tested by simply exchanging one or two parts of the injector. The parameters that the experimenters would like to investigate are the effect of frequencies ranging from 1.6 kHz to 10.0 kHz, the effect of varying the length of the pulse for a given frequency, and the effect of having all of the injection ports firing at once versus having them be offset.

The injector is composed of a rotating valve housed within a cavity that has been machined into two mating plates (Figure 81, Figure 83, and Figure 82). A gasket is placed between the two plates to prevent the carbon dioxide from leaking. Carbon dioxide gas enters the injector through plastic tubing which is attached to the fuel inlet ports at the back of the injector (Figure 81, Figure 83, and Figure 82). As the valve rotates the “teeth” of the valve block and unblock the injection ports causing the carbon dioxide to be injected in pulses. The first injector face plate has been designed with eight injection ports. The first valve has been designed with eight teeth to simultaneously block all of the injection ports. As the valve rotates all of the injection ports open and close at the same time and carbon dioxide is injected simultaneously from the ports.

The valve shaft is supported by a ceramic bearing and a stainless steel bearing and is attached via a vibration dampening coupling to a pneumatic die grinder. The ceramic bearings were originally chosen over steel bearings as they can withstand higher RPMs without suffering damage due to friction induced heating, but the vibration of the shaft caused the rear ceramic bearing the crack so it was replaced with a stainless steel bearing. The bearing specifications are given in Table 1 below. The frequency of the pulses can be controlled by varying the RPM of the die grinder and a Monarch PLT200 optical laser tachometer is used to verify the die grinder RPM. The injector and pneumatic die grinder can be seen installed beneath the test section step in Figure 84.

Table 1: Bearing Specifications

Bearing	R-44-T9/P58 LD ZRO2 Radial Full Ceramic Bearings	
Inner diameter	0.125”	
Outer diameter	0.25”	
Width	0.0937”	
Cost	$48.95 each	
Lubricant	None	
Bearing	BB001 Dental Tool Bearing	
Inner diameter	0.125”	
Outer diameter	0.25”	
Width	0.0937”	
Cost	$15.95	
Lubricant	AGS Powdered Graphite Lubricant	

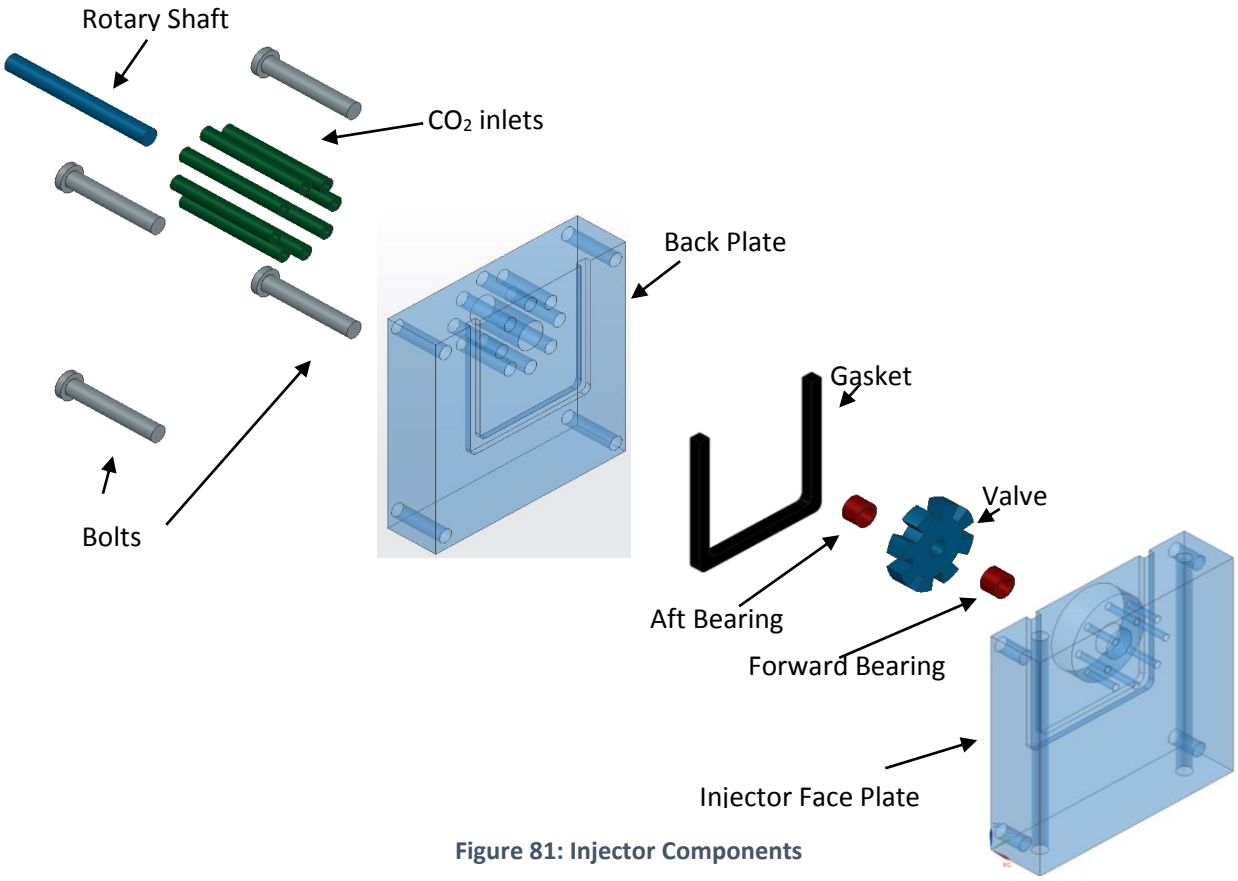

Figure 81: Injector Components

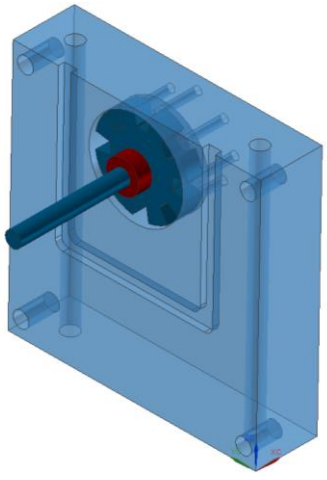

Figure 82: Injector Face Plate and Valve

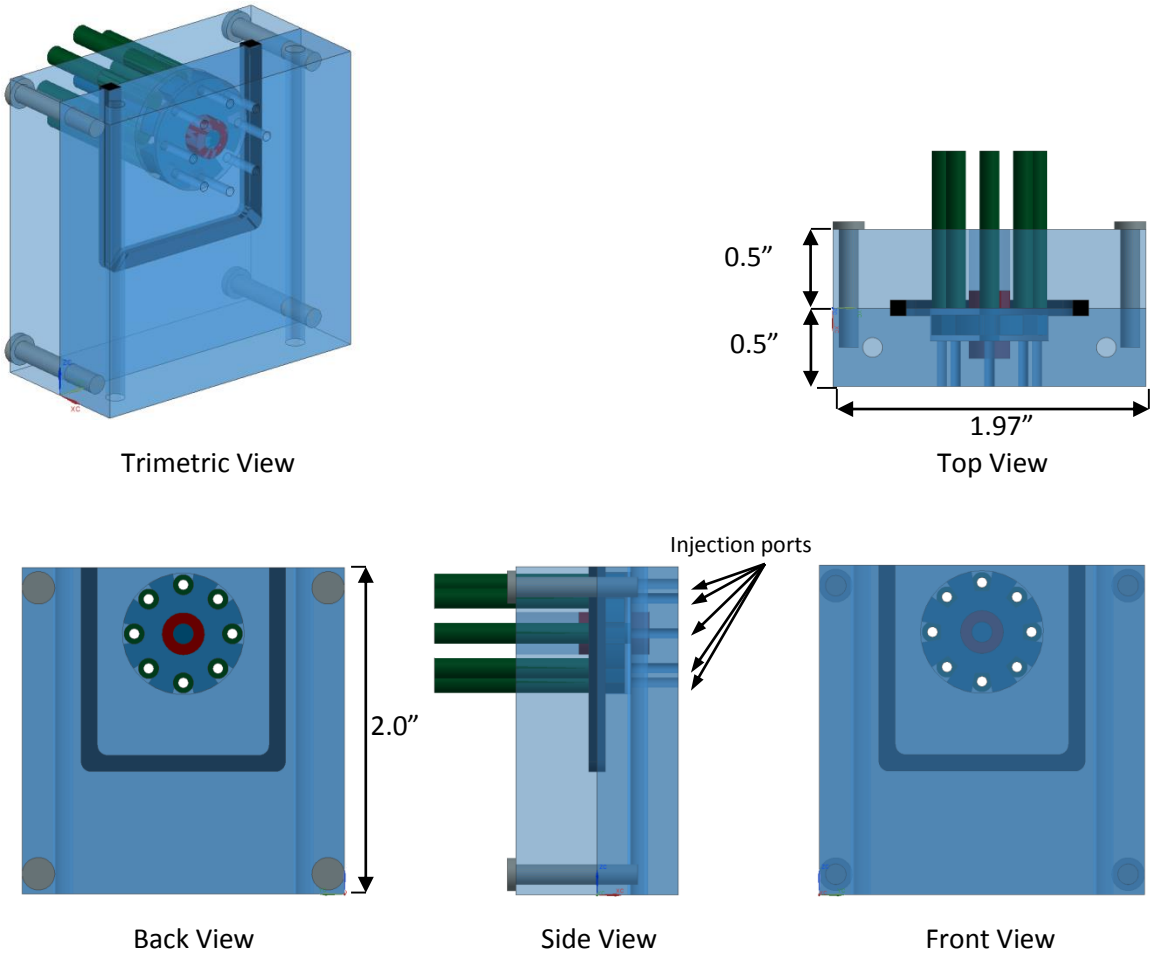

Figure 83: Injector Views

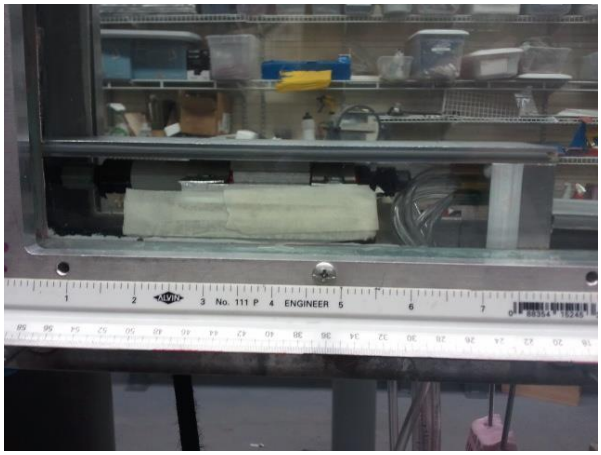

Figure 84: Installed Injector

Four other valves have been designed one with 16 teeth evenly spaced and three other valves have been designed with five teeth each. For one of the valves the widths of the teeth and the gaps between

the teeth are equal. For the second valve the widths of the teeth are one third of the width of the gaps between the teeth and for the third valve the gaps between the teeth are one third of the width of the teeth. This allows for the effect of three different duty cycles on shear layer excitation to be tested at each frequency (Figure 85).

A second face plate has been designed that has five injection ports so that when paired with the valves with five teeth all of the injection ports will still be open at once. The five port injector face plate can also be paired with the eight tooth valve so that each of the injection ports will open and close sequentially (Figure 86). Thus the effect of simultaneous vs. sequential injection on shear layer excitation can be tested.

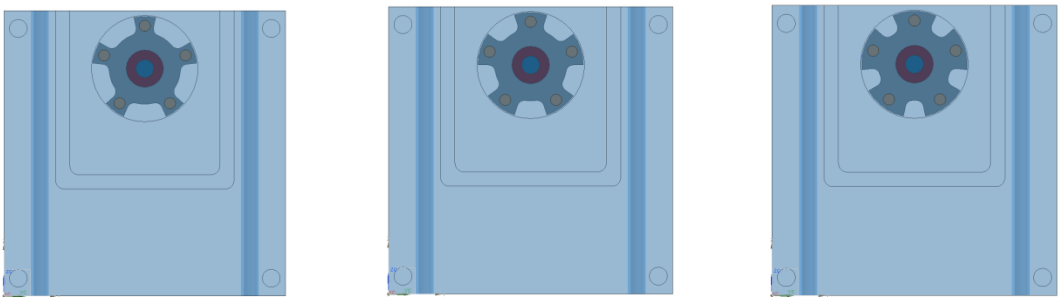

Figure 85: Five Port Injector Plate with Five Tooth Valves for Varying Pulse Duration

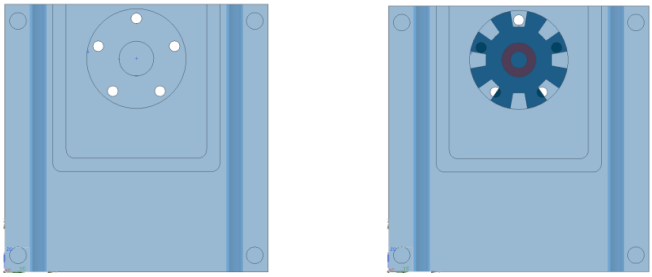

Figure 86: Five Port injector Plate and Five Port Injector Plate with Eight Tooth Valve

The initial eight port face plate can be paired with the various five tooth valves to determine the effect of pulse width on shear layer excitation when the ports are not opening simultaneously (Figure 87).

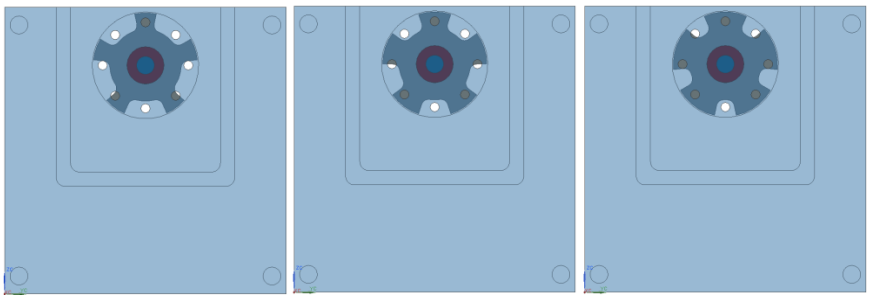

Figure 87: Eight Port Injector Plate with Five Tooth Valves for Varying Pulse Duration

In the future studies of the effect of pulsed injection angle can also be studied. This will require the construction of several new injectors each with the injection ports machined at various angles (Figure 88). The current injectors could also be mounted at a 90˚ angle to study pulsed normal injection. If the injectors with angled injection ports were also mounted at 90˚ then the range of angles of injection between 0˚ and 90˚ could be tested.

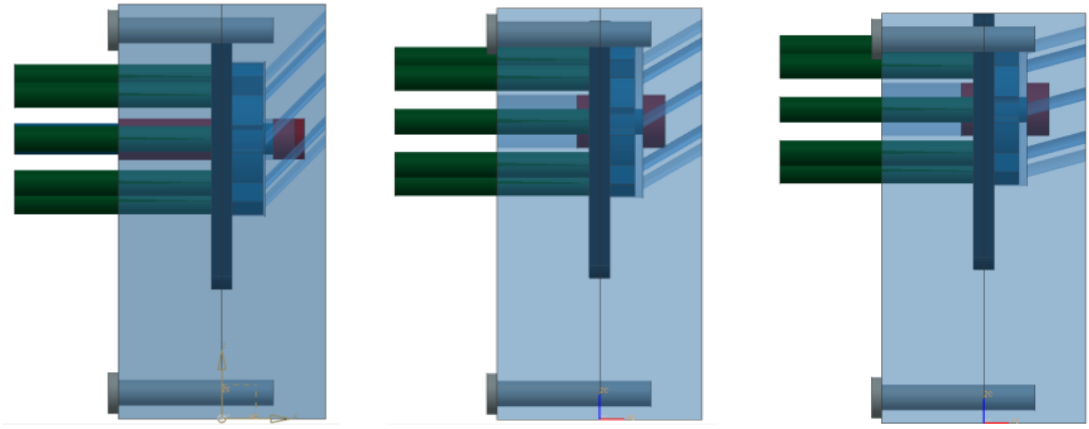

Figure 88: Injectors for 45˚, 30˚, and 15˚ respectively

Table 2 shows a comparison of the capabilities of the current injector design to previous pulsed injectors.

Internal static pressures in scramjet combustors are in the range of 100 psi to 3000 psi. Fuel injectors in jet engines commonly have line pressures between 5000 and 8000 psi with modern fuel injectors even being as high as 15000 psi. As modern injectors and fuel lines are capable of higher pressures than those found in scramjet combustion chambers this injector design could be scaled up to operate in a scramjet combustion chamber.

Table 2: Comparison of Pulsed Injector Capabilities

	Frequency Range	Pulse length	Angle of injection
Bueno et al.	10 Hz and 100 Hz	5 ms	Normal
Culter et al. 2001	Up to 12.8 kHz		Normal
Cutler and Harding	Up to 13 kHz		Normal
Kalidas and Kurian	1 Hz, 2 Hz	150 ms and 220 ms	Normal
Kouchi et al.	1 kHz	0.75 ms	Normal
Kouchi et al. 2007	Up to 1 kHz	100 ms, 150 ms, 200 ms, 250 ms, 350 ms	Normal
Miller et al.			Normal
Randolph and Chew	1 Hz	250 ms	Normal
Farokhi and Smith	1.6 kHz to 12 kHz	0.3125 ms to 0.04167 ms	0˚, 15˚, 30˚, 45˚, 60˚, 75˚, 90˚

4.3 Instrumentation Setup and Calibration

Initially, the pressure transducers used to measure the static pressure distribution along the upper and lower walls of the wind tunnel was an array of MPX2200DP differential pressure transducers (Figure 89), with a response time of 1 ms and a maximum pressure of 29 psi. The signals from the pressure transducers are read into a Labview program which converts the millivolt signal from the pressure transducers into PSI and records the data for analysis.

Figure 89: MPX2200DP Differential Pressure Transducer

Later, during testing, there was some concern that the response time of the MPX2200DP pressure transducers was not fast enough to accurately capture higher frequency fluctuations so they were replaced by an array of PXSDX-015GV differential pressure transducers (Figure 90), which has a response time of 0.1 ms and a maximum pressure of 30 psi.

Figure 90: PXSDX-015GV Differential Pressure Transducer

The static pressure transducers were calibrated using an Omega PX 309 pressure transducer (Figure 91).

Figure 91: Omega PX 309

A Labview program was created that compared the pressure readings from an MPX2200 pressure transducer and the Omega PX 309 transducer (Figure 92 and Figure 93).

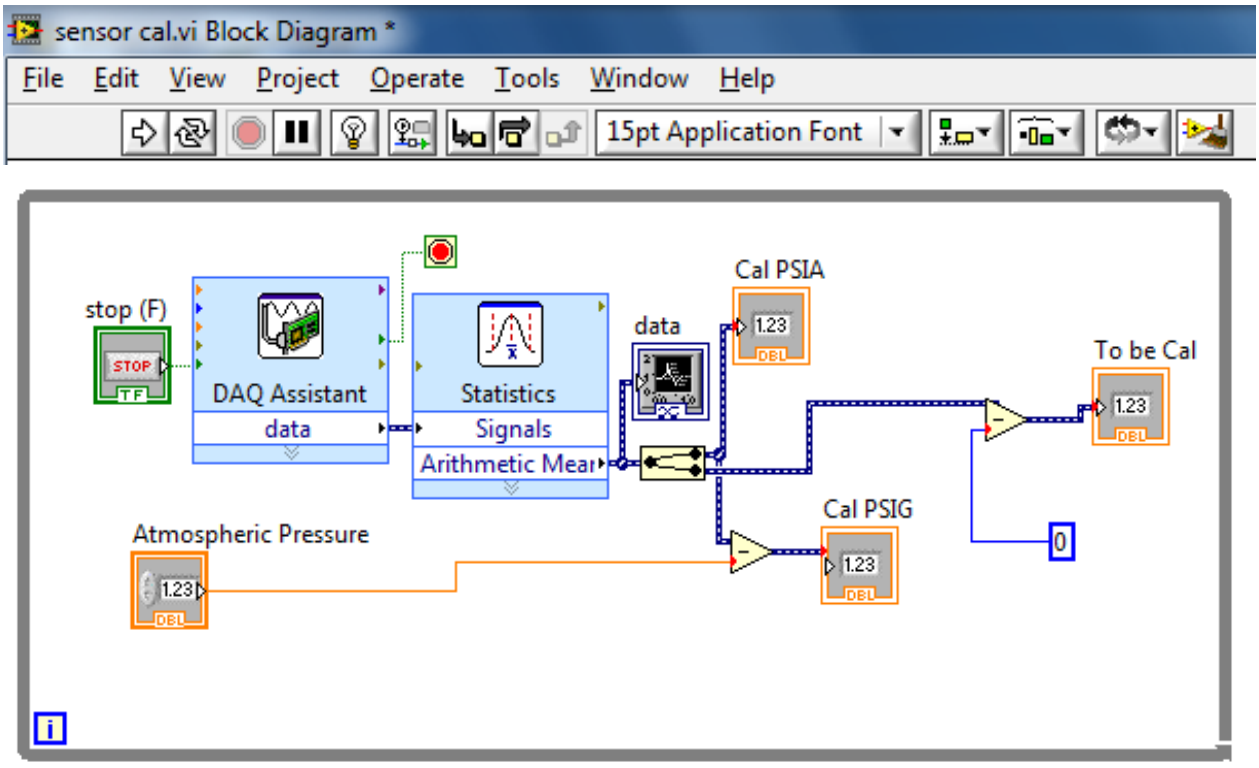

Figure 92: Static Pressure Transducer Calibration Labview vi

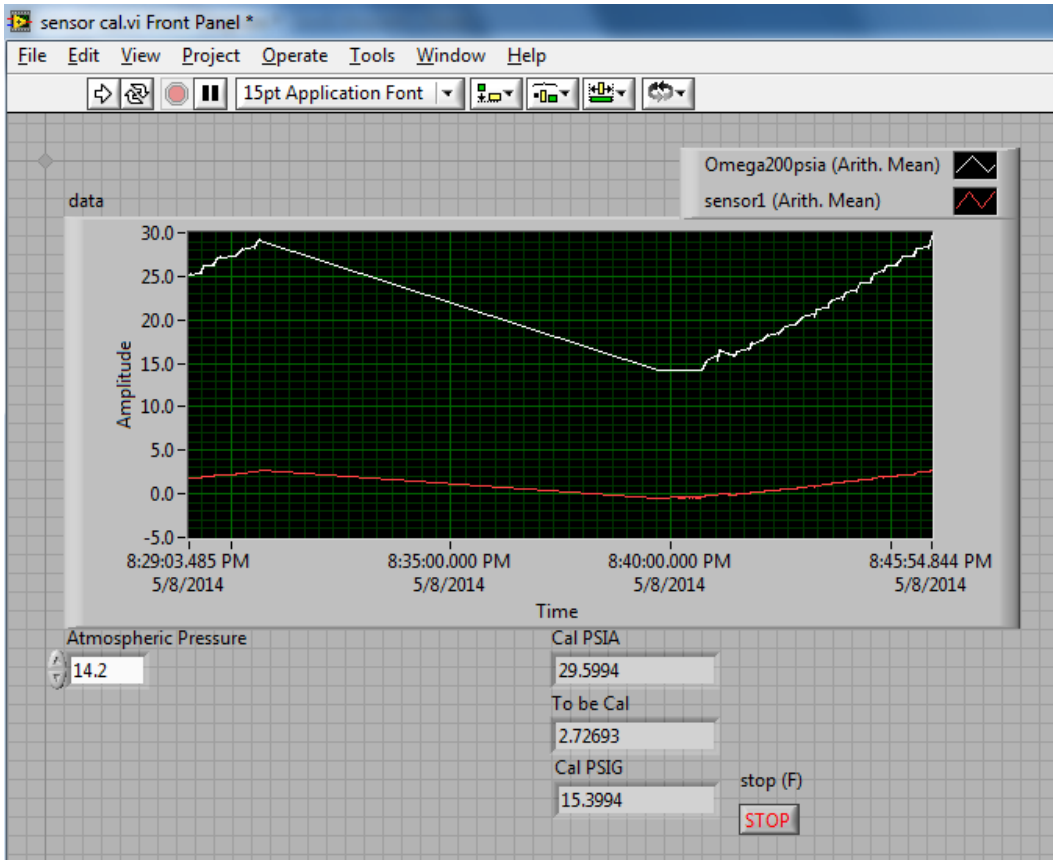

Figure 93: Static Pressure Transducer Calibration Labview vi

Using the DAQ Assistant in the Labview block diagram, the slope and intercept of the equation that the Labview program uses to convert millivolts to PSI were modified for each of the MPX2200 and PXSDS pressure transducers, individually, until the readings from the MPX2200 and PXSDX pressure transducers matched the reading from the Omega PX 309 transducer (Figure 94).

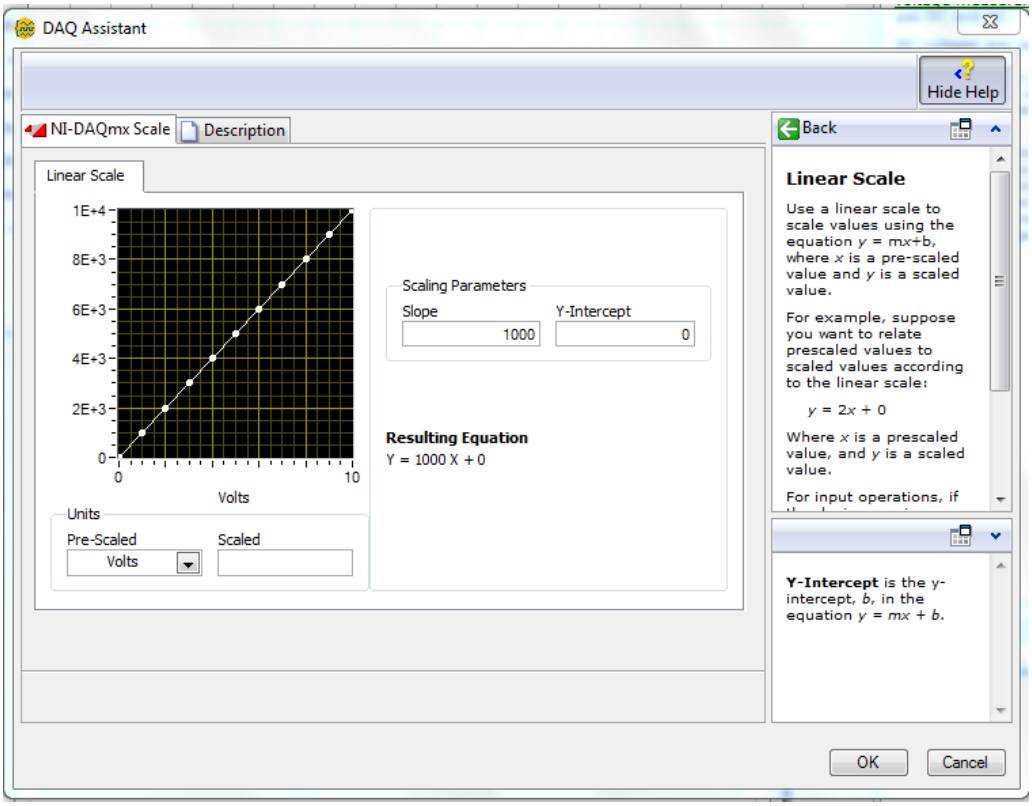

Figure 94: Labview Voltage Linear Scaling Menu

Another Labview program was created that reads millivolt data in from 8 pressure transducers, converts the data from millivolts to psi, and outputs the data to an Excel file (Figure 95 and Figure 96). The DAQ assistant for this program was used to modify the scaling equations for each of the pressure transducers to match the scaling equations from the calibration program.

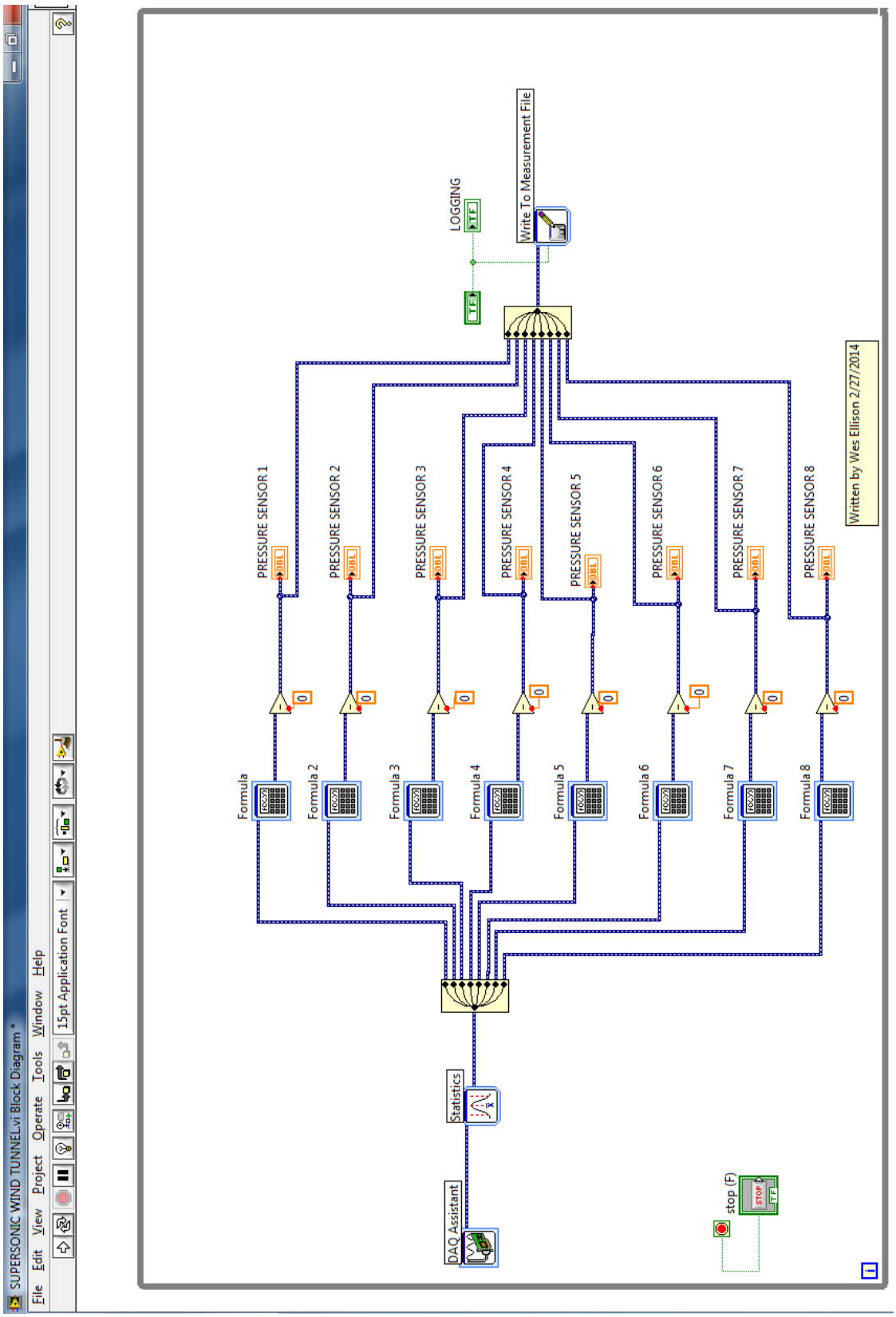

Figure 95: Supersonic Wind Tunnel Static Pressure Acquisition Labview Block Diagram

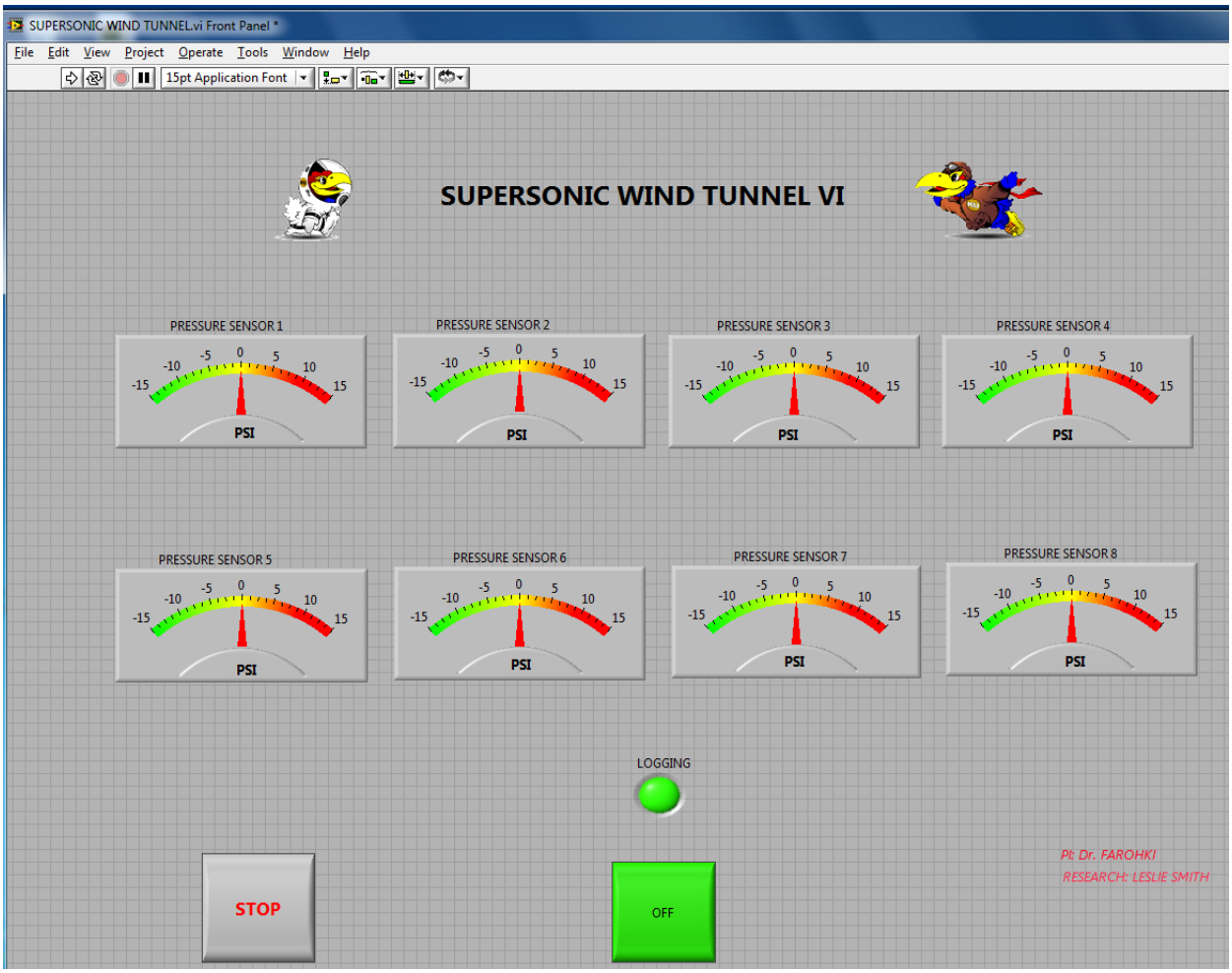

Figure 96: Supersonic Wind Tunnel Static Pressure Acquisition Labview vi

4.4 Injector Testing

4.4.1 Preliminary Testing

A baseline test was performed with no injection and the static pressure data was collected along the upper and lower walls of the tunnel via the pressure transducers. This data was used to ensure that the initial pressure conditions in the STAR-CCM+ model were the same as in the wind tunnel test. The throats of the supersonic wind tunnel were set so that the test section had a Mach number of 1.8. Theoretical calculations show that the supersonic wind tunnel should be able to sustain a Mach number of around Mach 1.8 for 43.75 seconds. The supersonic wind tunnel data from the test run showed that the tunnel can sustain a Mach number of 1.8 through the test section for 43.16 seconds before the

pressure in the vacuum tanks rises to the point where the pressure differential needed to sustain that air speed can no longer be met. However, the pressure recorded by the pressure tap furthest downstream begins to rise significantly after just 18.42 seconds. This is because shocks are traveling upstream in the wind tunnel at a speed of 0.141 ft/s until the tunnel un-chokes. To prevent these travelling shocks from affecting the data, the duration of each test was 15 seconds.

4.4.2 Proof of Concept Testing

The Injector was first tested into still air using the eight tooth valve paired with the eight port injector face. These tests were conducted with a carbon dioxide back pressure of 180 psi and an injection frequency of 1.6 kHz. No pressure data was recorded for these tests.

4.4.3 Testing

For the cold flow experiments, carbon dioxide gas was injected at a back pressure of 180 psi. The first test performed was for constant injection so that it can be determined what effect the pulsation has on the shear layer as opposed to simply mass addition. For the pulsed injection tests, the pulse frequency of the injector was varied from 1.6 kHz to 4.8 kHz at intervals of 400 Hz for the 8 tooth valve. This is done by varying the pressure to the pneumatic motor which in turn varies the rpm of the motor. For the 16 tooth valve the frequency was varied from 4.8 kHz to 10 kHz at intervals of 400 Hz. All three of the 5 toothed valves were tested at frequencies ranging from 1 kHz to 4 kHz at intervals of 500 Hz.

There are a total of 32 pressure ports along the upper and lower walls of the wind tunnel with 16 ports on the upper wall and 16 ports on the lower wall. The DQE is only able to read data in from 8 channels at a time. For each data point at each frequency four separate tests were run, one for each group of eight pressure taps.

4.5 3D CFD Modeling

Three 3 dimensional volume meshes representing the 8 injection port injector and three 3 dimensional volume meshes representing the 5 injection port injector were created using the mesh building software incorporated into STAR-CCM+. This was done by first creating the three dimensional geometry modeled after the 8 injection port injector and the three dimensional geometry modeled after the 5 injection port injector in 3D-CAD, the parametric solid modeler available within STAR-CCM+. On the injector face plates the injection ports are arranged in a ring. The models, therefore, were designed as half of the wind tunnel geometry with one side declared a plane of symmetry, thus only one injector is shown at each of the vertical coordinates leaving 5 injection ports in the model representing the 8

port injector and 3 injection ports in the model representing the 5 port injector. This was done to decrease the run time of the simulation and to prevent instabilities that can occur in the simulation if the geometry is symmetrical but the mesh is not. The geometry used for the Wind Tunnel models is shown in Figure 97, Figure 98, and Figure 99, below.

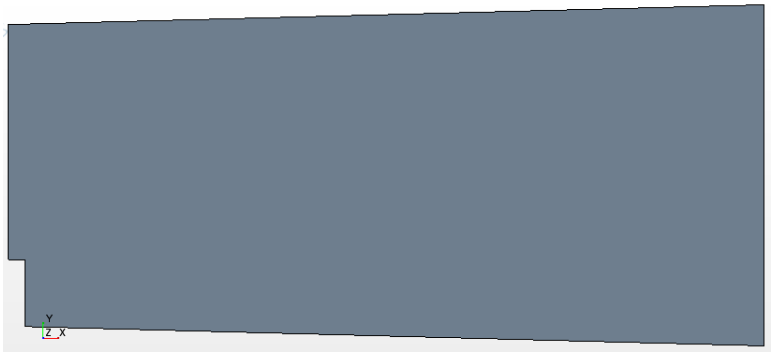

Figure 97: Geometry of the Two Dimensional Wind Tunnel Model

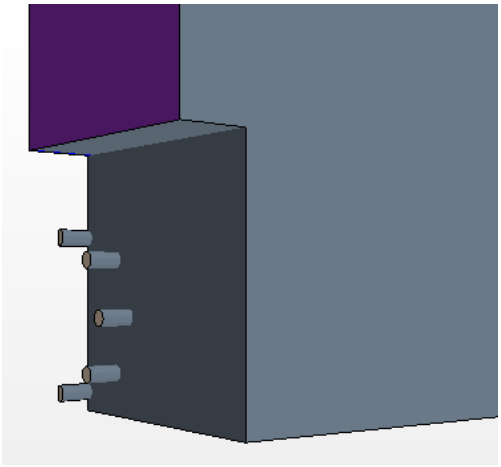

Figure 98: Geometry of the Section near the Step in the Wind Tunnel Model for the 8 Injection Port Model

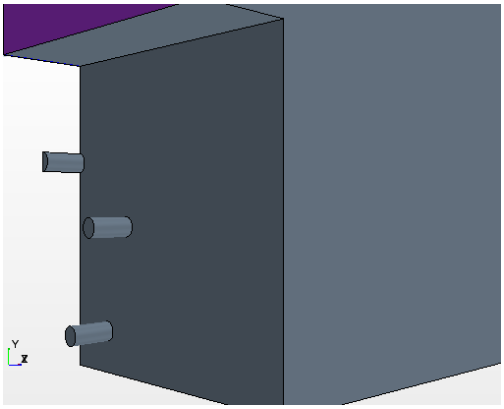

Figure 99: Geometry of the Section near the Step in the Wind Tunnel Model for the 5 Injection Port Model

The meshes were generated by declaring a global element size. Fine, medium, and coarse meshes were created to model each the injector with 8 ports and the injector with 5 ports. The coarse meshes had an average mesh size of 0.0833" x 0.0833" x 0.0833". The medium meshes had an average mesh size of 0.0625" x 0.0625". The fine meshes had an average mesh size of 0.04167" x 0.04167" x 0.04167". Thus the grid refinement ratio between each mesh is 1.5. The apparent order of the method was calculated for the meshes using static pressure along the upper and lower walls as the variable of interest. (See Figure 100)

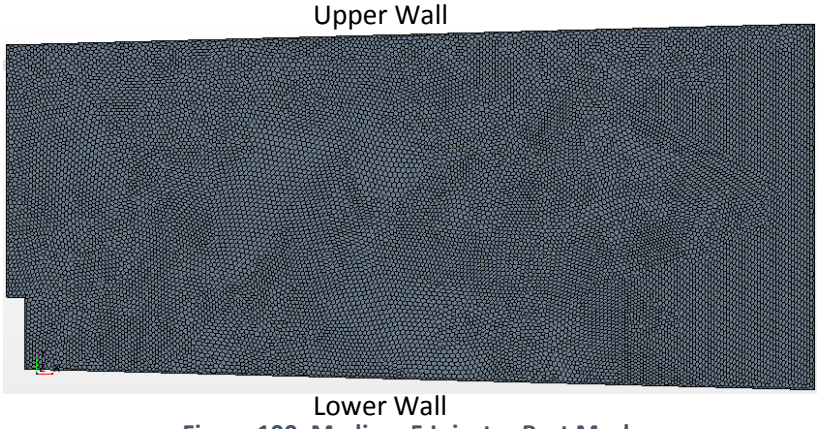

Figure 100: Medium 5 Injector Port Mesh

The meshes were run by the STAR-CCM+ solver. For cases where there is no injection or constant injection the model used was a steady model. All of the modeled cases are coupled flows. It is assumed in the STAR-CCM+ models that all gases are ideal gases and thus the energy equation is taken into account. The CFL number used for all steady cases was 5. The turbulence model used for all of the cases was the Standard K-Epsilon turbulence model. A turbulence intensity of 3.05% and a turbulent length scale of 0.0062 m were specified. The solver used for each of the models was first order implicit in time. The first order upwind scheme was used to solve for the flow. A second order scheme was used for the turbulent kinetic energy, and the turbulence dissipation rate. The flux type was ROE-FDS. The velocity at the inlet for all cases was Mach 1.8, and the inlet temperature for all cases was 300 K. To match the conditions in the supersonic wind tunnel, the inlet static pressure was specified to be -88213.9 Pa and the exit static pressure was specified to be -90000.0 Pa.

As the grid refinement ratio is constant between the meshes, the apparent order of the method can be calculated by using Equation 4.1.

$$p = \frac{1}{\ln(r_{21})}\left|ln\left|\frac{\varepsilon_{32}}{\varepsilon_{21}}\right|\right| \qquad \text{Equation 4.1}$$

Where: $\varepsilon_{32} = \phi_3 - \phi_2$, $\varepsilon_{21} = \phi_2 - \phi_1$, ϕ is equal to static pressure and r_{21}=2. Table 3 shows the average apparent order for each variable.

Table 3: Average Apparent Order

	P
Lower Wall Static Pressure for Mesh with 8 injection ports	1.98
Upper Wall Static Pressure for Mesh with 8 injection ports	1.97
Lower Wall Static Pressure for Mesh with 5 injection ports	1.99
Upper Wall Static Pressure for Mesh with 5 injection ports	1.50

Next the GCI method was used to calculate the discretization error. First the extrapolated ϕ values were calculated using Equation 4.2.

$$\phi_{ext}^{21} = \left(r_{21}^{p}\phi_1 - \phi_2\right)/\left(r_{21}^{p} - 1\right) \quad \text{Equation 4.2a}$$

$$\phi_{ext}^{32} = \left(r_{32}^{p}\phi_2 - \phi_3\right)/\left(r_{32}^{p} - 1\right) \quad \text{Equation 4.2b}$$

Then the approximate relative error was calculated using Equation 4.3.

$$e_a^{21} = \left|\frac{\phi_1 - \phi_2}{\phi_1}\right| \quad \text{Equation 4.3a}$$

$$e_a^{32} = \left|\frac{\phi_2 - \phi_3}{\phi_2}\right| \quad \text{Equation 4.3b}$$

The extrapolated relative error was calculated using Equation 4.4.

$$e_{ext}^{21} = \left|\frac{\phi_{ext}^{12} - \phi_1}{\phi_{ext}^{12}}\right| \quad \text{Equation 4.4a}$$

$$e_{ext}^{21} = \left|\frac{\phi_{ext}^{12} - \phi_1}{\phi_{ext}^{12}}\right| \quad \text{Equation 4.4b}$$

Finally the fine grid convergence index was calculated using Equation 4.5.

$$GCI_{fine}^{21} = \frac{1.25e_a^{21}}{r_{21}^{p} - 1} \quad \text{Equation 4.5}$$

Table 4 shows the average error values for each of the pertinent variables.

Table 4: Average Error Values

	e_a^{21}	e_a^{32}	e_{ext}^{21}	e_{ext}^{21}	GCI_{fine}^{21}
Lower Wall Static Pressure for Mesh with 8 injection ports	1.25%	1.58%	3.60%	3.75%	1.60%
Upper Wall Static Pressure for Mesh with 8 injection ports	0.67%	0.80%	5.50%	6.14%	0.75%
Lower Wall Static Pressure for Mesh with 5 injection ports	2.31%	1.49%	6.84%	4.50%	1.50%
Upper Wall Static Pressure for Mesh with 5 injection ports	1.27%	0.95%	4.45%	3.89%	1.42%

The fine grid convergence indices were used to calculate the error bars for the fine grid solutions presented below.

Figure 101 and Figure 103 show the static pressure curves for the three 8 injection port meshes for the lower and upper walls, respectively. Figure 102 and Figure 104 show the fine grid solution with error bars representing the discretization error. The highest errors occur where the static pressure rises sharply due to a shockwave. Figure 105, Figure 106, and Figure 107 show the static pressure contours for each of the meshes with eight injector ports.

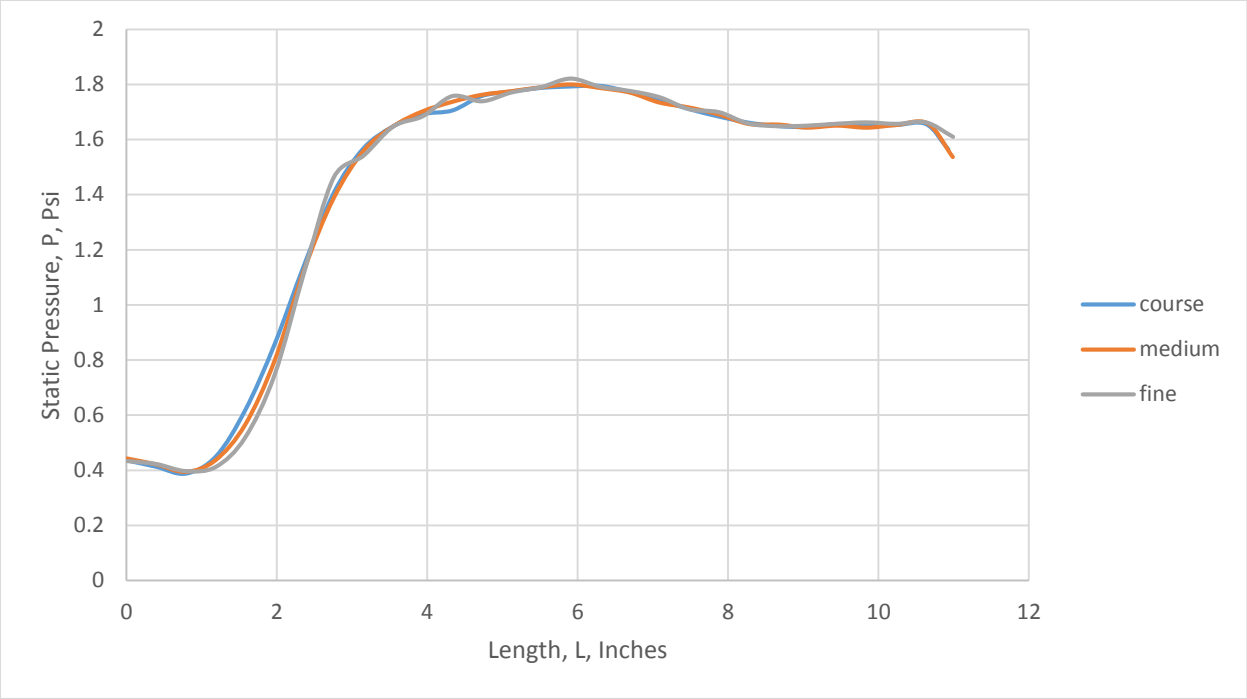

Figure 101: Static Pressure along the Bottom Wall for the 3D Mesh with 8 Injector Ports

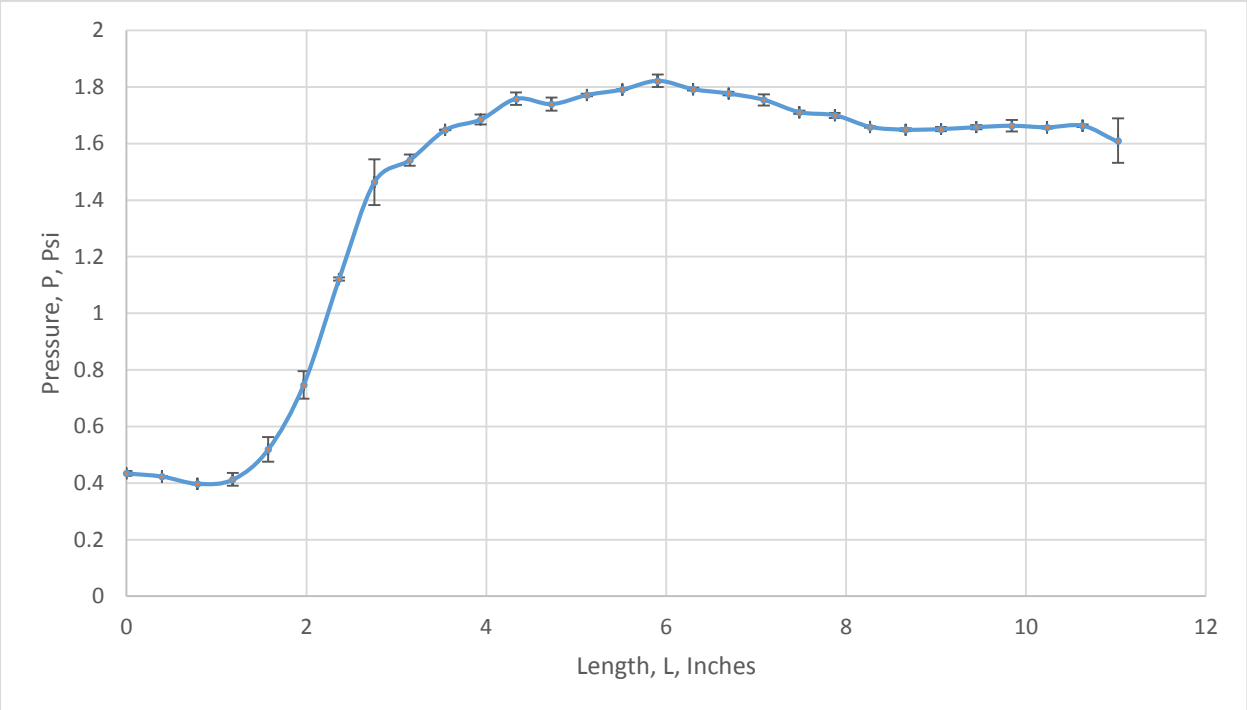

Figure 102: Fine Grid Solution with Error Bars for Static Pressure along the Bottom Wall of the 3D Mesh with 8 Injector Ports

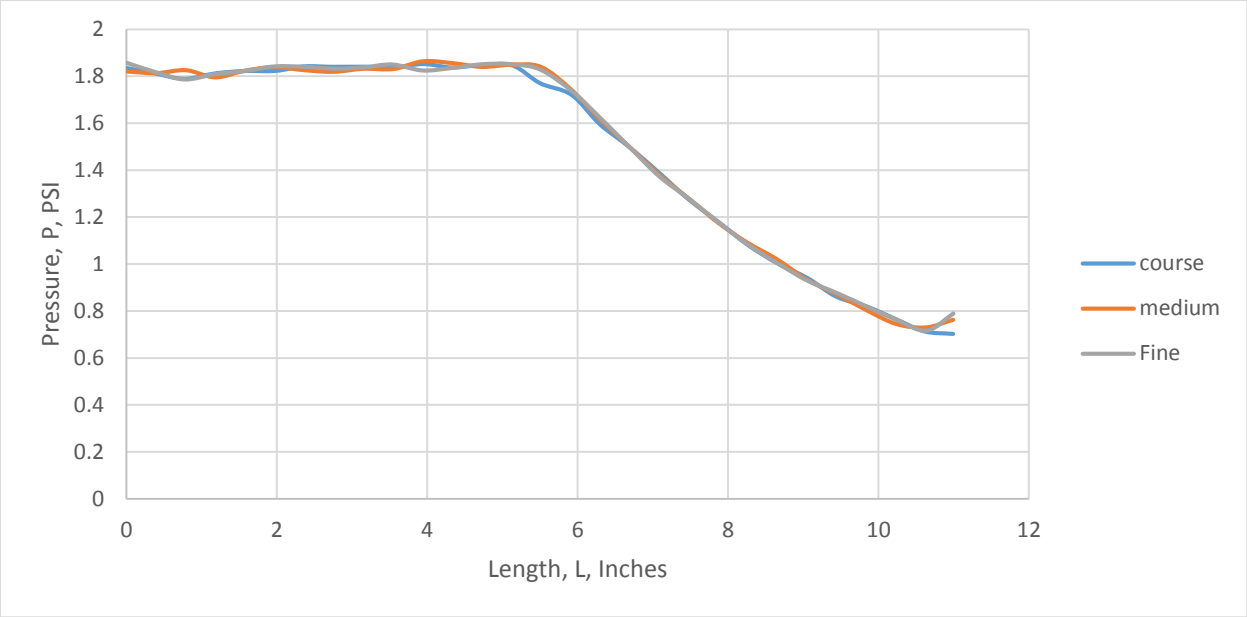

Figure 103: Static Pressure along the Top Wall for the 3D Mesh with 8 Injector Ports

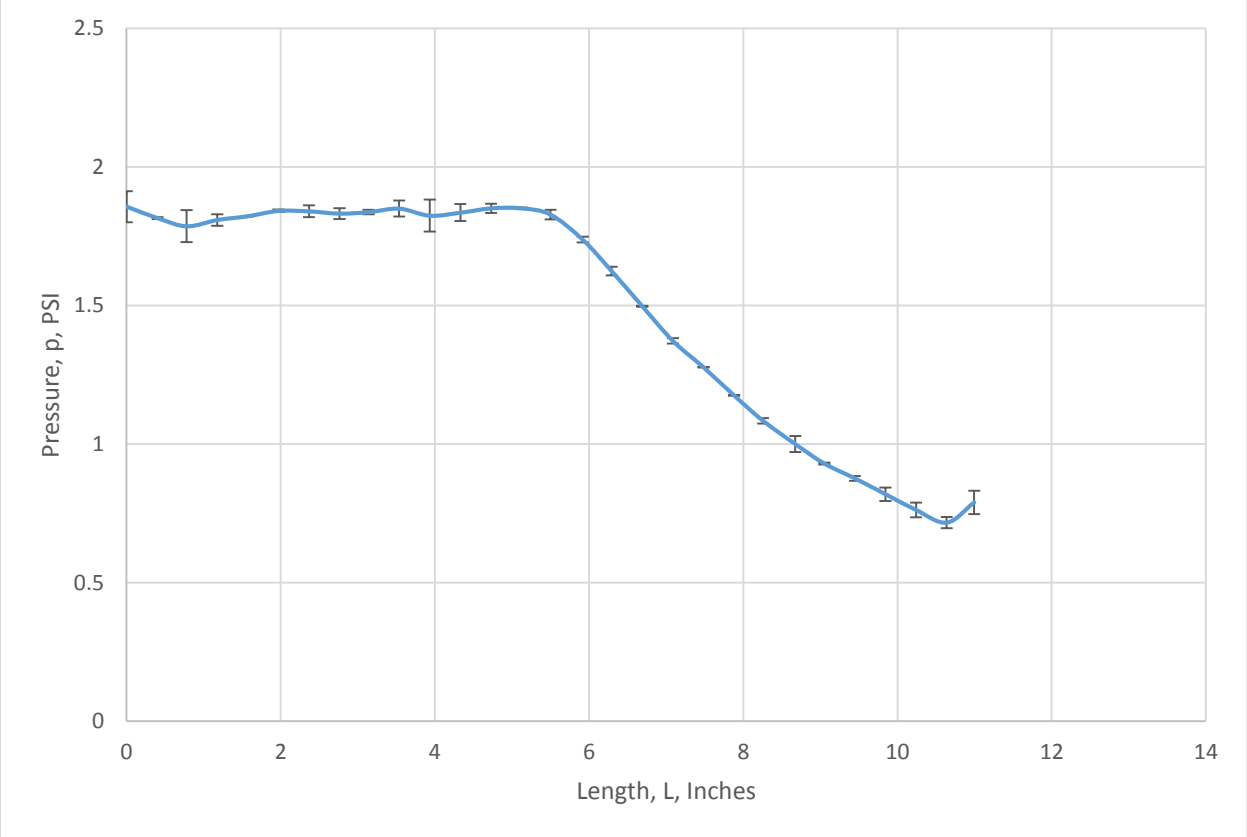

Figure 104: Fine Grid Solution with Error Bars for Static Pressure along the Top Wall of the 3D Mesh with 8 Injector Ports

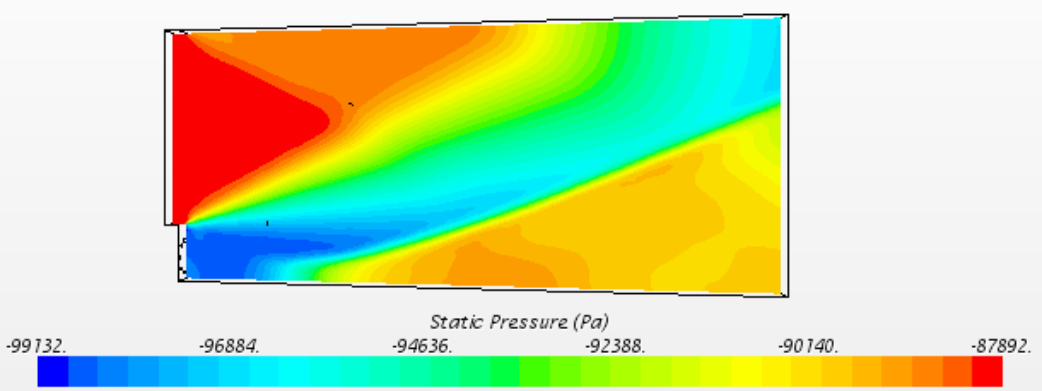

Figure 105: Static Pressure, Pa, Coarse Mesh with 8 Injector Ports

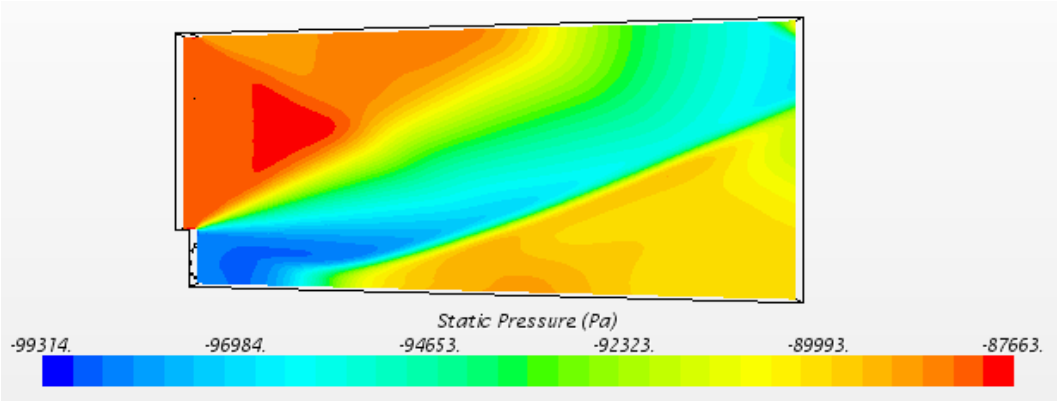

Figure 106: Static Pressure, Pa, Medium Mesh with 8 Injector Ports

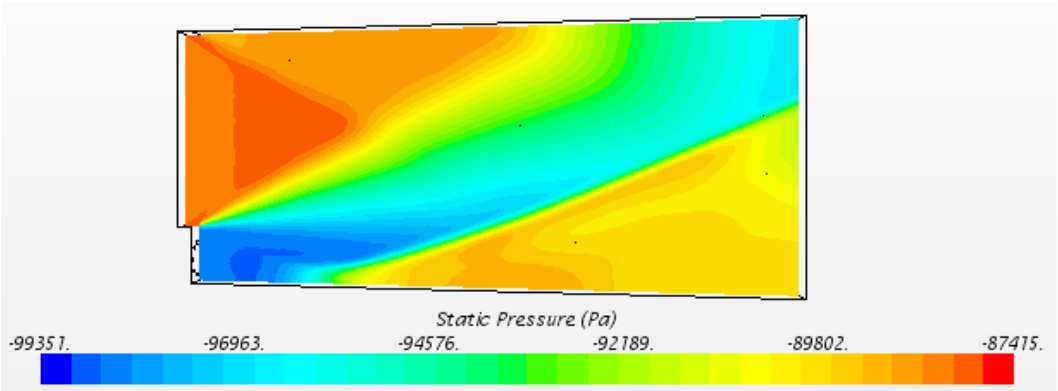

Figure 107: Static Pressure, Pa, Fine Mesh with 8 Injector Ports

Figure 108 and Figure 110 show the static pressure curves for the three 5 injection port meshes for the lower and upper walls, respectively. Figure 109 and Figure 111 show the fine grid solution with error bars representing the discretization error. The highest errors occur where the static pressure rises

sharply due to a shockwave. Figure 112, Figure 113, and Figure 114 show the static pressure contours for each of the meshes with eight injector ports.

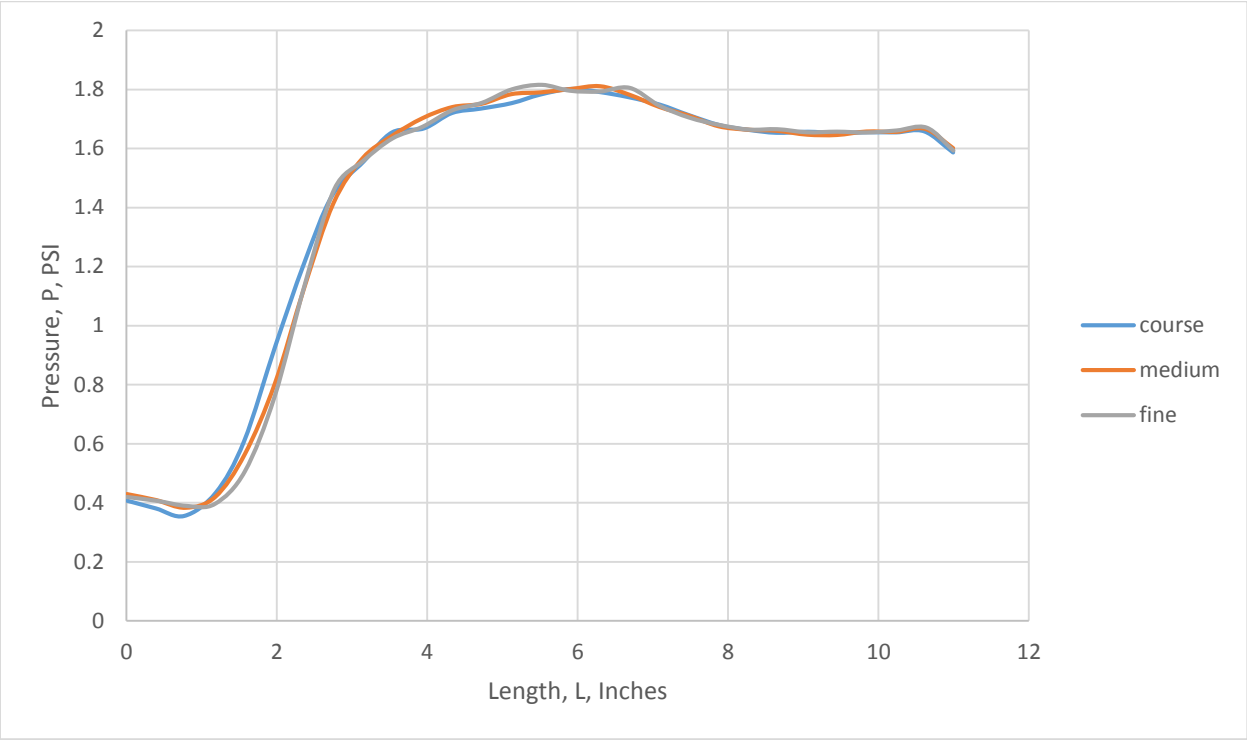

Figure 108: Static Pressure along the Bottom Wall for the Mesh with 5 Injector Ports

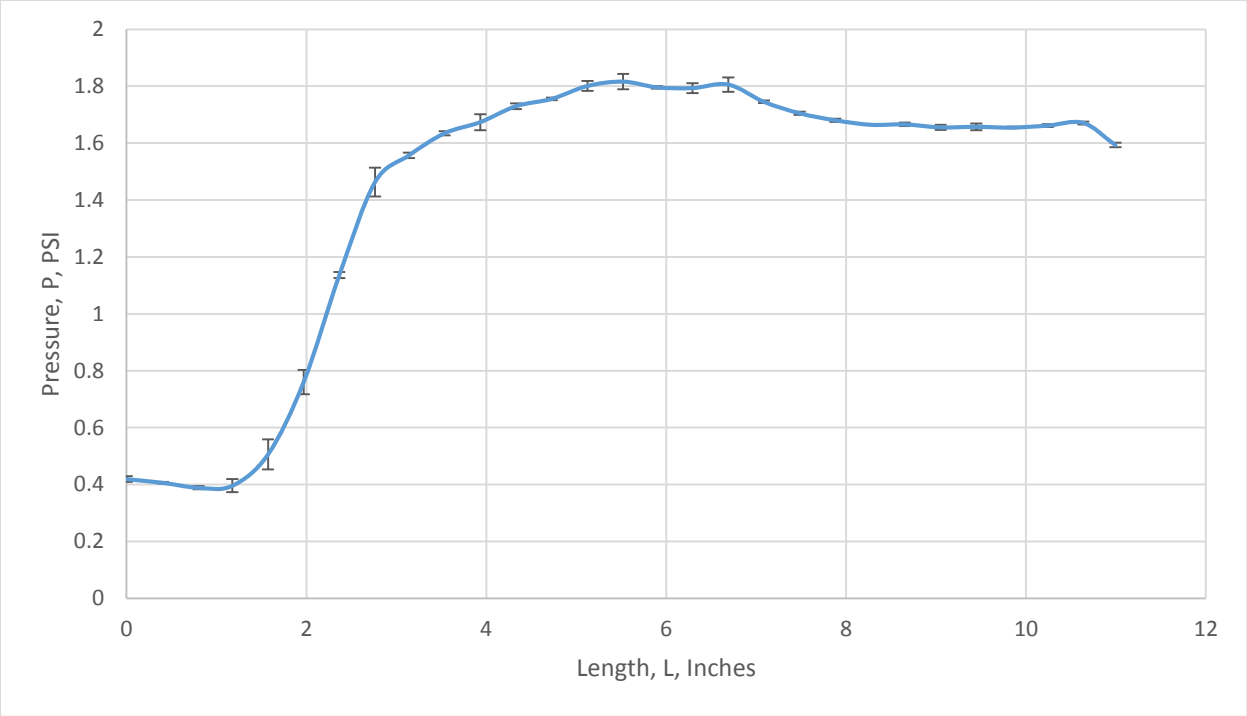

Figure 109: Fine Grid Solution with Error Bars for Static Pressure along the Bottom Wall of the Mesh with 5 Injector Ports

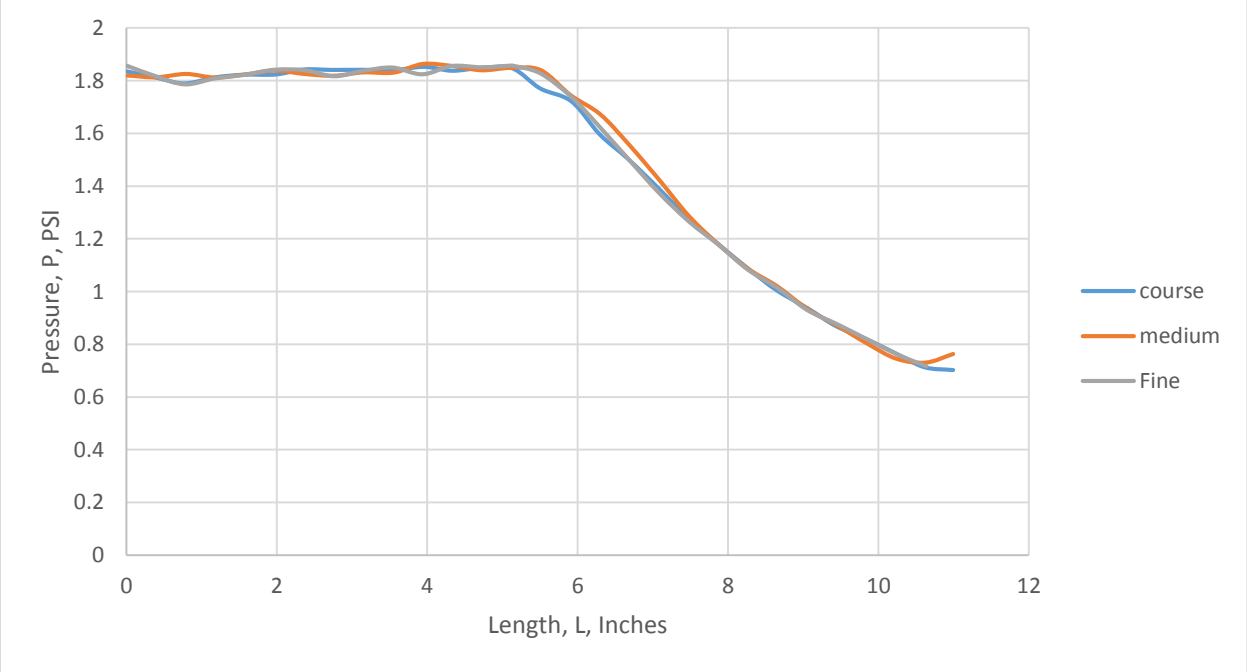

Figure 110: Static Pressure along the Top Wall for the Mesh with 5 Injector Ports

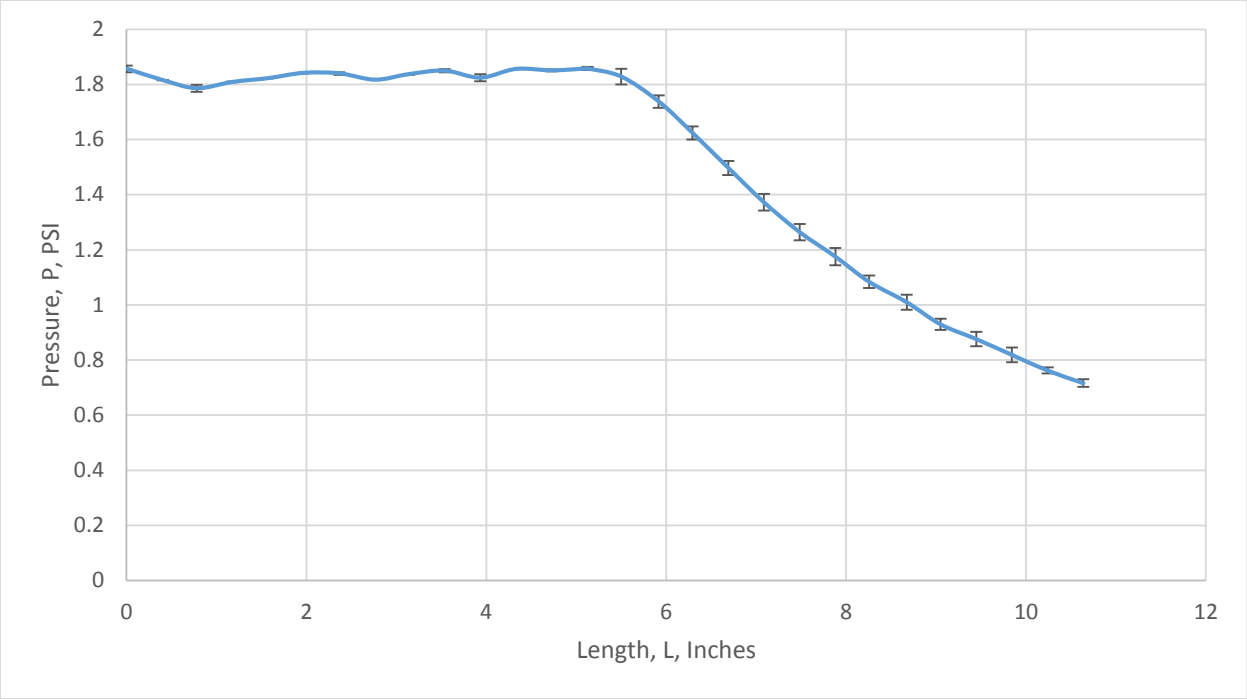

Figure 111: Fine Grid Solution with Error Bars for Static Pressure along the Top Wall of the Mesh with 5 Injector Ports

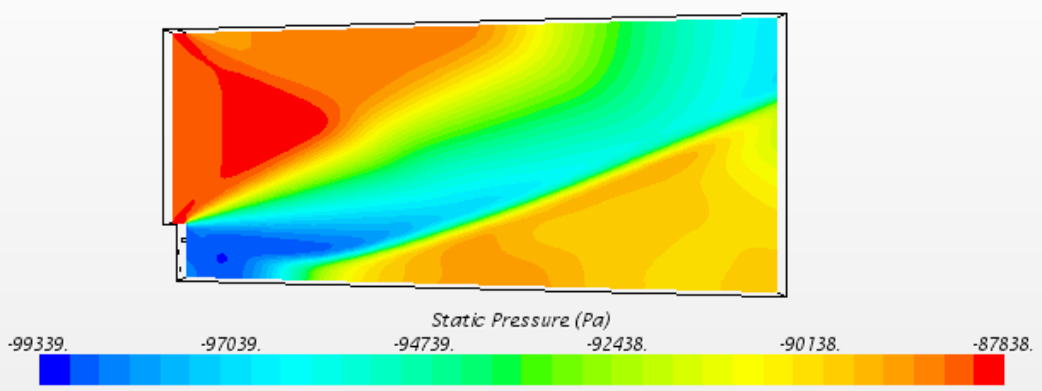

Figure 112: Static Pressure, Pa, Coarse Mesh with 5 Injector Ports

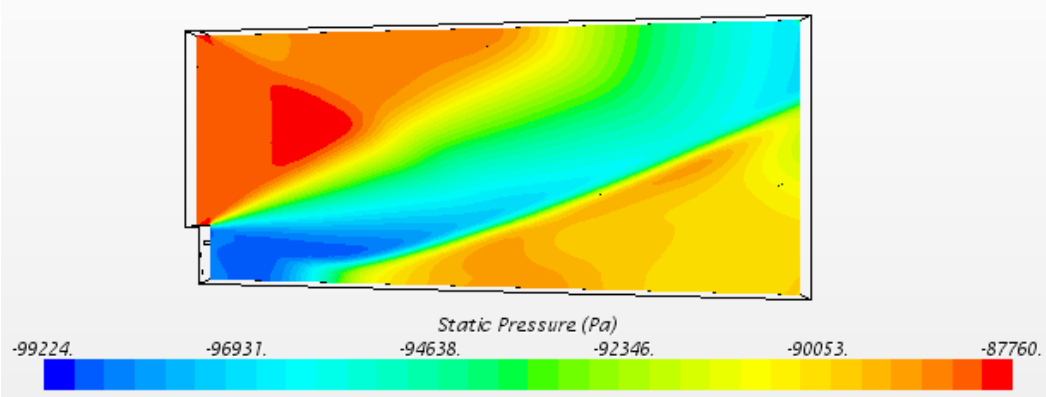

Figure 113: Static Pressure, Pa, Medium Mesh with 5 Injector Ports

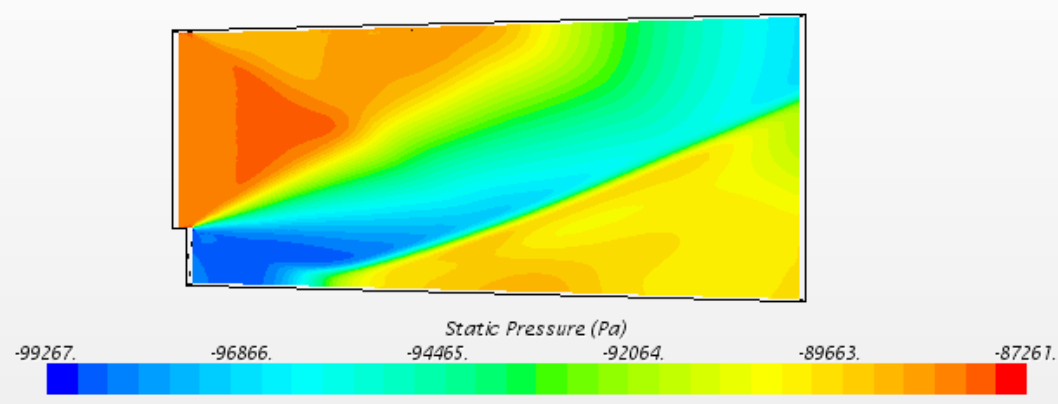

Figure 114: Static Pressure, Pa, Fine Mesh with 5 Injector Ports

Because all of the errors for each of the variables tested were so small, it can be assumed that the mesh solutions are grid independent.

For all models for constant and pulsed injection simulations thereafter the medium mesh was used because it was felt that it would capture fine vortical structures better than the coarse mesh while not taking as long to run as the fine mesh. Modeling unsteady velocities in STAR-CCM+ requires tables with one column for the time and one column for the mass flow rate profile with respect to time to be uploaded to STAR-CCM+. These profiles were created to represent the output of each of the valves.

The turbulent Intensity for the injected gas was specified to be 3.05% and the turbulence length scale was specified to be 0.0062. The injected gas was also assumed to be an ideal gas. For the constant injection case an air velocity of Mach 1 was assumed. All injected gases were specified to be at a temperature of 450 K. The CFL number used for these cases was also 5.

The model for constant flow used steady conditions but all of the pulsed injection models were transient. The transient models used the first order upwind method in space and an implicit method in time. The residuals for each case were set to be converge at 10^-4. The total run time for each model was 0.0110 seconds. For the 8 injection port mesh, 1000 time steps at a step size of 10^{-5} seconds was used. For the 5 injection port mesh 1,000 time steps at a step size of 10^{-5} seconds used for the cases representing the three different injectors. All of the pulsed injection models had a CFL number of 50, as CFL number scales with time step.

The y+ parameter is a dimensionless parameter in the viscous sub-layer, and is used in CFD studies to determine if the simulation is accurately resolving the boundary layer on the walls of a given model. A y+ analysis was performed on the walls of each of the meshes over the range of conditions tested to determine if the STAR-CCM+ model was accurately resolving the boundary layer on the walls of the simulated wind tunnel test section. Wall y+ is given by equation 4.6:

$$y^+ = \frac{u_* y}{\nu} \qquad [4.6]$$

Where y is the wall distance, v is the kinematic viscosity, and u_* is the friction velocity given by equation 4.7:

$$u_* = \sqrt{\frac{\tau_w}{\rho}} \qquad [4.7]$$

Where ρ is density, and τ_w is the wall shear stress given by equation 4.8:

$$\tau_w = \mu \left(\frac{du}{dy}\right)_{y=0} \qquad [4.8]$$

There are two wall treatment options available in the STAR-CCM+ software. The low y+ wall treatment option which is valid for when the y+ values are less than 1 and the high y+ wall treatment option which is valid for when the y+ values are greater than 1. In all cases the y+ values are in the acceptable range given by STAR-CCM+ for the high y+ wall treatment (y+ > 1).

5 Results

This section presents the results from pulsed injector testing in the supersonic wind tunnel and the results from the STAR-CCM+ CFD models. For the 8 Port injector the results for no base injection and steady injection are presented. Also presented for the 8 port injector and 5 port injector with varying pulse lengths are the results for pulsed injection at 1.0 kHz. The wind tunnel results are from the 8 port injector face plate with the 8 tooth injector valve, the 8 port injector face plate with the 16 tooth injector valve and the 5 port injector face plate with the evenly spaced 5 tooth injector valve. Figure 115 shows sketches of the front view and side view of the eight port injector. Figure 116 shows sketches of the front view and side view of the five port injector.

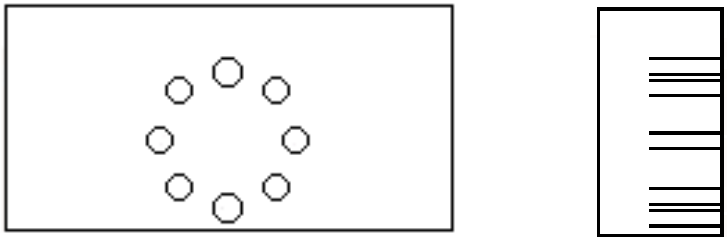

Figure 115: Sketch of 8 Port Injector Face Plate Front and Side Views

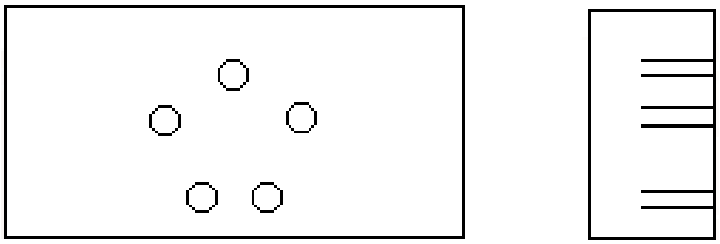

Figure 116: Sketch of 5 Port Injector Face Plate Front and Side Views

5.1 STAR-CCM+ 3D CFD Results

As the injector design is three dimensional in nature and produces a three dimensional flow field it was decided that a three dimensional CFD model is better suited for comparison with the wind tunnel data than a two dimensional CFD model. Below are presented the results of the three dimensional CFD models created in STAR-CCM+ to represent steady and pulsed injection from the 8 port and 5 port injectors.

5.1.1 No Base Injection

A no base injection case was used as a baseline condition to which all of the other test conditions could be compared. The entrance and exit conditions used in the STAR-CCM+ CFD model for the no base injection test were taken from data from the supersonic wind tunnel. Figure 117 shows the

definition sketch for the no base injection case. At station 1 the Mach number is 1.8 and the entrance static pressure is 21,000 Pa. When no base injection is present, the step causes the supersonic flow to expand and to turn around the step. An expansion wave forms at the lip of the step which turns and accelerates the flow. When the turned flow encounters the lower wall a shockwave is formed as the flow turns back to parallel condition with the duct wall. The shock wave also abruptly decelerates the flow. A zone of low speed, recirculating air is created in the separated region in the corner of the step (region 3). The flow in region 2 has a higher velocity than the recirculating air in region 3 so a shear layer forms between the recirculating air and the main flow which can be seen between the step and the lower wall. When the shear layer impinges on the lower wall it is reflected as a shock wave. The expansion waves and shock waves reflect from the upper and lower walls of the tunnel as they propagate downstream. As the supersonic flow evolves through the expansion waves and shock waves it undergoes periodic expansion and compression. As the flow is expanded through the expansion fans it is accelerated and the static pressure declines. As the flow is compressed by the reflected shock waves it is decelerated and the static pressure rises.

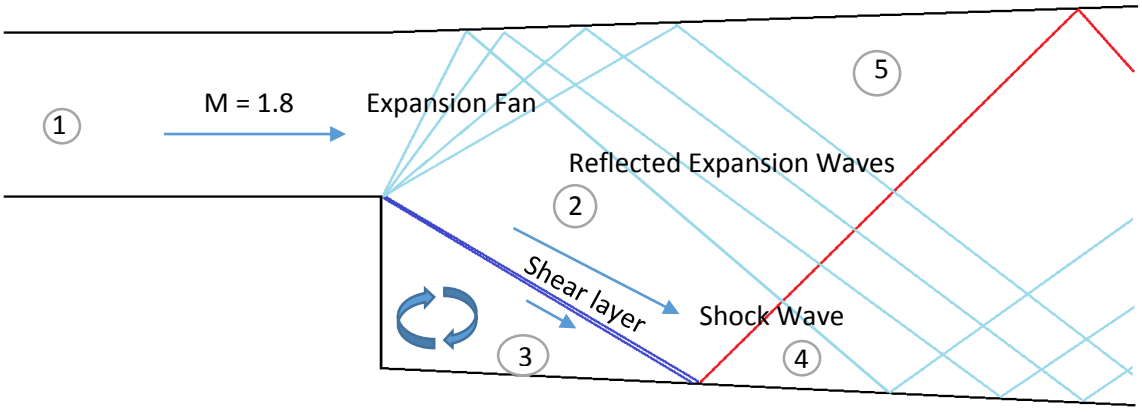

Figure 117: No Base Injection Definition Sketch

Figure 118 shows the contours of Mach number at the plane of symmetry. In these images the plane of symmetry is the right hand side of the cross section. The expansion fan and reflected expansion waves can be seen as regions where the Mach number increases incrementally. The shock waves exist where the Mach number drops abruptly after passing through a wave. The recirculation region can be seen as the region of separated, subsonic flow in the corner of the step. The shear layer impinges on the lower wall approximately 3 base heights downstream of the step. The spanwise cross sections show that near the step, where the boundary layer is thin the Mach number varies little the regardless of distance from the plane of symmetry. Further downstream where the boundary layer is

thicker and the shock wave interacts with the boundary layer, the Mach number is lower near the left hand wall. Following the definition sketch, Figure 117, the convective Mach number is expressed as:

$$M_c = \frac{2(U_2 - U_3)}{a_2 + a_3} \tag{5.1}$$

Where U_2 and U_3 are the freestream velocities of regions 2 and 3, respectively, and a_2 and a_3 are the speed of sound in regions 2 and 3, respectively. The convective Mach number of the shear layer for the no base injection case is 0.83. U_2 and U_3 were taken from the contours of velocity generated by the STAR-CCM+ model and a_2 and a_3 were calculated from the temperature contours. The non-dimensional shear layer growth rate $\Delta\delta^*/L$ is 0.005, where $\Delta\delta^*$ is the change in shear layer thickness (the thickness to where the velocity is half the freestream velocity on both sides of the shear layer) and L is the characteristic length of the shear layer in the streamwise direction. Shear layers grow more slowly at supersonic convective Mach numbers than at subsonic convective Mach numbers due to compressibility effects. As the convective Mach number in this range is still subsonic little suppression of the growth rate is expected. However, it is possible that due to velocity variations along the shear layer there will be regions where the convective Mach number is supersonic and, therefore, the growth rate is locally suppressed. In the no injection case the shear layer impinges on the wall at 3 step heights downstream of the step. This is in consistent with earlier work in literature where at Mach 2 shear layer reattachment lengths of 3 step heights to 3.5 step heights were noted.[60,61,62]

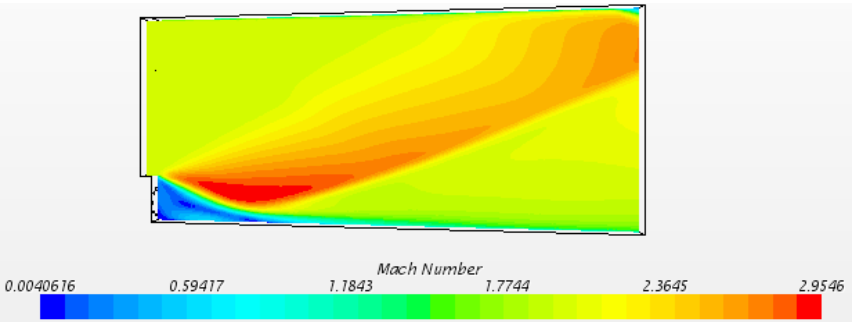

Figure 118: 3D Contours of Mach number for No Base Injection of the 8 Port Injector

Shear layers form in regions of flow where the flow velocity is greater on one side of the flow than on the other but where the static pressure is the same on both sides (in cases of planar shear layers with no curvature). In Figure 119, the contours of static pressure are shown for the no base injection case. The shear layer and recirculation region by the step cannot be discerned because the static pressure is relatively constant in that region. The static pressure can be seen to continuously decrease as the flow passes through the expansion fans and abruptly increase as the flow passes through the shockwaves. As

with the contours of Mach number, the cross sections for the contours of static pressure show very little variation with span until the flow is further downstream where the boundary layer is thicker and the shock wave interaction causes separation.

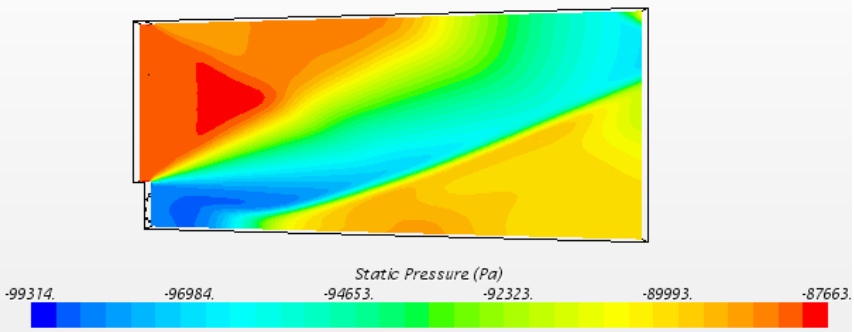

Figure 119: 3D Contours of Vorticity (Pa) for No Base Injection of the 8 Port Injector

Figure 120 shows the contours of vorticity for the no base injection case at the plane of symmetry. The vorticity dynamics equation is:

$$\frac{D\vec{\Omega}}{Dt} = (\vec{\Omega}\cdot\nabla)\vec{V} - \vec{\Omega}(\nabla\cdot\vec{V}) - \nabla x\left(\frac{1}{\rho}\nabla p\right) + \nabla x\vec{X} + \nabla x\overrightarrow{F_{visc}} \qquad (5.2)$$

The term on the left side of the equation is the time rate of change of vorticity vector following a fluid particle. The first term on the right-hand side of the equation is time rate of change of vorticity due to vortex stretching, which is inherently a three dimensional phenomenon. The second term on the right is the time rate of change of vorticity due to compressibility effects. The third term on the right is the creation of vorticity due to baroclinic torque caused when the pressure gradient and density gradient are not aligned. The fourth term on the right is the contribution of a non-conservative body force and the fifth term is the viscous contribution term.

The region of greatest vorticity naturally occurs in the shear layer generated by the separated flow at the step. In the shear layer the difference in velocity excites the Kelvin-Helmholtz instability waves which causes the interface between the two regions of differing velocity to roll up into spanwise or ring vortices. The cross section contours also show heightened levels of vorticity in the boundary layers, especially where the oblique shock interacts with the left hand side boundary layer. This vorticity is due to baroclinic torque.

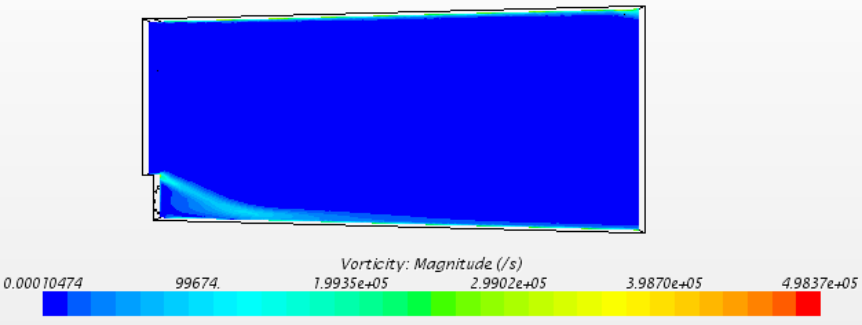

Figure 120: 3D Contours of Vorticity (1/s) for No base Injection of the 8 Port Injector at the Plane of Symmetry

Figure 121 and Figure 122 show the contours of turbulent kinetic energy for the no base injection case at the plane of symmetry and at spanwise cross sections of the three dimensional model at 0.25, 0.5, 1, 2, and 5 step heights downstream of the step. Turbulent kinetic energy is the kinetic energy per unit mass that has been generated by eddies in a turbulent flow. For the no base injection case turbulent kinetic energy is generated along the shear layer and boundary layers and in the recirculation region of the step. The turbulent kinetic energy reaches its maximum where the shear layer impinges on the lower wall and a shock wave is formed. The three dimensional model also shows large regions of turbulent flow in the region of the expansion fan and shock wave. This turbulence is generated by three dimensional compressibility effects and as shown in the cross plane this turbulence is stronger where the shock and expansion waves are stronger and weaker near the wall where the waves are weaker.

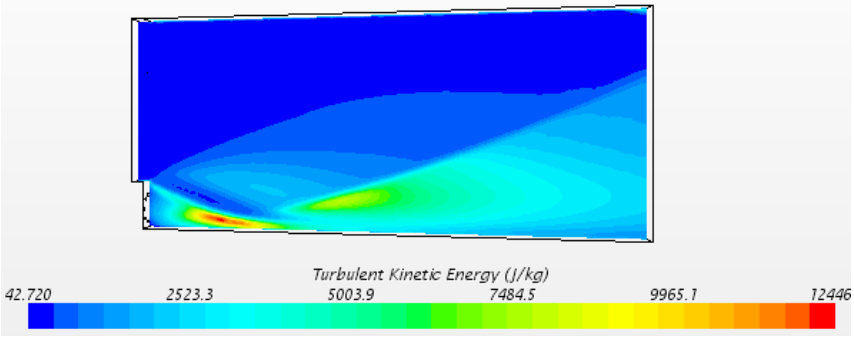

Figure 121: 3D Contours of Turbulent Kinetic Energy (m^2/s^2) for No base Injection of the 8 Port Injector

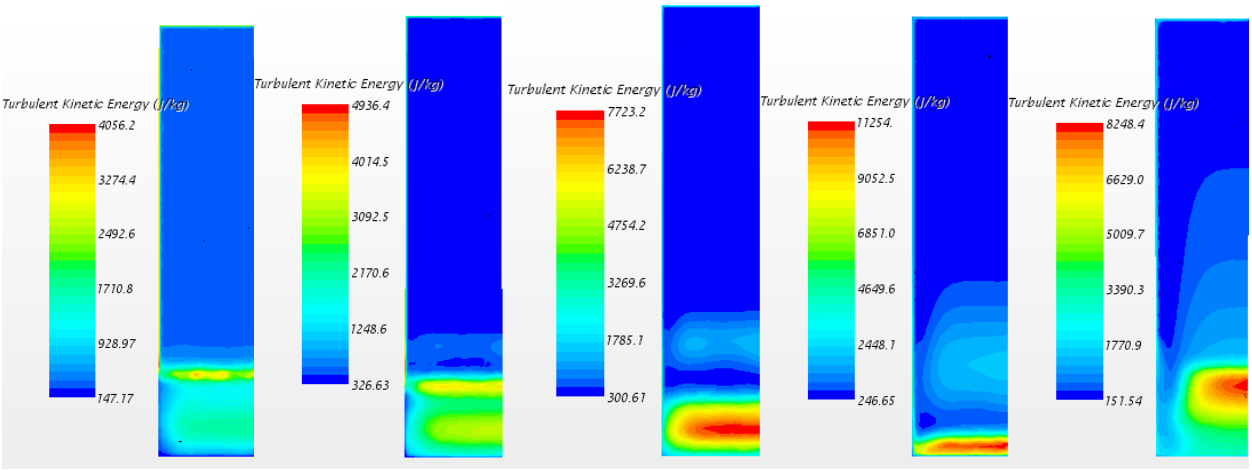

Figure 122: Cross Section Contours of Vorticity (1/s) at 0.25, 0.5, 1, 2, and 5 base heights downstream of the step

5.1.2 8 Port Injector Steady Injection

A steady injection case for the 8 port injector was run to compare with the 8 injection port pulsed injection cases to determine the effects of pulsation on mass addition from injection. Figure 123 shows the definition sketch for the steady injection case. As in the no base injection case, at station 1 the Mach number is 1.8 and the entrance static pressure is 21,000 Pa. In region 2, the injected jet is choked, i.e. the Mach number is 1. The nozzle pressure ratio of the injected gas, (NPR) the ratio of the total pressure of the injected gas to the static pressure in the tunnel, is 7. This means that the injection stream is under-expanded. As the gas is injected it expands outward and accelerates. Due to the increase in pressure from the injected mass addition the shear layer produced by the step is forced upward slightly so that the static pressure on either side of the shear layer is once again in balance. This means that slightly less flow turning by the main flow is needed, so the shockwave and expansion fans produced by the main flow are slightly weaker than in the main flow for steady injection for the case with no base injection.

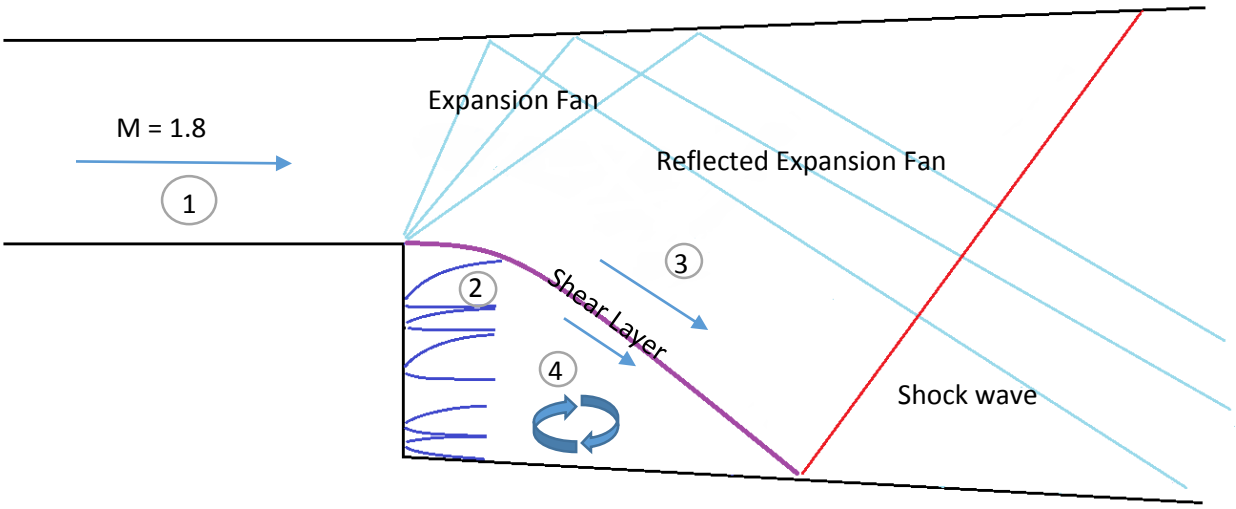

Figure 123: Steady Injection Definition Sketch

Following the definition sketch, Figure 123, the convective Mach number of the shear layer can be expressed as in equation 3 and the convective Mach number of the shear layers at the edge of the jets can be expressed in equation 4:

$$M_c = \frac{(U_2 - U_3)}{a_2 + a_3} \tag{5.3}$$

$$M_c = \frac{2(U_2 - U_4)}{a_2 + a_4} \quad M_c = \frac{(U_2 - U_4)}{a_2 + a_4} \tag{5.4}$$

Where U_2, U_3, and U_4 are the freestream velocities of regions 2, 3, and 4, respectively, and a_2, a_3, and a_4 are the speed of sound in regions 2, 3, and 4, respectively. The convective Mach number for the shear layers produced along the edges of the jets is 0.32. The convective Mach number of the step produced shear layer in the steady injection case is 0.08. U_2, U_3, and U_4 were taken from the contours of velocity generated by the STAR-CCM+ model and a_2, a_3, and a_4 were calculated from the temperature contours. These convective Mach numbers are subsonic so there is no suppression of shear layer growth due to compressibility effects. The shear layer growth rates are hard to quantify from the contours of velocity as the shear layers of the jets merge as the jets expand and the shear layer generated by the step merges with the shear layer of the upper most jet. The interaction between neighboring jets in merging introduces a complex interaction that cannot be resolved or explained by an isolated jet or shear layer growth. Consequently, the multi-port injector problem results in complex shear layer interaction demanding a new parameter besides the convective Mach number expressions of equations 3 and 4.

To examine the effect of injection, a cross section was taken of the three dimensional flow field at the plane of symmetry. The contours of Mach number show how the shear layer curves upward as a

result of injection and the effect this has on the shear layer, the expansion fan, and the oblique shock wave. It can be seen in Figure 124, the injectors force the shear layer up resulting in a weaker expansion fan and shock wave in the region of injection. This prevents strong wave formations and the attendant acceleration and deceleration. Outside the region of injection the shear layer, expansion fan and shock wave behave as in the no injection case. The nozzle pressure ratio, NPR, is 7 so the jets are under-expanded and expand and accelerate outward from the point of injection. At the plane of symmetry, the shear layer impinges on the lower wall at approximately 3.5 step heights downstream. The cross sections show that the injection has forced the shear layer to impinge further downstream than in the region where no injection is present. However, the Mach contours show a region of lower. Further downstream the effects of injection on Mach number wash out and the variation across the span declines. The Mach contours across the span at 5 base heights downstream have a lower peak Mach number than in the no base injection case.

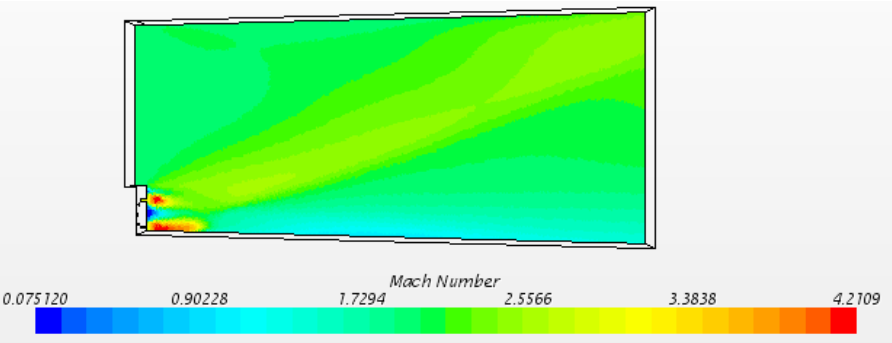

Figure 124: 3D Contours of Mach Number for Steady Injection of the 8 Port Injector

In steady injection, at the plane of symmetry, the shear layer has been forced upward resulting in a weaker expansion fan and shock wave. This results in less of a change in static pressure as the flow moves through the wind tunnel. This can be seen in Figure 125. Away from the injectors the shear layer has not been perturbed and the contours resemble the no base injection contours. Near the injector the jets raise the static pressure, but further downstream the effects of injection wash out and there is little variation in static pressure across the span.

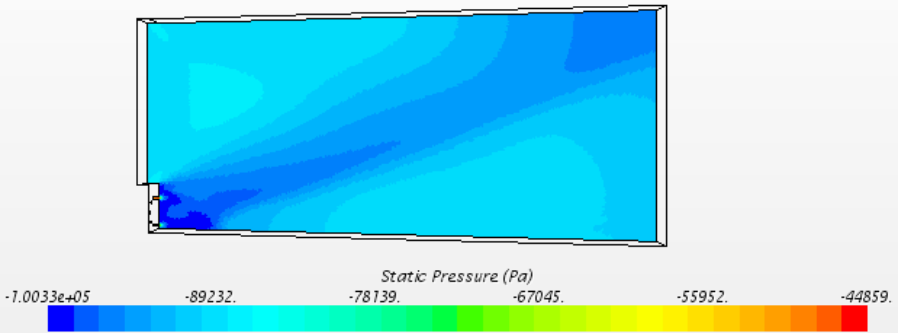

Figure 125: 3D Contours of Static Pressure (Pa) for Steady Injection of the 8 Port Injector

As we observe in Figure 126 and Figure 127, for steady injection, unlike the no base injection case, the peak vorticity strength is in the shear layers along the edges of the jets, but the vorticity in the jets themselves is very low. The vorticity strength along the shear layer is diminished near the region of injection as the velocity differential is much lower due to injection. This results in a much weaker shear layer near the point of injection in the steady injection case than in the no base injection case. In essence, injection fills the base with high pressure fluid and thus weakens the separated shear layer at the step corner. Away from the injectors the shear layer is stronger, as reasoned above.

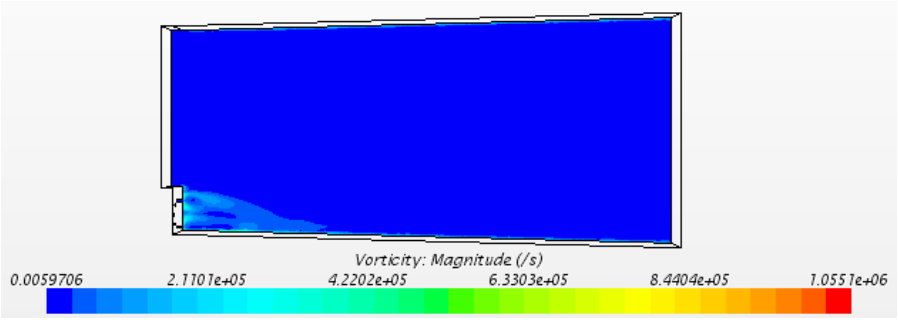

Figure 126: 3D Contours of Vorticity (1/s) for Steady Injection of the 8 Port Injector

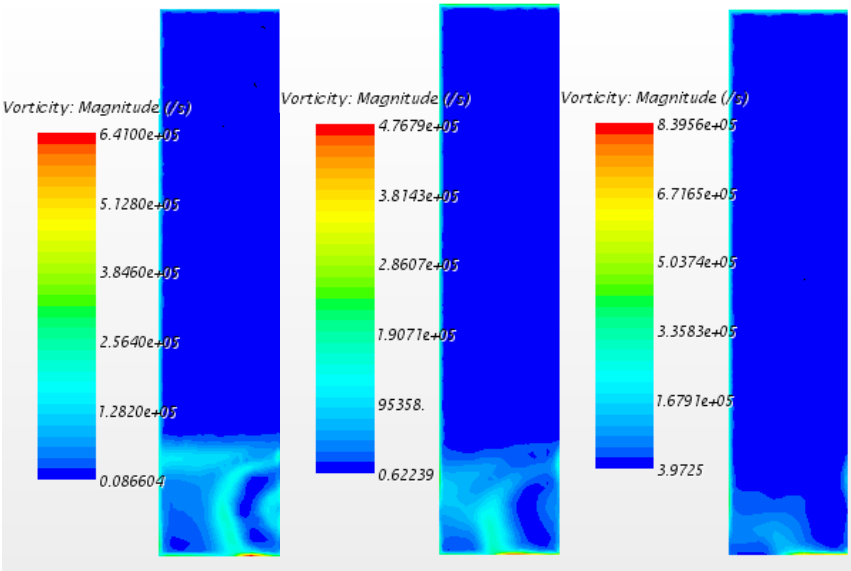

Figure 127: Steady Injection Cross Section Contours of Vorticity (1/s) at 0.25, 0.5, and 1 base heights downstream of the step

The regions with the highest turbulent kinetic energy in the three dimensional model are the shear layers around the jets, as we observe in Figure 128 and Figure 129. The turbulent kinetic energy in the shear layer is quite low where the injected jets interact with it. This is because of the lower vorticity due to the change in velocity across the shear layer being smaller. As in the no base injection case the expansion fan region and the region just downstream of the oblique shock are also characterized by regions of higher turbulence. The turbulent kinetic energy in these regions is not as strong as in the no injection case which further suggests that this turbulence is partially due to compressibility effects as the expansion fan and shock waves are weaker for the steady injection case than in the no injection case. Another contributor to turbulent kinetic energy is due to the curvature of the shear layer, which is suppressed by multi-port injection.

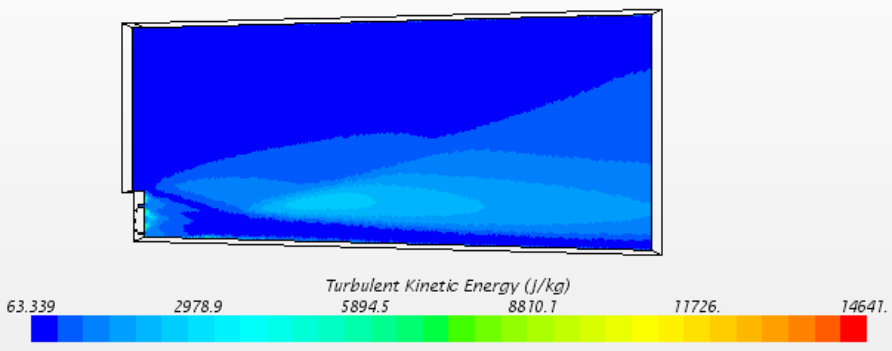

Figure 128: 3D Contours of Turbulent Kinetic Energy (m^2/s^2) for Steady Injection of the 8 Port Injector

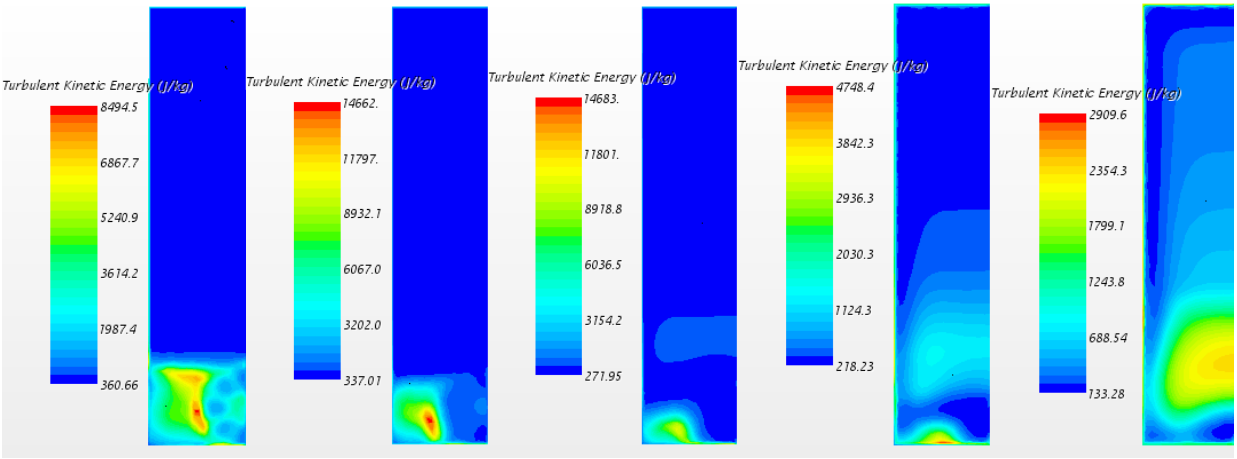

Figure 129: Steady Injection Cross Section Contours of Turbulent Kinetic Energy (m^2/s^2) at 0.25, 0.5, 1, 2, and 5 base heights downstream of the step

5.1.3 8 Port Injector 1.0 kHz Injection

The pulsed injection was modelled at 1.0 kHz. Figure 130 shows the definition sketch for all pulsed injection cases. As in the previous cases, at station 1 the Mach number is 1.8 and the entrance static pressure is 21,000 Pa. At region 2, the injected jet, each pulse is injected at Mach number is 1. As in the steady injection case, the nozzle pressure ratio of the injected gas, (NPR) is 7, so the injection is under-expanded. At the beginning of each pulse the shear layer resembles the shear layer in the no base injection case. An expansion fan forms at the lip of the step to turn the flow and a separated recirculation zone exists in the corner of the step (region 4). A shear layer forms between the supersonic turned flow of region 3 and the subsonic recirculating flow of region 4.

As a pulse is injected, the shear layer generated by the step is forced slightly upward. At the peak of injection, the shear layer produced by the step is in the same position as the shear layer in the steady

injection case. At a frequency of 1.0 kHz the period of injection is 1 millisecond. At 100% of the period of pulsation the shear layer generated by the step recovers its position at the beginning of the pulse.

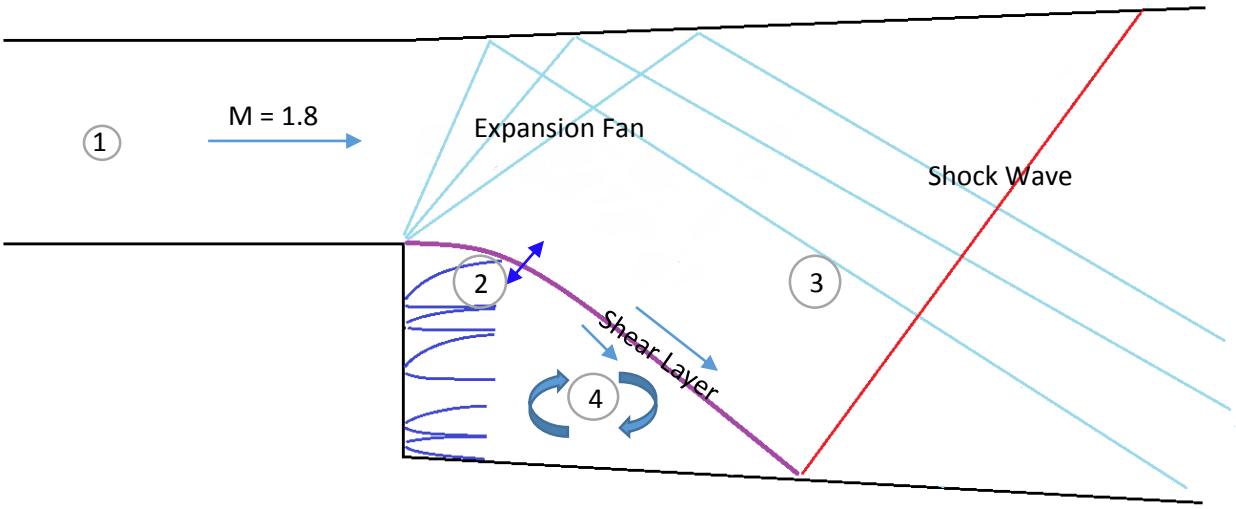

Figure 130: Pulsed Injection Definition Sketch

The same cross sections that were used to examine steady state injection of the 8 port injector were also used to examine pulsed injection at 1.0 kHz. The contours of Mach number over the pulse are shown in Figure 131. It can be seen that at the beginning of the pulse the shear layer approximates the shear layer of the no base injection case. At this early stage of injection the injected jets have little effect on the position of the shear layer. Thus, the Mach contours of the main flow have not varied much from their injector off positions. The nozzle pressure ratio, NPR, is 7 so the jets are under-expanded and expand and accelerate outward from the point of injection. As can also be seen in Figure 131, the shear layer impinges on the lower wall at approximately 3.7 step heights. At 20% of the period of pulsation, i.e. 0.2T, there is some slight curvature in the shear layer near the region of injection, but overall there is little spanwise variation in the Mach contours.

The contours of Mach number at 0.4T, show the shear layer begin to curve upward at each of the injectors as a result of increased injection. At the plane of symmetry, the injection forces the shear layer up slightly resulting in a weaker expansion fan and shock wave. This results in less variation in Mach number as the flow passes through the test section. The shear layer impinges on the lower wall at approximately 4.4 step heights, which in essence is delayed from the 3.5 in the base injection case. At 0.4T the increased injection has resulted in more spanwise shear layer curvature, but the effects of injection are less noticeable further downstream.

The contours of Mach number at 0.6T show the shear layer curve upward at each of the injectors as a result of increased injection to, at this stage of injection approximate the steady injection case. At the plane of symmetry the injectors force the shear layer up resulting in a weaker expansion fan and shock wave. This results in less variation in Mach number as the flow passes through the test section. The shear layer impinges on the lower wall at approximately 5 step heights. The greatest spanwise shear layer curvature occurs at 0.6T, when injection is at its peak.

The contours of Mach number at 0.8T show the shear layer curve has decreased as a result of decreased injection. At the plane of symmetry, the injection once again only forces the shear layer up slightly resulting in a weaker expansion fan and shock wave, but less so than when the injection was at its peak. The shear layer impinges on the lower wall at approximately 4.8 step heights. At 0.8T, as the pulse begins to recede, the spanwise curvature of the shear layer decreases and the effects of injection further downstream become less profound.

At the end of the pulse, the shear layer once again approximates the shear layer of the no base injection case. Thus, the Mach contours of the main flow once again also match their injector off positions. The shear layer impinges on the lower wall at approximately 3.4 step heights, as noted earlier. At 1T the spanwise contours of Mach number approximate those of the no base injection case. The contours of pulsed injection seem to merely oscillate between the contours of the no base injection case and the steady state injection case.

In terms of Figure 130, the convective Mach number of the shear layer can be expressed as in equation 6 and the convective Mach number of the shear layers at the edge of the jets can be expressed in equation 7:

$$M_c = \frac{2(U_3 - U_4)}{a_3 + a_4} \tag{5.5}$$

$$M_c = \frac{2(U_2 - U_3)}{a_2 + a_3} \tag{5.6}$$

Where U_2, U_3, and U_4 are the freestream velocities of regions 2, 3, and 4, respectively, and a_2, a_3, and a_4 are the speed of sound in regions 2, 3, and 4, respectively. The velocities were taken from the contours of velocity generated by STAR-CCM+ and the speeds of sound were calculated from the temperature contours. The shear layer convective Mach number oscillates between 0.83 and 0.08 and the shear layers along the edges of the jets have a convective Mach number of 0.32. Both of these convective Mach numbers are subsonic so no suppression of shear layer growth is expected from compressibility effects.

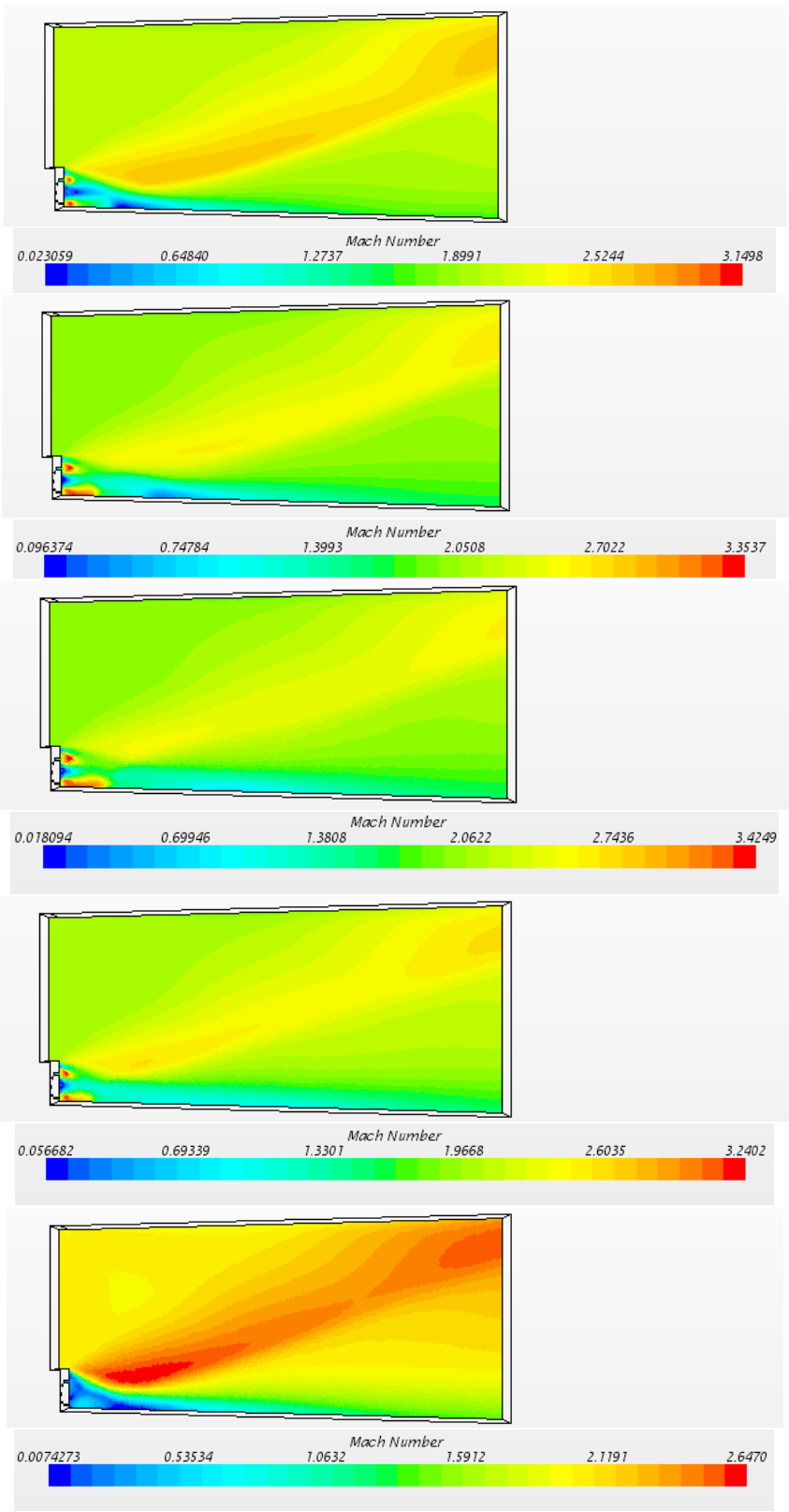

Figure 131: Contours of Mach number for the 8 port Injector at 0.2T, 0.4T, 0.6T 0.8T and 1T

In pulsed injection, when the injectors are off the contours of static pressure mimic the no base injection case at all cross sections. As the injectors begin to inject gas, the shear layer is forced upward weakening the expansion fan and shock wave. This results in less variation in static pressure as the flow progresses through the expansion fan and shock wave in the test section. As injection increases the shear layer is forced up further and the expansion fan is further weakened. Figure 133 shows this phenomenon at the plane of symmetry where the effect is the strongest. In the plane of symmetry the static pressure is lower across the height of the tunnel. The static pressure increase moving to the left, away from the plane of symmetry and towards the wall, as the injectors become lower, outside the influence of the injectors the static pressure contours resemble the no base injection contours throughout the pulse. As injection reaches its peak the static pressure contours come to resemble the steady injection contours. As the pulse begins to recede the change in static pressure across the expansion fan and shock begins to increase. When the pulse ends the static pressure contours again resemble the no base injection case.

Figure 132 shows the pressure variation with time along the lower wall. There is some initial pressure variation due to injection, but the changes in pressure are much smaller beyond the shear layer reattachment point.

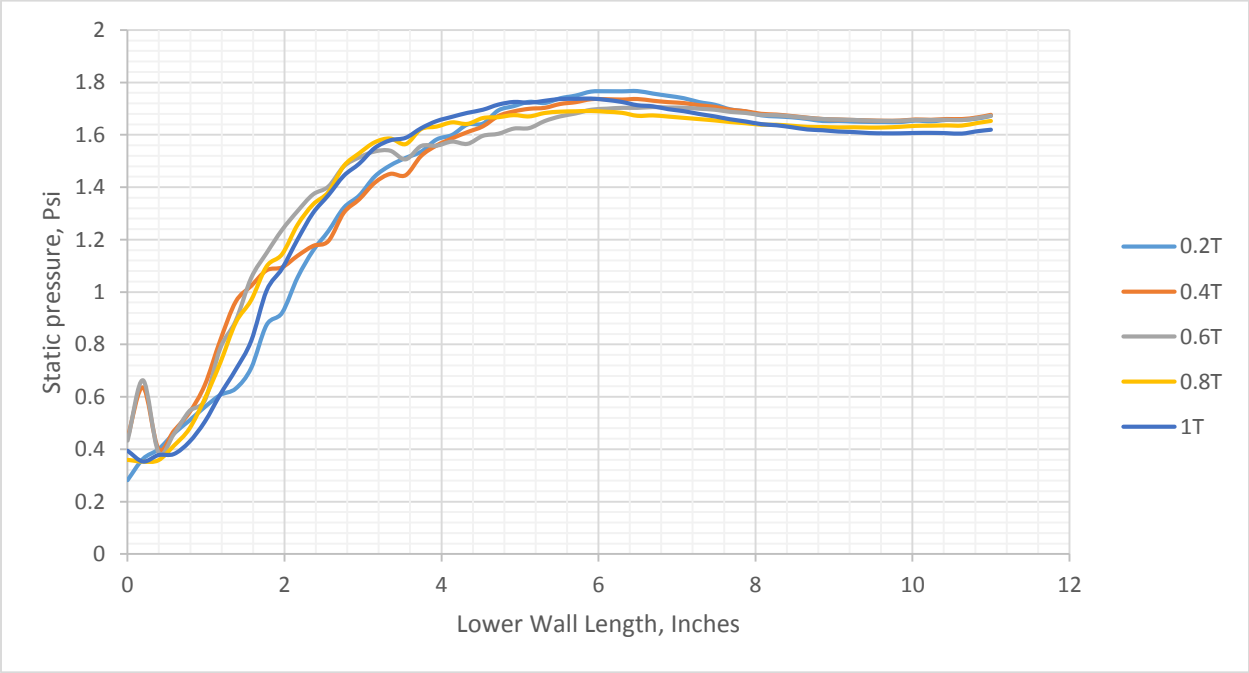

Figure 132: 1.0 kHz Lower Wall Static Pressure Variation over One Pulse for the 3D 8 Port Model (note 1 inches is the step height)

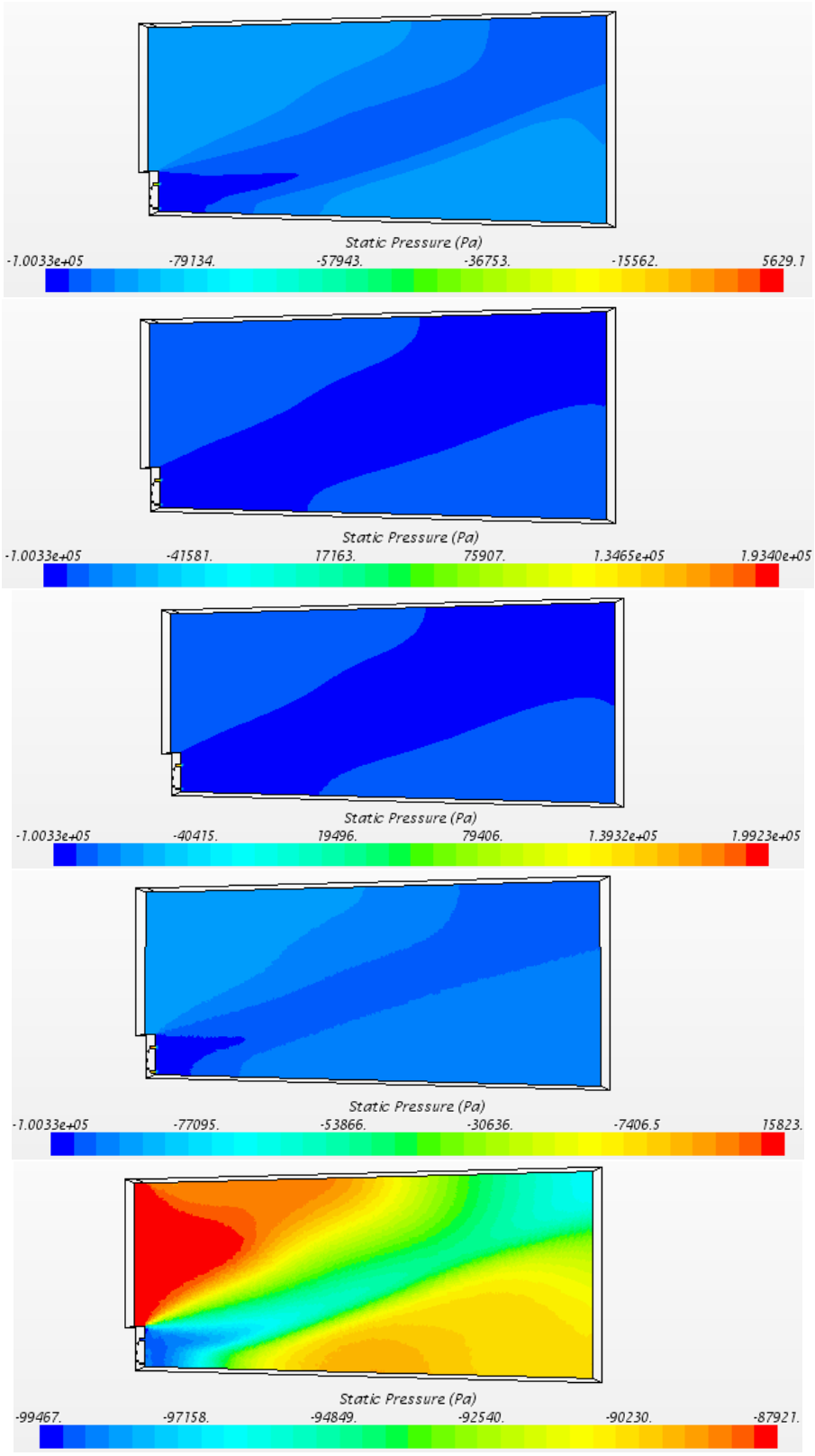

Figure 133: Contours of Static Pressure for the 8 port Injector at 0.2T, 0.4T 0.6T 0.8T, and 1T

In pulsed injection when, the injectors are off the peak vorticity levels can be found in the shear layer, like in the no base injection case, where the Kelvin-Helmholtz instability has been excited by the differing velocities to create vorticial structures. When the injection pulse begins at 0.2T of pulsation, the peak vorticity strength begins to shift to the shear layers along the edges of the jets as shown in Figure 134, Figure 135, and Figure 136. At the beginning of each pulse the convective Mach number of the shear layer is the same as for the no base injection case.

As injection continues, at 0.4T, the vorticity strength in the shear layers along the edges of the jets becomes stronger and the vorticity in the shear layer shed from the step becomes weaker in the region of injection. The strength of the vorticity along the shear layer is diminished because the velocity differential is much lower due to increased injection. This results in a progressively weaker shear layer in the region of injection in the pulsed injection case compared to the no base injection case. Outside the region of injection the strength of vorticity in the shear layer is amplified.

As injection reaches its peak, at 0.6T, the vorticity strength in the shear layers along the edges of the jets continue to increase and the vorticity in the shear layer shed from the step continue to decrease in the region of injection. The vorticity strength along the shear layer is weaker because the velocity differential is at its lowest due to the velocities induced by injection being at their highest during the pulse. This results in a weak shear layer, in the region of injection. The convective Mach number of the shear layers along the jets when injection is at its peak are 0.32, while the convective Mach number along the shear layer when injection is at its peak is 0.08 at the plane of symmetry.

As injection begins its downward cycle, at 0.8T, the vorticity strength in the shear layers along the edges of the jets is weaker and the vorticity in the shear layer shed from the step becomes amplified.

At the end of injection, at 1T, the vorticity contours come to resemble the vorticity contours of the no base injection case. The convective Mach numbers are the same as for the no base injection case.

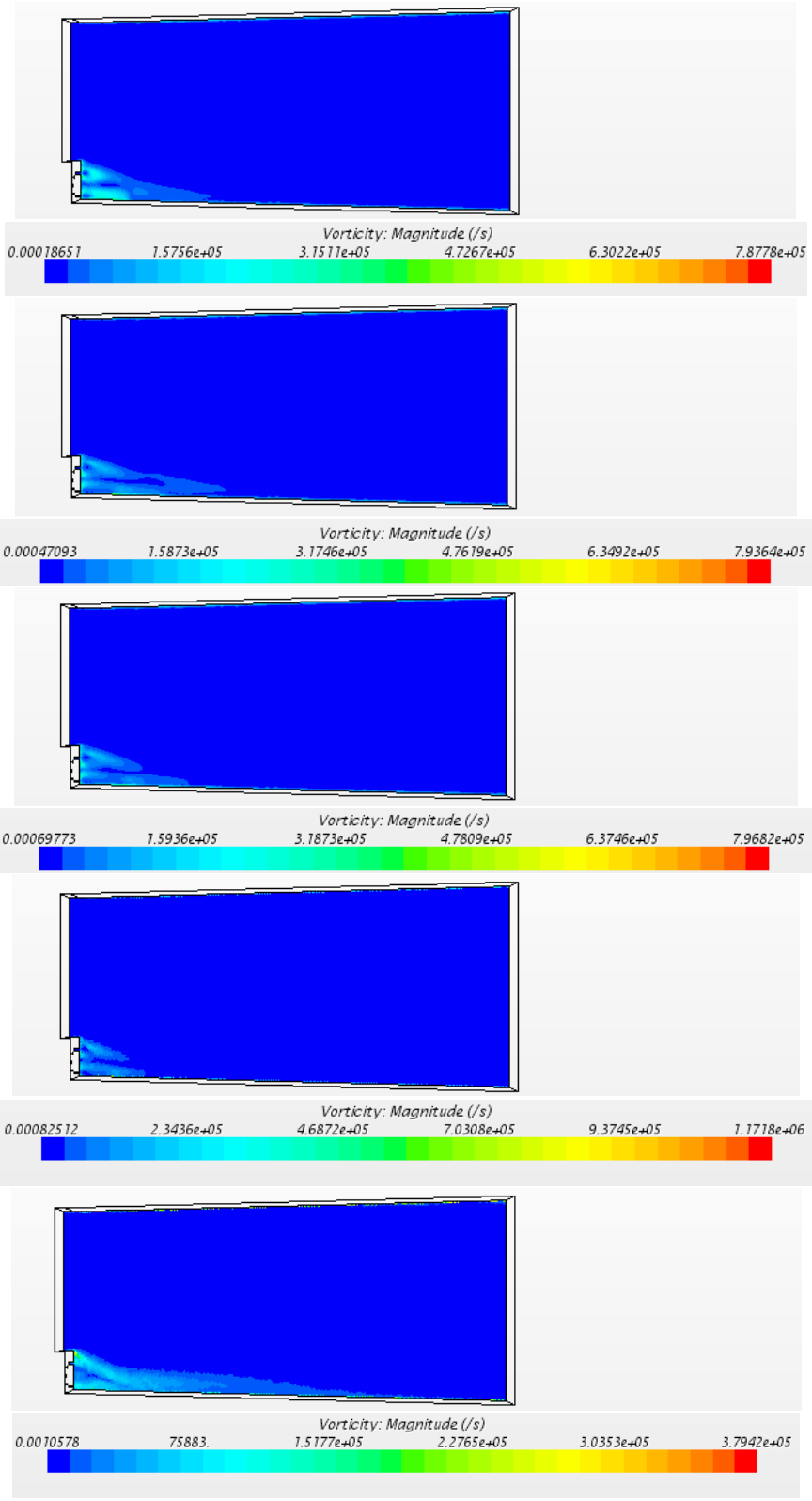

Figure 134: Contours of Vorticity (1/s) for the 8 port Injector at 0.2T, 0.4T, 0.6T, 0.8T, and 1T

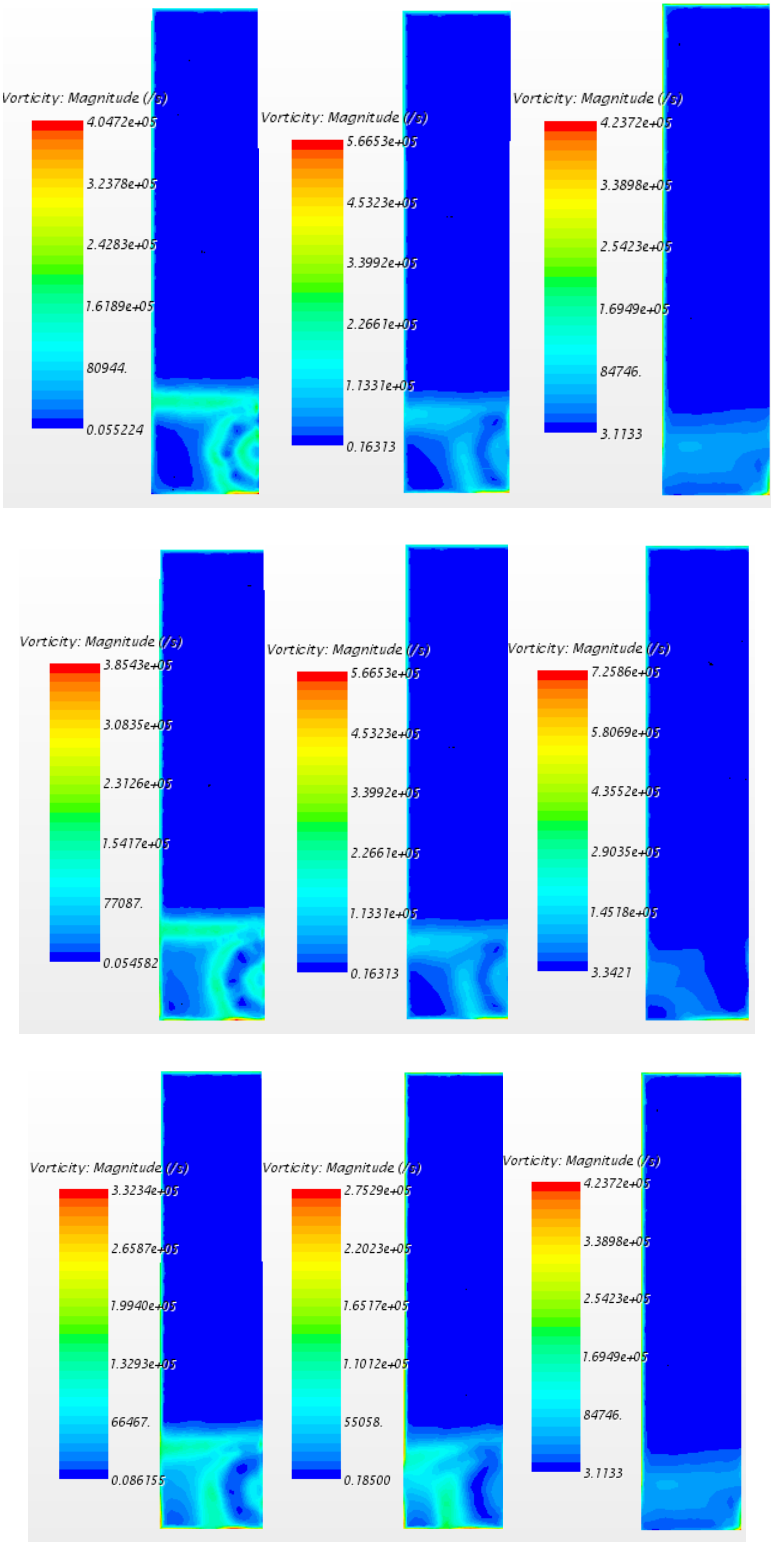

Figure 135: Pulsed Injection Cross Section Contours of Vorticity (1/s) at 0.25, 0.5, and 1 base heights downstream of the step at 0.2T, 0.4T, and 0.6T

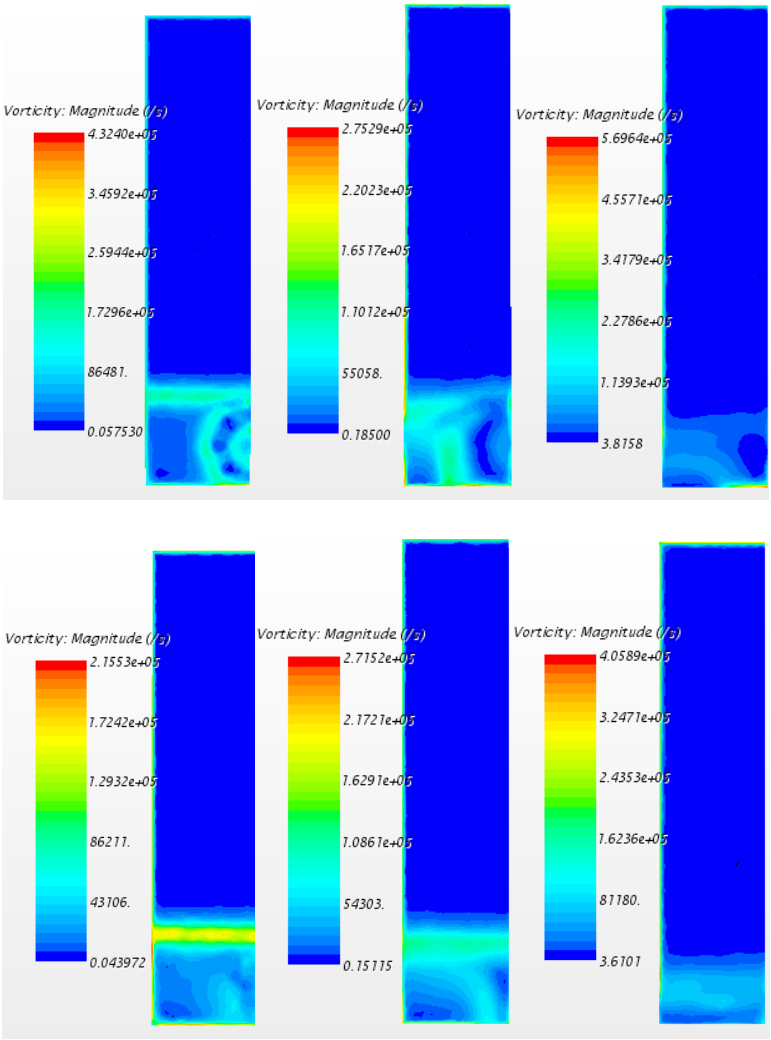

Figure 136: Pulsed Injection Cross Section Contours of Vorticity (1/s) at 0.25, 0.5, and 1 base heights downstream of the step at 0.8T and 1T

We observe that in Figure 137, Figure 138, and Figure 139, the turbulent kinetic energy in the pulsed injection case peaks near the shear layer impingement point at the beginning of the pulse, as in the no base injection case. Also as in the no injection case, the pulsed injection model shows large regions of turbulent flow in the region of the expansion fan and shock wave, which is partially due to three dimensional compressibility effects and is partially caused by flow curvature.

At 0.4T, the regions with the highest turbulent kinetic energy are the shear layers around the jets right as they are injected into the recirculation region. Outside the region influenced by the injectors the turbulent kinetic energy in the shear layer is still high. The lower vorticity due to the change in velocity across the shear layer being smaller causes the turbulent kinetic energy in the shear layer to diminish near the injectors as the pulse begins. As in the no base injection case the expansion fan region and the region just downstream of the oblique shock are also characterized by regions of higher turbulence. The turbulent kinetic energy in these regions is not as strong as in the no base injection case suggesting that this turbulence is due to compressibility effects and reduced flow curvature.

At 0.6T, the regions with the highest turbulent kinetic energy are still the shear layers around the jets as they are injected into the recirculation region. The jets themselves have a remarkably low level of turbulence. The vorticity due to the change in velocity across the shear layer is at its lowest at this point in the pulse which causes the turbulent kinetic energy in the shear layer near the injectors to be quite low. The expansion fan region and the region just downstream of the oblique shock are also characterized by regions of higher turbulence, mainly due to flow curvature.

At 0.8T, the regions with the highest turbulent kinetic energy are still the shear layers around the jets right as they are injected into the recirculation region. The lower vorticity due to the change in velocity across the shear layer near the injectors being slightly larger than at the peak of the pulse causes the turbulent kinetic energy in the shear layer to increase as the pulse recedes. The expansion fan region and the region just downstream of the oblique shock are also characterized by regions of higher turbulence. At 1T, the turbulent kinetic energy contours come to resemble the no injection contours.

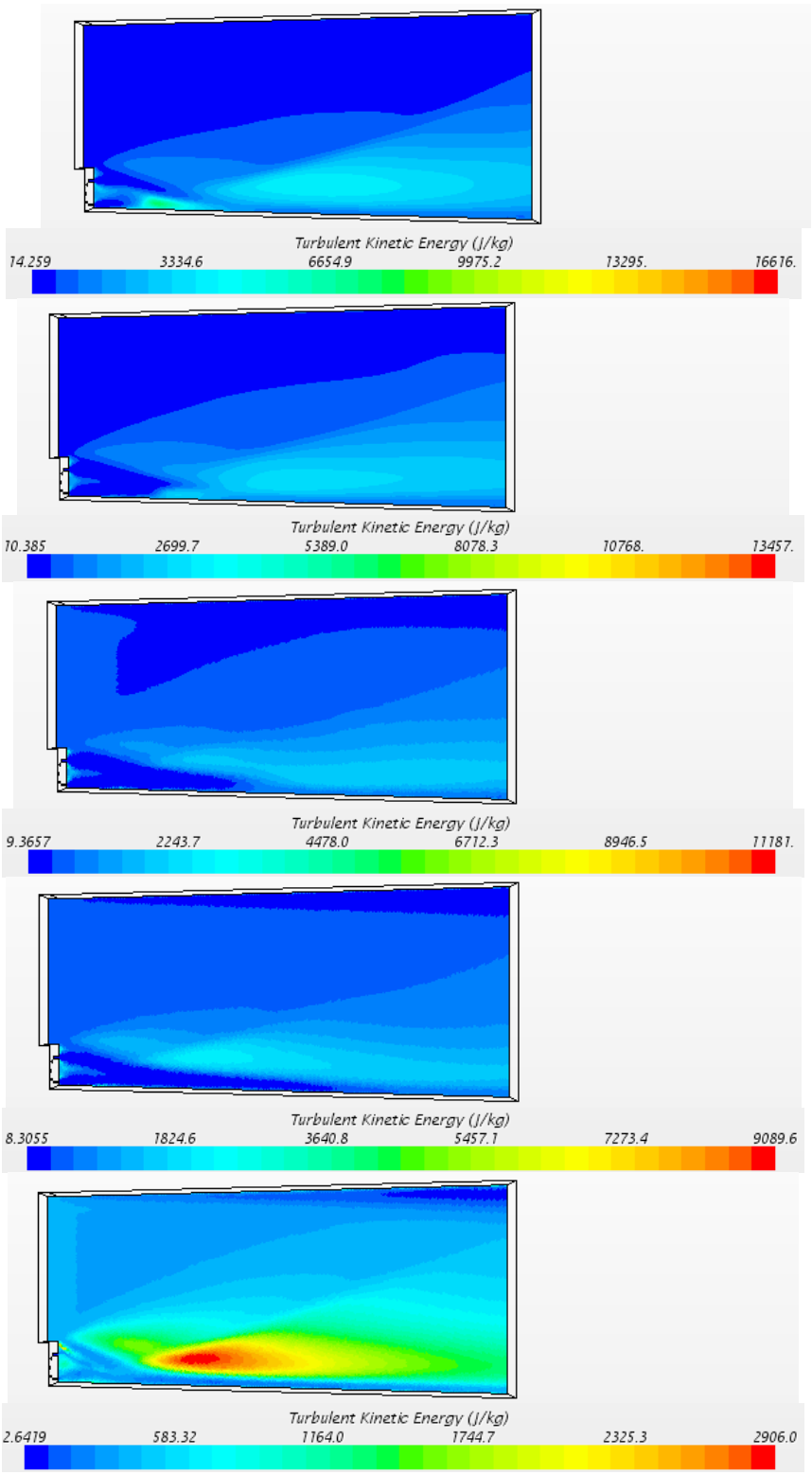

Figure 137: Contours of Turbulent Kinetic Energy (m^2/s^2) for the 8 port Injector at 0.2T, 0.4T, 0.6T, 0.8T, and 1T

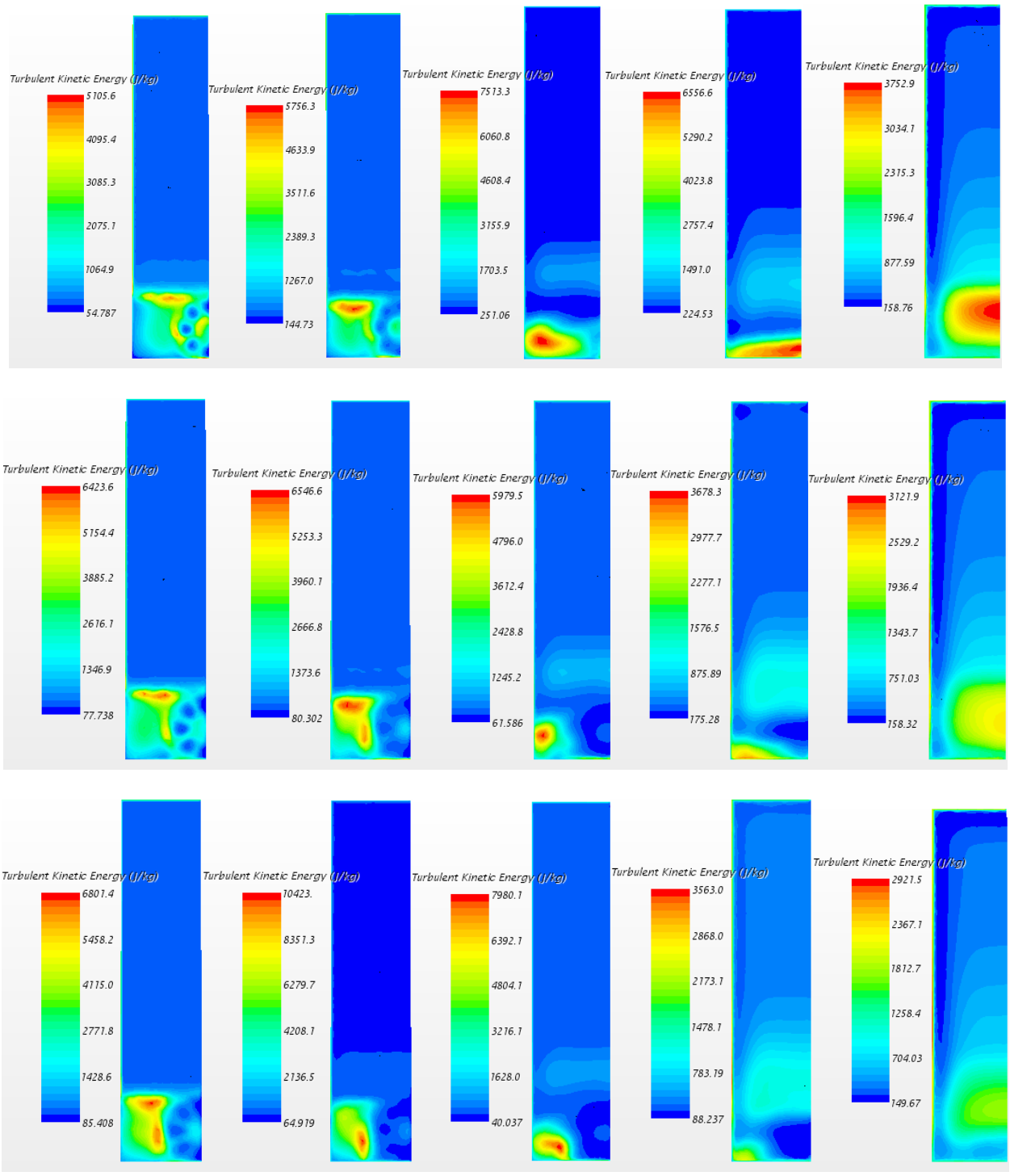

Figure 138: Pulsed Injection Cross Section Contours of Turbulent Kinetic Energy (m^2/s^2) at 0.25, 0.5, 1, 2, and 5 base heights downstream of the step at 0.2T, 0.4T, and 0.6T

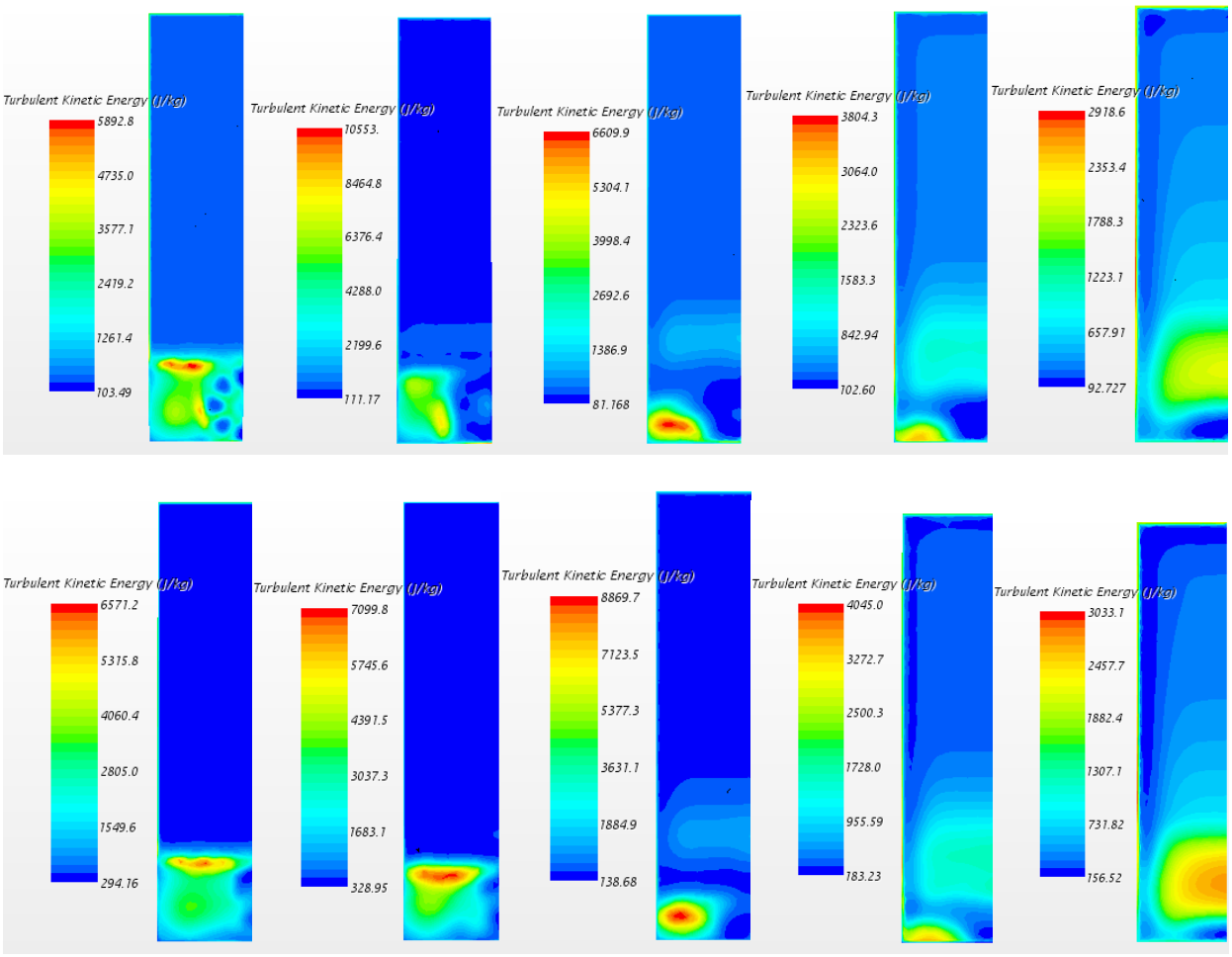

Figure 139: Pulsed Injection Cross Section Contours of Turbulent Kinetic Energy (m^2/s^2) at 0.25, 0.5, 1, 2, and 5 base heights downstream of the step at 0.8T and 1T

5.1.4 5 Port Injector Steady Injection

A three dimensional steady injection model for the 5 port injector was also created so that the effects of pulsed injection could be differentiated from the effects of mass addition. As with the 8 port injector, a cross section at the plane of symmetry is used to present the contours for the 5 port injector cases. The contours of Mach number show how the shear layer curves upward as a result of injection and the effect this has on the shear layer, the expansion fan, and the oblique shock wave. It can be seen in Figure 140 that at the injector forces the shear layer up slightly resulting in a weaker expansion fan and shock wave. This results in less variation in Mach number as the flow passes through the test section. The deformation of the shear layer is greatest near the plane of symmetry where the injection port is nearest the lip of the step. The lower the injection port with respect to the step, the impact of injection on the shear layer is diminished. The curvature of the shear layer is less pronounced for the 5 port injector than it was for the 8 port injector. This is partially attributed to the injection ports off the line of symmetry being lower than for the 8 injection port case and also partially due to the reduced mass flow rate. As with the 8 port injector the nozzle pressure ratio, NPR, is 7 so the jets are under-expanded and expand and accelerate outward from the point of injection. The shear layer impinges on the lower wall at approximately 3.25 step heights.

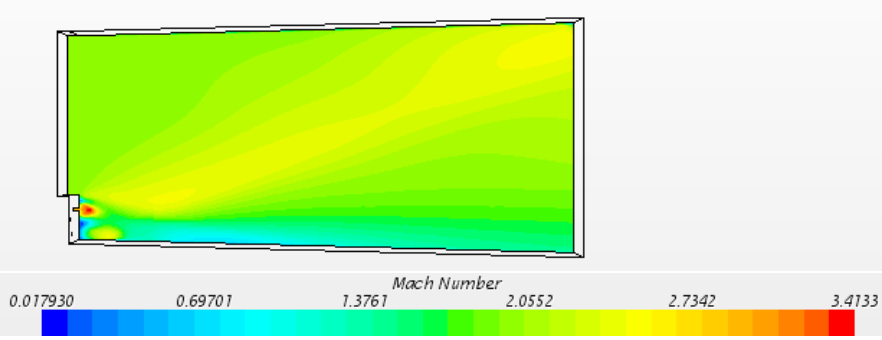

Figure 140: Contours of Mach number for Steady Injection from the 5 port Injector

In steady injection for the 5 port injector, at the plane of symmetry, the shear layer has been forced upward resulting in a weaker expansion fan and shock wave. The reduced intensity waves affect the static pressure variation in the flow as it moves through the wind tunnel. This behavior is observed in Figure 141. Away from the injectors, the shear layer has not been perturbed and the contours resemble the no base injection contours.

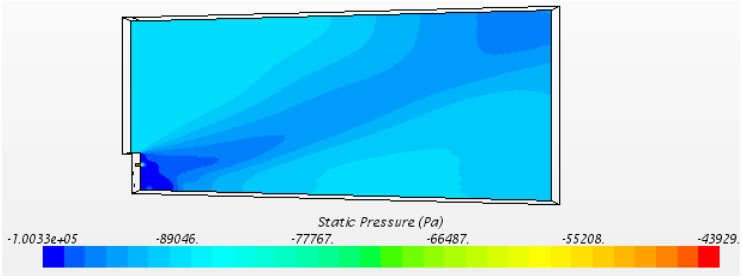

Figure 141: Contours of Static Pressure (Pa) for Steady Injection from the 5 port Injector

In steady injection from the 5 port injector, like the 8 injection port steady injection case the peak vorticity strength is in the shear layers along the edges of the jets. The vorticity strength along the shear layer is diminished for the steady injection case than for the no base injection case as the velocity differential is much lower near the injectors due to the decrease in velocity differential. This results in a much weaker shear layer near the injectors in the steady injection case than in the no base injection case. Further from the injectors the shear layer vorticity is stronger. The convective Mach number of the shear layers along the jets is 0.32, while the convective Mach numbers along the shear layer is 0.076 at the plane of symmetry.

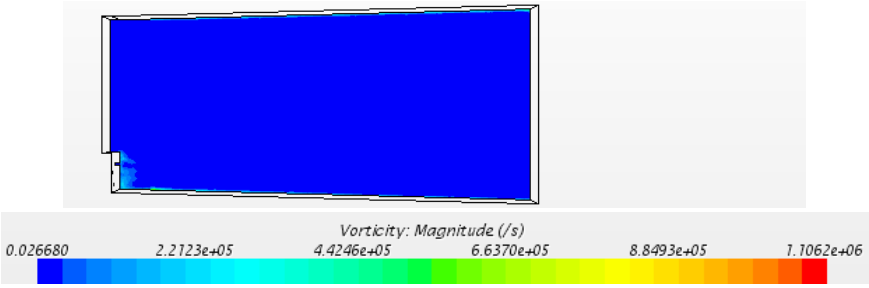

Figure 142: Contours of Vorticity (1/s) for Steady Injection from the 5 port Injector

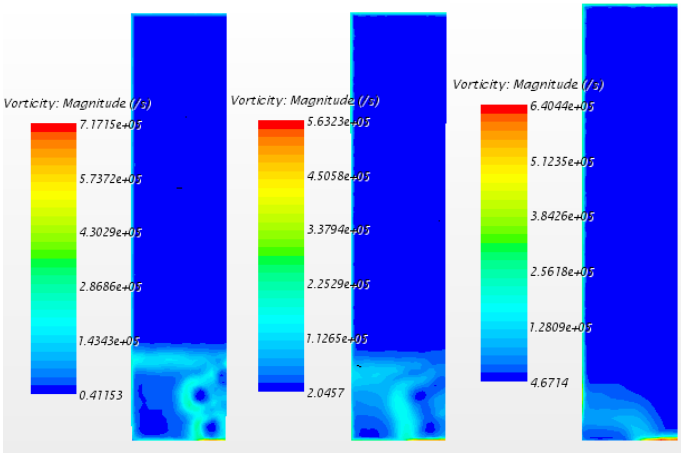

Figure 143: Steady Injection Cross Section Vorticity (1/s) at 0.25, 0.5, and 1 base heights downstream of the step

As in the 8 port model, the regions with the highest turbulent kinetic energy in the three dimensional model are the shear layers around the jets, as we observe in Figure 144 and Figure 145. The turbulent kinetic energy in the shear layer of the 5 injection port model is quite low. As with the 8 injection port model, the shear layer strength is reduced. As in the no base injection case the expansion fan region and the region just downstream of the oblique shock are also characterized by regions of higher turbulence. The turbulent kinetic energy in these regions, as with the 8 port injector, is not as strong as in the no injection case.

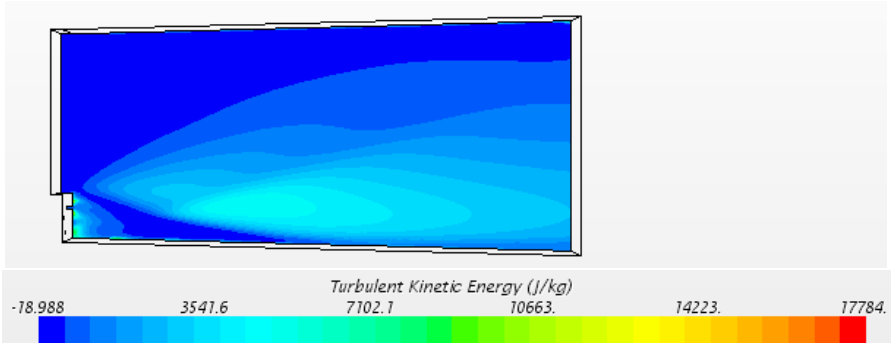

Figure 144: Contours of Turbulent Kinetic Energy (m^2/s^2) for Steady Injection from the 5 port Injector

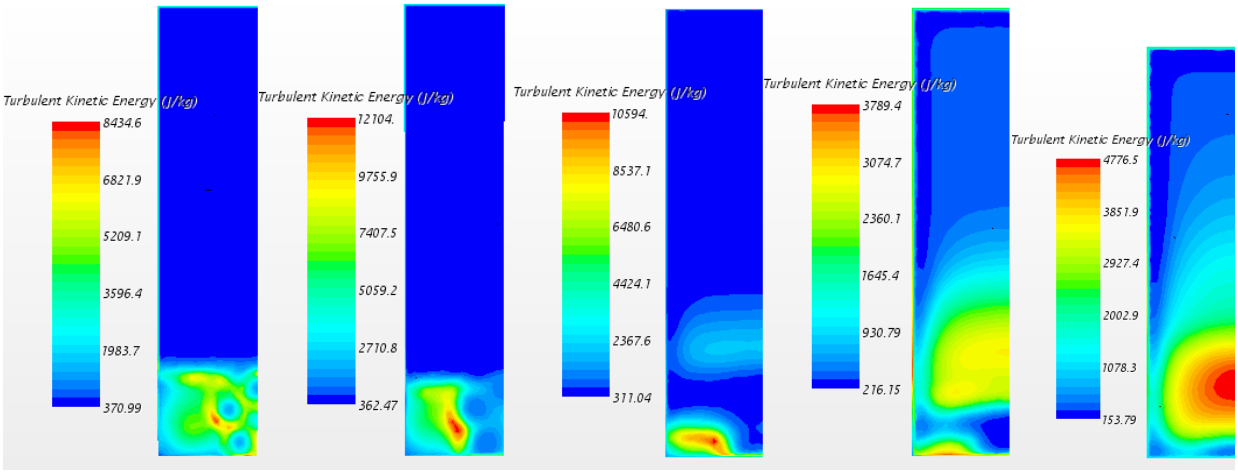

Figure 145: Steady Injection Cross Section Contours of Turbulent Kinetic Energy (m^2/s^2) at 0.25, 0.5, 1, 2, and 5 base heights downstream of the step

5.1.5 5 Port Injector 1.0 kHz Injection 50% on

The same cross section that was used to examine steady state injection of the 5 port injector was also used to examine pulsed injection at 1.0 kHz for when the injector is on for 50% of the time. The contours of Mach number over the pulse are shown in Figure 146. It can be seen that at the beginning of the pulse the shear layer approximates the shear layer of the no base injection case, as expected. At this early stage of injection, 0.2T, the injected jets have little effect on the position of the shear layer. Thus, the Mach contours of the main flow have not varied much from their injector off positions. As with the 8 port injector model the nozzle pressure ratio, NPR, is 7 so the jets are under-expanded and expand and accelerate outward from the point of injection. The shear layer impinges on the lower wall at approximately 2.8 step heights.

The contours of Mach number at 0.4T show the shear layer begin to curve upward as a result of increased injection. At the plane of symmetry the jet forces the shear layer up slightly resulting in a slightly weaker expansion fan. The shear layer impinges on the lower wall at approximately 4.3 step heights.

The contours of Mach number at 0.6T show the shear layer curve upward as a result of increased injection to, at this stage of injection, approximate the steady injection case. At the plane of symmetry, the injector forces the shear layer up resulting in a weaker expansion fan and shock wave. This results in less variation in Mach number as the flow passes through the test section. The shear layer impinges on the lower wall at approximately 4.3 step heights.

The contours of Mach number at 0.8T show the shear layer curve has decreased as a result of decreased injection. At the plane of symmetry, the injection forces the shear layer up slightly resulting in a weaker expansion fan and shock wave, but less so that when the injection was at its peak. The shear layer impinges on the lower wall at approximately 3.8 step heights.

At 1T that the shear layer once again approximates the shear layer of the no base injection case. Thus, the Mach contours of the main flow have once again also match their injector off positions. The shear layer impinges on the lower wall at approximately 3.0 step heights.

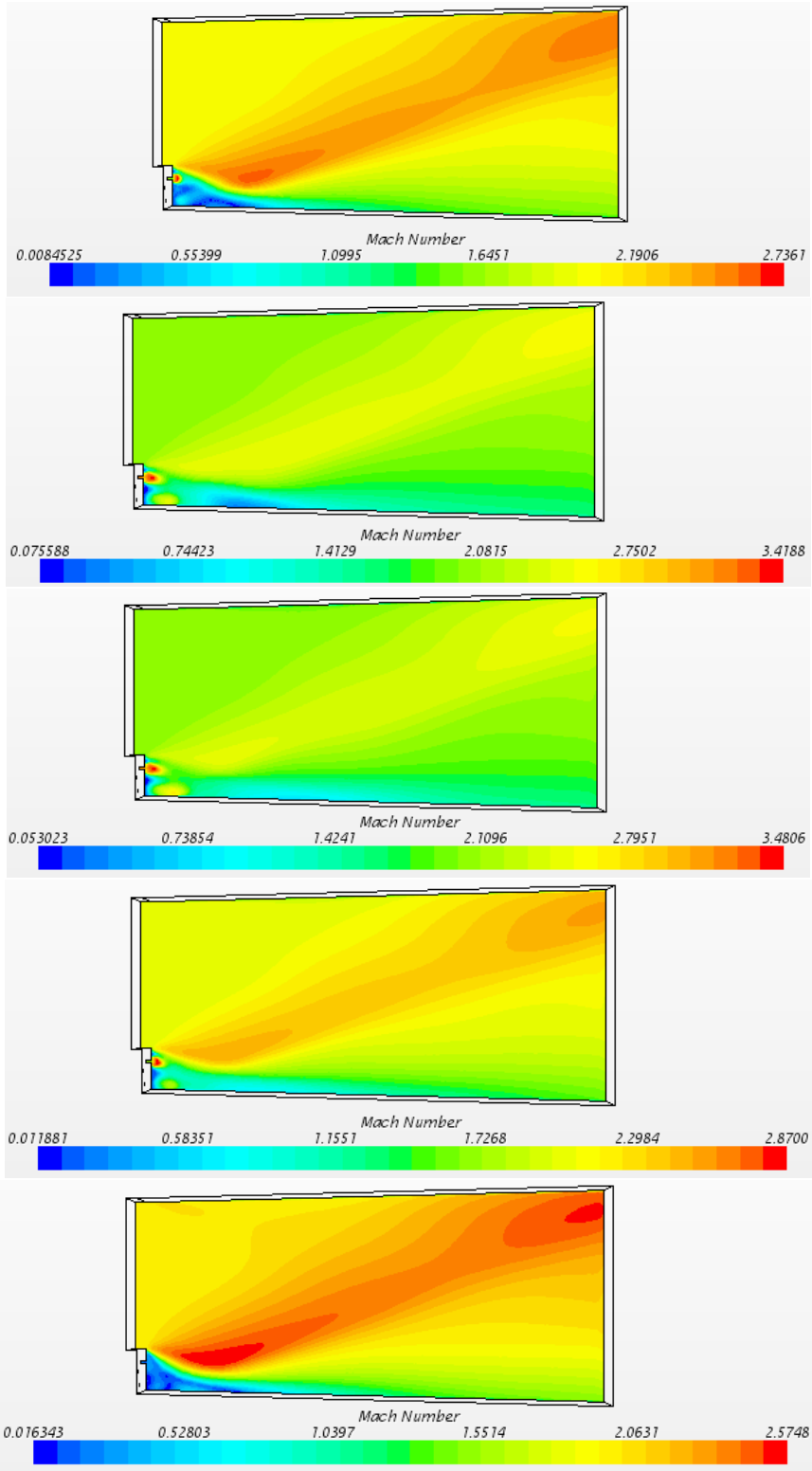

Figure 146: Contours of Mach number for the 5 port Injector on 50% at 0.2T, 0.4T, 0.6T, 0.8T, and 1T

In pulsed injection for the 5 port injector, when the injectors are off the contours of static pressure mimic the no base injection case at all cross sections. As the injectors begin to inject gas, at 0.2T, the shear layer is forced upward weakening the expansion fan and shock wave. This results in less variation in static pressure as the flow progresses through the expansion fan and shock wave. At 0.4T, as injection increases the shear layer is forced up further and the expansion fan is further weakened. The impact on shear layer curvature is less for the 5 port injector than for the 8 port injector so the expansion fan and shock are not weakened as much with the 5 port injector as with the 8 port injector. Figure 148 shows this phenomenon at the plane of symmetry where the effect is the strongest. Where the injection ports are lower, the effect is weaker, and outside the influence of the injectors the static pressure contours resemble the no base injection contours throughout the pulse. As injection reaches its peak, at 0.6T the static pressure contours come to resemble the steady injection contours. At 0.8T, the change in static pressure across the expansion fan and shock begins to increase. When the pulse ends at 1T the static pressure contours again resemble the no base injection case, as expected.

Figure 147 shows the pressure variation with time along the lower wall for the 5 port injector. There is some initial pressure variation due to injection, but the pressure variation after the shear layer reattachment point is minor. This behavior is consistent with the flow simulation results.

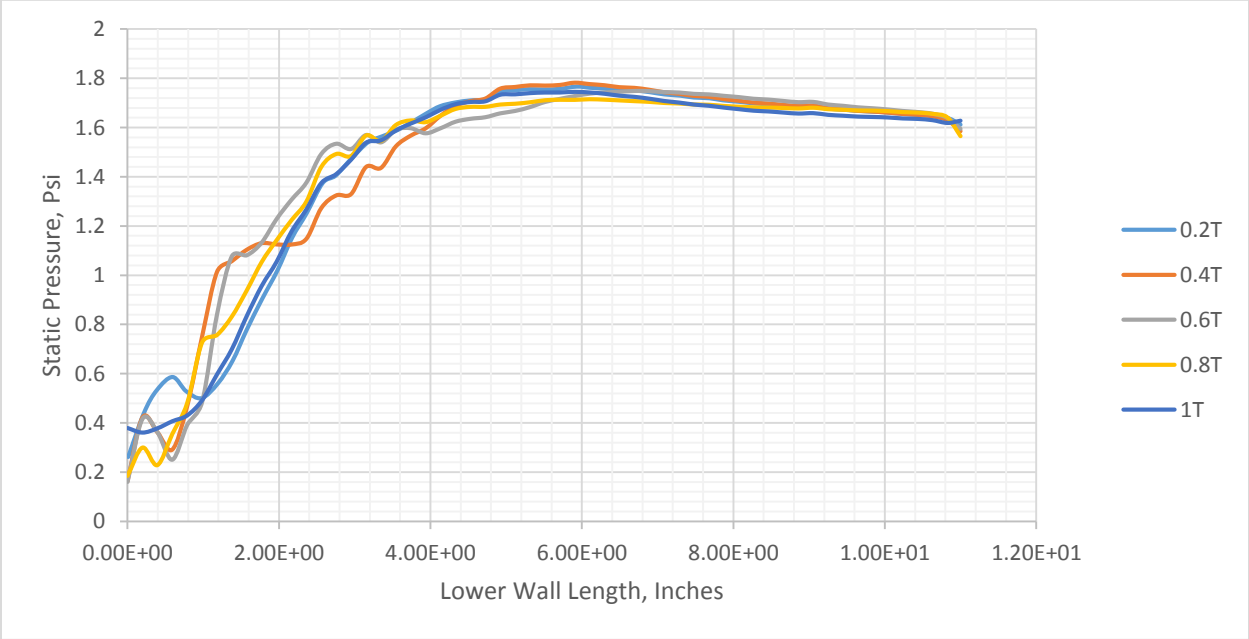

Figure 147: 1.0 kHz Lower Wall Static Pressure Variation over One Pulse for the 3D 5 Port 50% on Model

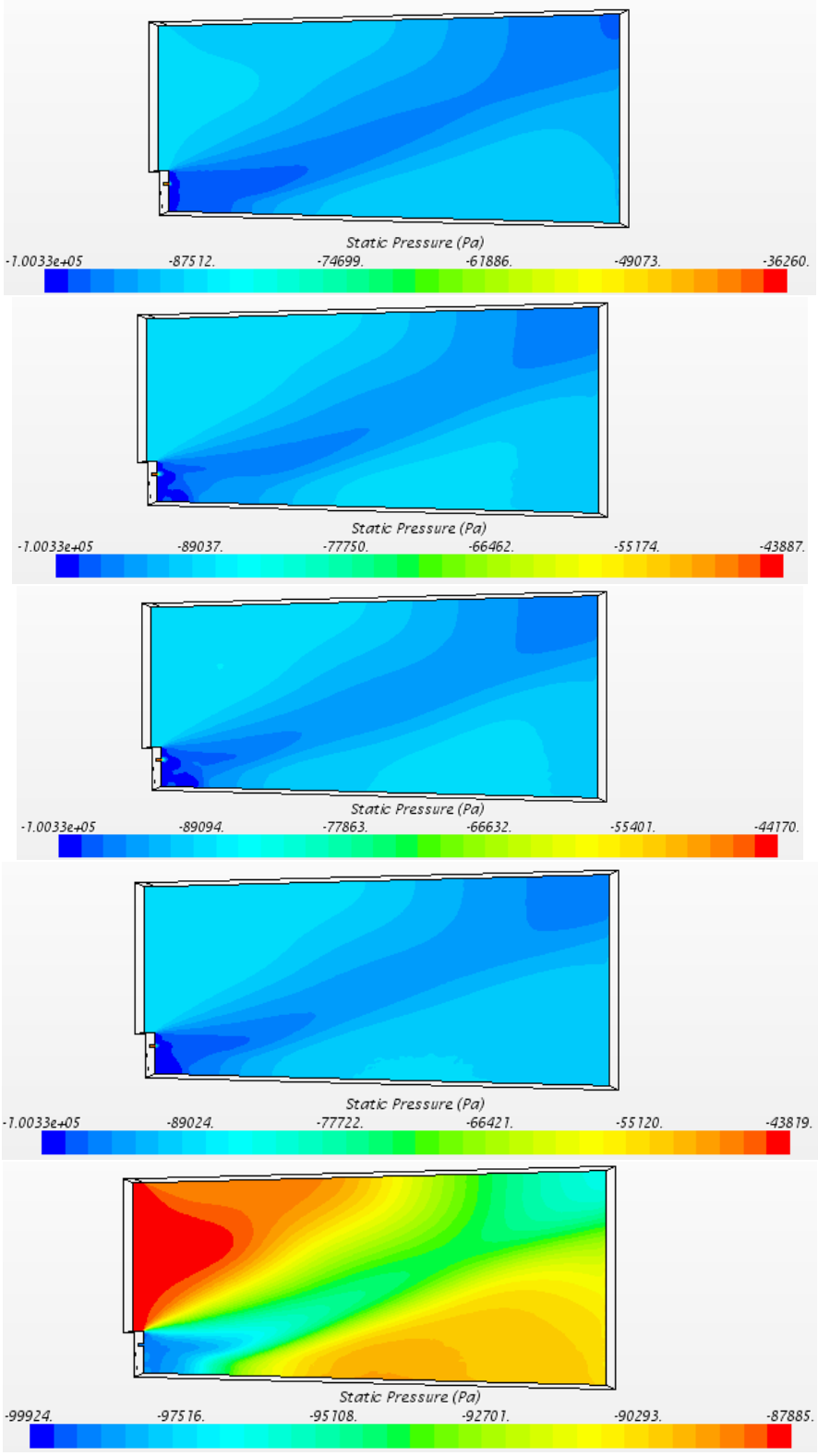

Figure 148: Contours of Static Pressure (Pa) for the 5 port Injector on 50% at 0.2T, 0.4T, 0.6T, 0.8T, and 1T

In pulsed injection when the injectors are off the peak vorticity levels can be found in the shear layer, like in the no base injection case. When the injection pulse begins, the peak vorticity strength begins to shift to the shear layers along the edges of the jets, as we observe in Figure 149. At the beginning of each pulse the convective Mach number of the shear layer is the same as for the no base injection case.

At 0.4T, the vorticity strength in the shear layers along the edges of the jets becomes stronger and the vorticity in the shear layer shed from the step becomes weaker. The vorticity strength along the shear layer is diminished due to a reduced shear layer curvature caused by increased injection. This results in a progressively weaker shear layer in the pulsed injection case compared to the no base injection case.

As injection reaches its peak intensity, at 0.6T, the vorticity strength in the shear layers along the edges of the jets continue to increase and the vorticity in the shear layer shed from the step continue to decrease. The vorticity strength along the shear layer is weak because the velocity differential is at its lowest due to the velocities induced by injection being at their highest during the pulse. This results in a weak shear layer. The convective Mach number of the shear layers along the jets when injection is at its peak are 0.32, while the convective Mach number along the shear layer is 0.076 at the plane of symmetry.

At 0.8 T, as injection begins to diminish the vorticity strength in the shear layers along the edges of the jets becomes weaker and the vorticity in the shear layer shed from the step becomes stronger.

At the end of injection, at 1T, the vorticity contours come to resemble the vorticity contours of the no base injection case. The convective Mach numbers are the same as for the no base injection case.

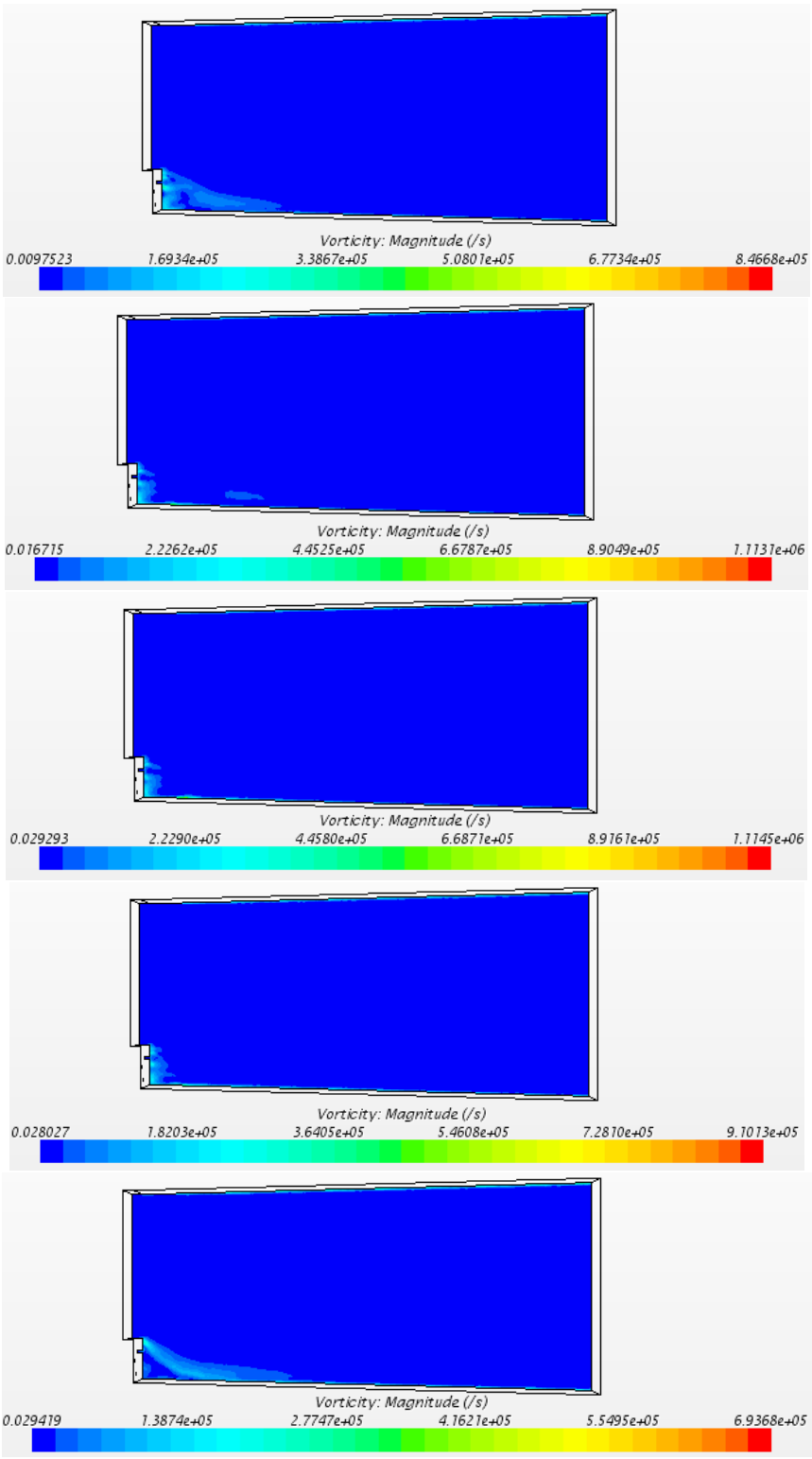

Figure 149: Contours of Vorticity (1/s) for the 5 port Injector on 50% at 0.2T, 0.4T, 0.6T, 0.8T, and 1T

As we observe in Figure 150, the turbulent kinetic energy in the pulsed injection case peaks near the shear layer impingement point at the beginning of the pulse, as in the no injection case. Also as in the no injection case, the pulsed injection model shows large regions of turbulent flow in the region of the expansion fan and shock wave, which is likely being generated partially by three dimensional compressibility effects and partially by flow curvature.

At 0.4T, the vorticity strength in the shear layers along the edges of the jets become stronger and thus these regions become more turbulent and the vorticity in the shear layer shed from the step becomes weaker. The vorticity strength along the shear layer is decreased because the velocity differential is much lower due to increased injection. This results in a progressively weaker less turbulent shear layer in the pulsed injection case compared to the no base injection case.

At 0.6T, the regions with the highest turbulent kinetic energy are still the shear layers around the jets as they are injected into the recirculation region, but these regions are quite small. The jets themselves have a remarkably low level of turbulence. The vorticity due to the change in velocity across the shear layer is at its lowest at this point in the pulse which causes the turbulent kinetic energy in the shear layer to be quite low. The expansion fan region and the region just downstream of the oblique shock are also characterized by regions of higher turbulence, mainly due to flow curvature.

At 0.8T, the regions with the highest turbulent kinetic energy are still the shear layers around the jets right as they are injected into the recirculation region. The lower vorticity due to the change in velocity across the shear layer being slightly larger than at the peak of the pulse causes the turbulent kinetic energy in the shear layer to increase as the pulse recedes. The expansion fan region and the region just downstream of the oblique shock are also characterized by regions of higher turbulence.

As the pulse comes to an end at 1T, the turbulent kinetic energy contours come to resemble the no injection contours

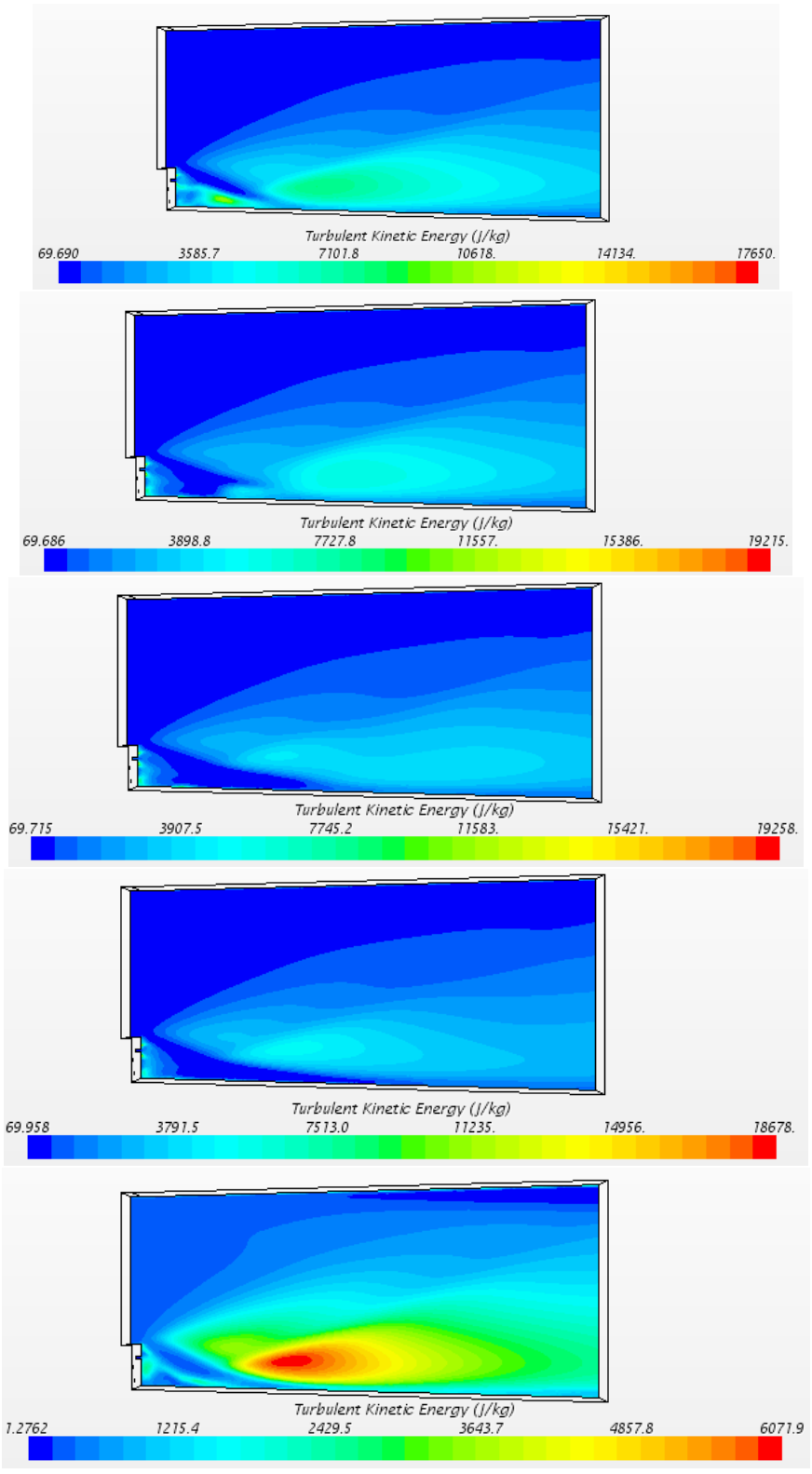

Figure 150: Contours of Turbulent Kinetic Energy (m^2/s^2) for the 5 port Injector on 50% at 0.2T, 0.4T, 0.6T, 0.8T, and 1T

5.1.6 5 Port Injector 1.0 kHz Injection 66% on

The same cross section used in the previous two sections was also used to examine pulsed injection at 1.0 kHz for when the injector is on for 66% of the time. The contours of Mach number over the pulse are shown in Figure 151. It can be seen that at the beginning of the pulse the shear layer approximates the shear layer of the no base injection case, as expected. It can be seen in Figure 151 that at this early stage of injection the injected jets have little effect on the position of the shear layer. Thus, the Mach contours of the main flow have not varied much from their injector off positions. As with the previous 5 port injector model the nozzle pressure ratio, NPR, is 7 so the jets are under-expanded and expand and accelerate outward from the point of injection. The shear layer impinges on the lower wall at approximately 2.75 step heights.

The contours of Mach number at 0.4T show the shear layer curve upward at the injector as a result of increased injection, in this case the pulse has nearly reached its peak. The flow at this point has come to approximate the steady injection Mach contours. At the plane of symmetry the jet forces the shear layer up resulting in a much weaker expansion fan. The shear layer impinges on the lower wall at approximately 3.9 step heights.

At 0.6T, the contours of Mach number show the shear layer curve upward at the injector as a result of maintained injection, in this case the pulse has reached its peak. As at the previous time step, the flow at this point approximates the steady injection Mach contours. At the plane of symmetry the jet forces the shear layer up resulting in a much weaker expansion fan and shock wave. The shear layer impinges on the lower wall at approximately 3.9 step heights.

The contours of Mach number show the shear layer maintain their upward curve as a result of maintained injection. As at the previous time step, the flow at this point approximates the steady injection Mach contours. At the plane of symmetry the jet forces the shear layer up resulting in a much weaker expansion fan. The shear layer impinges on the lower wall at approximately 3.9 step heights.

At the end of the pulse at 1T, the shear layer once again approximates the shear layer of the no base injection case. Thus, the Mach contours of the main flow have once again also match their injector off positions. The shear layer impinges on the lower wall at approximately 3.0 step heights.

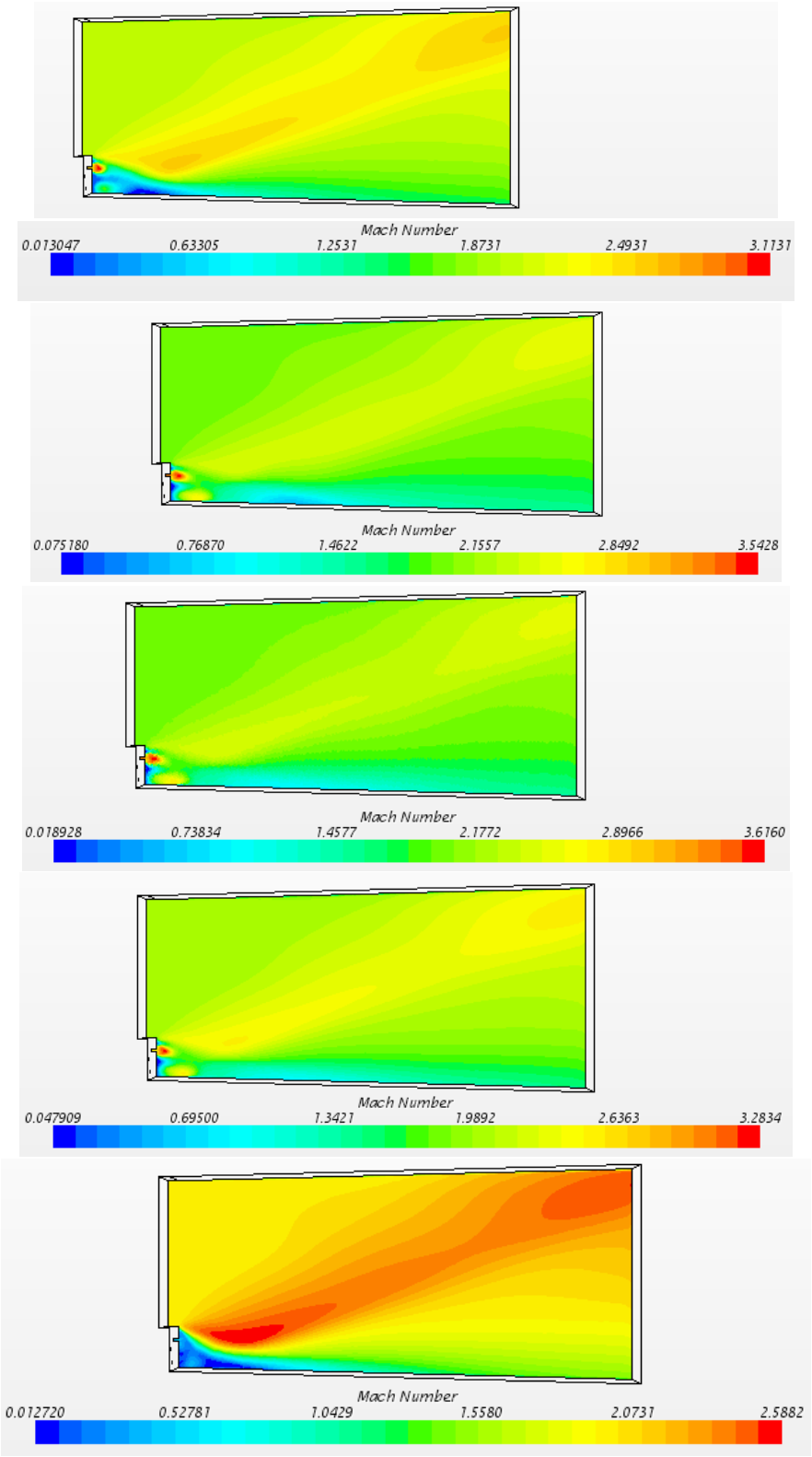

Figure 151: Contours of Mach Number for the 5 port Injector on 66% at 0.2T, 0.4T, 0.6T, 0.8T, and 1T

When the injectors are off the contours of static pressure mimic the no base injection case at all cross sections. As the injectors begin to inject gas, the impact of shear layer curvature is the weakening of the expansion fan and shock wave. The expansion fan and shock wave are weakened more in the 8 port injector case than in the 5 port injector case because the shear layer curvature is reduced for the 5 port injector compared to the 8 port injector. The curving shear layer results in less variation in static pressure as the flow progresses through the expansion fan and shock wave in the test section. As injection increases, at 0.4T, the shear layer is forced up to where it mimics the steady injection case, further weakening the expansion fan and shock. Figure 153 shows this at the plane of symmetry where the effect is the strongest. Where the injection ports are lower, the effect is weaker, and outside the influence of the injectors the static pressure contours resemble the no base injection contours throughout the pulse. The injection for the 66% on injector maintains its peak, at 0.6T, and the contours continue to resemble the steady injection contours. As the pulse begins to recede the change in static pressure across the expansion fan and shock begins to increase. When the pulse ends the static pressure contours again resemble the no base injection case, as expected.

Figure 152 shows the pressure variation with time along the lower wall for the 5 port injector. The pressure curves are very similar at 0.4T, 0.6T, and 0.8T when the injector is on. The pressure varies as injection is increased and decreased but beyond the shear layer reattachment point the variation is minor. This behavior is consistent with the flow simulation results.

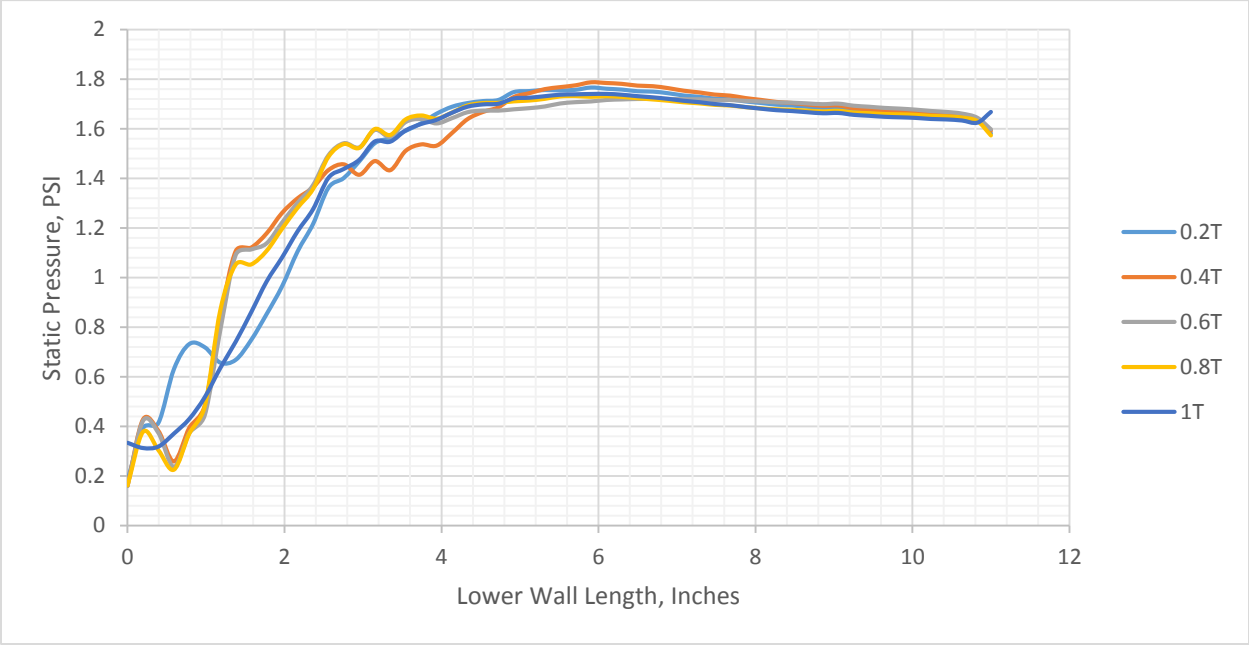

Figure 152: 1.0 kHz Lower Wall Static Pressure Variation over One Pulse for the 3D 5 Port 66% on Model

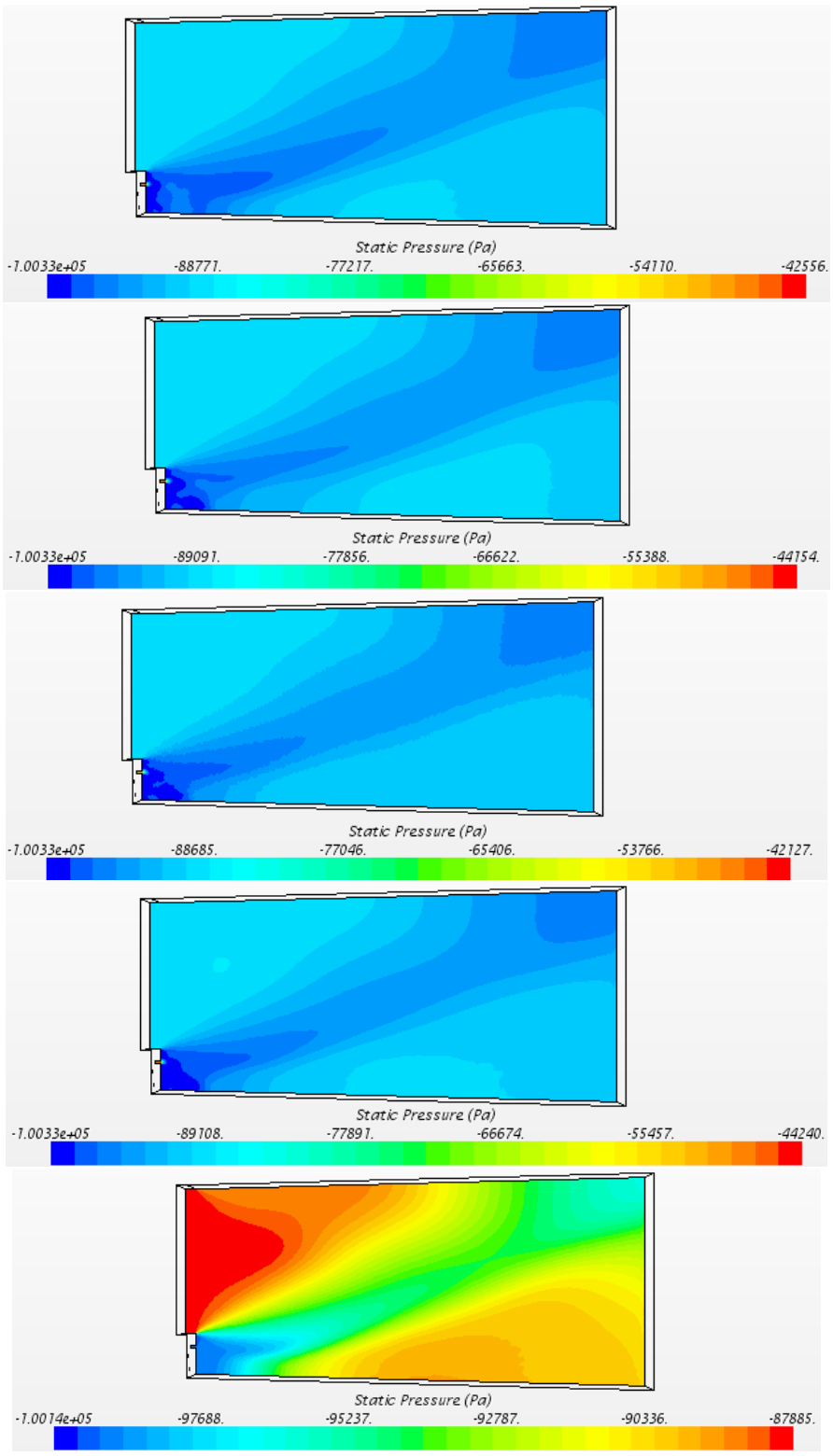

Figure 153: Contours of Mach Number for the 5 port Injector on 66% at 0.2T, 0.4T, 0.6T, 0.8T, and 1T

In pulsed injection when the injectors are off the peak vorticity levels can be found in the shear layer, like in the no base injection case. When the injection pulse begins, the peak vorticity strength begins to shift to the shear layers along the edges of the jets as can be we observe Figure 154. At the beginning of each pulse, at 0.2T, the convective Mach number of the shear layer is the same as for the no base injection case.

As injection reaches its peak the vorticity strength in the shear layers along the edges of the jets continue to increase and the vorticity in the shear layer shed from the step continues to diminish. The vorticity strength along the shear layer is diminished because the velocity differential is at its lowest due to the velocities induced by injection being at their highest during the pulse. This results in a weak shear layer. The convective Mach number of the shear layers along the jets when injection is at its peak are 0.32, while the convective Mach number along the shear layer at the plane of symmetry is 0.076.

The 66% on injector maintains its peak injection intensity at 0.6T, thus the vorticity strength in the shear layers along the edges of the jets remain at their elevated levels and the vorticity strength in the shear layer shed from the step remains low. The vorticity strength along the shear layer is diminished because the velocity differential is at its lowest due to the velocities induced by injection being at their highest during the pulse. This results in a weak shear layer.

As injection begins to diminish, at 0.8T, the vorticity strength in the shear layers along the edges of the jets becomes weaker and the vorticity strength in the shear layer shed from the step becomes stronger.

At the end of injection, at 1T, the vorticity contours come to resemble the vorticity contours of the no base injection case. The convective Mach numbers are the same as for the no base injection case.

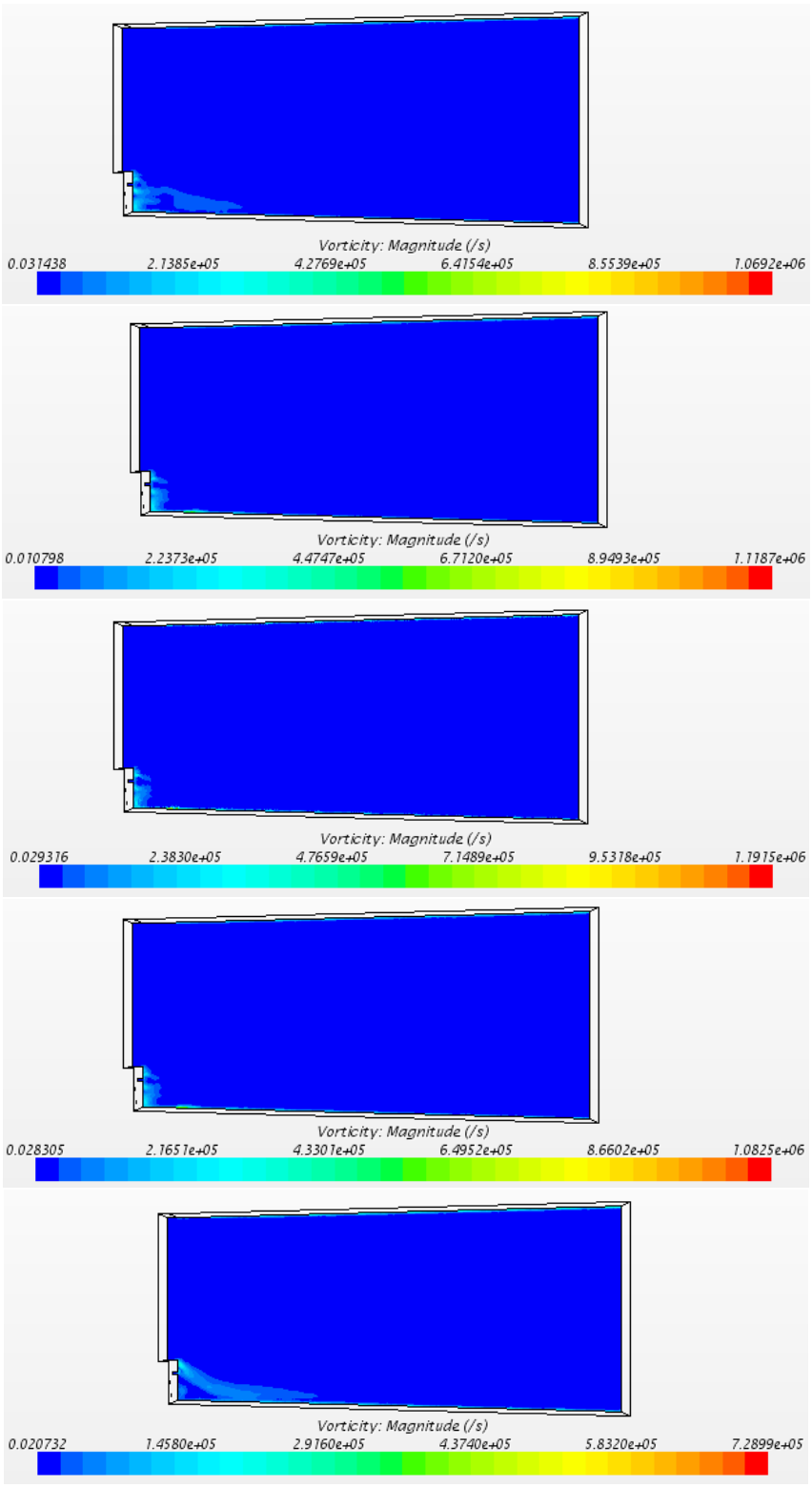

Figure 154: Contours of Vorticity (1/s) for the 5 port Injector on 66% at 0.2T, 0.4T, 0.6T, 0.8T, and 1T

As we observe in Figure 155, the turbulent kinetic energy in the pulsed injection case peaks near the shear layer impingement point at the beginning of the pulse, as in the no injection case. Also as in the no injection case, the pulsed injection model shows large regions of highly turbulent flow in the region of the expansion fan and shock wave, which is likely being generated partially by three dimensional compressibility effects and also partially by flow curvature.

As the pulse reaches its the peak intensity at 0.4T, the regions with the highest turbulent kinetic energy are the shear layers around the jets right as they are injected into the recirculation region, but these regions are quite small. The jets themselves have a remarkably low level of turbulence. The vorticity due to the change in velocity across the shear layer is at its lowest at this point in the pulse which causes the turbulent kinetic energy in the shear layer to be quite low. The expansion fan region and the region just downstream of the oblique shock are also characterized by regions of higher turbulence caused by three dimensional compressibility effects and reduced flow curvature.

At 0.6T, the regions with the highest turbulent kinetic energy are still the shear layers around the jets, but these regions are still quite small. The jets still have extremely low levels of turbulence. The expansion fan region and the region just downstream of the oblique shock are also characterized by regions of higher turbulence.

At 0.8T, the regions with the highest turbulent kinetic energy are still the shear layers around the jets, but these regions are once again quite small. The jets still have extremely low levels of turbulence. The expansion fan region and the region just downstream of the oblique shock are also characterized by regions of higher turbulence.

As the pulse comes to an end at 1T, the turbulent kinetic energy peaks in the region of the expansion fan and shockwave while still having a high level of turbulence in along the shear layer and in the recirculation region. The turbulence is higher in this region than in the shear layer or recirculation region.

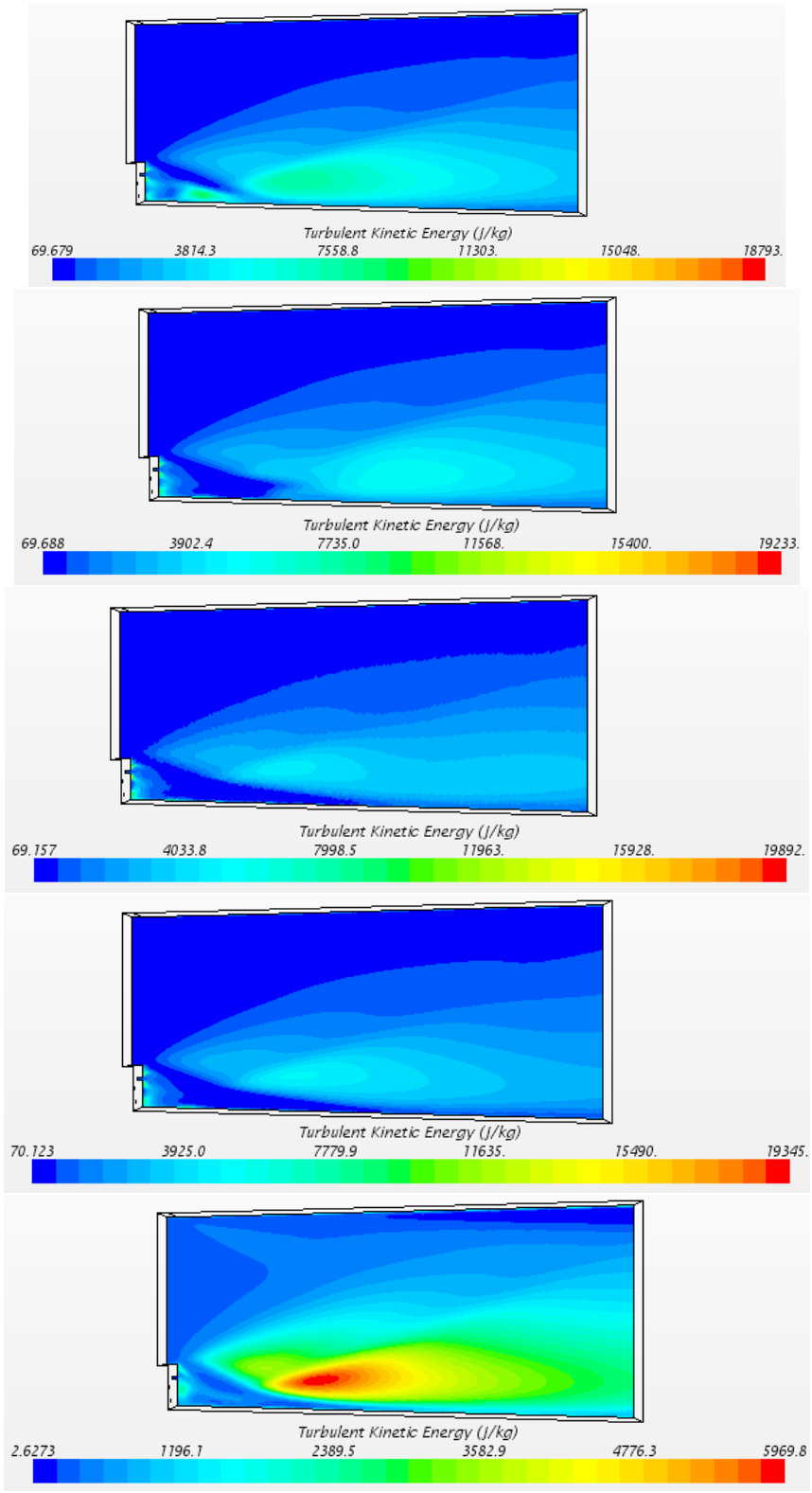

Figure 155: Contours of Turbulent Kinetic Energy (m^2/s^2) for the 5 port Injector on 66% at 0.2T, 0.4T, 0.6T, 0.8T, and 1T

5.1.7 5 Port Injector 1.0 kHz Injection 33% on

The same cross section used in the previous two sections was also used to examine pulsed injection at 1.0 kHz for when the injector is on for 33% of the time. The contours of Mach number over the pulse are shown in Figure 156. It can be seen that at the beginning of the pulse the shear layer approximates the shear layer of the no base injection case, as expected. At 0.2T injection has not begun and thus the shear layer is unaffected. Thus, the Mach contours of the main flow have not varied much from their injector off positions. The shear layer impinges on the lower wall at approximately 2.50 step heights.

At 0.4T injection has just begun with the injected jets not having much of an effect on the shape of the shear layer. Thus, the Mach contours of the main flow have not varied much from their injector off positions. As with the previous 5 port injector model the nozzle pressure ratio, NPR, is 7 so the jets are under-expanded and expand and accelerate outward from the point of injection. The shear layer impinges on the lower wall at approximately 2.75 step heights.

The contours of Mach number show that at 0.6T the shear layer curves upward at the injectors as a result of increased injection to, at this stage of injection, approximate the steady injection case. At the plane of symmetry the jet pushed the shear layer up resulting in a weakened expansion fan and shock wave. This results in less variation in Mach number as the flow passes through. The shear layer impinges on the lower wall at approximately 3.5 step heights.

The contours of Mach number show that at 0.8T the shear layer curve has decreased as a result of decreased injection. At the plane of symmetry the decreased injection is still causing the shear layer to curve upward slightly. The shear layer impinges on the lower wall at approximately 3.25 step heights.

At the end of the pulse that the shear layer once again approximates the shear layer of the no base injection case. Thus, the Mach contours of the main flow have once again also match their injector off positions. The shear layer impinges on the lower wall at approximately 3.0 step heights.

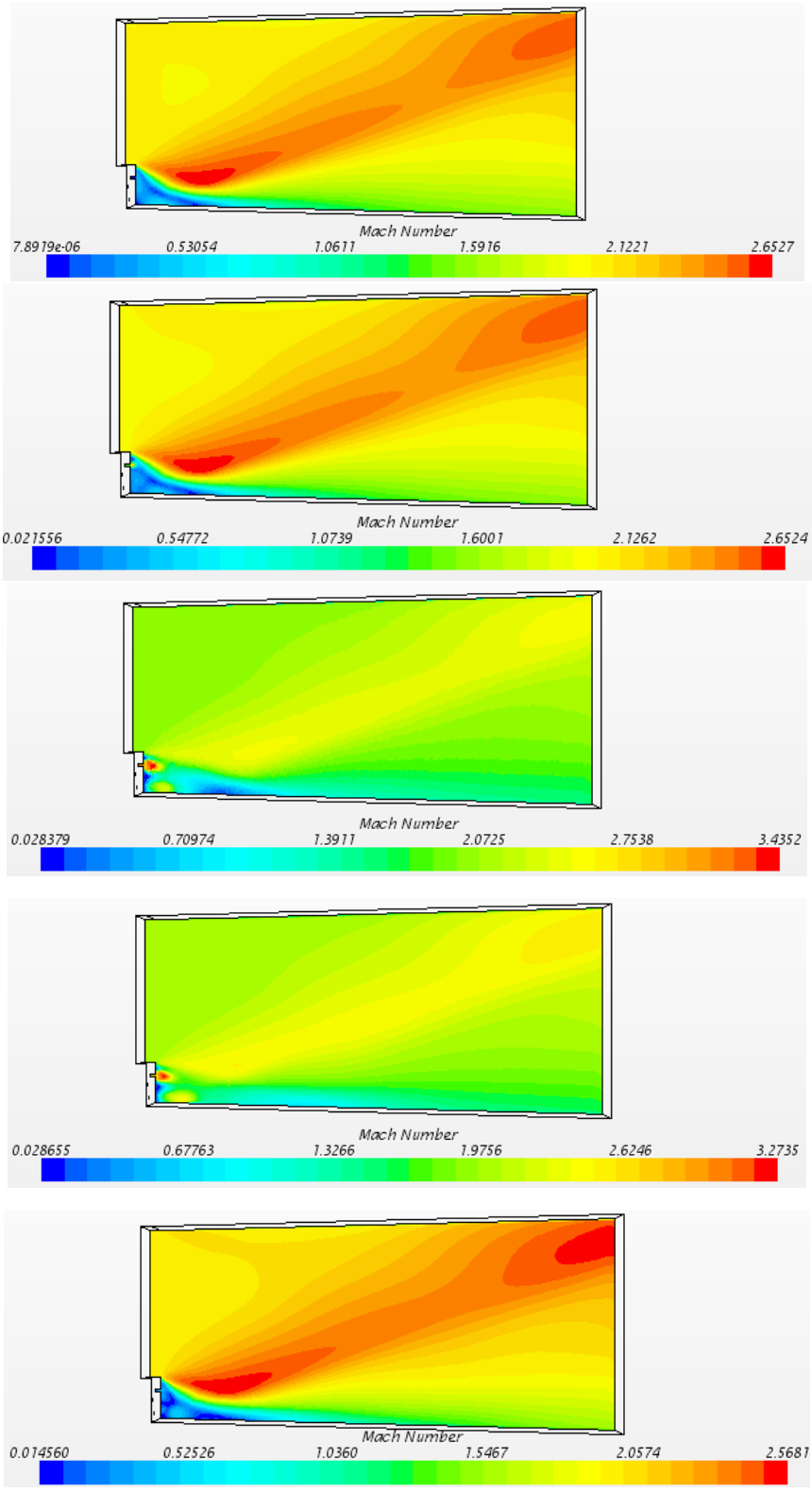

Figure 156: Contours of Mach number for the 5 port Injector on 33% at 0.2T, 0.4T, 0.6T, 0.8T, and 1T

When the injectors are off the contours of static pressure mimic the no base injection case at all cross sections. As the injector is off for a longer percentage of time in the 33% on case the contours at 0.4T still resemble the injector off contours. As the injectors begin to inject gas, the shear layer is forced upward weakening the expansion fan and shock wave. The expansion fan and shock wave are weakened more in the 8 port injector case than in the 5 port injector case because the shear layer curvature is reduced for the 5 port injector. The shear layer curvature results in less variation in static pressure as the flow progresses through the expansion fan and shock wave. As injection increases, at 0.6T, the impact of shear layer curvature is that the flow comes to mimic the steady injection case, further weakening the expansion fan and shock. Figure 153 shows this phenomenon at the plane of symmetry where the effect is the strongest. Where the injection ports are lower, the effect is weaker, and outside the influence of the injectors the static pressure contours resemble the no base injection contours throughout the pulse. As the pulse begins to recede, at 0.8T, the change in static pressure across the expansion fan and shock begins to increase. When the pulse ends the static pressure contours again resemble the no base injection case.

Figure 157 shows the pressure variation with time along the lower wall for the 5 port injector. The pressure curves are very similar at 0.2T, 0.4T, and 1T when the injector is off. The pressure varies as injection is increased and decreased but beyond the shear layer reattachment point the variation is minor. This behavior is consistent with the flow simulation results.

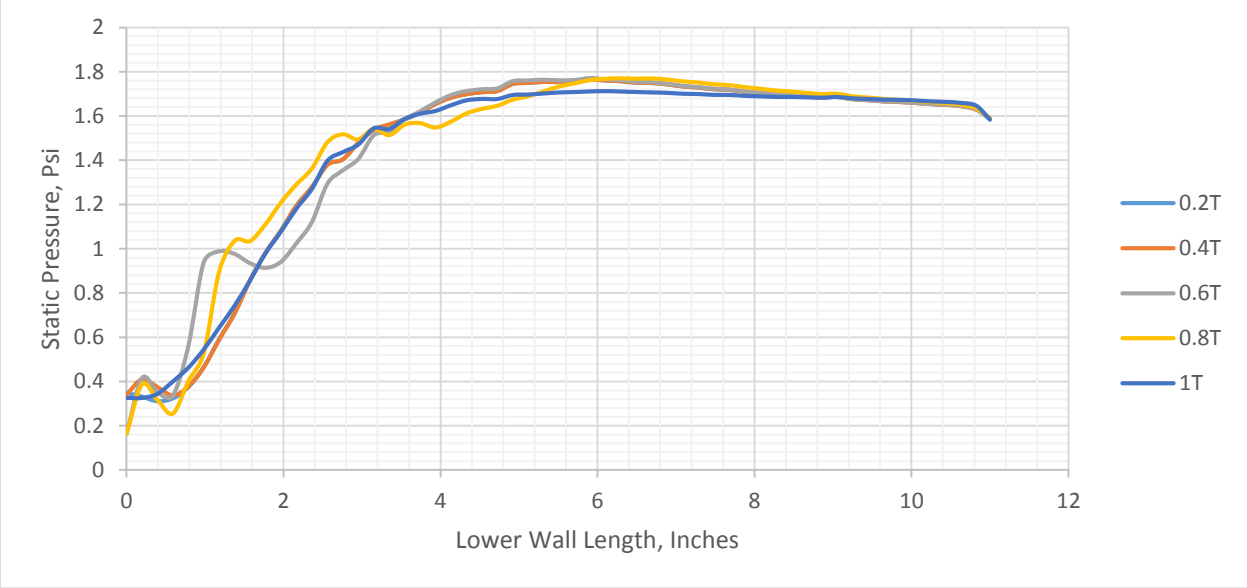

Figure 157: 1.0 kHz Lower Wall Static Pressure Variation over One Pulse for the 3D 5 Port 33% on Model

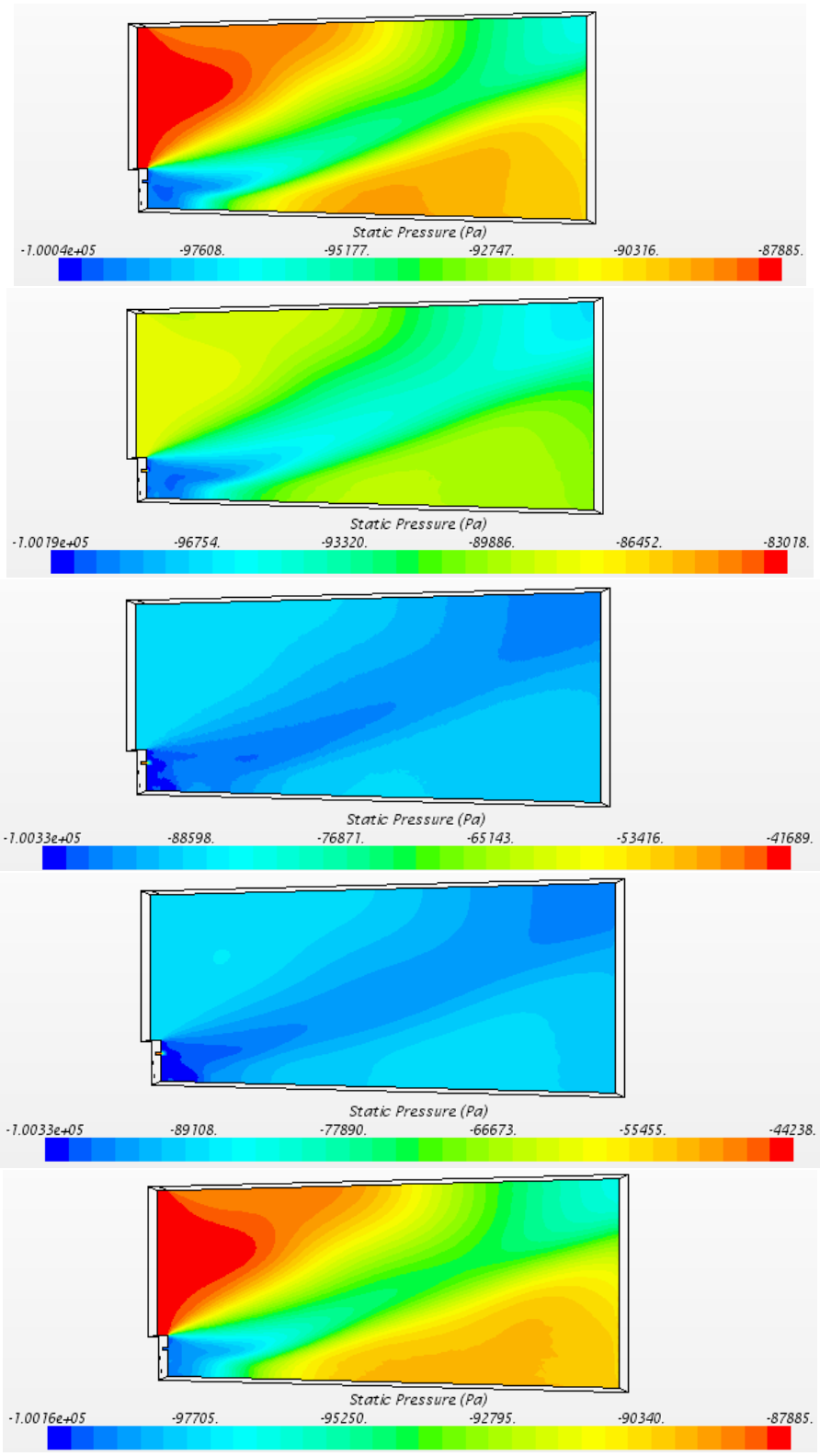

Figure 158: Contours of Static Pressure (Pa) for the 5 port Injector on 33% at 0.2T, 0.4T, 0.6T, 0.8T, and 1T

In pulsed injection when the injectors are off the peak vorticity levels can be found in the shear layer, like in the no base injection case, as we observe Figure 159. At the beginning of each pulse, the convective Mach number of the shear layer is the same as for the no base injection case.

When the injection pulse begins, at 0.4T, the peak vorticity strength begins to shift to the shear layers along the edges of the jets. At the beginning of each pulse the convective Mach number of the shear layer is the same as for the no base injection case.

As injection reaches its peak intensity, at 0.6T, the vorticity strength in the shear layers along the edges of the jets continues to increase and the vorticity strength in the shear layer shed from the step continues to diminish. The vorticity strength along the shear layer is diminished because the velocity differential is at its lowest due to the velocities induced by injection being at their highest during the pulse. This results in a weak shear layer. The convective Mach number of the shear layers along the jets when injection is at its peak are 0.32, while the convective Mach number along the shear layer at the plane of symmetry is 0.076.

As injection begins to diminish the vorticity strength in the shear layers along the edges of the jets become lower and the vorticity in the shear layer shed from the step becomes stronger.

At the end of injection, at 1T, the vorticity contours come to resemble the vorticity contours of the no base injection case. The convective Mach numbers are the same as for the no base injection case.

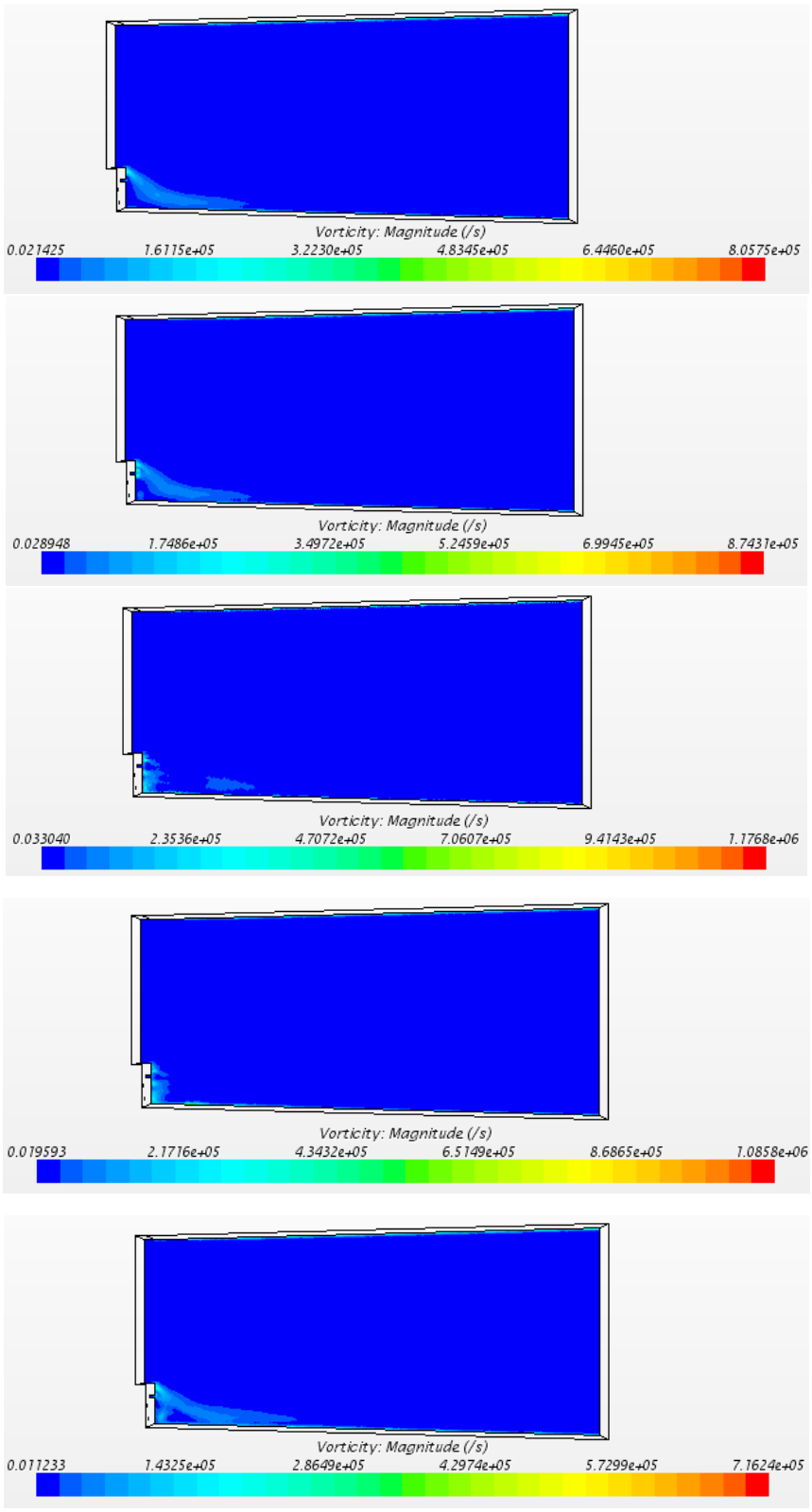

Figure 159: Contours of Vorticity (1/s) for the 5 port Injector on 33% at 0.2T, 0.4T, 0.6T, 0.8T, and 1T

As we observe in Figure 160, the turbulent kinetic energy in the pulsed injection case peaks near the shear layer impingement point at the beginning of the pulse at 0.2T, as in the no injection case. Also as in the no injection case, the pulsed injection model shows large regions of turbulent flow in the region of the expansion fan and shock wave, which is likely being generated partially by three dimensional compressibility effects and partially by flow curvature.

At 0.4T, the turbulent kinetic energy in the pulsed injection case is still at its peak near the shear layer impingement point at the beginning of the pulse, as in the no base injection case. The pulsed injection model shows large regions of turbulent flow in the region of the expansion fan and shock wave.

At 0.6T, the regions with the highest turbulent kinetic energy are the shear layers around the jets right as they are injected into the recirculation region but these regions are quite small. The jets themselves have a remarkably low level of turbulence. The vorticity due to the change in velocity across the shear layer is at its lowest at this point in the pulse which causes the turbulent kinetic energy in the shear layer to be quite low. The expansion fan region and the region just downstream of the oblique shock are also characterized by regions of higher turbulence.

As the pulse begins to recede, at 0.8T, the regions with the highest turbulent kinetic energy are still the shear layers around the jets but these regions are still quite small. The jets still have extremely low levels of turbulence. The expansion fan region and the region just downstream of the oblique shock are also characterized by regions of higher turbulence.

As the pulse comes to an end at 1T, the turbulent kinetic energy peaks in the region of the expansion fan and shockwave while still having a high level of turbulence in along the shear layer and in the recirculation region. The turbulence is higher in this region than in the shear layer or recirculation region.

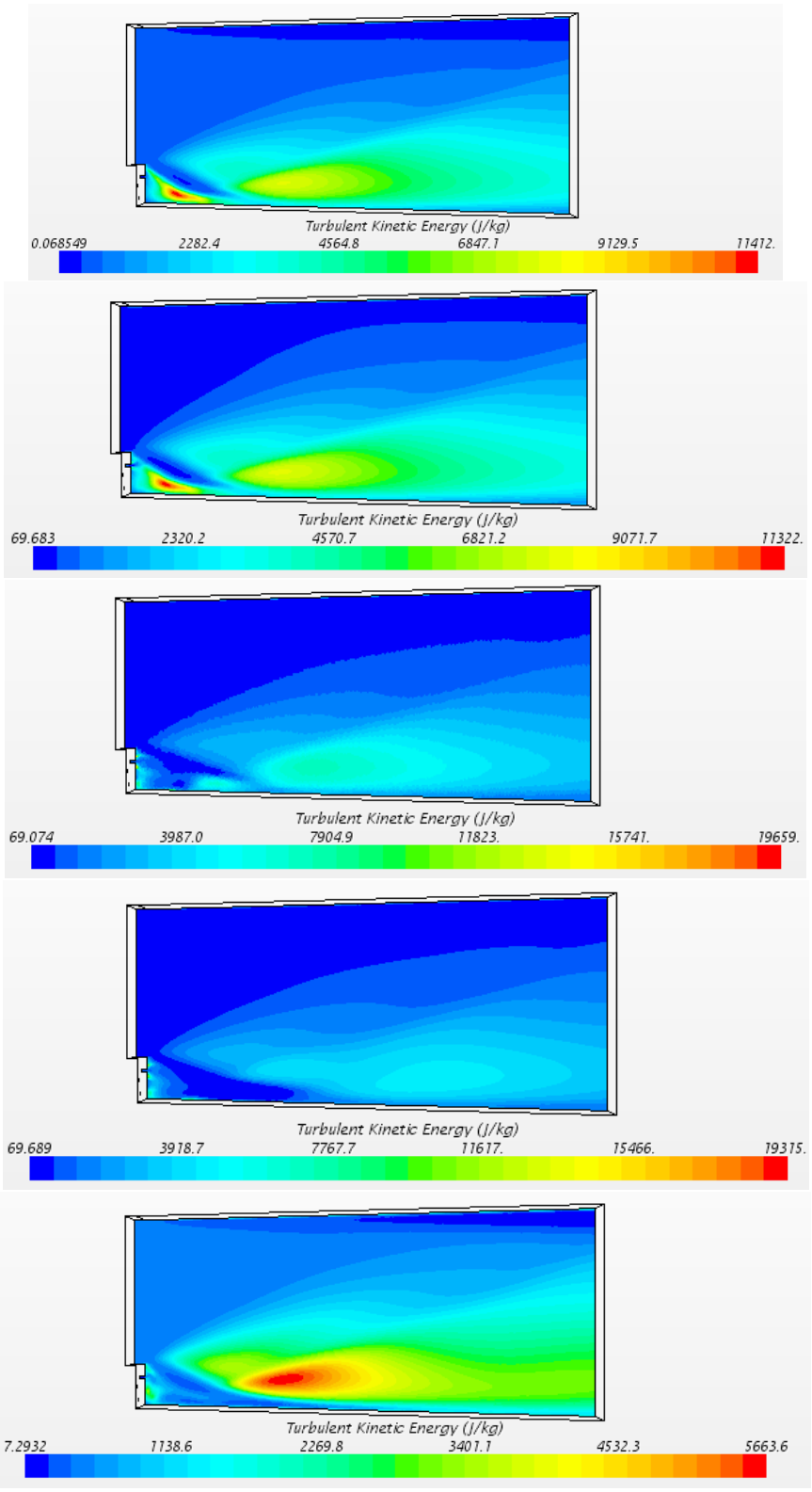

Figure 160: Contours of Turbulent Kinetic Energy (m^2/s^2) for the 5 port Injector on 33% at 0.2T, 0.4T, 0.6T, 0.8T, and 1T

5.2 Supersonic Wind Tunnel Data

Below are presented data taken from the static pressure ports of the supersonic wind tunnel at each of the different test conditions. The data points represent the average pressure values for over one second at that pressure port during the test. The data points are presented with the static pressure curve from their respective CFD case for comparison.

5.2.1 No Base Injection

Figure 161 shows a comparison between the test section and the three dimensional CFD model when no base injection is present. For the lower wall, in wind tunnel cases from wind tunnel runs B1 and B2 the eight pressure port data points appear to match well with the CFD Data with the exceptions that the pressures recorded at the first pressure port and the sixth pressure port are slightly higher than the pressure calculated by the CFD model.

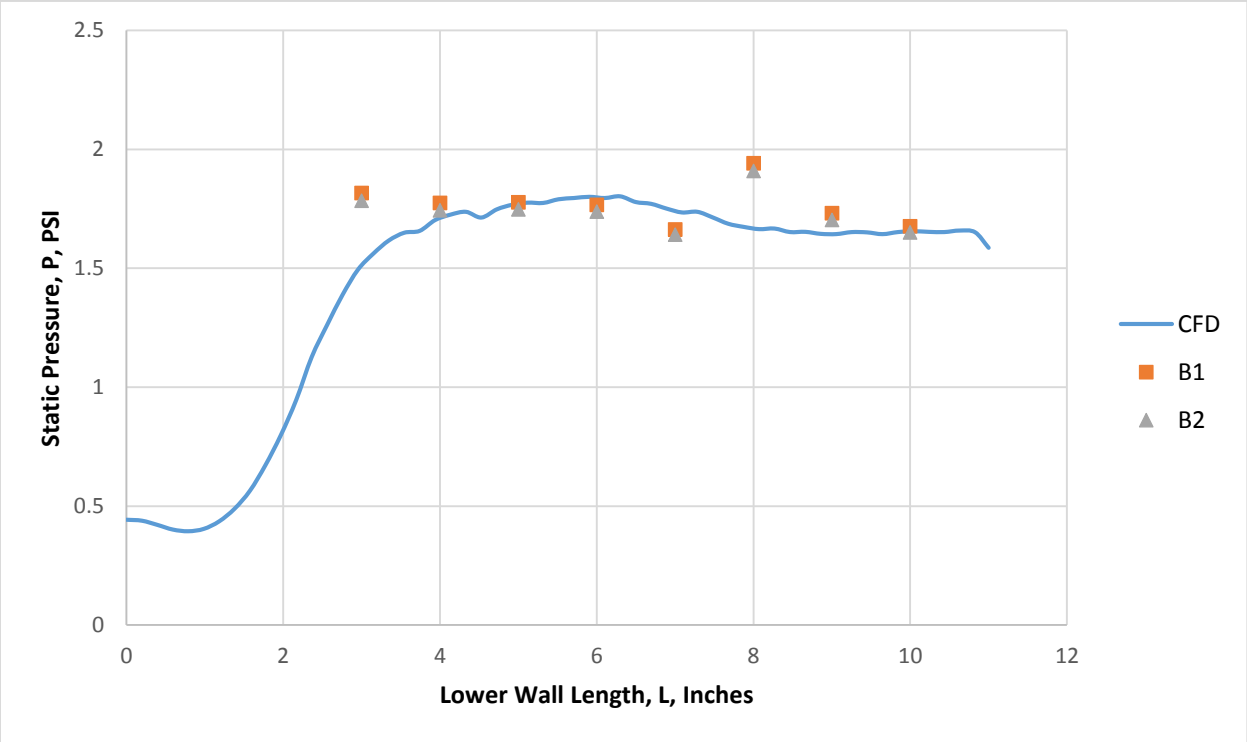

Figure 161: Comparison between Wind Tunnel Pressure Data and STAR-CCM+ CFD Data for the No Base Injection Case along the Lower Wall

5.2.2 Steady State Injection

Figure 162 shows a comparison between the test section wind tunnel runs B1, B2, and B3 and the CFD case with constant injection. As with the no base injection case, for the steady state injection case

on the lower wall the eight pressure ports match well with the CFD data, although there are a few points that are slightly lower or higher.

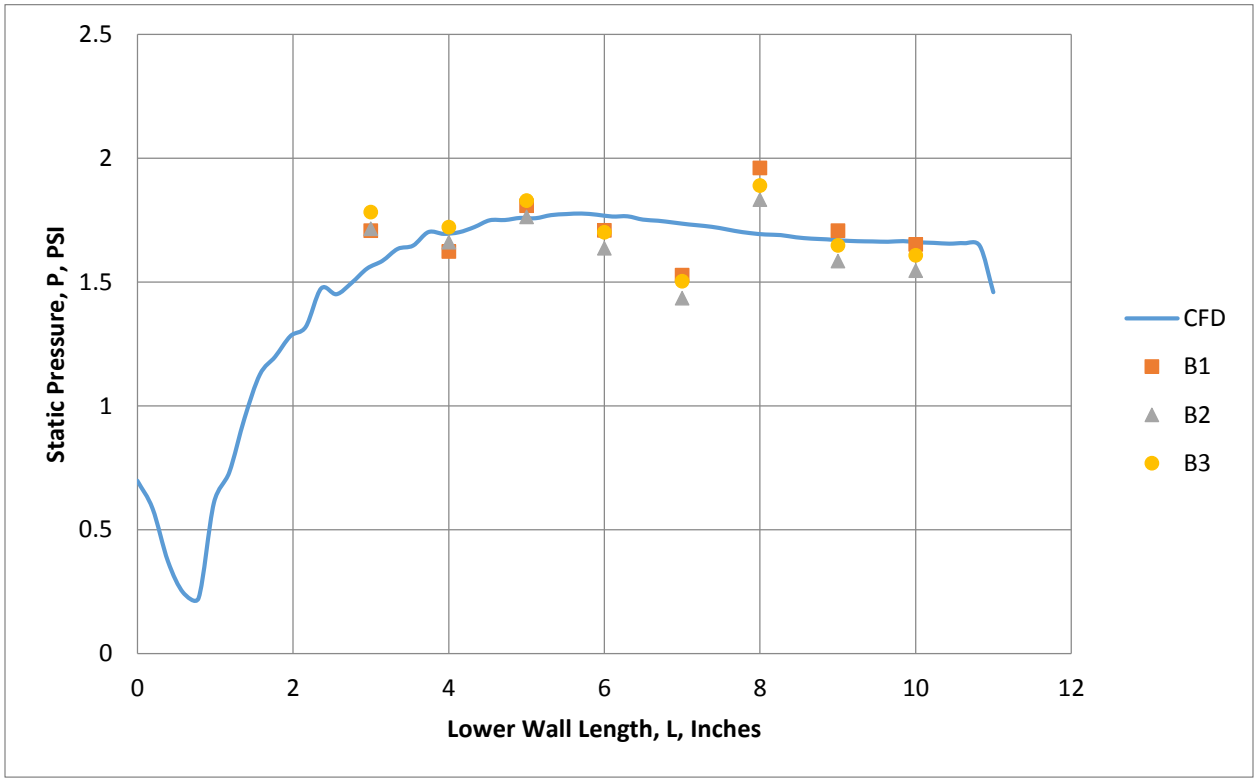

Figure 162: Comparison between Wind Tunnel Pressure Data and STAR-CCM+ CFD Data for the Constant Injection Case along the Bottom Wall

5.2.3 Pulsed Injection at 1.6 kHz

Figure 163 shows a comparison between the test section wind tunnel runs B1, B2, and B3 and the CFD case with injection at a frequency of 1.6 kHz. As with the no base injection case and steady injection case, for the pulsed injection case on the lower wall the eight pressure ports match well with the CFD data, although there are a few points that are slightly lower or higher.

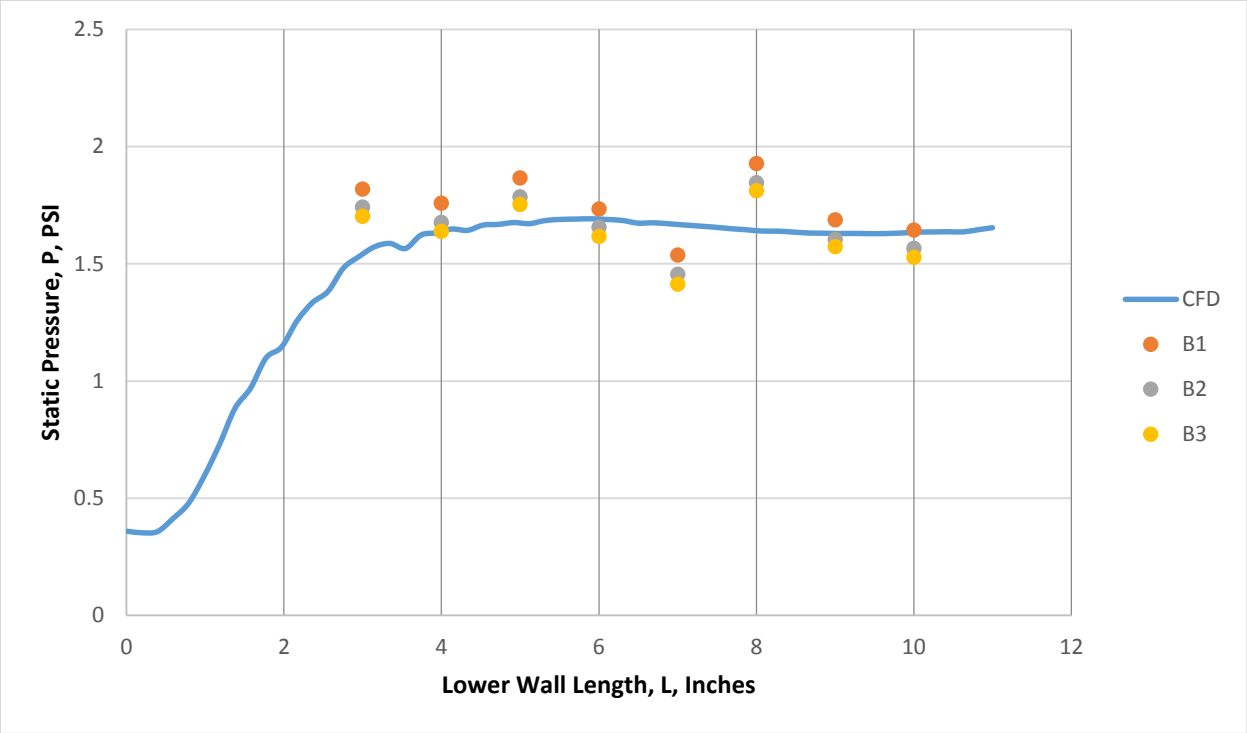

Figure 163: Comparison between Wind Tunnel Pressure Data and STAR-CCM+ CFD Data for Injection at 1.6 kHz along the Lower Wall

5.2.4 Spectral Analysis of Unsteady Wall Pressure Data

The following section plots the data collected from pressure ports on the lower wall for various test conditions. In each case the root mean squared value of the sample pressure data was taken. This value was then subtracted from each point of the unsteady data so that only the fluctuations about the RMS value are shown. This allows the pressure fluctuations to be analyzed for frequency and fluctuation strength. In each case the data has been collected over a period of 0.1 seconds at a sampling frequency of 20 kHz. A fast Fourier analysis was performed on the normalized pressure data to give the frequency response of the pressure at different test conditions.

The first set of data is for the no base injection case which will be used as a baseline to compare the responses of the pressure to other conditions. Figure 164 shows the fluctuations in static pressure about the RMS pressure as recorded at the first Injection port, 1 step height downstream of the step. Figure 165 shows enhanced views of the frequency response from 0 to 10 kHz, plotted in terms of sound pressure level (dB). It can be seen that for the no base injection case the peak sound pressure levels occur at around 110 dB SPL and all of these peaks occur at less than 70 Hz. Between 70 Hz and 10000 Hz the sound pressure levels at each frequency drop off exponentially.

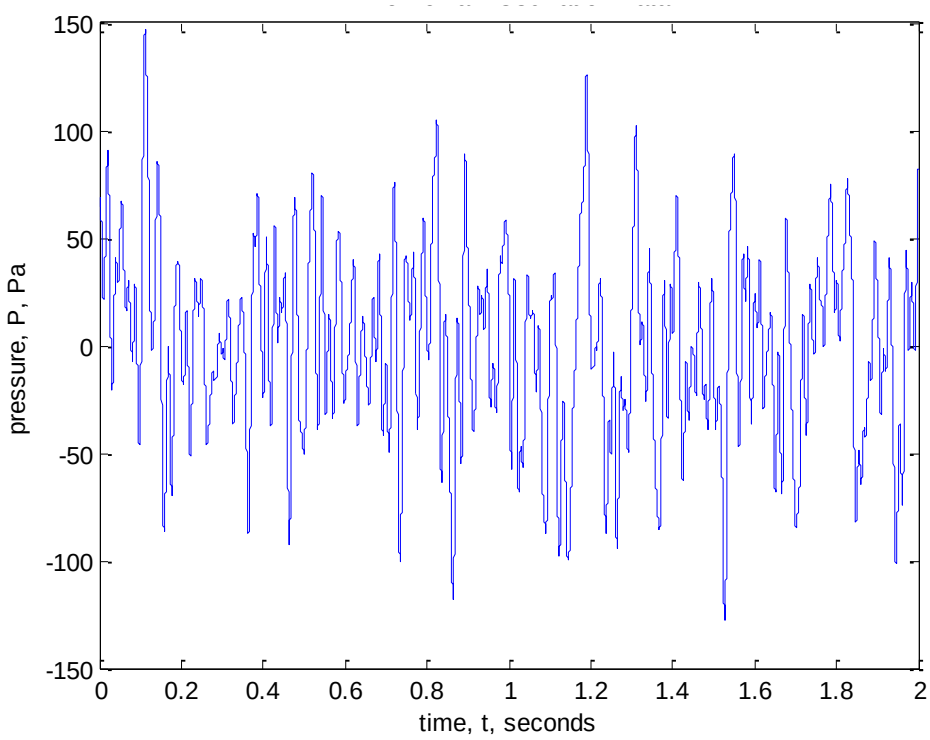

Figure 164: Unsteady Data for the No Base Injection Case

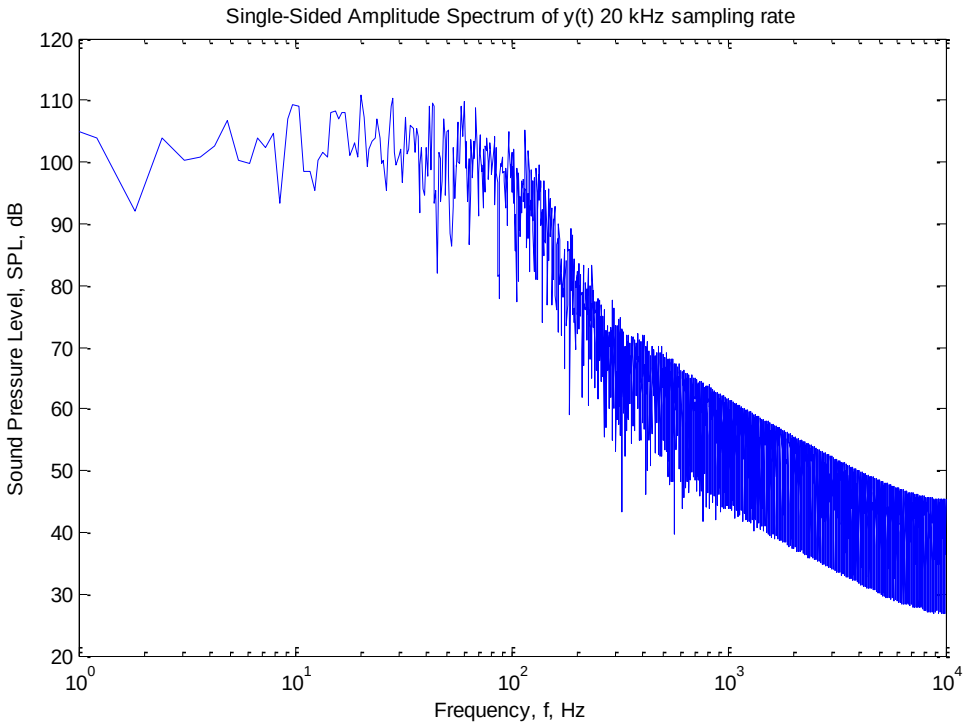

Figure 165: Single-Sided Amplitude Spectrum of Y(t) for the No Base Injection case, 0 to 10 kHz

The second set of data is for the steady injection from the 8 port injector case. Figure 166 shows the unsteady wall pressure fluctuations of the static pressure at the first Injection port 1 step height downstream of the step. Figure 167 show enhanced views of the frequency response from 0 to 10 kHz. It can be seen that for steady injection from the 8 port injector the peak sound pressure levels once again occur at around 110 dB SPL and all of these peaks occur at less than 70 Hz. As with the no base injection case, between 70 Hz and 10000 Hz the sound pressure levels at each frequency drop off exponentially.

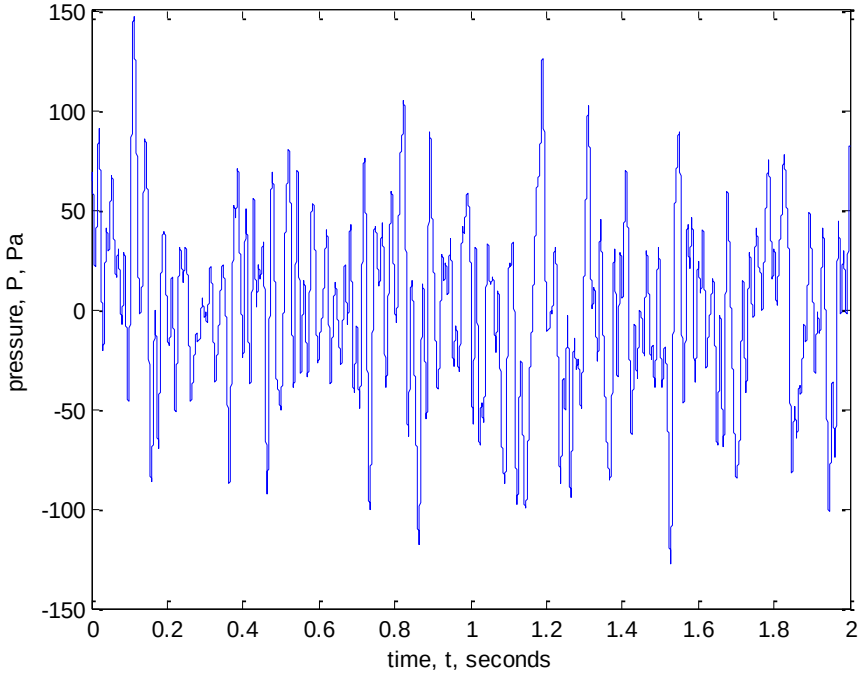

Figure 166: Unsteady Data for Steady Injection from the 8 Port Injector

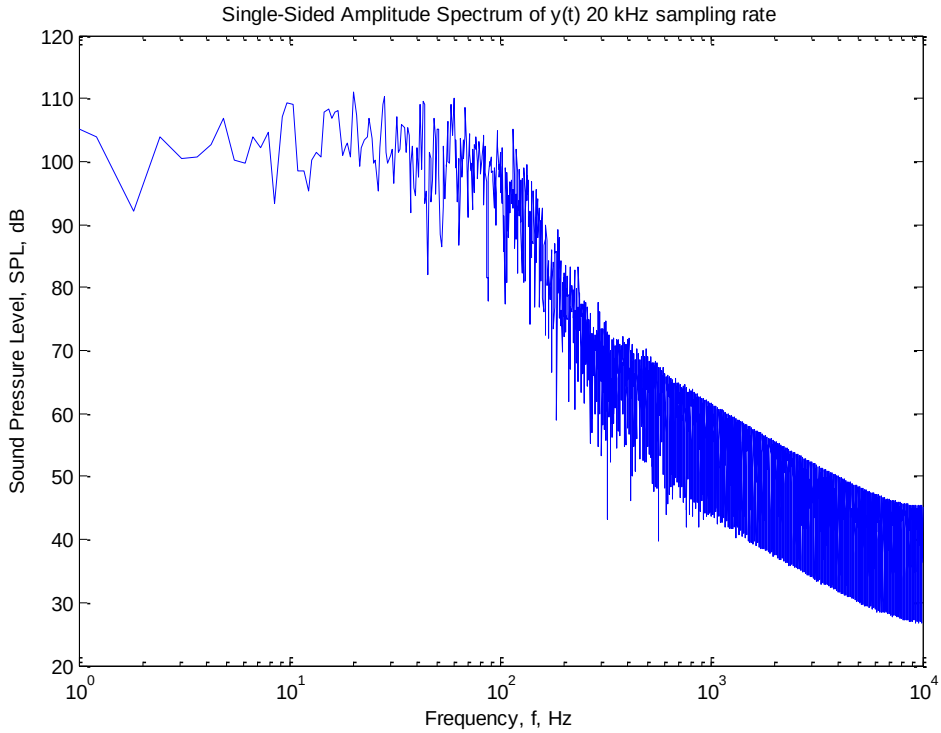

Figure 167: Single-Sided Amplitude Spectrum of Y(t) for Steady Injection from the 8 Port Injector, 0 to 10 kHz

The third set of data is for the pulsed injection from the 8 port injector at 1.6 kHz case. Figure 168 shows the unsteady static pressure fluctuations of the static pressure at the first Injection port 1 step height downstream of the step. Figure 169 show enhanced views of the frequency response from 0 to 10 kHz. It can be seen that for pulsed injection from the 8 port injector the peak sound pressure levels once again occur at around 110 dB SPL and all of these peaks occur at less than 70 Hz. As with the no base injection case, between 70 Hz and 10000 Hz the sound pressure levels at each frequency drop off exponentially.

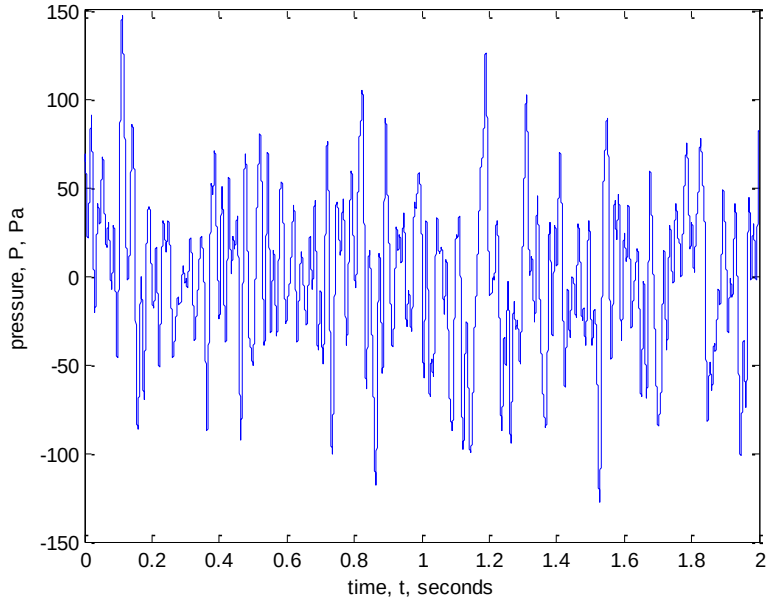

Figure 168: Unsteady Data for Pulsed Injection from the 8 Port Injector at 1.6 kHz

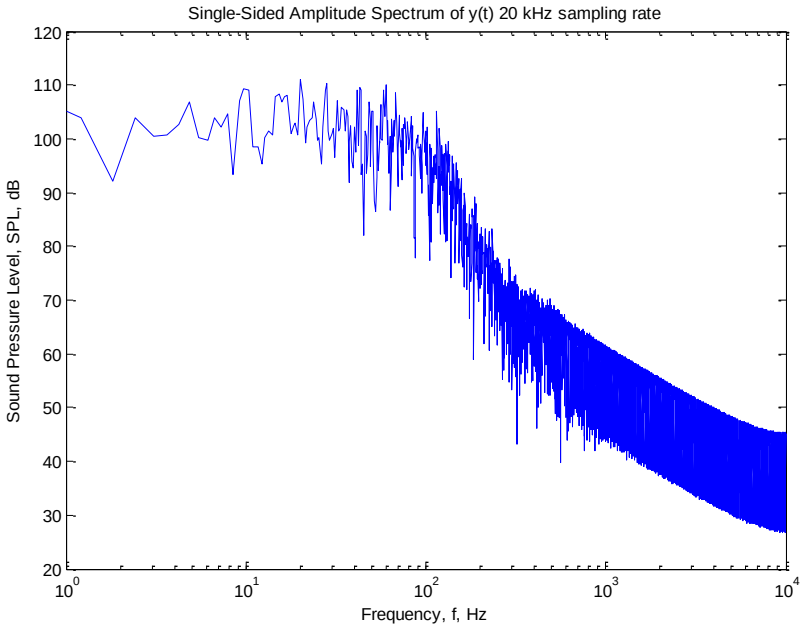

Figure 169: Single-Sided Amplitude Spectrum of Y(t) for Pulsed Injection from 8 port Injector at 1.6 kHz, 0 to 10 kHz

The fourth set of data is for the steady injection from the 5 port injector case. Figure 170 shows the unsteady static pressure fluctuations of at the first Injection port 1 step height downstream of the step. Figure 171 show the frequency response from 0 to 10 kHz. It can be seen that for steady injection from the 5 port injector the peak sound pressure levels once again occur at around 110 dB SPL and all of

these peaks occur at less than 70 Hz. As with the no base injection case, between 70 Hz and 10000 Hz the sound pressure levels at each frequency drop off exponentially.

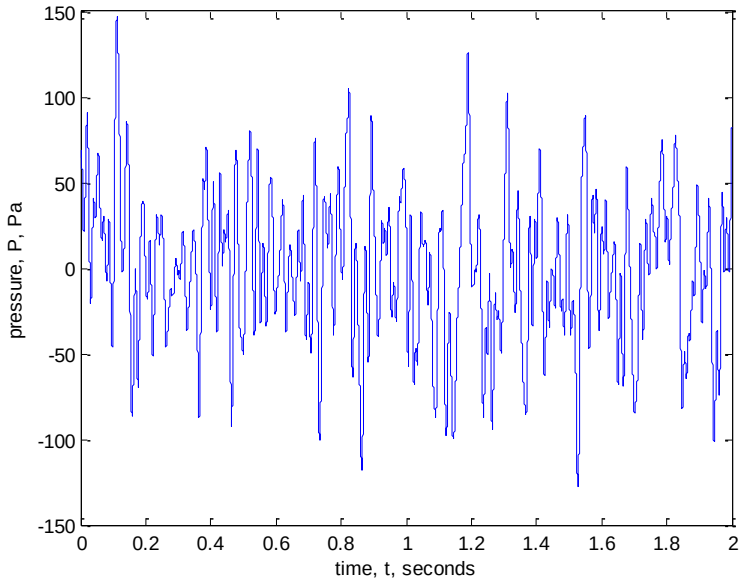

Figure 170: Unsteady Data for Steady Injection from the 5 Port Injector

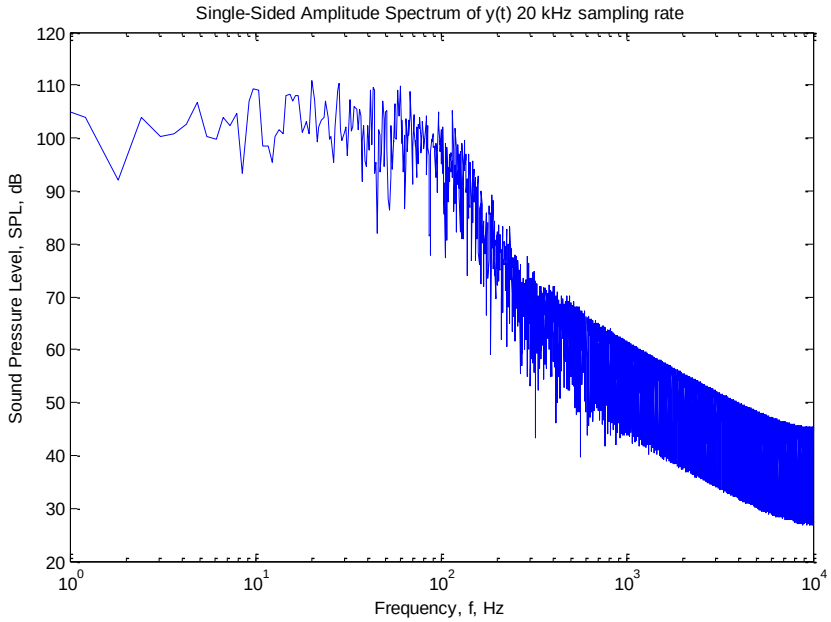

Figure 171: Single-Sided Amplitude Spectrum of Y(t) for Steady Injection from the 5 Port Injector, 0 to 10 kHz

The third set of data is for the pulsed injection from the 5 port injector at 1.0 kHz case. Figure 172 shows the unsteady fluctuations of the static pressure at the first Injection port 1 step height downstream of the step. Figure 173 show the frequency response from 0 to 10 kHz. It can be seen that

for pulsed injection from the 5 port injector the peak sound pressure levels once again occur at around 110 dB SPL and all of these peaks occur at less than 70 Hz. As with the no base injection case, between 70 Hz and 10000 Hz the sound pressure levels at each frequency drop off exponentially.

Spectral analysis of unsteady pressure data did not reveal significant variation between the baseline with no base injection and the cases with pulse injection.

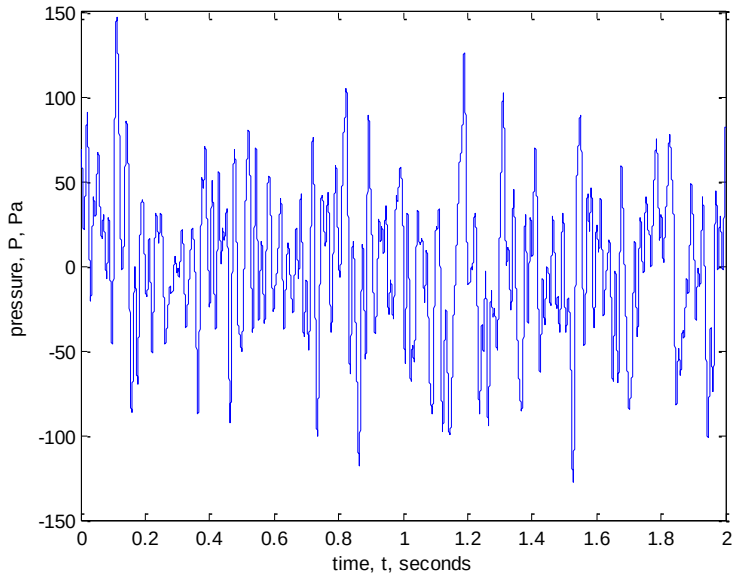

Figure 172: Unsteady Data for the Pulsed Injection from the 5 Port Injector at 1.0 kHz

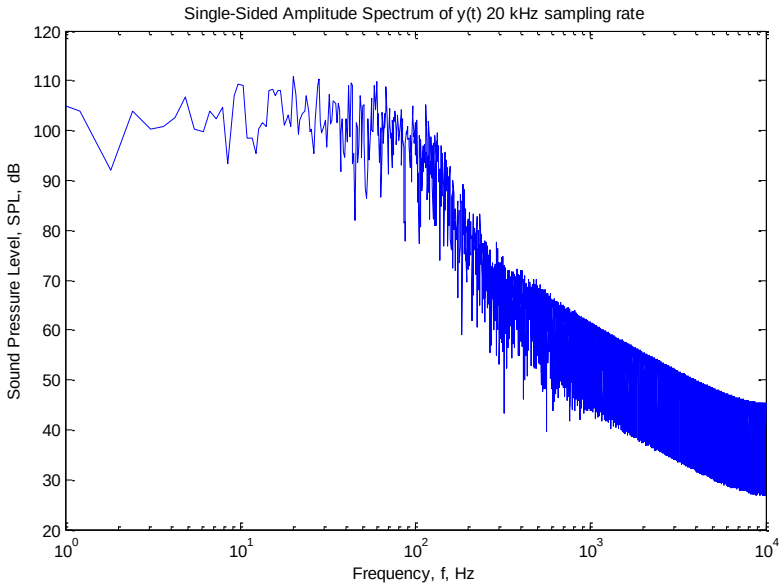

Figure 173: Single-Sided Amplitude Spectrum of Y(t) for Pulsed Injection from the 5 Port Injector at 1.0 kHz, 0 to 10 kHz

6 Conclusions

From the results presented in the previous section a number of conclusions can be drawn regarding the three dimensional STAR-CCM+ simulation results and the supersonic wind tunnel test section data. The results from the three dimensional STAR-CCM+ simulation show the behavior of the shear layer during injection, as seen in Figure 174. Injection causes a reduced curvature in the shear layer at each point of injection. This weakens the strength of the expansion fan and shock wave at these cross sections. Away from the injection ports the shear layer is unaffected and the contours resemble the no injection contours.

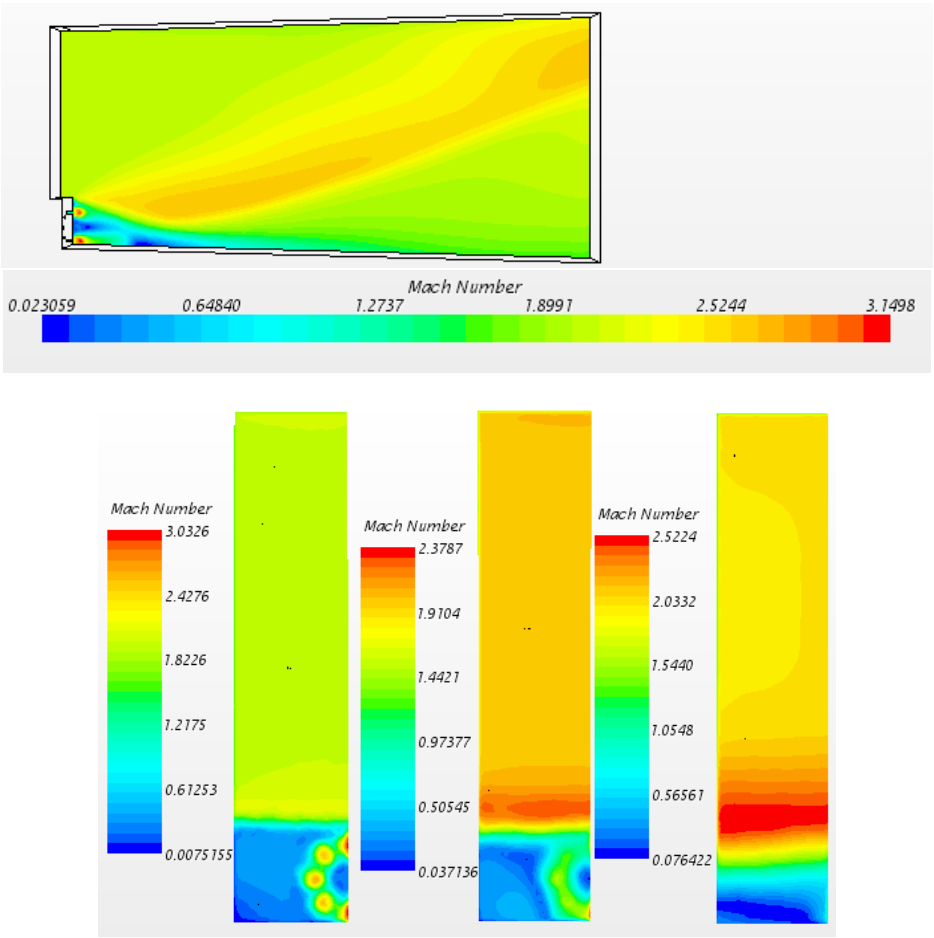

Figure 174: Contours of Mach number for the 8 port Injector at the Plane of symmetry and Cross Sections at 0.25, 0.5, and 1 Base Heights downstream of the Step at t=20% of the pulse period

Since vorticity dynamics plays a central role in mixing flow physics, as in scramjet combustors, it is repeated here for discussion purposes. The equation defining the dynamics of the vorticity vector field, which is the curl of the velocity vector field is:

$$\frac{D\vec{\Omega}}{Dt} = (\vec{\Omega} \cdot \nabla)\vec{V} - \vec{\Omega}(\nabla \cdot \vec{V}) - \nabla x \left(\frac{1}{\rho}\nabla p\right) + \nabla x \vec{X} + \nabla x \overrightarrow{F_{visc}} \quad (6.1)$$

Where $\vec{V}$ is the velocity vector field, $\vec{\Omega}$ is the vorticity vector field, $\vec{X}$ represents the body forces, p is pressure, ρ is density, and $\overrightarrow{F_{visc}}$ represents the viscous forces. The interaction between the velocity field and vorticity is governed by the vorticity dynamics equation. For example, vortex stretching caused by a three dimensional flowfield locally intensifies the vorticity field. In addition, the compressibility effect, which is a dominant feature in the scramjet flow simulation affects vorticity production.

This behavior appears to be somewhat analogous to the breaking down of a free shear mixing layer. Consequently, high-intensity vortical regions in the shear layer promote turbulence production and experience diminished intensity.

In the three dimensional models the injection actually decreased the vorticity across the shear layer by decreasing the velocity differential, as can be seen in Figure 175. Turbulence production was also diminished along the shear layer. Also in all three dimensional models, turbulence can be found in the expansion fan region (Figure 176). The reduction of shear layer curvature caused by base injection is deemed partially responsible for reduced turbulence generation and reduced vorticity strength.

The impact of base injection on the shear layer growth rate and turbulence kinetic energy production may be addressed through convective Mach number. The Convective Mach numbers in the shear layers is repeated here in equation 6.2:

$$M_c = \frac{2(U_1 - U_2)}{a_1 + a_2} \quad (6.2)$$

Where U_1 and U_2 are the freestream velocities on either side of the shear layer and a_1 and a_2 are the speed of sound on either side of the shear layer. The convective Mach number for the shear layer of the three dimensional no injection model is 0.83. The convective Mach number for the shear layer in the steady injection case is 0.08. The convective Mach number for the shear layers at the edges of the jets is 0.32. In the pulsed injection case the convective Mach number of the shear layer oscillates between 0.83 and 0.08, with the lower value being at the height of injection. This means that base injection is decreasing the velocity differential across the shear layer, thereby weakening the shear layer, thus reducing the shear layer's capacity to mix fuel and air.

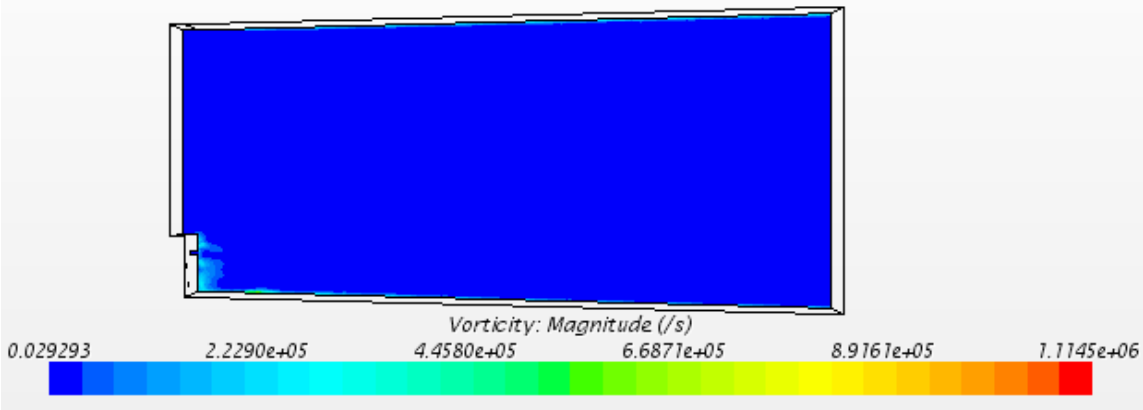

Figure 175: Contours of Vorticity (1/s) for the 5 port Injector on 50% at t=0.01006

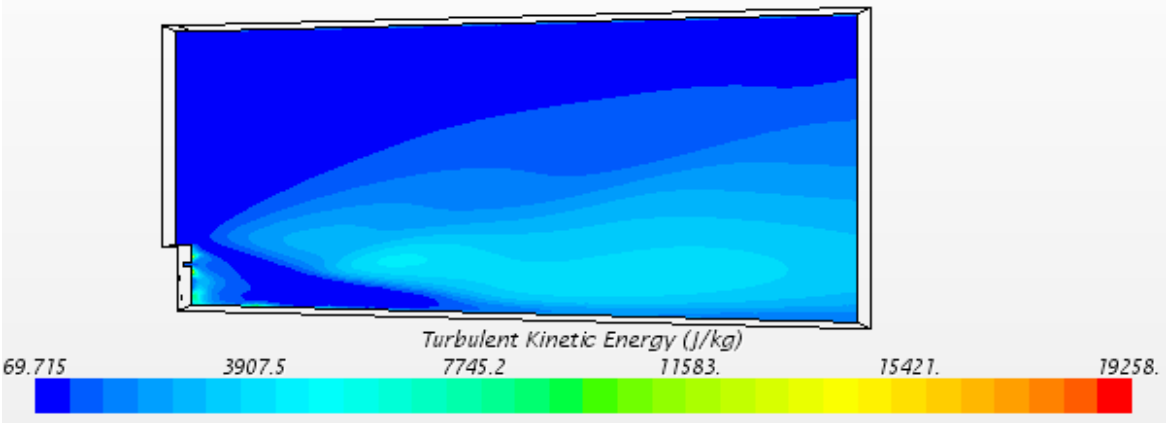

Figure 176: Contours of Turbulent Kinetic Energy (m^2/s^2) for the 5 port Injector on 50% at t=0.01006

The Strouhal Number is a useful non-dimensional parameter in oscillating flows that is the ratio of two characteristic time scales of the problem, namely the convective time scale and oscillation period, i.e.:

$$St = \frac{fL}{V} \tag{6.3}$$

Flows with Strouhal numbers between 10^-4 and 1 are characterized by vortex shedding. At an injection frequency of 1.0 kHz the Strouhal number of the injection port is 0.005, which is within the range where vortex shedding would be expected, but no vortex shedding was noted in any of the three dimensional simulations. The suppression of vortex shedding may be attributed to the complex dynamics of multi-jet interaction in the simulated injector problem. Also, it is possible that no vortex shedding was noted due to the insufficient grid resolution to capture the vortices and rapid dissipation of these vortices in the shear layer.

For the supersonic wind tunnel tests, the steady state static pressure data from the supersonic wind tunnel was closely replicated by the STAR-CCM+ CFD simulation for the wind tunnel wall in all cases.

Spectral analysis of unsteady pressure data from the wind tunnel did not reveal significant variation between the baseline with no injection and the cases with pulsed injection. This is in agreement with the STAR-CCM+ simulations which show only minor static pressure variation along the lower wall throughout the pulse. Thus, it must be concluded that pulsed injection from a backward facing step within the range of parameters tested did not excite resonance behavior in the shear layer. However, the flow physics captured by the interaction of pulsed jets in the base of a backward-facing step and supersonic shear layer provides valuable lessons in scramjet design.

7 Future Research

All supersonic wind tunnel data presented in this report was performed using the eight injection port face plate in conjunction with the eight tooth valve and sixteen tooth valve and the five injection port face plate in conjunction with the three five tooth valves for varying pulse duration.

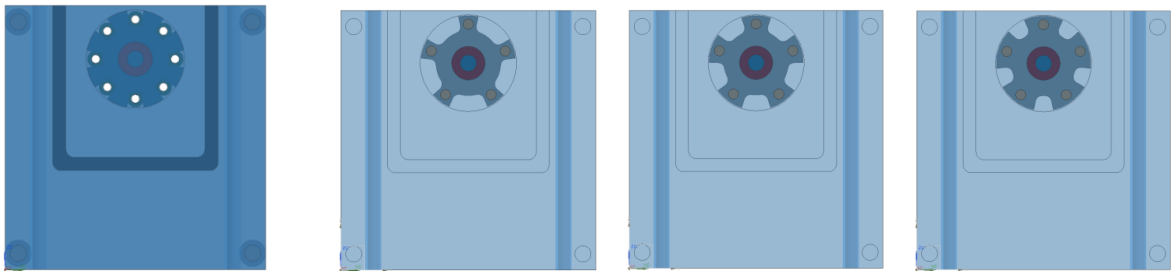

Figure 177: Eight Tooth Valve with Eight Port Injector and Five Port Injector Plate with Five Tooth Valves for Varying Pulse Duration

Even through orifice injection from the backward facing step has not been shown to have the desired effect of fuel and air mixing the injector concept could still be modified to test other variables. For example the injector could be turned at 90^{o} and various face plates could be designed that would allow for pulsed injection testing from 45^{o} to 90^{o}. The effects of frequency, duty cycle, orifice location and injection staging could all easily be tested with only minor modifications to the injector itself.

Two dimensional Fluent Simulations were also performed as part of this research, but showed no agreement with the three dimensional simulations or the wind tunnel test results. This is because the two dimensional injector would be more accurately represented by a slit injector rather than an orifice injector. The two dimensional model shows regions of vorticity that dissipate into regions of turbulence

being shed along the lower wall. It is recommended that slit nozzle injection from a backward facing step be studied experimentally and with three dimensional CFD simulations.

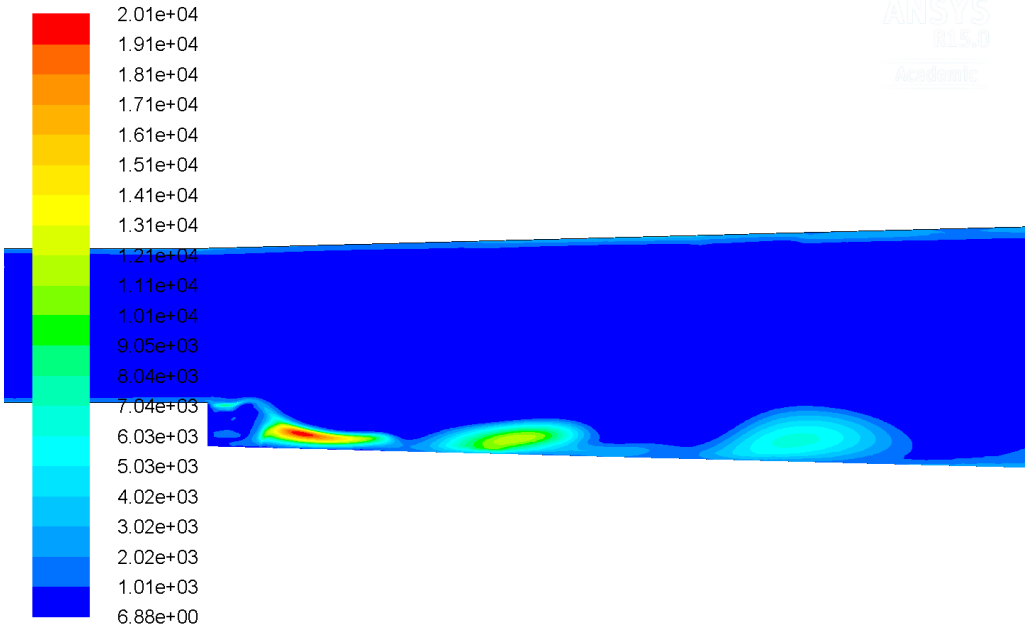

Figure 178: Two Dimensional Vortex shedding

8 Works Cited

1. Hieser, W.; Pratt, D. Hypersonic Airbreathing Propulsion, American Institute of Aeronautics and Astronautics, Inc., Washington D.C. 1994
2. "Ramjet/Scramjet Thrust," NASA Glenn Research Center Website, https://www.grc.nasa.gov/www/k-12/airplane/ramth.html
3. "How Scramjets Work," NASA Fact Sheet, http://www.nasa.gov/centers/langley/news/factsheets/X43A_2006_5.html
4. Lachman, G. *Boundary Layer and Flow Control: Its principals and application, Vol. 2*. Pergamon Press, New York, 1961 pp. 602-632
5. Dryden, H. 1955 Transition From Laminar to Turbulent Flow at Subsonic and Supersonic Speeds. *Proceedings of the Conference on High-Speed Aeronautics,* pp. 41-74
6. Betchov, R. & Criminale, W. *Stability of Parallel Flows.* Academic Press, New York, 1967, pp. 171-197
7. Chandrasekhar, S. *Hydrodynamic and Hydromagnetic Stability.* Dover Publications inc., New York, 1961, pp. 481-514
8. "Kelvin-Helmholtz Instability Cloud Structures," http://www.brockmann-consult.de/CloudStructures/kelvin-helmholtz-instability-description.htm
9. Brown, G. & Roshko, A. "On Density Effects and Large Structure in Turbulent Mixing Layers," *Journal of Fluid Mechanics*, Vol.64, part 4, 1974, pp. 775-816
10. Doty, M. & Mclaughlin, D. "Experiments on Mach-Wave Interactions in a Compressible Shear Layer," *AIAA Journal,* Vol. 38, No. 10, 2000, pp. 1871-1878
11. Papamoschou, D., 1990 Communication Paths in the Compressible Shear Layer. AIAA-90-0155
12. Plesniak, M., Bell, J., & Mehta, R. 1991 Effects of Initial Spanwise Perturbations and Three-Dimensionality in a Plane Mixing Layer. AIAA-91-0622
13. Bell, J., & Mehta, R. 1990 Effects of Streamwise Vorticity Injection on Turbulent Mixing Layer Development. AIAA-90-1459
14. Disimile, P. "Transverse Vorticity Observations in Large Coherent Structures," *AIAA Journal*, Vol. 33, No. 12, pp. 2427-2428
15. Wiecek, K. & Mehta, R. 1996 Effects of Velocity Ratio on Mixing Layer Three-Dimensionality. AIAA 1996-1932
16. Papamoschou, D., & Roshko, A. "The Compressible Turbulent Shear Layer: An Experimental Study," *Journal of Fluid Mechanics*, Vol. 197, 1988, pp.453-447
17. Krothapalli, A. 1999 Control of High Convective Mach Number Free Shear Layers. AIAA 99-3508
18. Maddalena, L., & Dimotakis, P. 2010 On the Effects of Transverse-Jet Injection into a Supersonic Shear Layer. AIAA 2010-755
19. Bunyajitradulya, A., & Papamoschou D. 1994 Acetone PLIF Imaging of the Turbulent Shear-Layer Structure at High Convective Mach Number. AIAA-94-0617
20. Soetrisno, M., Greenough, J., Eberhardt, D., & Riley, J. 1989 Confined Compressible Mixing Layers: Part 1. Three-dimensional Instabilities. AIAA-89-1810
21. Papamoschou, D. 1993 Total Pressure loss in Supersonic Parallel Mixing. AIAA-93-0216
22. Clemens, N., Petullo, S., & Dolling, D. "Large-Scale Structure Evolution in Supersonic Interacting Shear Layers," *AIAA Journal,* Vol. 34, No. 10, 1996
23. Demetriades, A. & Brower, T. 1990 Experiments on the Free Shear Layer between Two Supersonic Streams. AIAA 1990-0710
24. Papmoschou, D., Lin, M., Bunyajitradulya, A., & Robey, H. 1993, Non-Intrusive Technique for Measurement of Power Spectra in Compressible Turbulence

25. Watanabe, S., & Mungal, M. 1999, Velocity Field Measurements of Mixing-Enhanced Compressible Shear Layers, AIAA 99-0088
26. Sarkar, S. The Stabilizing Influence of Compressibility on Turbulence in High-Speed Shear Flows. AIAA 94-2243
27. Urban, W., Watanabe, S., & Mungal, M. 1998, Velocity Field of the Planar Shear Layer: Compressibility Effects, AIAA 98-0697
28. Elliot, G. & Samimy, M. 1990 Compressibility Effects in Free Shear Layers. AIAA 90-0705
29. Menaa, M. & Dussauge, J. 2003 Density and Compressibility Effects on the Structure of Supersonic Mixing Layer: Experimental Results and Similarity Analysis. AIAA 2003-6907
30. Samimy, M. & Elliott, G. "Effects of Compressibility on the Characteristics of Free Shear Layers," *AIAA Journal,* Volume 28, No. 3, 1990, pp. 439-445
31. Zhuang, M. Kubota, T., & Dimotakis, P. "Instability of Inviscid, Compressible Free Shear Layers," *AIAA Journal,* Vol. 28, No. 10, 1990, pp. 1728-1733
32. Gruber, M. Messersmith, N., & Dutton, J. "Three-Dimensional Velocity Field in a Compressible Mixing Layer," *AIAA Journal,* Vol. 31, No. 11, 1993, pp. 2061-2067
33. Goebel, S., & Dutton, J., 1990. Velocity Measurements of Compressible, Turbulent Mixing Layers, AIAA-90-0709
34. Bogdanoff, D. "Compressibility Effects in Turbulent Shear Layers," *AIAA Journal*, Vol. 28, No. 6, pp. 926-927
35. Petullo, S. & Dolling, D. 1993 Large-Scale Structure Orientation in a Compressible Turbulent Shear-Layer. AIAA-93-0545
36. Bowersox, R., & Schetz, J. "Measurements of Compressible Turbulent Flow Structure in a Supersonic Mixing Layer," *AIAA Journal,* Vol.33, No. 11, 1995, pp. 2101-2106
37. Shau, Y. & Dolling, D. 1990 The Detection of Large Scale Structure in Undisturbed and Disturbed Compressible Turbulent Free Shear Layers. AIAA 90-0711
38. Papamoschou, D., & Bunyajitradulya, A., 1995 Double-Exposure PLIF Imaging of Compressible Shear Layers. AIAA-95-0513
39. Papamoschou, D. 1989 Structure of the Compressible Turbulent Shear Layer. AIAA-89-0126
40. Hall, J., Dimotakis, P., &Rosemann, H. "Experiments in Nonreacting Compressible Shear Layers," *AIAA Journal,* Vol. 31, No. 12, 1993, pp. 2247-2253
41. Tang, W., Sankar, L., & Komerath, N. 1989 Mixing Enhancement in Supersonic Free Shear Layers. AIAA 89-0981
42. Ragab, S. & Sheen, S. 1990 Numerical Simulation of a Compressible Mixing Layer. AIAA-90-1669
43. Calhoon, W., Kannepalli, C., Papp, J., & Dash, S. 2002 Analysis of Scalar Fluctuations at High Convective Mach Numbers. AIAA-2002-1087
44. Risha, D. 1995 Analysis of Growth Rates in Three-Dimensional Air-to-Air, Supersonic Shear Layers Using Direct Numerical Simulation. AIAA 95-0523
45. Risha, D. 1995 Analysis of Turbulence Statistics in Three-Dimensional, Air-to-Air Supersonic Shear Layers Using Direct Numerical Simulation. AIAA-95-6072
46. Clemens, N. & Mungal, M. 1990 Two- and Three-Dimensional Effects in the Supersonic Mixing Layer. AIAA-90-1978
47. Hataue, I. 1990. Study of Compressibility Effects in Mixing Layer by Numerical Simulation. AIAA 1990-1464
48. Papamoschou, D., "Effect of Three-Dimensionality on Compressible Mixing," *Journal of Propulsion and Power*, Vol. 8, No. 1, 1992, pp. 247-249
49. Wantanbe, D., Kensuke, A., & Maekawa, H. 2011 Effects of Oblique Unstable Modes on the Development of a Turbulent Mixing Layer at High Convective Mach Numbers. AIAA 2011-41

50. Island, T., Urban, W., & Mungal, M., 1997. Small-perturbation mixing enhancement in compressible shear layers, AIAA-97-0395
51. Martens, S., Kinzie, K., & McLaughlin, D. "Measurements of Kelvin-Helmholtz Instabilities in a Supersonic Shear Layer," *AIAA Journal*, Vol. 32, No. 8, 1994, pp. 1633-1639
52. Martens, S., Kinzie, K., McLaughlin, D. "Structure of Coherent Instabilities in a Supersonic Shear Layer," *AIAA Journal,* Vol. 34, No. 8, 1996, pp. 1555-1561
53. Birch, S. 1997 On the Role of Structure in Turbulent Mixing. AIAA 1997-2636
54. Choong, K. & Loth, E. 1994 A numerical investigation of supersonic Turbulent Shear Layers: Compressibility Effects. AIAA-94-2244
55. Billig, F.& Schetz, J. "Penetration and Mixing of Gas Jets in Supersonic Cross Flow," *AIAA Journal*, Vol. 32, No. 7, pp. 1533-1535
56. Kouchi, T., Sasaya, K., Watanabe, J., Sibayama, H. & Masuya, G. 2010 Penetration Characteristics of Pulsed Injection into Supersonic Crossflow. AIAA 2010-6645
57. Ota, D., & Goldberg, U. "Computation of supersonic turbulent shear layer mixing with mild compressibility effects," *AIAA Journal*, Vol. 29, 1991, pp. 1156-1160
58. Claus, R., Huang, P., & MacInnes, J. "Time-Accurate Simulations of a Shear Layer Forced at a Single Frequency," *AIAA Journal,* Vol. 28, No. 2 1990, pp. 267-275
59. Papamoschou, D. 1993 Thrust Loss Due to Supersonic Mixing. AIAA-1993-2140
60. Liu, H.X., Wang, B., Guo, Y.C., Zhang, H.Q., & Lin, W. Y. 2013 "Effects of Inflow Mach Number and Step Height on Supersonic Flows over a Backward-Facing Step". *Advances in Mechanical Engineering*, Vol 2013, Acticle ID 147916
61. Roshko, A. & Thomke, G. 1966 "Observation of Turbulent Reattachment Behind an Axisymmetric Downstream-Facing Step in Supersonic Flow". *AIAA Journal*, vol. 4, no. 6, pp. 975-980
62. Abdullah, K., Wijeyakulasurya, S. & Nalim, M. 2012 Numerical Study of supersonic flow over backward-facing step for scramjet application. AIAA-2012-4001
63. Sigalla, L., Eberhardt, S., Greenough, J., Riley, J. & Soetrisno, M. 1990 Numerical Simulation of Confined Spatially-Developing Mixing Layers: Comparison to the Temporal Shear Layer. AIAA-90-1462
64. Soetrisno, M., Eberhardt, S., Greenough, J., & Riley, J. 1990 Confined Compressible Mixing layer" Part II. 3D Kelvin-Helmholtz-2D Kelvin Helmholtz Interactions. AIAA-90-1466
65. Morris, P., Giridharan, M., & Viswanathan, K., 1990. Turbulent Mixing in Plane and Axisymmetric Shear Layer., AIAA-90-0708
66. Cenkner, A. "Laser Doppler Velocimeter Measurements on Supersonic Mixing Nozzle that Employ Gas-Trips," *AIAA Journal,* Vol.20, No.3, 1982, pp.383-389
67. Cenkner, A. & Driscoll, R. "Laser-Induced Fluorescence Visualization of Supersonic Mixing Nozzles that Employ Gas-Trips," *AIAA Journal*, Vol. 20, No. 6, pp. 812-819
68. Davis, D. 1993 Scramjet Fuel Air Mixing Enhancement by Cross-Stream Pressure Gradients. AIAA-93-2139
69. Gouskov, O., Kopchenov, V., Lomkov, K. 2001 Numerical and experimental Investigation of Supersonic Mixing and Combustion. AIAA 2001-1821
70. Gutmark, E., Schadow, K., & Wilson, K., 1989 Mixing Enhancement in Coaxial Supersonic Jets. AIAA-89-1812
71. Murakani, E. & Papamoschou, D. 1998 PLIF Investigation of Coannular Supersonic Jets,
72. Yu, K., Gutmark, E. & Schadow, K. 1993 Passive Control of Coherent Vortices in Compressible Mixing Layers. AIAA 93-3262
73. Samitha, Z., Davis, D., & Balachandran, P. 2009 Computational Study of Supersonic Mixing Using Clover Nozzle. AIAA 2009-30

74. Samitha, Z., Swaraj Kumar, B., & Balchandran, P. 2007 Experimental Study on Supersonic Mixing Using Clover Nozzle. AIAA 2007-839
75. Tew, D., & Waitz, I. “Impact of Compressibility on mixing Downstream of Lobed Mixers,” *AIAA Journal*, Vol. 42, No. 11, pp. 2393-2396
76. VanLerberghe, W. Dutton, J., Lucht, R., & Yuen, L., 1994 Penetration and Mixing Studies of a Sonic Transverse Jet Injected into a Mach 1.6 Crossflow. AIAA-94-2246
77. Ben-Yakar, A., & Hanson, R. “Cavity Flame-Holders for Ignition and Flame Stabilization in Scramjets: An Overview,” *Journal of Propulsion and Power,* Vol. 17, No. 4, 2001, pp. 869-877
78. Takahashi, H., Oso, H., Kouchi, T., & Masuya, G., “Scalar Spatial Correlations in a Supersonic Mixing Flowfield,” *AIAA Journal,* Vol. 48, No. 2, February 2010, pp. 443-452
79. M. R. Gruber, A. S. Nejad, T. H. Chen, and J. C. Dutton. "Transverse Injection from Circular and Elliptic Nozzles into a Supersonic Crossflow", Journal of Propulsion and Power, Vol. 16, No. 3 (2000), pp. 449-457
80. Sunami, T., Wendt, M., & Nishioka, M. 1998 Supersonic Mixing and Combustion Control Using Streamwise Vortices. AIAA 1998
81. Arai, T., Sakaue, S., Hayase, H., & Hiejima, T. 2011 Streamwise Vortices Introduced by “Hyper-Mixer” on Supersonic Mixing. AIAA 2011-2342
82. Kawano, S., Aso, S. & Orino, M. 2000 A Study of a New Injector for Improvement of Supersonic Mixing. AIAA 2000-0089
83. Aso, S., Yamane, Y., Ando, Y., Umii, K., Tokunaga, K., & Sakata, K. 1997 A Study on Supersonic Mixing Flowfield with Swept Ramp Injectors. AIAA 97-0397
84. Sunami, T. & Scheel, F. 2002 Analysis of Mixing Enhancement Using Streamwise Vortices in a Supersonic Combustor by Application of Laser Diagnostics. AIAA 2002-5203
85. Abdel-Salam, T.M., Tiwari, S. & Mohieldin, T. “Effects of Ramp Side Angle in Supersonic Mixing” *AIAA Journal*, Vol. 41, No. 6, June 2003, pp. 1199-1201
86. Yamauchi, Y., Kodama, Y., Sakaue, S., & Arai, T. 2012 Effect of Mach Number on Supersonic Mixing by “Hyper-Mixer Injector.” AIAA 2012-5816
87. Parent, B. & Sislian, J. “Hypersonic Mixing Enhancement by Compression at a High Convective Mach Number,” *AIAA Journal*, Vol. 42, No. 4, April 2004, pp. 787-795
88. Parent, B., & Sislian, J. “Impact of Axial Vortices on Mixing at a High Convective Mach Number,” *AIAA Journal*, Vol. 41, No. 7, July 2003, pp. 1386-1388
89. Tumin, A., “Optimal Streamwise Vortices Intended for Supersonic Mixing Enhancement” *AIAA Journal*, Vol. 41, No. 8, August 2003, pp. 1542-1546
90. Inoue, Kei, Yamaguchi, K., Aso, S., & Tani, Y. 2005 A Study on the Enhancement of Supersonic Mixing by Using RMP Shaped Injector with Shock Generator and Cavity
91. Rougeux, A., & Malo-Molina, F. 2012 Numerical Studies for 3D Supersonic Cavity Based Flows. AIAA 2012-0776
92. Zang, A., Tempel, T., & Yu, K. 2005 Experimental Characterization of Cavity-Augmented Supersonic Mixing. AIAA 2005-1423
93. Yaga, M., Shinsaku, T., Doerffer, P., & Oyakawa, K. 2003 Numerical Simulation of Supersonic Mixing Enhancement with Porous Cavity. AIAA 2003-3461
94. Bueno, P., Unalmis, O., Clemens, N., & Dolling, D. 2002 The Effects of Upstream Mass Injection on a Mach 2 Cavity Flow. AIAA 2002-0663
95. Cutler, A., Harding, G., & Diskin, G. “High Frequency Pulsed Injection into a Supersonic Duct Flow,” *AIAA Journal*, Vol. 51, No. 4, April 2013, pp. 809-818
96. Miller, D., Yagle, P., Bender, E., Smith, B., & Vermeulen, P. 2001 A Computational Investigation of Pulsed Injection into a Confined, Expanding Crossflow. AIAA 2001-3026

97. Bueno, P., Hou, Y., Clemens, N., & Dolling, D. 2004 Wide Field PIV study of Pulsed Jet injection Upstream of Mach 2 Shock Wave/Boundary Layer Interaction. AIAA 2004-0707
98. Kalidas, S., & Kurian, J. 2007 Enhancement of Supersonic Mixing with the help of Pulsed Injection. AIAA 2007-5032
99. Malo-Molina, F., & Ebrahimi, H. 2012 High Fidelity Analysis of a Non-Reacting Pulsed Supersonic Combustor. AIAA 2012-0946
100. Cutler, A., Harding, G., Diskin, G. 2001 Supersonic Pulsed Injection. AIAA-2001-0517
101. Kouchi, T. Sakuranaka, N., Izumikawa, M. & Tomioka, S. 2007 Pulsed Transverse Injection Applied to a Supersonic Flow. AIAA 2007-5405
102. Randolph, H., & Chew, L. 1994 Pulsed Jets in Supersonic Cross Flow. AIAA 1994-0256
103. Donovan, A., Goddard, F., Lawrence, H., Gilruth, R., Editors, *High Speed Problems of Aircraft and Experimental Methods*, Goddard, F. "Section G: Supersonic Tunnels," Princeton, New Jersey, Princeton University Press, 1961, pp. 491-532
104. "Schlieren System," NASA Wind Tunnel Index, http://www.grc.nasa.gov/WWW/k-12/airplane/tunvschlrn.html
105. "Schlieren Photography," McGraw Hill Science and Technology Encyclopedia, http://www.answers.com/topic/schlieren-photography
106. Clemens, N. & Mungal, M. "A Planar Mie Scattering Technique for Visualizing Supersonic Mixing Flows," *Experiments in Fluids*, Vol. 11, 1991, pp. 175-185
107. Bugden, W., Fitton, K., Folinas, G., Fournier, N., Hogan, G., Ito, M., Lambert, J., Patel, N., Shin, D., Wong, G., Ziegler, E., *Design and Construction of a Supersonic Wind Tunnel with Diagnostics*, JB3-SWT3, April 2013
108. Kondo, A., Sakaue, S., & Arai, T. 2008 Fluctuation of Mass Flux and Concentration on Supersonic Mixing Using Streamwise Vortices. AIAA 2008-2535
109. AIAA Aerodynamic Measurement Technology Technical Committee, "Technique Overview," https://info.aiaa.org/tac/ASG/AMTTC/Shared%20Documents/Technique%20Overviews/lv.html
110. Takahashi, H., Ikegami, S., Oso, H., Masuya, G. & Hirota, M. "Quantitative Imaging of Injectant Mole Fraction and Density in Supersonic Mixing," *AIAA Journal*, Vol. 46, No. 11, November 2008, pp. 2935-2943
111. Seitzman, J. & Hanson, R. "Instrumentation for Flows with Combustion: Chapter 6: Planar Fluorescence Imaging in Gases," pp. 403-466
112. Escoda, M., & Long, M. "Rayleigh Scattering Measurements of the Gas Concentration Field in Turbulent Jets," *AIAA Journal,* Vol. 21, No. 1, 1983, pp. 81-84